



# **Mechanisms behind the assembly and stabilization of hyaluronan-rich extracellular matrices**

Dissertation presented to the Department of Biochemistry and  
Molecular Biology to obtain the degree of Doctor from the  
University of Basque Country

by

Natalia S. Baranova

Thesis supervisor: Dr. Ralf P. Richter  
University Tutor: Prof. Felix Goñi Urcelay

Donostia-San Sebastian 2013





The research work related to this thesis has been performed at:

CIC biomaGUNE,  
Donostia-San Sebastian,  
Basque Country,  
Spain

Biosurfaces Unit,  
Group of Ralf Richter



*для К.*



Понять - значит упростить.

Д. Строгов

эпиграф к «*Волны гасят ветер*» А. и Б. Стругацких

---

To understand – is to simplify.

D. Strogov

epigraph to the “*The Time Wanderers*” by A. & B. Strugatski





# Acknowledgements

---

This thesis would not have been possible without the help of several individuals who in one way or another contributed and extended their valuable assistance in the completion of this project and my life in Spain.

Foremost, I would like to express my sincere gratitude to my supervisor Dr. Ralf Richter. From the beginning of my PhD you constantly challenged me with the physicist point of view on biology, by this inspiring me to dig deep into my knowledge. Your high scientific requirements, deep understanding of matter and perfect organization is the best example which students can get from their supervisor. Without your strong support in and outside of lab this dissertation definitely would not have been possible.

I would like also to express my deepest gratitude to Prof. Anthony Day for many fruitful discussions crucial to shape the project and of course for the constant supply of proteins. My gratitude also goes to Dr. David Briggs and Dr. Antonio Inforzato, who were always ready to provide me with proteins and shared their motivating ideas. This project would not be completed without efforts of the members of the Tony Day's group in the University of Manchester - Viranga Tilakaratna and Simon Foulcer.

I also would like to extend by sincere gratitude to Dr. Natalia Yevdokimova, thanks to whom I had decided to do my PhD - you grew my passion to research, under conditions where research itself was not possible.

My gratitude goes to my former and current colleagues in the group. The discussions we carried and often technical help were valuable to complete the project. Many thanks also for the fun times we had outside of the lab. Basque hospitality and the warm welcome of Ixaskun Carton helped me to overcome life obstacles at the beginning of my PhD. Marta Gallego and Leire Diaz were ready to support me at all times. Thank you all for your unselfish and unfailing help.

The best recharge of energy during my PhD I found hiking in the Basque mountains with the `cuadrilla`. Thank you for many unforgettable moments. I also want to thanks my friends in Ukraine – I am happy to know that the distance has not affected our friendship.

And of course my warmest gratitude goes to my family who has always supported me as I chase my dreams, however extreme they are. Спасибо большое, родители, за ту свободу выбора, которую вы мне давали с самого детства и за вашу постоянную поддержку. “Все приходит в свое время для тех, кто умеет ждать”, - спасибо моему мужу за бесконечную веру в меня. И конечно же спасибо малышу Тимуру за его ежедневную улыбку.



# Abstract

---

Many eukaryotic cells surround themselves with a hydrogel-like, polysaccharide-rich matrix. A crucial component of such coats is hyaluronan (HA), a regular, linear polysaccharide of the glycosaminoglycan family of typically several micrometers in contour length. The coats do also contain a number of HA-binding proteins that engage in the self-assembly of HA into relatively thick, soft and highly hydrated coats. An example of such pericellular coats is the cumulus cell-oocyte complex (COC) matrix, an extended viscoelastic coat that grows around oocytes just before ovulation and that is required for fertilization. The secreted product of tumor necrosis factor-stimulated gene-6 (TSG-6), inter- $\alpha$ -inhibitor (I $\alpha$ I) and pentraxin 3 (PTX3) proteins were shown to be crucial for COC matrix stabilization, but how they form a functional and stable HA matrix remains poorly understood.

The *aim* of this thesis was to gain mechanistic insight into the supramolecular self-assembly processes that lead to the formation of HA-rich matrices, to understand how such matrices are stabilized, and to relate the physico-chemical properties of the matrices to their biological functions. To this end, we used a simplified yet well-defined model system of pericellular coats: films of end-grafted HA. The HA films were created on solid supports, enabling the application of surface-sensitive techniques like quartz crystal microbalance with dissipation monitoring (QCM-D), spectroscopic ellipsometry (SE) and reflection interference contrast microscopy (RICM) for their detailed characterization, and allowing for highly controlled, quantitative experiments to be realized.

HA matrices of increasing complexity were reconstituted by external addition of proteins to the HA films which are known to be involved in matrix assembly and stabilization. We found that the inflammation-associated protein TSG-6, when presented alone to the HA film, forms oligomers upon binding to HA. The TSG-6 oligomers cross-link HA and induce a pronounced collapse of the HA matrix. In contrast, when TSG-6 is presented together with I $\alpha$ I, its cross-linking properties are impaired. Instead, TSG-6 acts as an enzyme for the covalent transfer of heavy chain subunits from I $\alpha$ I to HA. The ternary interaction of HA, TSG-6 and I $\alpha$ I results in a matrix containing several different and very stably incorporated proteins and protein complexes. We also found that, in order to incorporate PTX3 into HA matrices, the encounter between I $\alpha$ I, TSG-6 and PTX3 prior to their interaction with HA is required. In the presence of all three proteins, the HA film becomes cross-linked but not collapsed.

Based on these results we propose that the spatio-temporal regulation of HA/protein interactions *in vivo* is responsible for the balance between effective expansion of the COC matrix during ovulation on one hand and matrix stabilization through cross-linking on the other. Our results highlight that a hierarchy of interactions between the molecular players determines the proteins' functions and the properties of the supramolecular assembly. The discovered mechanisms of HA matrix stabilization illustrate the significance of matrix remodeling under inflammatory conditions.

# Resumen

---

Muchas células eucariotas se rodean de una matriz rica en polisacáridos similar a un hidrogel. Un ejemplo de estas matrices pericelulares es la matriz del cumulus-oophorus (COC), un recubrimiento viscoelástico y extendido que crece alrededor del ovocito solo antes de la ovulación y que se requiere para la fertilización.

Un componente crucial de estos recubrimientos es ácido hialurónico (AH). El AH es un polisacárido lineal, posee una estructura simple que se ha preservado durante la evolución. Sus unidades repetitivas son disacáridos de ácido glucurónico y N-acetilglucosamina. El número de unidades repetitivas de disacárido puede llegar hasta 10000 o más, con un peso molecular alto ( $10^5$ - $10^7$  Da). La longitud de un disacárido es de aproximadamente 1 nm, por tanto la cadena entera de AH puede llegar a extenderse varios micrómetros  $\sim 10 \mu\text{m}$  si la molécula está extendida de extremo a extremo. Desde el punto de vista de la física de polímeros, el AH está descrito como un polielectrolito. En solución, el AH adopta una conformación hidratada y enrollada al azar. Los polímeros de AH de tamaño típico, el contenido de agua de dicha conformación está en torno al 99.9%. La cadena de AH es muy larga y por tanto puede albergar cientos de ligandos para las hialadherinas.

Las capas también tienen proteínas con ligandos para el AH que participan en la autoorganización de la matriz gruesa, suave y hidratada. El TSG-6 (factor estimulador de necrosis tumoral gen 6), el inter- $\alpha$ -inhibidor, (I $\alpha$ I) y la pentraxina 3 (PTX3) son proteínas que han demostrado ser muy relevantes para la estabilización de la matriz COC, pero el cómo forman una matriz estable y funcional todavía permanece poco entendido.

TSG-6 es una proteína multifuncional que se expresa bajo condiciones inflamatorias y por las células cumulus en el folículo preovulatorio. Tiene muchos ligandos, entre los cuales se encuentran el AH, I $\alpha$ I y PTX3. El TSG-6 está compuesto de dos dominios: el módulo Link

tiene capacidad interaccionar con el AH y el módulo CUB. El módulo Link en algunos casos tiene efectos biológicos comparables con la proteína entera.

Inter- $\alpha$ -inhibidor es un complejo proteoglicano constitutivo de la sangre; consiste en dos cadenas pesadas HC1 y HC2 covalentemente ligadas via condroitín sulfato a otra subunidad ligera la bikunina. Las interacciones entre el I $\alpha$ I, el TSG-6 y el AH llevan a la formación de complejos covalentes HA•HCs. La modificación covalente de la matriz COC con las HCs tiene una consecuencia particular en la formación de la matriz – los ratones que no producen bikunina (que no pueden producir I $\alpha$ I) son incapaces de formar una matriz estable. Sin embargo, la presencia de TSG-6, I $\alpha$ I es no suficiente para estabilización de la matriz COC, porque los ratones que no producen PTX3 mostraron inestabilidad de la matriz y falta de fertilidad.

PTX3, el receptor reconocedor de patrones soluble pentraxina 3, es un miembro de la familia de la pentraxina. La proteína la forma un complejo de 8 subunidades idénticas (PM ~42.5 kDa) estabilizadas por enlaces disulfuro. Cada protómero de PTX3 consiste de un dominio C-terminal de tipo pentraxina, homólogo a la clásica pentraxina corta y un dominio N-terminal único. Las células cumulus de los ratones con PTX3<sup>-/-</sup> son incapaces de organizar una matriz funcional. La adición exógena de PTX3 recupera la formación de la matriz COC. Aunque PTX3 no interacciona con el AH, existe la hipótesis que su incorporación en la matriz-AH esta mediada por el dominio Link del TSG-6 o HCs unidos covalentemente al AH.

Es más, los datos *in vivo* sugieren la importancia de la regulación espacio-temporal en la organización de la matriz COC. En particular, se ha establecido que las expresiones de TSG-6, PTX3 y AH tienen perfiles temporales similares. El TSG-6 se ha encontrado co-localizado con el AH a lo largo de la matriz desde la periferia de las células cumulus a la zona pelúcida. El I $\alpha$ I es un constitutivo de la sangre y penetra el folículo tras la activación hormonal de la ovulación, cuando la barrera de permeabilidad se vuelve permeable, y con el tiempo se difunde hacia el ovocito. Tras 6 horas de inducción de la ovulación se retiene un gradiente de PTX3 en la matriz COC. Dicha organización espacio-temporal puede ser crucial para la regulación de la interacción AH/proteína y el correcto autoorganización de la matriz COC.

El *objetivo* de esta tesis ha sido adquirir conocimiento sobre los procesos de autoensamblaje supramolecular que conducen a la formación de matrices ricas en AH para saber

cómo se estabilizan dichas matrices y para relacionar las propiedades físico-químicas de las matrices con sus funciones biológicas. Para este propósito utilizamos un sistema-modelo bien definido y simplificado de capas pericelulares: películas de AH, donde el polímero está unido a superficie en uno de sus extremos. Las películas de AH se crearon sobre soportes sólidos, permitiendo la aplicación de técnicas de superficie como quartz cristal microbalance (QCM-D), elipsometría espectroscópica (SE) y reflection interference contrast microscopy (RICM) para caracterizarlas en detalle y permitiendo la realización de experimentos cuantitativos altamente controlados.

Ha sido necesario desarrollar diferentes metodologías en el diseño y manipulación de las películas de AH necesarias para la tesis. En particular, el AH polimérico puede ser reemplazado por AH oligomérico, permitiendo así controlar el número de puntos de enlace por cadena de AH. Al cambiar entre plataformas de OEG y SLB los puntos de anclaje pueden mantenerse, potencialmente, bien lateralmente móviles o bien inmovilizados. Los modelos basados tanto en OEG como en SLB fueron notablemente resistentes al tratamiento con GuHCl. Por último, establecimos un protocolo para la desecación/rehidratación de películas de AH basadas en OEG sin que su comportamiento fuera afectado de forma significativa, facilitando así el uso de películas de AH fuera del laboratorio en el que han sido producidas. Estas modificaciones demuestran que las propiedades de las películas de AH se pueden ajustar a las aplicaciones deseadas.

Las matrices de AH crecientemente complejas fueron reconstituidas por adición externa de proteínas a las capas de AH, proteínas que se sabe que están involucradas en el ensamblaje y estabilización de las matrices. Los datos cuantitativos del sistema modelo demuestran que TSG-6 forma oligómeros al interactuar con AH que actúan como reticulantes efectivos de AH. En concentraciones que podrían ser fisiológicamente relevantes, TSG-6 es capaz de transformar las capas de Ah de un estado altamente expandido en una capa condensada y bastante rígida. Este tipo de remodelación podría ocurrir en el glicocáliz endotelial y hacer la función de señal primaria para atraer a los leucocitos. La remodelación de la matriz extracelular de los TSG-6 podría afectar también a las propiedades mecánicas de las células y cambiar significativamente su fenotipo. En la artritis la retención de AH por la reticulación con del TSG-6 en la capa de los condrocitos podría contribuir a su función condroprotectora.

I $\alpha$ I dicta la actividad de TSG-6 y remodela las propiedades de la matriz de AH. La reticulación y compactación inducida por TSG-6 de las películas de AH se ve inhibida por la presencia de I $\alpha$ I. Esto lleva a la inhibición del enlace de AH con las células positivas en CD44 mediado por TSG-6. Una incubación prolongada con TSG-6 y I $\alpha$ I resulta en películas de AH que contienen, además de HCs enlazadas covalentemente a AH, varias especies moleculares que están firmemente pero no covalentemente enlazadas. El material no covalentemente enlazado, que incluía TSG-6, tiene la habilidad de transferir HCs a AH.

También demostramos que la interacción entre las proteínas TSG-6, I $\alpha$ I y PTX3 determina las propiedades estructurales y morfológicas de la matriz de AH. PTX3 era inerte a la interacción con una matriz de AH que fuera resultante de la interacción ternaria entre I $\alpha$ I, TSG-6 y AH, a pesar de que dichas matrices contienen el complejo HA•HC; se ha sugerido que dichos complejos son potencialmente ligantes de PTX3. Además, PTX3 no puede ser introducido en una matriz de AH únicamente mediante TSG-6. Al contrario, observamos que la interacción de PTX3 con I $\alpha$ I y TSG6 antes de encontrarse con A H es necesaria para que pueda incorporarse eficientemente a la matriz. PTX3 parece estar involucrado en la reticulación. A pesar de haber incorporado con éxito todas las proteínas que se han visto que son cruciales para la estabilidad de las matrices de COC en las capas de AH, todavía no se conoce la estructura exacta de los nódulos de reticulación en la matriz de AH. Próximos estudios con dominios seleccionados de proteínas (en particular HCs recombinantes) o formas mutantes (por ejemplo PTX3 que forme dímeros o tetrámeros), utilizando las pruebas desarrolladas en esta tesis, deberían permitir esclarecer aún más esta cuestión.

Basados en los hallazgos enumerados arriba, postulamos que hay una interacción funcional entre los diferentes mecanismos reticulantes en el ensamblaje de la matriz de COC. En particular, la reticulación inducida por TSG-6 podría ser importante en las primeras fases de ensamblaje de la matriz de COC, cuando la síntesis de AH y TSG-6 es elevada. TSG-6 podría ayudar a retener en la matriz del cúmulo de células el exceso de AH producido antes de que la pared de folículos se haga permeable a otro ligante de TSG-6 – I $\alpha$ I. Cuando I $\alpha$ I entra en el folículo, la reticulación de TSG6 se vería perjudicada. Para estabilizar la estructura en su totalidad, PTX3 se incorpora a la matriz de AH en las regiones donde las proteínas (o sus subunidades) se topan. Esto llevaría a la formación de estructuras reticuladas



que son transitorias y por tanto permiten la incorporación de nuevas cadenas de AH y, en última instancia, la expansión de la matriz de COC.

En el futuro esta hipótesis podrá ser verificada en sistemas modelo tridimensionales (3D). Con este fin, microesferas recubiertas de AH podrían ser incrustadas a una matriz de AH por medio de la adición externa de proteínas y AH. Las propiedades mecánicas de las matrices artificiales que tengan composiciones diferentes se pueden comprobar y comparar a las de una matriz de COC real. La reconstitución de un material 3D extenso debería brindar una valiosa prueba si AH, TSG-6, I $\alpha$ I y PTX3 juntos pudieran, de hecho, componer el sistema mínimo requerido para el ensamblaje, expansión y estabilización de la matriz de COC.



# Contents

<b>1</b>	<b>Introduction.....</b>	<b>1-1</b>
1.1	Objective and outline.....	1-1
1.2	Biological relevance of HA-rich matrices.....	1-2
1.3	The cumulus cell-oocyte complex matrix.....	1-4
1.4	Composition of the COC matrix.....	1-6
1.4.1	Hyaluronan.....	1-6
1.4.2	TSG-6.....	1-8
1.4.3	IαI.....	1-10
1.4.4	PTX3.....	1-12
1.5	On the spatial and temporal regulation of COC matrix assembly.....	1-13
1.6	Model system to reconstruct HA matrix assembly.....	1-14
1.7	Characterization techniques.....	1-17
1.7.1	Quartz crystal microbalance with dissipation monitoring (QCM-D).....	1-18
1.7.2	Spectroscopic ellipsometry.....	1-21
1.7.3	Colloidal probe reflection interference contrast microscopy (RICM). ....	1-23
<b>2</b>	<b>Design of well-defined HA films to study complex HA-protein interactions .....</b>	<b>2-1</b>
2.1	Introduction.....	2-2
2.2	Experimental procedures.....	2-3
2.3	Results.....	2-6
2.3.1	Design of well-defined HA films.....	2-6
2.3.2	Surface density of pHA films.....	2-10
2.3.3	Resistance of HA films against the dissociating agent GuHCl.....	2-11
2.3.4	Drying and rehydration of OEG-based HA films.....	2-13
2.4	Discussion.....	2-17
2.4.1	OEG- versus SLB-based model system. ....	2-17
2.4.2	Applications of oligo HA films. ....	2-17
2.4.3	Stability of HA films against GuHCl.....	2-18
2.4.4	Drying/rehydration of OEG-based pHA films. ....	2-18
2.4.5	Potential applications of rehydrated HA films. ....	2-18
<b>3</b>	<b>The inflammation-associated protein TSG-6 cross-links hyaluronan via hyaluronan-induced TSG-6 oligomers.....</b>	<b>3-1</b>
3.1	Introduction.....	3-2
3.2	Experimental procedures.....	3-4
3.3	Results.....	3-7
3.3.1	Binding of full length TSG-6 to HA films. ....	3-9
3.3.2	Full-length TSG-6 oligomers can cross-link HA.....	3-12
3.3.3	Full-length TSG-6 induces strong condensation of HA films. ....	3-15
3.3.4	Binding of Link_TSG6 to HA films. ....	3-17

3.3.5	Condensation of HA films by Link_TSG6. ....	3-20
3.3.6	Link_TSG6 induces total film collapse at low ionic strength. ....	3-22
3.4	Discussion .....	3-25
3.4.1	Implications for the function of TSG-6 in vivo.....	3-26
3.4.2	Relevance of the cross-linking of HA-rich pericellular coats for leukocyte homing.....	3-27
<b>4</b>	<b>Inter-<math>\alpha</math>-inhibitor impairs TSG-6 induced hyaluronan cross-linking.....</b>	<b>4-1</b>
4.1	Introduction.....	4-2
4.2	Experimental procedures .....	4-4
4.3	Results .....	4-8
4.3.1	I $\alpha$ I partially impairs TSG-6 binding to HA .....	4-8
4.3.2	Retained TSG-6 promotes slow incorporation of I $\alpha$ I (or its subunits). ....	4-10
4.3.3	TSG-6 can bind tightly but non-covalently to HCs.....	4-11
4.3.4	Pre-mixing of TSG-6 and I $\alpha$ I affects protein incorporation into HA films .....	4-12
4.3.5	I $\alpha$ I-binding and HC transfer activity are retained, albeit reduced .....	4-15
4.3.6	Effect of I $\alpha$ I incubation on the thickness of the HA film. ....	4-16
4.3.7	Effect of I $\alpha$ I on TSG-6-enhanced HA cell coats.....	4-17
4.4	Discussion .....	4-19
4.4.1	A hierarchy of interactions determines protein function. ....	4-19
4.4.2	Possible mechanisms for the I $\alpha$ I-induced displacement of TSG-6 from HA.....	4-20
4.4.3	The nature and physiological relevance of non-covalently HA-bound material. ....	4-21
4.4.4	Covalent modification of HA with HCs. ....	4-21
4.4.5	Is an HA film exposed to I $\alpha$ I/TSG-6 cross-linked? .....	4-22
4.4.6	Role of HC•HA in leukocyte adhesion.....	4-23
4.5	Supplemental Data .....	4-24
<b>5</b>	<b>PTX3 incorporation into HA-rich matrices .....</b>	<b>5-1</b>
5.1	Introduction.....	5-2
5.2	Experimental procedures .....	5-4
5.3	Results .....	5-7
5.3.1	PTX3 interacts with Link_TSG6, rhTSG-6 and I $\alpha$ I in the absence of HA. ....	5-7
5.3.2	Ternary interaction between TSG-6 constructs, PTX3 and HA.....	5-9
5.3.3	Interaction of PTX3 with HA films that were pre-exposed to TSG-6 and I $\alpha$ I. ....	5-14
5.3.4	Permeability of HA films for PTX3. ....	5-15
5.3.5	How to incorporate PTX3 into HA films?.....	5-16
5.3.6	Stability of PTX3 incorporation and effect of PTX3 on HA film composition. ....	5-19
5.3.7	Structural role of PTX3. ....	5-21
5.4	Discussion .....	5-26
5.4.1	TSG-6-mediated binding of PTX3 to HA. ....	5-26
5.4.2	The display of PTX3 binding sites in HA matrices appears to be tightly regulated. ....	5-27
5.4.3	Structural role of PTX3 in the assembly of COC matrix.....	5-28
<b>6</b>	<b>Conclusions and perspectives .....</b>	<b>6-1</b>

<b>7</b>	<b>Annex I .....</b>	<b>7-1</b>
	Polymer theory concepts for HA characterization .....	7-1
	2.1. Estimate of HA dimension in solution. ....	7-1
	2.2. End-grafted polymers.....	7-2
	2.3. The mesh size of an entangled polymer meshwork.....	7-3
<b>8</b>	<b>References .....</b>	<b>8-1</b>

# 1 Introduction

## 1.1 Objective and outline

The objective of this interdisciplinary work was to gain mechanistic insight into the supramolecular self-assembly processes that lead to the formation of hyaluronan (HA)-rich pericellular or extracellular matrices, to understand how such matrices are stabilized, and to relate the physico-chemical properties of the matrices to their biological functions. To this end, HA-rich matrices were reconstituted in vitro using surface-confined films of end-grafted HA. A toolbox of surface-sensitive characterization techniques such as quartz crystal microbalance with dissipation monitoring (QCM-D), spectroscopic ellipsometry (SE) and reflection interference contrast microscopy (RICM) was used to obtain quantitative information on the mechanisms behind HA-rich matrix assembly.

Chapter 1 provides a general introduction into HA-rich matrices. Of particular relevance for this thesis work is the cumulus cell-oocyte complex (COC) matrix with its key proteins TSG-6, inter- $\alpha$ -inhibitor (I $\alpha$ I) and pentraxin 3 (PTX3). The research work accomplished is presented in Chapters 2 to 5. Novel developments in the design of the surface-based model systems are presented in Chapter 2. Chapter 3 is dedicated to the investigation of interaction between TSG-6 and HA. Chapter 4 covers the ternary interaction between HA, TSG-6 and I $\alpha$ I. Another level of complexity will be added in Chapter 5, where we will look at the quaternary interaction between HA, TSG-6, I $\alpha$ I and PTX3. Chapters 2 to 5 do also contain more detailed introductions of the investigated proteins and their known interactions, as well as detailed descriptions of the materials and methods used. Concluding remarks and perspectives will be covered in Chapter 6. A short summary of polymer theory concepts to describe behaviour of HA in solution, on surfaces and upon cross-linking can be found in Annex 1.

This work has given rise to several manuscripts for peer-reviewed journals. Chapter 3 is already published, Chapter 4 submitted and Chapter 5 in preparation.

## 1.2 Biological relevance of HA-rich matrices

In tissues, cells are embedded in extracellular matrix (ECM) which is made from components that are produced and then secreted by the cells. This matrix has many functions: it serves as integrative support to anchor cells, it distinguishes tissues from one another, it regulates inter-cellular communication and it ensures the mechanical stability of the tissue <sup>1</sup>. Many mammalian cells additionally endow themselves with a pericellular matrix (PCM), also referred to as a cellular coat or glycocalyx, which is located at the interface between the ECM and the cellular membrane, and typically defined by its direct anchorage to the plasma membrane <sup>2</sup>. Pericellular matrices have been reported for a variety of cells *in vivo* and in tissue culture such as fibroblasts <sup>3</sup>, chondrocytes <sup>2, 4</sup>, epithelial cells <sup>5</sup>, prostate cells <sup>6</sup>, monocytes <sup>7</sup> and endothelial cells <sup>8, 9</sup>. The thickness of the coat varies from one cell type to another and depends strongly on the state of the cell (Fig. 1.1) <sup>10, 11</sup>. For example, monocyte coats typically extends outwards by only 10 to 20 nm <sup>7</sup>, whereas 20  $\mu\text{m}$  thick coats were observed on chondrocytes <sup>2, 12</sup>.

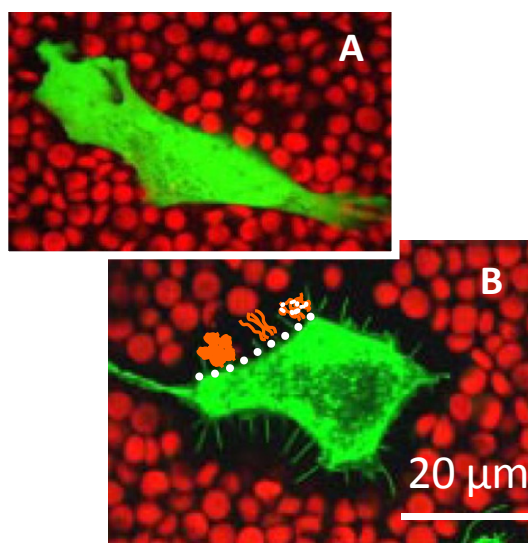


**Fig. 1.1 Visualization of a PCM by a particle exclusion assay.** Red blood cells (red) were settled on a culture of human breast adenocarcinoma cell line, MCF-7, and pericellular matrices become visible because they cannot be penetrated by red blood cells. Membranes of MCF-7 cells were stained with a fluorescent dye (green) A. Native MCF-7 cell. B. MCF-7 cell transfected to overproduce hyaluronan (HA); membrane protrusions, so called microvilli (visible as green lines) were induced by transfection. Schematics (orange) were drawn into the micrograph to illustrate that the thick coat can be the result of different HA configurations: a cross-linked multilayer, extended chains in a brush-like conformation, or extended chains decorated with additional proteins (from left to right). Adapted from <sup>10</sup>.

For a long time, the PCM was considered as a passive lubricating layer around the cells, because of its strongly hydrated gel-like nature. Later, it was found that it also plays an active

role in many biological processes<sup>13</sup>, including cell adhesion<sup>14, 15</sup>, cell proliferation<sup>16, 17</sup>, cell migration<sup>6, 18</sup>, the display of growth factors<sup>19</sup>, embryogenesis<sup>13</sup> and fertilization<sup>20</sup>. Although the PCM is involved in a diverse range of fundamental biological processes the relation between its structure and functions remains poorly understood.

A key structural component of many pericellular matrices is the polysaccharide hyaluronan (HA, chapter 1.4.1). It is synthesized directly at the cellular membrane and can remain anchored to the cell surface either at the HA-synthase that produced the HA chain or it can bind to the cell surface through HA-binding receptors. The linear HA chains of typically several micrometer in contour length alone are not enough to assemble PCMs of several microns in thickness<sup>21</sup>. Instead, they serve as a scaffold or polyvalent template<sup>22</sup> for the incorporation of members of the family of hyaluronan-binding proteins, also called hyaladherins. For example, the attachment of aggrecan, a proteoglycan that has the form of a bottle brush, to HA chains results in the formation of extended and highly hydrated<sup>4</sup> that can give rise to thick cellular coats.

Variations in the length of HA chains, the confinement of HA to the cell surface, and the non-uniform distribution of various hyadherins along one chain can give rise to a spatial organization of the PCM. In cultures of rat chondrocytes, for example, the density of the coat was shown to be relatively high at a distance of about 1  $\mu\text{m}$  from the cell membrane, with a mesh size of  $\sim 100$  nm, as compared to the periphery, where the mesh size reached 500 nm<sup>11</sup>. Such density gradients in the PCM create an osmotic force which decays with the distance from the cell surface<sup>11</sup>. Also, when cells were transfected with HA synthases, the thickness of the HA-rich coat was found to increase drastically, driven by the formation of membrane protrusions (microvilli; Fig. 1.1). Interestingly, the increase in the density of HA on the cellular membrane was proposed as the driving force for microvillus formation<sup>10, 23</sup>.

PCMs are highly dynamic structures<sup>24</sup>, they reorganize constantly as a function of external stimuli. The dynamic rearrangement of the coat can be observed when cells detach from the surface or from surrounding cells, like during mitosis or migration<sup>17, 25</sup>. Detachment of the cells in these cases is characterized by a swollen PCM and a rounded cell shape<sup>17</sup>.

Under inflammation, for example in arthritis, the PCM undergoes remodeling – the HA matrix needs to be cross-linked to stabilize the entire assembly and to prevent the loss of tissue<sup>26</sup>. Remodeling of the PCM structure by HA cross-linking was proposed as a pathway to regulate inflammatory process. For example, the formation of cable-like structures, larger than 200 microns in length, with altered leukocyte-binding properties, were observed in response to inflammatory stimuli<sup>27</sup>. These cable-like structures were suggested to be formed by cross-linked HA chains<sup>26</sup>. The mechanisms of PCM cross-linking as well as how cross-linking alters the physico-chemical properties of the HA matrix and its functional activity remain poorly understood. Various proteins and protein complexes were proposed to cross-link HA meshworks (Fig. 1.2).



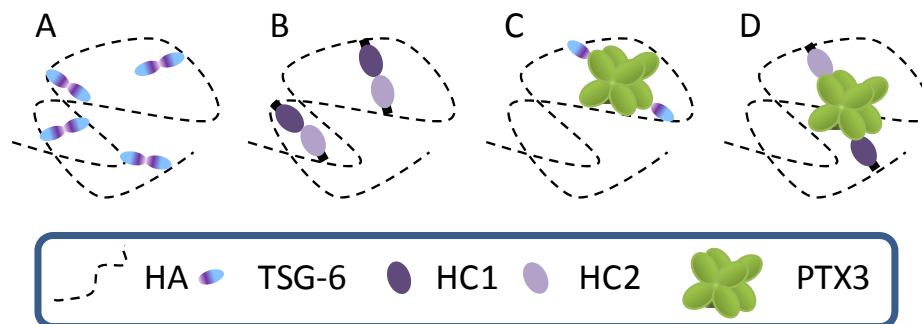


Fig. 1.2 **Hypothesized mechanisms of TSG-6 mediated HA cross-linking.** A. Direct cross-linking of HA chains through self-association between TSG-6 monomers. B. HA cross-linking via non-covalent interaction between heavy chains (HCs) of inter- $\alpha$ -inhibitor (I $\alpha$ I), covalently transferred onto HA by TSG-6. C. A cross-linking node formed by a complex of TSG-6 and PTX3. PTX3 is a multimeric protein, which does not bind HA directly but that interacts with TSG-6 and I $\alpha$ I. D. Incorporation of PTX3 cross-linker can be mediated via HCs of I $\alpha$ I.

Several different cross-linking pathways might be at play simultaneously in a given tissue. Considering the highly dynamic nature of HA and the PCM, it is likely that HA-rich matrices are typically stabilized by transient cross-linking interactions, allowing for continuous matrix remodeling and a constantly changing network of interactions.

## 1.3 The cumulus cell-oocyte complex matrix

An illustrative example of a cross-linked PCM is the cumulus cell-oocyte complex (COC) matrix. This extended viscoelastic coat forms around oocytes just a few hours before ovulation and surrounds the oocyte on its journey towards fertilization in the oviduct. Before hormonal stimulation, the ovulating follicle represents a cavity filled with follicular fluid, where the wall of the follicle is formed by several layers of granulosa cells attached to the basement membrane. The oocyte is attached to the follicle wall and surrounded by ~1000 closely packed cumulus cells, such close packing is needed to maintain communication between the cumulus cells and oocyte<sup>1</sup>. At the time of hormonal stimulation, there is very thin PCM around cumulus cells (Fig. 1.3), but during the following hours a progressive accumulation of HA takes place leading to COC matrix expansion. Shortly before ovulation the COC matrix reaches its maximal volume (~20 times its initial state)<sup>28</sup>. While HA is the predominant structural component of the COC matrix, matrix expansion is also driven by the ingress of water because of the polyanionic nature of HA (Chapter 1.4.1).

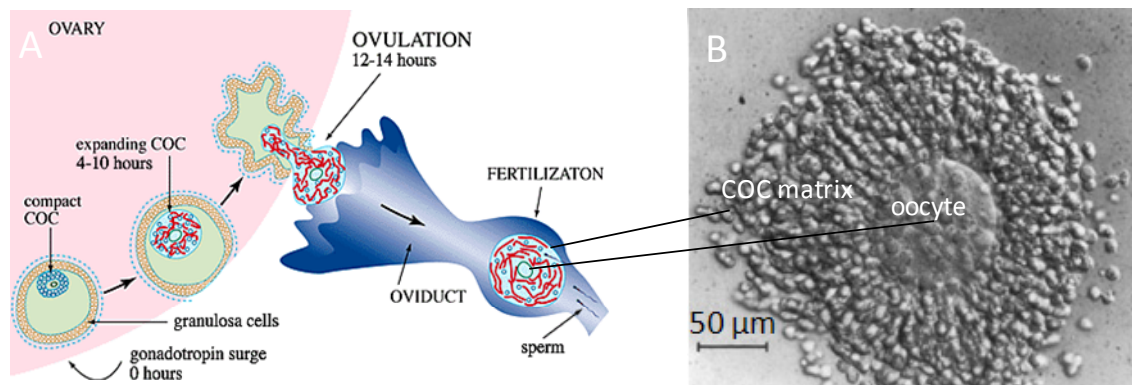


Fig. 1.3 COC matrix in ovulation. *A*. A hydrogel-like polysaccharide-rich coat growth around oocyte before ovulation. The stability, mechanics and chemistry of the COC matrix are designed for successful follicle rupture (ovulation), pick-up, transport and selection of the best sperm for fertilization of the oocyte. *B*. Micrograph of an expanded HA-rich matrix around an oocyte. Adapted from <sup>28</sup> and <sup>29</sup>

In order to keep the expanded COC matrix cohesive, i.e. to stabilize its structure, HA chains need to be cross-linked. Treatment with protease demonstrated that the matrix can be completely dissolved, revealing a fundamental role of proteins in the stabilization of the COC matrix <sup>30</sup>. Several proteins were identified to participate in matrix organization, (i) a group of the proteins which bind HA directly: TSG-6 (<sup>31-33</sup>; Chapter 1.4.1 and Chapter 3), versican <sup>34</sup>, heavy chains (HC) of IαI (<sup>35</sup>; Chapter 1.4.2 and Chapter 4) and cartilage link protein <sup>36</sup>, and (ii) proteins that does not possess a HA-binding motif: PTX3 (<sup>37, 38</sup>; Chapter 5), fibronectin, tenascin and laminin <sup>39</sup>.

The typical way to demonstrate the structural role of proteins in the assembly of the COC matrix is to disrupt their synthesis. In this way, it was demonstrated that loss of either TSG-6 or IαI expression perturbed matrix expansion and ovulation, although HA production was not affected. This led to a drastic decrease in the rate of *in vivo* fertilization (<sup>35, 40, 41</sup>). Notably, COC matrix expansion could be completely blocked by addition of short HA oligosaccharides that compete for TSG-6 <sup>42</sup>, suggesting that TSG-6 is a key player in matrix stabilization. Furthermore the literature demonstrates that COC matrix expansion and successful ovulation depend on the interaction of IαI, in addition to TSG-6, with HA <sup>31-33, 43</sup>. Moreover, PTX3 deficient mice could achieve cumulus expansion *in vivo*, but failed to fertilize because of the rapid disassembly and loss of the COC matrix during release from the follicle <sup>37, 44</sup>. Thus, PTX3 can additionally stabilize the COC matrix and support its retention around the oocyte. The bottle-shaped proteoglycan versican, closely related to aggrecan of cartilage tissue, was also suggested to be evolved in matrix assembly <sup>45</sup>. Whether it is critical for COC matrix expansion has not been confirmed, because removal of versican is lethal making direct knockout studies impossible <sup>34</sup>. However, there is no indirect evidence that cross-linking by versican might take place, but rapid cleavage of the versican in the COC matrix is required for successful ovulation <sup>46</sup>.

It is likely that COC matrix expansion is required for successful ovulation. Together with the thinning of the follicle wall by proteolytic degradation, the expansion of the COC matrix could exhibit an additional pressure on the wall promoting follicle rupture<sup>45</sup>. A cohesive and thick COC matrix is also important for the capture of the oocyte by the oviduct and subsequent transport through the oviduct. In particular, there is a selective adhesion between the cilia of the oviduct epithelium and the COC matrix<sup>47</sup>. Only an oocyte endowed with a proper matrix can efficiently pass through the oviductal lumen<sup>47, 48</sup>. In addition, the COC matrix may present a selective barrier that screens for sperm with high fertility potential<sup>49</sup>. PTX3 was shown to bind sperm cells and attract sperm to the COC in the oviduct<sup>37</sup>. Another protein of unknown identity, yet with a size that would be consistent with versican, was shown to promote acrosomal reaction – the release of hyaluronidases by sperm<sup>50, 51</sup>. The degree of cumulus expansion has been found to be indicative of high oocyte quality and has been used as a criterion for selection of oocytes for *in vitro* fertilization during many years<sup>52</sup>. All this *in vivo* data provide compelling evidence that the correct self-assembly of HA and proteins into the COC matrix is functionally important.

## 1.4 Composition of the COC matrix

As outlined above, much of what is known about the mechanism of HA cross-linking comes from studies on the expansion of cumulus matrix. In particular, it was demonstrated that the presence of HA, TSG-6, IαI and PTX3 is essential for COC matrix expansion and stabilization. In the following, these components will be described briefly. More detailed descriptions are provided in the introductory parts of Chapter 3 to 5.

### 1.4.1 Hyaluronan

Hyaluronan (HA), or hyaluronic acid, is the main carbohydrate component of the PCM, and defined together with collagen and fibronectin the entire structure of extracellular matrix<sup>53</sup>. HA was discovered in 1934 by Meyer in the vitreous humor of the eye<sup>54</sup>, and belongs to the family of glycosaminoglycans. In contrast to all other carbohydrates, HA is synthesized directly on the plasma membrane and thus it does not undergo typical chemical modifications in the golgi apparatus as others glycosaminoglycans<sup>55</sup>. HA hence has a simple structure that has been highly preserved during evolution<sup>56</sup>. As all glycosaminoglycans, HA is linear. HA is a regular polymer of disaccharides, with the repeating unit consisting of glucuronic acid and N-acetylglucosamine (Fig. 1.4). The number of disaccharides,  $n$ , per chain can reach 10000<sup>53</sup>. With each disaccharide (HA<sub>ds</sub>) having a molecular weight of 378 Da, the polymer chain can hence reach a molecular weight of 4 MDa. The length of HA<sub>ds</sub> is approximately 1 nm, and thus a single HA chain can reach a length of 10 μm if it is fully extended (i.e. the so-called contour length)<sup>18, 57</sup>.

From a polymer physics point of view, HA is well described as polyelectrolyte<sup>58-60</sup>. The  $pK_a$  of the glucuronic acid is about 3-4, and thus at physiological pH the carboxyl groups are predominantly ionized, rendering the HA chain highly negatively charged<sup>61</sup>. Intramolecular hydrogen bonds stiffen the chain<sup>62</sup>. Because the HA chains are relatively stiff and repel each other, and because of thermal energy, isolated HA chain in solution adopts the conformation of a swollen random coil. For the typical size of HA polymers, the water content in such a coil is around  $\sim 99.9\%$ <sup>59, 63</sup>.

A single HA chain is very long and hence can have hundreds of binding sites for hyaladherins<sup>64</sup>. Hyaladherins typically bind to between 6 and 20 monosaccharides of HA<sup>65</sup>. The persistent length of an HA chain, a measure of chain flexibility, is 4.2 or 7 nm<sup>60, 66</sup>. On the length scale of a hyaladherin binding cite, the hyaluronan chain therefore appears rather rigid.

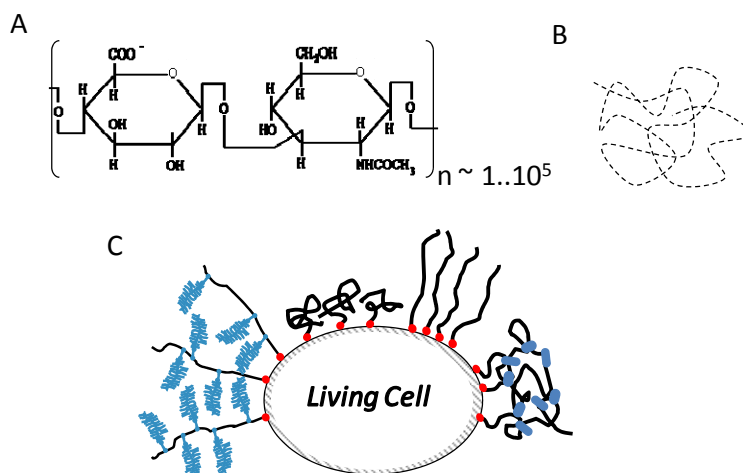


Fig. 1.4 **Chemical structure and conformation of HA.** *A.* HA has a regular polymer that can reach a contour length up to 10  $\mu\text{m}$ . It is unbranched and does not undergo chemical modification by sulfatation as other glycosaminoglycans. *B.* In solution, HA forms a dynamic swollen random coil which contains about 99.9% of water. *C.* The different conformations of HA can be induced by the interaction with hyaladherins which can crosslink or swell HA chains, or confine HA to the cell surface. A single HA chain has many binding sites for hyaladherins.

The concentration of HA in tissues varies from 0.01  $\mu\text{g}/\text{ml}$  in blood plasma to about 4 mg/ml in synovial fluid and umbilical cord<sup>67</sup>. In the expanded COC matrix, for example, the HA concentration is about 0.5 mg/ml<sup>28</sup>. At this concentration, the swollen random coils formed by individual HA chains start to overlap and hence pervade the entire solution, forming a transient meshwork of entangled polymer chains. The typical size of a transient mesh in such an meshwork would be about 50 to 100 nm (Annex 7.3). As discussed above, the HA meshwork in the COC matrix is stabilized by protein cross-linkers. The mesh size in a cross-linked meshwork should depend on the density and stability of cross-links.

Although HA has a several micrometers long contour length and can adapt a random coil conformation in solution occupying a large volume (the radius of gyration, a measure for the coil size, for longest HA chains is about 500 nm (Annex 1.1), this alone cannot explain the origin of the extended matrices with thicknesses of several micrometers. In the literature different models were proposed to explain the formation of the thick coats (Fig. 1.4 C): 1) the PCM might consist of multiple layers of cross-linked and entangled HA chains<sup>14</sup>; 2) the cell membrane might be extremely rough to form microvilli<sup>10, 23</sup>; 3) it is also possible that there is a formation of a dense HA brush, because on the cell surface HA chain remains attached via HA synthases<sup>4, 16</sup>. In addition, steric repulsion between bottle-brush shaped proteoglycans, like versican of the COC matrix<sup>34</sup> can also affect HA configuration by stretching individual HA chains in similar manner as aggrecan<sup>4, 24</sup> (Attili & Richter, unpublished data). The mentioned mechanisms may be specific to a given tissue or they might act together. Overall, the interactions between HA and hyaladherins, but not HA alone, dictate the final properties of the PCM such as thickness, permeability and mechanical properties.

### 1.4.2 TSG-6

The secreted product of tumor necrosis factor-stimulated gene-6 (TSG-6) is a 35 kDa protein composed of a Link and a CUB module. The mRNA encoding the protein was originally identified following tumor necrosis factor treatment of human fibroblasts<sup>68, 69</sup>. The protein TSG-6 has been reported in the synovial fluid of arthritis patients at concentrations of ~ nM<sup>70</sup> or 0.6  $\mu$ M<sup>71</sup>, but it is not constitutively expressed under healthy conditions. The precise role of TSG-6 in inflammation is still unclear, though it was demonstrated that it protects from the cartilage destruction in the mice model of arthritis<sup>72-74</sup>. In ovulation, TSG-6 was shown to be critical for COC matrix expansion<sup>43</sup>.

The Link module contains the hyaluronan binding domain which is conserved among HA binding proteins<sup>75, 76</sup>. The three dimensional structure of a protein construct containing essentially the Link module (Link\_TSG6) has been determined in HA-free and HA-bound conformations<sup>75, 77</sup> ( Fig. 1.5). Link\_TSG6 has a molecular weight of 10.9 kDa and dimension of ~ 3 × 5 × 2 nm<sup>3</sup>(*Protein Data Bank code* 1O7C).

It is demonstrated that HA<sub>8</sub> is the minimal sugar length that can stably bind to the protein. By site directed mutagenesis five main amino acids, mostly aromatic residues (i.e. Tyr<sup>12</sup>, Tyr<sup>59</sup>, Phe<sup>70</sup> and Tyr<sup>78</sup>), were identified to be involved in HA binding<sup>78</sup>. In addition, Arg<sup>81</sup> and Lys<sup>81</sup> were proposed to make a salt bridge with GlcA on the basis of NMR data<sup>76</sup>. The presence of salt bridges was confirmed by isothermal calorimetry performed over a range of NaCl concentrations<sup>79</sup>.

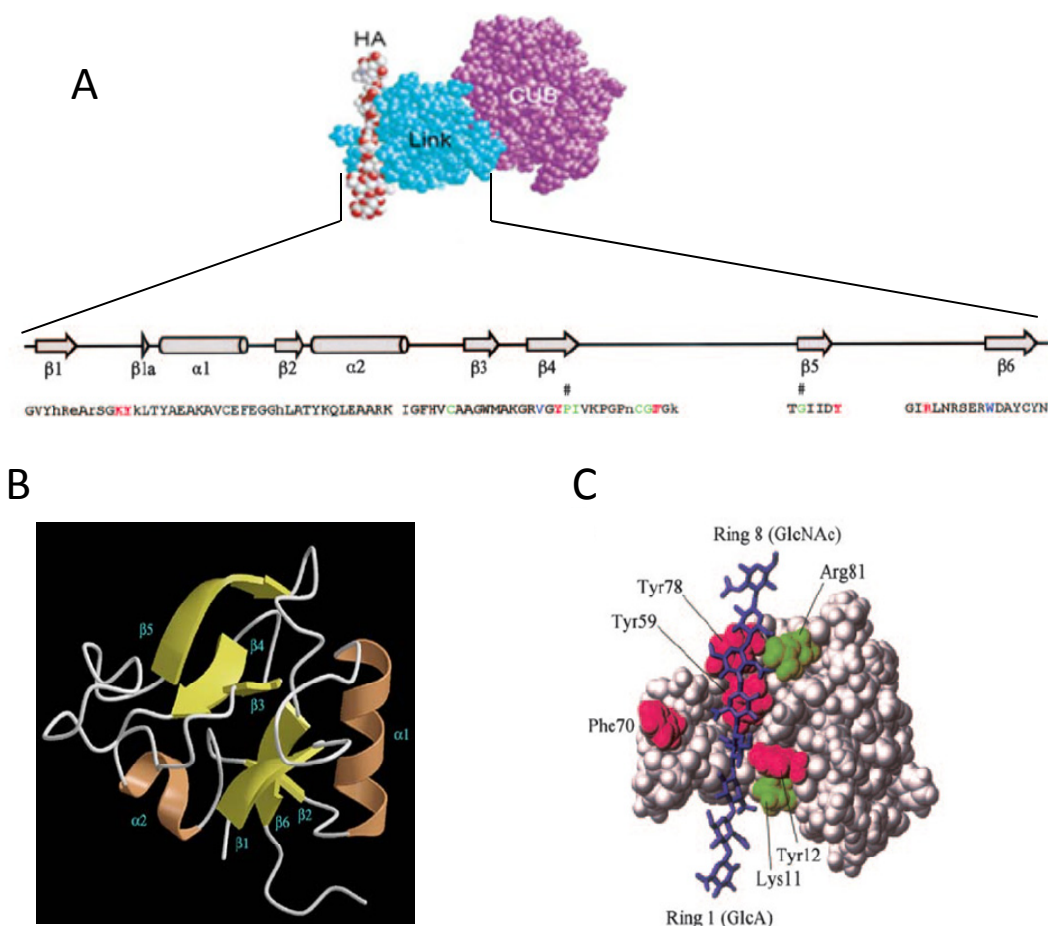


Fig. 1.5 **The structure of TSG-6.** *A.* Structural model of full length TSG-6 with Link module (in blue) and CUB module (in violet), and schematic diagram of the sequence of Link\_TSG6, adapted from <sup>26</sup> and <sup>76</sup>, respectively. *B.* The secondary structure of Link\_TSG6 which consists of two  $\alpha$  helices ( $\alpha 1$  and  $\alpha 2$ ) and two antiparallel  $\beta$  sheets (sheet 1 is composed of strands  $\beta 1$ ,  $\beta 2$  and  $\beta 6$ , and sheet 2 of  $\beta 3$ ,  $\beta 4$  and  $\beta 5$ ) <sup>77</sup>. *C.* Model of HA<sub>8</sub> built into the binding groove of Link\_TSG6. Key binding residues on the protein are marked in red (aromatic) and green (basic), taken from <sup>76</sup>.

The CUB module is not known to have HA binding properties. Its structure is currently not solved, but molecular modeling suggested that it is involved in the bonding of TSG-6 to IaI (31). Also, it was demonstrated that the CUB domain is responsible for the interaction between TSG-6 and fibronectin <sup>80</sup>.

Small angle X-ray scattering data suggested full length TSG-6 to form dimers in the presence of HA octasaccharides in solution <sup>81</sup>. The TSG-6 dimer was estimated to be  $\sim 13 \pm 1$  nm in length. Based on this finding, self-association between TSG-6 monomers was proposed as one of the mechanisms to cross-link HA matrices and thereby to stabilize the matrix against destruction like in arthritis <sup>82</sup> (Fig. 1.2 A).

### 1.4.3 IαI

Inter- $\alpha$ -inhibitor (I $\alpha$ I) is a proteoglycan. It is composed of two heavy chains (HC1 and HC2) and the serine protease inhibitor bikunin<sup>83, 84</sup>. The HCs are interconnected with the bikunin subunit by a chondroitin sulfate (CS) chain. The CS chain is 12 to 18 disaccharides long. The HC1 and HC2 subunits (~80 kDa each) are located in close proximity to each other, in a region of less sulfated CS, with HC1 attached farther away from bikunin than HC2<sup>85</sup>. The attachment of bikunin to CS is through a common O-glycosidic bond on Ser, while the HCs are attached via ester bonds formed between the carboxyl group of aspartic acid on the HCs and the C-6 carboxyl group of N-acetylgalactosamine in CS<sup>86</sup>. By electron microscopy, it was shown that bikunin has a spherical shape with a diameter of ~2 nm, whereas the two HCs have a globular shape (diameter of ~11 nm)<sup>87</sup>. I $\alpha$ I is present in blood plasma (the circulating level is 150 to 500  $\mu$ g/ml<sup>88, 89</sup>), and in extracellular matrix<sup>35, 90, 91</sup>.

Its name reflects that I $\alpha$ I was initially extensively studied as a protease inhibitor, but its inhibitory activity on proteases, realized through the bikunin subunit, is rather weak<sup>89</sup>. It was suggested that I $\alpha$ I functions as a shuttle that traps proteases and then transfers them to the physiological inhibitors<sup>92</sup>. Most of circulating bikunin though corresponds to I $\alpha$ I, rather than bikunin-CS, presumably due to the longer half-life of intact I $\alpha$ I<sup>35, 93</sup>.

In the ECM, I $\alpha$ I was found to be associated with HA although it does not bind directly to HA<sup>93, 94</sup>. In particular, HA can be covalently modified with HCs, and increased modification of HA with HCs of I $\alpha$ I was found in synovial fluid of patients with rheumatoid arthritis compared to healthy patients. The extracted HA containing covalent HC modifications had properties of a gel, suggesting that HCs can cross-link HA<sup>94</sup>. HA•HC complexes have also been found in follicular fluid<sup>95</sup>. Structural analysis of the complexes revealed that HCs are bound to HA via an ester bond between the Asp residue at the C-terminus of HCs and the C-6 hydroxyl group of N-acetylglucosamine in HA, analogous to the original bond between HCs and CS in intact I $\alpha$ I<sup>96</sup>. Because HA in the ECM has rather large contour length, a single chain can accommodate several HCs. The HA length in rheumatoid arthritis synovial fluid is rather heterogeneous, but HA chains of ~2 MDa were found to carry 3 to 5 HCs on average<sup>97</sup>.

Several requirements need to be fulfilled to allow for covalent HA•HC complexes to form. The first requirement is the presence of an enzyme which facilitates the transesterification reaction. TSG-6 has been identified to fulfill this function by formation of an intermediate 120 kDa complex with HCs of I $\alpha$ I<sup>98</sup>. The covalent TSG-6•HC complex has been detected in arthritis synovial fluid, in air pouch exudates and in the COC matrix<sup>99, 100</sup>. Rugg et al.<sup>98</sup> suggested the following mechanism of transfer: (1) TSG-6 displaces HCs from I $\alpha$ I, with formation of a TSG-6•HC complex, subsequently (2) HCs from the TSG-6•HC complex become transferred to HA and (3) TSG-6 is released and engaged into a new interaction with I $\alpha$ I, i.e. it is recycled (Fig. 1.6). Another important requirement for the formation of HA•HC complexes is the presence of divalent cations, particularly Mn<sup>2+</sup> or

$Mg^{2+}$ . Both TSG-6•HC complex formation and HCs transfer on HA are metal ion dependent processes<sup>98</sup>.

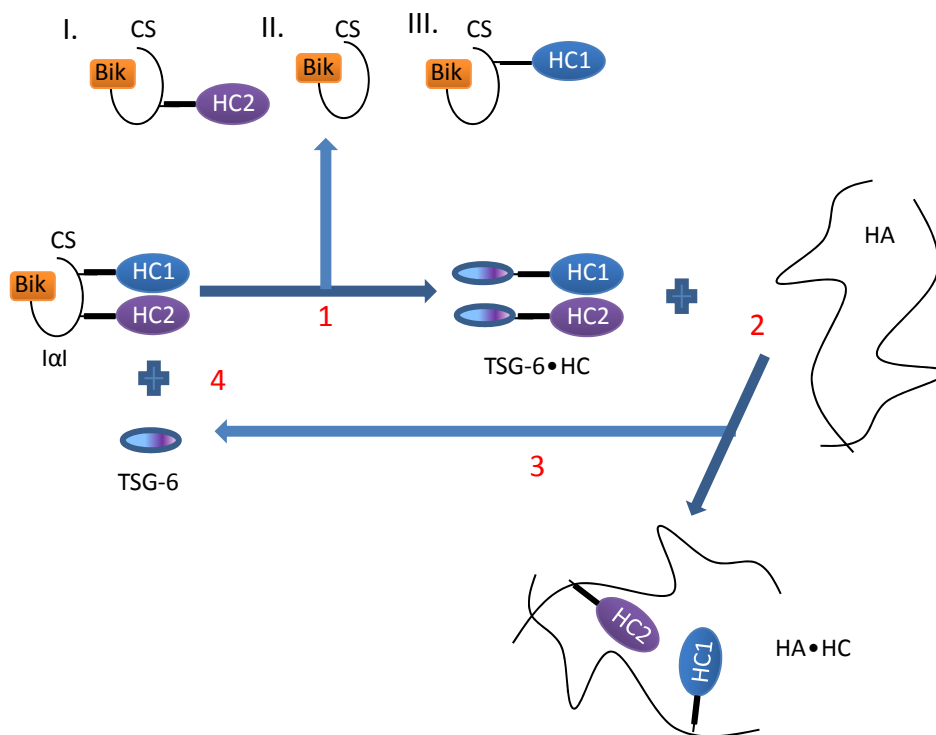


Fig. 1.6 **The mechanism of HA•HC complex formation.** IαI consists of three protein subunits (HC1, HC2 and bikunin) linked together by a CS chain. In a first transesterification reaction (1) TSG-6 reacts with IαI and cleaves HCs resulting in the formation of a covalent TSG-6•HC1 or TSG-6•HC2 complex with release of CS•bikunin, HC1•bikunin or HC2•bikunin products. In the second reaction (2) HCs are transferred from TSG-6 to HA. After transfer, TSG-6 is released (3) and can interact with new IαI (4), thus acting as an enzyme in the covalent modification of HA. Adapted from reference<sup>98</sup>.

Binding of IαI (or its subunits) to HA is of great importance for the normal expansion of the COC. In the absence of serum as an IαI source, cultured cumulus cells are not able to organize a stable matrix<sup>101</sup>. While bikunin can be detected in follicular fluid at the point of ovulation, indicating the presence of IαI<sup>102</sup>, COC matrices that were isolated after 24 h contained HCs but not bikunin. This correlates with the proposal that bikunin is released upon formation of HC•HA complexes and does not play any structural role in the HA matrix<sup>95, 99, 100</sup>. Bikunin knockout mice, even though they were producing free HCs, were not able to form HC•HA complexes or to assemble a functional matrix<sup>35</sup>. This highlights that the presence of the intact form of IαI is essential for the formation of HC•HA complexes. In particular, it is important to have the ester bond between CS and HCs which later can be transferred to HA.



Self-association between HCs was hypothesized<sup>82</sup> based on the findings that HA from synovial fluid of arthritis patients aggregates and gels at low pH<sup>97</sup>. However, for the organization of functional COC matrix, the presence of the three components HA, TSG-6 and IαI is still not sufficient<sup>37, 38</sup>.

### 1.4.4 PTX3

Long pentraxin 3 (PTX3) is an acute phase glycoprotein produced at sites of inflammation by both somatic and immune cells<sup>103-105</sup>. Similar to TSG-6, PTX3 expression can be induced by treatment with interleukin-1 and TNF<sup>105</sup>. PTX3 plays an important role in innate immunity, vascular biology and fertility<sup>44, 106-108</sup>. PTX3 forms octamers with a molecular weight of ~340 kDa in which the quaternary structure is held together by disulfide bonding. Each protomer of ~42.5 kDa contains N- and C-terminal globular domains<sup>105, 109</sup>. The N-terminal region (178 amino acids) has a unique structure that has not been found in any other protein. It contains three  $\alpha$ -helices which form a coiled-coil assembly<sup>110</sup>. The C-terminal region (203 amino acids) corresponds to a pentraxin-like domain, which is homologous to the short pentraxins C-reactive protein and serum amyloid P component<sup>105, 109, 111, 112</sup>.

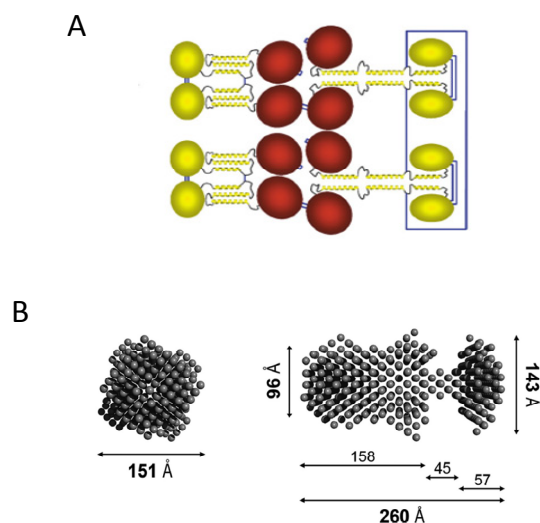


Fig. 1.7 **Quaternary structure of PTX3.** *A.* Arrangement of protomer subunits in a PTX3 octamer. Protomers of PTX3 assemble into a helix bundle, a long tube like structure around which both the N-terminal domains (yellow) and the C-terminal domains (red) are arranged. *B.* Model of PTX3 based on small angle X-ray scattering with the respective maximum dimensions. Taken from<sup>113</sup>.

Structural analysis of recombinant PTX3 revealed that it is an elongated, asymmetric molecule with two lobes of tetramers connected via a stalk part (Fig. 1.7)<sup>113</sup>. The structural

complexity of PTX3 can explain the existence of the broad spectrum of binding ligands among which are TSG-6<sup>37, 114</sup> and HCs of I $\alpha$ I<sup>38, 115</sup>.

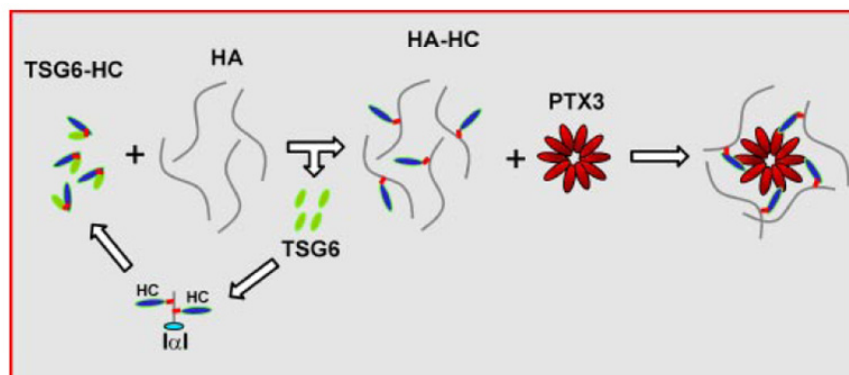


Fig. 1.8 **The structure of a hypothesized PTX3 cross-link in HA matrices.** In this model, it was proposed that HC transferred to HA by enzymatic activity of TSG-6 can bind different subunits of PTX3 and thereby cross-link HA chains in the COC matrix. Reproduced from<sup>38</sup> (at that time PTX3 was believed to form a decamer).

The oligomeric status of PTX3 is of particular importance for the stabilization of the COC matrix. In the COC matrix, PTX3 was found to be co-localized with HCs of I $\alpha$ I, suggesting that the HA•HC is the binding ligand for PTX3<sup>38</sup> (Fig. 1.8). It was demonstrated that Cys/Ser mutated forms of the N-terminal domains of PTX3 that form dimers were not able to rescue COC matrix assembly in PTX3<sup>-/-</sup> mice, while the native form which forms tetramers was active in restoring matrix expansion<sup>115</sup>. Although the N-PTX3 dimer binds both TSG-6 and I $\alpha$ I, the exact amount of binding site for TSG-6 and I $\alpha$ I on the PTX3 octamer remains unknown. The importance of PTX3 oligomerization for the stabilization of COC matrix suggests that PTX3 as a nodal molecule in the cross-linking of the HA matrix.

## 1.5 On the spatial and temporal regulation of COC matrix assembly

COC matrix formation is an illustrative case of spatio-temporal regulation of self-assembly. Because oocyte and cumulus cells are located in a special cavity, there is a spatial distribution of the crucial proteins: I $\alpha$ I is circulating in the blood and diffuses into the ovarian follicle only after initiation of ovulation, when the permeability barrier becomes leaky<sup>116, 117</sup>. In contrast, TSG-6 and PTX3 are produced by cumulus cells around the oocyte. The time required for I $\alpha$ I to diffuse towards oocyte remains unknown, but the first HA•HC complexes were detected only 6 h after the initiation of ovulation<sup>118, 119</sup>.

The expression of TSG-6, PTX3 and HA-synthases was found to have similar temporal profiles<sup>28, 37, 102, 120</sup>. TSG-6 was found to be homogeneously distributed throughout the

matrix from the periphery of the cumulus cells to the zona pellucida<sup>121</sup>. Cells in a close proximity to the zona pellucida produce more PTX3<sup>122</sup>. Thus, PTX3 distribution is spatially heterogeneous. A gradient of PTX3 was found to be preserved even 6h after initiation of ovulation. The gradient of PTX3 also correlates with another feature indicating a radial heterogeneity in the organization of the COC matrix: HA chains close to the oocyte are more packed than in the matrix periphery<sup>122</sup>. Such a spatio-temporal organization may be crucial for the regulation of HA/protein interaction and for the correct assembly of the COC matrix (Fig. 1.9).

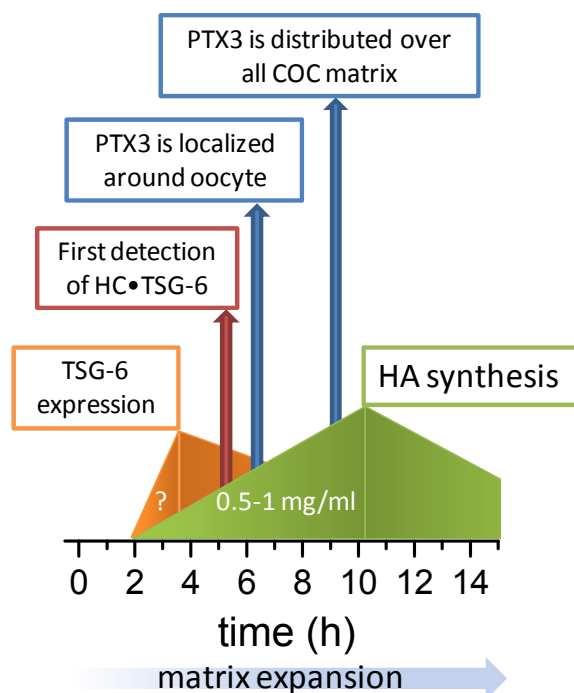


Fig. 1.9 **Spatio-temporal regulation of COC matrix formation.** Data from the literature<sup>28, 102, 118-120, 122</sup> are summarized in this sketch to highlight the events in the timeline of COC matrix expansion. The *x*-axis presents time after induction of ovulation. The orange and green figures display the evolution of expression of TSG-6 and HA-synthases. The HA concentration in COC matrix was measured by Salustri et al.<sup>28</sup> to be 0.5 to 1 mg/ml, while the concentrations of TSG-6, PTX3 and IaI (or its subunits) within the COC matrix remain unknown.

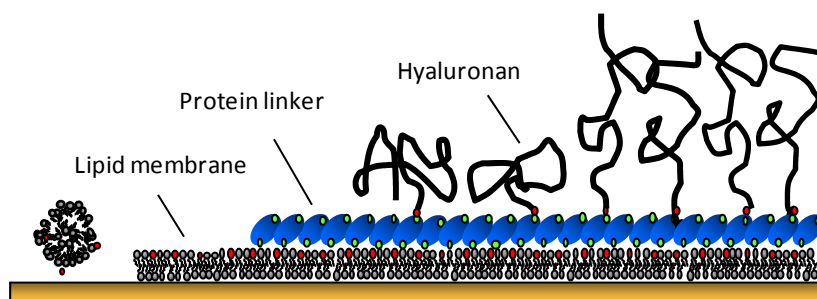
## 1.6 Model system to reconstruct HA matrix assembly

Biological surface science is an interdisciplinary field which provides powerful tools to study biological phenomena. Well-defined biomimetic systems can be created thanks to numerous methods of surface fabrication. Information about the structural properties of surface-assembled ultrastructures can be obtained on the micro- and nanoscale by highly

sensitive high resolution techniques <sup>123</sup>. A main scientific challenge for surface science is to reproduce the interactions, structures and kinetics of the biological systems in a similar way as it has been done by nature. To reconstitute the biological structure, the molecular building blocks should be brought on the surface in proper order and at the right concentrations. Surface biofunctionalization allows controlling the distribution, surface density and orientation of molecules of interest on the surface of choice.

Definitely, the main advantage of model systems is their simplicity. The reduced complexity compared to the native system allows for highly controlled measurements and to derive quantitative information on specific interactions. On the other hand, the translation of the properties of model systems to the functions of real biological systems remains a bottle neck. Direct comparison of the knowledge gathered in the model systems with the real biological system is essential to fill the gap between the reductionist approach of the models systems and the complexity of the real biological systems. However, starting from a simplified point of view on a specific question, the entire puzzle of the biological assembly can potentially be solved.

Surface-confined model systems are of particular relevance for the investigation of PCM structure. Currently, progress has been made on the understanding of the PCM functions on the cellular and molecular levels, but there is a limited understanding at the intermediate level – the supramolecular organization. It remains poorly understood, how different hyaladherins interact simultaneously with HA and how each protein contributes to the organization of cellular coats. A model system displaying surface-bound HA can shed light on these questions and serve as appropriate mimic of PCM, since HA in the PCM also remains attached to the cell surface and is able to self-organize with proteins into different structures.



1.10 The surface-based model system of HA matrix <sup>124</sup>. The construction of films of end-grafted HA was performed on a solid support (silica) which was first functionalized with a supported lipid bilayer, where some lipids carry biotin groups (red). A monolayer of the linker protein streptavidin (blue) was then immobilized on the surface, in order to attach the next layer – end-biotinylated HA chains. Reproduced from <sup>124</sup>.

The main strategy for PCM reconstitution is HA immobilization on the surface. Several approaches exist to modify surfaces with HA <sup>125</sup>. Among them are: passive adsorption on the surface <sup>126</sup>, formation of polyelectrolyte multilayers, where HA is mixed with chitosan or

poly-*L*-lysine<sup>127, 128</sup>, covalent coupling of HA to a variety of solid supports and functionalized layers, like glass<sup>58</sup>, polystyrene<sup>129</sup> and mixed supported lipid bilayers<sup>130</sup>. Coupling of HA was also performed via the HA-binding protein p32 which was grafted to NTA- functionalized supported lipid bilayers (SLB) via a histidine-tag<sup>131</sup>. More sophisticated immobilization of HA, with controlled density of anchorage points, was presented by Wolny et al, where HA was immobilized to the SLB via the extracellular part of the cell-surface HA-receptor CD44<sup>132</sup>. In all mentioned immobilization strategies, HA was immobilized to the surface via side-grafting, i.e. via numerous grafting points along one HA chain. This type of immobilization results in the formation of thin HA films<sup>131, 132</sup>, in which the exact conformation of the HA chains is not well known because the number and location of binding sites along the HA chains is difficult to control.

Recently, Richter et al.<sup>124</sup> presented a model system, where HA chains that were biotinylated at their reducing end were end-grafted to a biotin-functionalized SLB surface via attachment to a linker layer of streptavidin<sup>124</sup>. This approach provides tight control on the attachment of HA to the surface and tenability of the grafting density. In addition, the underlying surface is inert to the nonspecific binding of most proteins, i.e. it provides a passive background. Tunable and well-controlled HA attachment is a high advantage compared to the other immobilization approaches mentioned above. Films of end-grafted HA were intensively used throughout this thesis. Different modifications of the initial model system have been implemented in order to optimize the performance for the studies performed in this thesis. These developments are described in Chapter 2.

## 1.7 Characterization techniques

Even though pericellular coats play a crucial role in many fundamental biological processes, the understanding of their internal organization and functionality is still limited. Why is it so difficult to get a clear view on the architecture of the coats? The reason lays in HA itself. Its highly hydrated nature results in very low imaging contrast. In addition matrix is constantly reorganized and does not have a fixed structure. An overview of methodological approaches used to study the organization of PCM, together with the limitations of each method, is presented in Table 1.1.

<b>Methodology</b>	<b>Gained information</b>	<b>Limitations</b>
<i>Particle exclusion assay</i>	Thickness of HA matrix around cells <sup>2, 133</sup> .	Lack of detailed structural information.
<i>Fluorescent HA labeling</i>	Presence of HA gradient –higher concentration on the cellular membrane <sup>23, 134</sup> .	Lack of detailed structural information. High risk of matrix perturbation by labeling.
<i>High resolution electron microscopy</i>	Fixed PCM forms fibers <sup>47</sup> .	Upon drying matrix is destroyed. Fibers might be artifact structures.
<i>Optical tweezer</i>	Measure mechanical properties of the HA matrix and the mesh size <sup>11, 134</sup> .	The measurement are influenced by the cell status.

Table 1.1 An overview of the methodological approaches to study the structure of HA-rich matrices

The surface-based model of the HA matrix allows to use state of art surface-sensitive techniques for their characterization. Each method by itself is powerful and can provide quantitative information about a few parameters. However no single method alone gives a comprehensive picture of the architecture of the HA film, but the information combined from the different techniques is required. With a toolbox of methods, presented below, many parameters of HA model systems can be quantified, including film thickness, hydration, permeability, amount of incorporated molecules, their orientation and the kinetics of self-organization.

### 1.7.1 Quartz crystal microbalance with dissipation monitoring (QCM-D)

The QCM-D technique is widely used to study soft and solvated interfaces, because it enables both quantification of adsorbed mass and characterization of the viscoelastic properties of the adsorbed layer<sup>135</sup>. This technique has found many applications to study fundamental biological and biotechnological questions as: adsorption of the proteins to the solid supports<sup>136-138</sup>, proteins cross-linking<sup>139</sup>, DNA hybridization<sup>140, 141</sup>, or DNA-drug interactions<sup>142</sup>, as well as the adhesion and spreading of cells<sup>143, 144</sup>. The technique is also widely used for the characterization of biofunctionalized surfaces<sup>145, 146</sup>, for example, in biosensors<sup>147</sup>.

In the frame of this thesis, QCM-D was a main technique to characterize the assembly of HA-films. QCM-D afforded monitoring of adsorption processes in real time, providing detailed yet mostly qualitative information about the kinetics of layer formation, morphology and stability. Results acquired by this technique are mostly presented in Chapters 2- 3. The initial screening of interactions between HA-films and the proteins used in other chapters has also typically been performed by QCM-D, although these data are not explicitly presented.

#### Working principle

The working principle of QCM-D is based on the piezoelectric nature of quartz. The QCM-D sensor is made of a quartz crystal that is sandwiched between two electrodes and excited into a shear oscillatory movement by applying an AC electric field ( Fig.1.11).

Cutting off the external electric field results in a dampened oscillation of the crystal. By fitting an exponentially decaying oscillating curve to the data (Fig. 1.11D), the resonance frequency,  $f$ , of the crystal and the energy dissipation,  $D$ , are extracted. Simplistically, one could say that changes in resonance frequency,  $\Delta f$ , relate to the mass (including hydrodynamically coupled water) or alternatively to the thickness of the adsorbed film, whereas changes in dissipation,  $\Delta D$ , relate to the mechanical (typically viscoelastic) properties of the material bound to or situated in the vicinity of the surface.

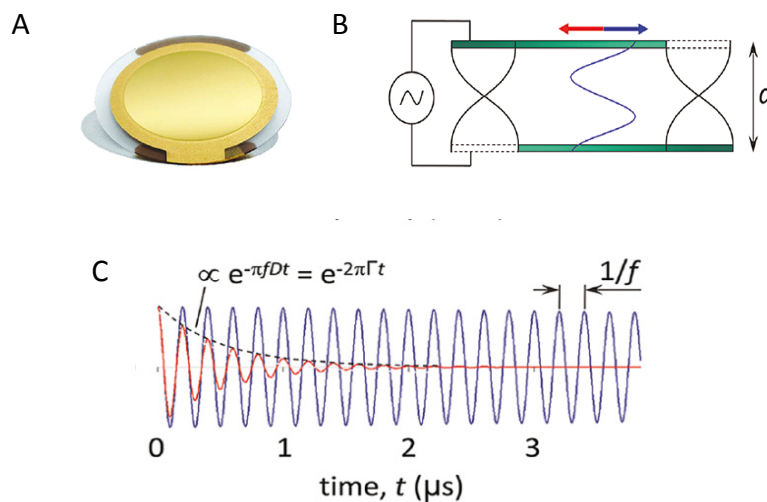


Fig. 1.11 **Schematic of QCM-D operation principle.** *A.* A picture of 4.95 MHz AT-quartz crystal sensor typically used for the measurements. *B.* Schematic side view of the crystal. Excitation of the sensor results in a cyclical deformation, where top and bottom surface move in an antiparallel fashion. The fundamental frequency (black wave at the edge of crystal) and third overtone (blue wave in the middle) are demonstrated. The lateral motion of the crystal is not drawn to scale, in reality it is in the nm range. *C.* QCM-D uses the so-called ring down method, where the driving voltage is transiently switched off and the decay of the oscillation is monitored. From the decay curve, the resonance frequency  $f$  and the energy dissipation  $D$  are extracted. Reproduced from <sup>135</sup>.

For biological applications, an important feature of QCM-D is that it operates in liquid. Work in liquid causes a response which reflects the bulk properties of the solution. The relation between the bulk properties – viscosity  $\eta_1$  and density  $\rho_1$  – of the liquid and the QCM-D response is following:

$$\Delta f_n = \frac{1}{\sqrt{\pi \rho_q v_q}} \sqrt{n f_0^3 \eta_1 \rho_1} \quad 1.1$$

$$\Delta D_n = \sqrt{\frac{f_0}{i}} \eta_1 \rho_1 \frac{1}{\sqrt{\pi \rho_q v_q}} \quad 1.2$$

where  $v_q$  is the speed of sound in quartz and  $\rho_q$  - density of the quartz crystal, respectively,  $f_0$  is fundamental frequency,  $i$  is the overtone number.

### Mass determination for thin and rigid, homogeneous film

The adsorbed mass per surface area of the sensor crystal can be determined through the direct relation between changes in frequency,  $\Delta f$ , and the areal mass density,  $m$ , also known as the Sauerbrey relation:



$$\Delta f_i = -\frac{i}{C}m = -\frac{i}{C}\rho d \quad 1.3$$

where  $i$  is the overtone number,  $C$  is the mass sensitivity constant,  $\rho$  is the density and  $d$  thickness of adsorbed film. The density of the film is often not accurately known, but fortunately, the density of most biomolecules (e.g.,  $\rho_{\text{lipids}} \approx 1.0 \text{ g/cm}^3$ ,  $\rho_{\text{proteins}} \approx 1.4 \text{ g/cm}^3$ ) or polymers is rather close to that of water ( $\rho_{\text{H}_2\text{O}} = 1.0 \text{ g/cm}^3$ ), i.e. the thickness can be determined with rather good accuracy by substituting  $\rho$  with the density of water. The mass sensitivity constant  $C$  depends solely on the material properties of the sensor crystal. For a sensor with a fundamental frequency of  $f_0 = 5 \text{ MHz}$ ,  $C = 18 \text{ ng/cm}^2/\text{Hz}$ .

The Sauerbrey equation is only valid for sufficiently rigid films. Sufficiently rigid films follow the oscillation of the sensor crystal with little dissipative losses. For homogeneous films, as a rule of thumb, the Sauerbrey equation can give a good approximation if the ratio  $\Delta D/(-\Delta f/i)$  is much smaller than  $0.4 \times 10^{-6} \text{ Hz}^{-1}$ .

### Homogeneous viscoelastic films

If the adsorbed film is sufficiently soft ( $\Delta D > 0$ ) and thick, the Sauerbrey equation typically underestimates the real mass of the layer. Here, QCM-D is also sensitive to viscoelastic properties of the layer. Soft and highly hydrated films can be treated as a homogeneous layer with a given thickness, density and effective viscoelastic properties. There are viscoelastic models<sup>148, 149</sup> available that relate the shifts in  $f$  and  $D$  to these film properties. By fitting the QCM data (at several overtones) with these models, quantitative information about the mechanical properties of the film can in some cases be obtained<sup>150</sup>. For the rather thick and very soft HA films used in this study, it was usually not possible to find a unique solution for thickness and viscoelastic properties. Therefore, this quantitative approach is not commonly used in this study.

### Morphological remodeling of the film

Nevertheless, QCM-D allowed monitoring of the remodeling of HA films upon protein incorporation (Chapter 3) as well as other surface functionalization and reorganization steps such as SLB formation<sup>151</sup> (Chapter 2). The detection of morphological changes by QCM-D is facilitated, because adsorbed material at the solid-liquid interface usually contains a large fraction of water. The QCM senses all material that is mechanically coupled to the sensor surface, i.e. both the adsorbent and the coupled water:

$$m_{\text{QCM-D}} = m_{\text{ads}} + m_{\text{solvent}} \quad 1.4$$

Moreover, morphological changes are usually also accompanied by changes in mechanical properties, to which QCM-D is also sensitive. Hence, QCM-D is exquisitely sensitive to structural variations of surface-confined films.

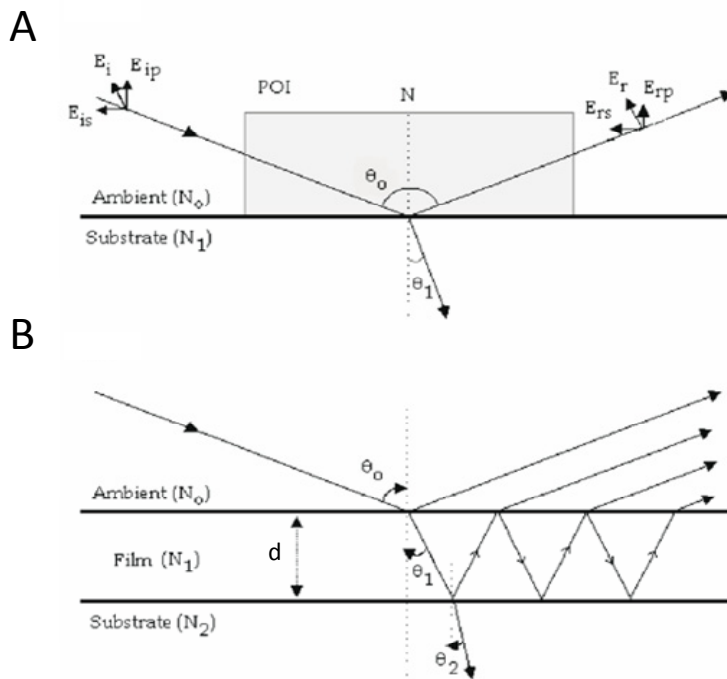
On the other hand, with the QCM-D alone, it is usually difficult to quantify the surface density of adsorbed biomolecules in absolute terms, because the contribution of adsorbent and solvent to the QCM-D response cannot be easily separated. Here, complementary techniques are useful<sup>152, 153</sup>. Optical mass-sensitive techniques that only rely on changes in the refractive index, such as ellipsometry, reflectometry, surface plasmon resonance (SPR) or optical waveguide light mode spectroscopy (OWLS) or their combination with QCM-D<sup>154</sup> can be used for the absolute quantification of surface densities and the hydration of adsorbed films.

## 1.7.2 Spectroscopic ellipsometry

Ellipsometry is an optical technique that can be used to measure the mass, thickness and refractive index of adsorbed layers. In the frame of this thesis, ellipsometry was used as the main method to quantify surface densities of end-grafted HA films and incorporated proteins, as well as binding affinities and kinetics of HA-protein interactions.

### **Working principle**

Ellipsometry is based on the measure of the changes in the polarization of elliptically polarized light upon reflection at the interface. Ellipsometry measures two parameters, the so-called ellipsometric angles  $\Psi$  and  $\Delta$ . In order to obtain information about the thickness, refractive index and adsorbed mass, the measured  $\Psi$  and  $\Delta$  values need to be fitted with an adequate model<sup>155</sup>.



1.12 **Reflection of polarized light.** *A.* From the bare substrate. *B.* From the surface with an adsorbed film. When light is reflected from the surface, it is partly adsorbed and partly reflected, and a change in the phase and in the amplitude of its components perpendicular ( $E_s$ ) and parallel ( $E_p$ ) to the plane of incidence occurs. The change depends on the substrate properties, and the properties of the adsorbed layer, and can be measured by ellipsometry.  $N_0$ ,  $N_1$ , and  $N_2$  are the complex refractive index of the ambient, the adsorbed film and the substrate, respectively.  $\theta_0$  is the angle of incidence,  $\theta_1$  the angle of transmission,  $\theta_2$  the angle of adsorption and  $d$  is the thickness of the adsorbed film<sup>156</sup>. Reproduced from<sup>156</sup>.

### Changes in the polarization of light upon reflection

Maxwell theory describes light as an electromagnetic wave, where its electric component is characterized by two vectors: parallel ( $E_p$ ) and perpendicular ( $E_s$ ) to the plain of incidence. Upon reflection from the surface, the phase and the amplitude of the reflected light are changed. The way how these parameters change depends on the optical properties of the adsorbed layer. For the reflection of lineary polarized light on a bare surface, the following equations are valid:

$$\Delta = \delta_{rp} - \delta_{rs} \quad \text{and} \quad \frac{|r_p|}{|r_s|} = \tan(\Psi) \quad 1.5$$

where  $\delta_{rp}$  and  $\delta_{rs}$  are phase shifts in parallel and perpendicular vectors,  $r_p$  and  $r_s$  are the complex Fresnel reflection coefficients for s- (perpendicular) and p- (parallel to the plane of incidence) polarized light. The relation between  $\Psi$  and  $\Delta$  can be expressed in the form of the ratio of the Fresnel coefficients:

$$\frac{r_p}{r_s} = \tan(\Psi) e^{(i\Delta)} = f(N_0, N_1, N_2, \lambda, d, \Theta_0) \quad 1.6$$

The ratio  $r_p/r_s$  depends on the wavelength ( $\lambda$ ) of the incident light, the thickness of the film ( $d$ ), the angle of incidence ( $\Theta_0$ ), and the complex refractive index of the ambient, the adsorbed film and the substrate ( $N_0$ ,  $N_1$ , and  $N_2$  respectively). Typically,  $N_0$ ,  $N_2$ ,  $\lambda$  and  $\Theta_0$  are known parameters. Moreover, we work with transparent films, i.e. the refractive index of the film is real ( $N_1 = n$ ). The measured  $\Psi$  and  $\Delta$  can then be directly related to the properties of the film ( $n$  and  $d$ ), i.e. the refractive index  $n$  and the film thickness  $d$  can be calculated through a fit to the experimental data. In particular for thick films, the thickness and refractive index of adsorbed layer can be fitted independently with good accuracy. In spectroscopic ellipsometry (SE),  $\Psi$  and  $\Delta$  are measured over a range of wavelengths, and  $n$  can then also be determined as a function of wavelength.

### Determination of adsorbed mass

Based on the measured  $n$  and  $d$ , the surface density ( $\Gamma$ ) can be calculated according to de Feijter<sup>157</sup>:

$$\Gamma = \frac{d(n_1 - n(\lambda)_2)}{dn/dc} \quad 1.7$$

where  $d$  is the average thickness of the film,  $n_1$  is the refractive index of the film,  $n_2$  the (real) refractive index of the solution, and  $dn/dc$  is the so-called refractive index increment of the molecules that constitute the film. Within this work  $dn/dc$  values of 0.169, 0.18 and 0.15 ml/g were used for SLBs<sup>153, 158</sup>, proteins<sup>157</sup> and HA<sup>66</sup>, respectively.

### 1.7.3 Colloidal probe reflection interference contrast microscopy (RICM).

The RICM technique was first introduced to study cell adhesion, in particular for the visualization of the area of the cell attached to the surface in the focal adhesion site<sup>159</sup>. In the 1980s, Sackmann *et al.* demonstrated that the distances between a planar transparent substrate and spherical objects, like a colloidal bead, hovering over the substrate can be well quantified by RICM<sup>160-162</sup>. In this thesis we applied colloidal probe RICM to determine the thickness of the HA films modified by proteins. Moreover, tracking the normal and lateral displacement of HA functionalized beads hovering above a planar HA film provided insight into interactions, such as cross-linking in and between HA assemblies.

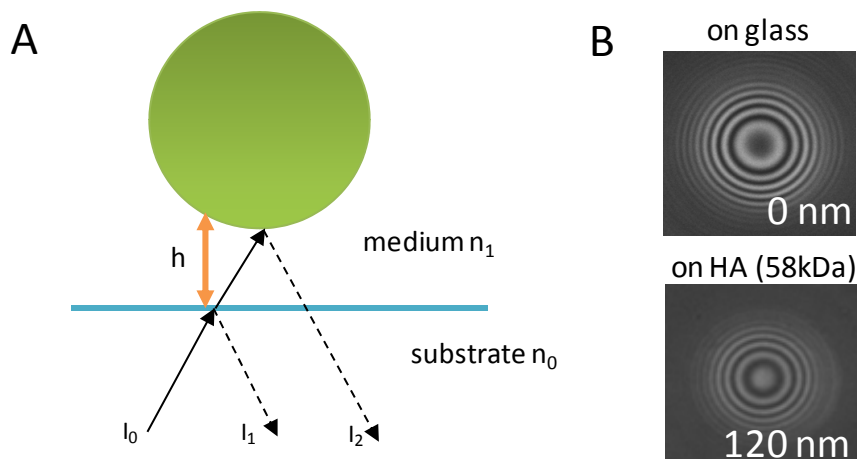


Fig. 1.13 **Schematic representation of the RICM working principle.** *A.* The incidence beam with intensity  $I_0$  is partly reflected from the substrate interface (bare glass or glass covered with a thin transparent gold layer) and partly from the surface of a colloidal bead. The reflected beams with intensities  $I_1$  and  $I_2$  interfere and give rise to an interference pattern. *B.* Interferographs of a colloidal bead sitting on the glass surface or on an HA-film of approximately 120 nm thickness, respectively.

### The working principle

RICM is based on the interference of light reflected from different interfaces (Fig. 1.13). The incidence light is first partly reflected at the glass/medium interface. The transmitted light is further partly reflected at the colloidal probe/medium interface. The reflected beams interfere and give rise to a pattern, so-called Newtonian rings of maximum ( $I_{max}$ ) and minimum intensity ( $I_{min}$ ). The relation between the intensity distribution and height of the bead above the surface is given by:

$$I(h(x,y)\lambda) = I_{min} + I_{max} + 2\sqrt{I_{min}I_{max}}\cos\left[\frac{4\pi n h(x,y)}{\lambda} + \delta\right] \quad 1.8$$

where  $h(x,y)$  is the distance at a given lateral position with coordinates  $x$  and  $y$ ,  $n_b$  is the refractive index of the medium,  $\delta$  is the phase shift of the reflected light and  $\lambda$  is the wavelength.

### Reconstruction of the film thickness

For a colloidal probe of spherical geometry, the interference pattern consists of circular fringes. The intensity in the center changes as the distance between probe and substrate varies (Fig.1.13B). The radius  $r_l$  from the center at which an extremum (maximum or minimum) occurs can be calculated with good accuracy from the radially averaged intensity profile. The probe-substrate distance can then be derived from the radial position of the selected extremum:

$$h(r_l) = \frac{\lambda l}{2n} - R + \sqrt{R^2 - r_l^2} \quad \text{for maximum} \quad 1.9$$

and

$$h(r_l) = \frac{\lambda(2l+1)}{4n} - R + \sqrt{R^2 - r_l^2} \quad \text{for minimum} \quad 1.10$$

where  $R$  is the radius of the bead, and  $l$  is the fringe order (which needs to be appropriately chosen).

### **Dual-/Triple –wavelength RICM**

From equations 1.9 and 1.10, it is obvious that the distance measured by RICM is not unambiguously defined. The RICM intensity response as a function of probe-substrate distance is periodic (Fig.1.14B), and several solutions are possible. Under the experimentally relevant conditions, the periodicity is on the order of a few 100 nm, but depends on the wavelength. Correlation of RICM data at multiple wavelength, therefore, enable unambiguous distance determination over a distance range that is much larger than the periodicity (Fig.1.14B). With triple-wavelength RICM the absolute height can be determined over a distance range of more than 1 micrometer with an accuracy of a few nanometers<sup>60, 124, 162, 163</sup>.

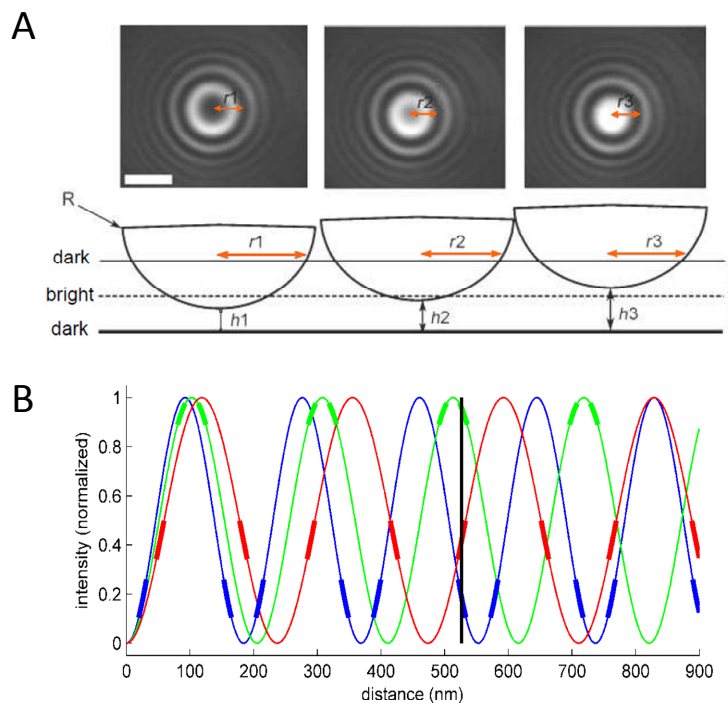


Fig.1.14 **Quantification of the film thickness from RICM images.** *A.* Height reconstruction. RICM fringes showing the fringe pattern of a colloidal bead of different heights from the surface ( $h_1$ ,  $h_2$  and  $h_3$ ). The intensity in the center changes as a function of the height, and the radius of first fringe changes accordingly. Figure reproduced from <sup>164</sup>. *B.* Normalized intensities in the center of the probe as a function of probe-substrate distance, for three selected wavelengths 490nm, 546 nm and 630 nm (triple-wavelength RICM, thin colored lines), reproduced from <sup>124</sup>. A given intensity, measured for a given wavelength (indicated by thick colored lines), would be consistent with various probe-substrate distances (“candidate distances”) at each individual wavelength. By comparing different wavelengths, many candidate distances can be discarded. A unique distance remains that is consistently found with all three wavelengths. This approach is used to reconstruct distances above 100 nm.

### Mean squared displacement

The thermal motion of the colloidal bead hovering above the HA film in the  $x$ ,  $y$  and  $z$  directions can be quantified by RICM with nm resolution. The thermally driven motion of the colloidal probe hence becomes detectable by microscopy. When unconstrained, the probe performs a random walk in  $x$  and  $y$  due to Brownian motion. The average of the squared distance which the bead has moved in, for example, the  $x$  direction within a given time step  $\tau$ , the so-called mean square displacement (MSD), is given by:

$$MSD = \langle x^2(\tau) \rangle = \langle |x(t) - x(t - \tau)|^2 \rangle$$

1.11

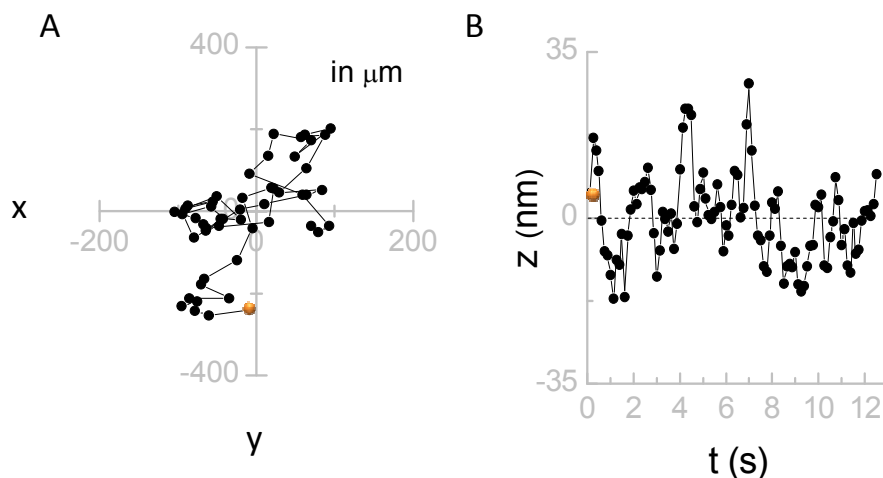


Fig. 1.15 **Colloidal bead undergoing thermal motion.** The track shows a typical random walk of HA-functionalized polystyrene beads of about  $25\ \mu\text{m}$  diameter hovering above a HA film. A. Movement in  $x$  and  $y$  directions. B. Movement in  $z$  direction. The length of the track corresponds to 100 data points recorded at 8 frames per second.

The MSD is a measure of the mobility of the probe, and can be correlated to diffusion. Sengupta et al. used the calculation of the MSD (in  $z$  direction) by colloidal probe RICM to characterize the viscoelastic properties of HA films<sup>131</sup>.





## 2 Design of well-defined HA films to study complex HA-protein interactions

---

Films of end-grafted HA permit to study hyaladherin incorporation in a quantitative manner by use of a toolbox of surface sensitive techniques. In 2007, Richter et al. established a first approach to prepared films of end-grafted HA, based on supported lipid bilayers (SLB). Here, we present a number of methodological developments with regard to the preparation and handling of films of end-grafted HA on solid supports, namely: (i) the preparation of HA films on self-assembled oligoethylene glycol (OEG) monolayers; (ii) the design of so-called oligo HA films, where each HA chain represents only one instead of many protein binding sites; (iii) the successful drying/rehydration of OEG-based HA films without significant loss of performance; and (iv) the demonstration that HA films are fully resistant to guanidine hydrochloride treatment. Developments (i), (ii) and (iv) found their application later in this thesis. Moreover, the establishment of a drying/rehydration protocol provides the potential for a wider use of HA films. In the field of HA, this may facilitate accumulation of the data directly on the supramolecular level and thus lead to a faster progress in the understanding how cellular coats are organized and function.

## 2.1 Introduction

Hyaluronan is a key molecular component of pericellular coats (PCCs), which play essential roles in many fundamental biological processes such as cell adhesion <sup>14, 15</sup>, proliferation <sup>16, 17</sup>, motility <sup>6, 18</sup>, embryogenesis <sup>13</sup> and fertility <sup>20</sup>. However, we still know too little about the mechanism of the coats' supramolecular assembly and their supramolecular architecture. The structural organization of HA in PCCs depends on its interaction with specific HA binding proteins. Over the last decade many of them have been identified and characterized on the molecular level. Although the interaction of some proteins and HA has been studied intensively, it remains largely elusive how the self-assembly of the coats is driven. Experimental data from studies on the molecular and cellular levels have provided some hypotheses about the organization of the coats. However, it remains difficult to directly assess coats assembly on the supramolecular level and to test these hypotheses.

Why it is so difficult to draw out a clear view on the architecture of the coats? The reason lays in HA itself. Its highly hydrated nature results in very low imaging contrast. The widely used particle exclusion assay for visualization of coats around living cells can provide some information about the extension of the coats but the internal structure remains obscure <sup>2, 133</sup>. To study self-assembly of such biologically complicated supramolecular structures it is reasonable to switch from the complexity of the cell to a well-defined model system with tunable properties.

Recently, Richter et al. presented a simple reconstruction of PCCs in the form of films of HA molecules grafted to a supported lipid bilayer (SLB) <sup>124</sup>. These HA films are well-defined in their molecular attachments (Fig. 2.1), the length of HA chains, and the HA surface density. Their controlled assembly makes such films highly useful for the reconstruction of different types of cellular coats by step-wise addition of relevant proteins.

The possibility to control the density of the HA films in our approach is a significant advantage compared to the numerous assays where uncontrolled immobilization of HA to the surface was used, like a simple passive adsorption to plastic labware, photoimmobilization on silanized glass <sup>125</sup>, side-grafting to concanavalin A modified plates by ECD chemistry <sup>165</sup> or ionic coupling in case of formation of polyelectrolyte multilayers <sup>127</sup>. The immobilization strategy can strongly influence the biological properties of HA and should be considered in protein and cell binding assays. In this regard, the end-grafted HA films represent the most controlled model system among the mentioned strategies for HA immobilization.

Here we present a number of methodological developments with regard to films of end-grafted HA on solid supports. Some of these developments became necessary on the course of this thesis work, to refine the experimental design and to be able to address specific

questions related to the mechanisms of self-assembly of the COC matrix. Others were triggered through discussions with colleagues and may find their use in future projects.

## 2.2 Experimental procedures

### **Buffer and hyaluronan preparations.**

A 'hepes' buffer (150 mM NaCl, 10 mM HEPES at pH 7.4, 3 mM  $\text{NaN}_3$ , 2 mM  $\text{CaCl}_2$ , 5 mM  $\text{MgCl}_2$ , in ultrapure water) was used throughout all measurements. Lyophilized HA, biotinylated at its reducing end and with well-defined molecular masses of  $58\pm 3$  kDa,  $1083\pm 53$  kDa or  $837\pm 54$  kDa (i.e. two different batches of Select-HA B1000) was purchased from Hyalose (Oklahoma City, OK, USA). For reconstitution, HA was taken up in ultrapure water at a stock concentration of 1 mg/ml, gently shaken over night, aliquoted, and stored at  $-20^\circ\text{C}$ . Films of end-grafted HA on biotin-functionalized protein-repellent surfaces were assembled as described in Chapters 3 and 4.

### **Substrate preparation.**

Silica-coated QCM-D sensors (QSX303 and QSX335; Biolin Scientific, Västra Frölunda, Sweden), silicon wafers with a native oxide layer of about 2 nm thickness (University Wafers, South Boston, MA, USA) and glass cover slips (#1,  $24\times 24$  mm<sup>2</sup>; Menzel-Gläser, Thermo Scientific, Germany) were used as substrates for QCM-D, ellipsometric and RICM measurements, respectively, on HA films on supported lipid bilayers (SLBs). Before each use, the QCM-D sensors and the silicon wafers were cleaned in an aqueous solution of 2% sodium dodecyl sulfate (15 min), rinsed with ultrapure water, blow-dried in  $\text{N}_2$  and treated with UV/ozone (Bioforce Nanoscience, Ames, IA, USA) for 30 min. Glass cover slips were immersed in freshly prepared piranya solution, i.e. a 1:1 (v/v) mixture of 50%  $\text{H}_2\text{O}_2$  and concentrated  $\text{H}_2\text{SO}_4$  for 1 h, rinsed with ultrapure water, blow-dried with  $\text{N}_2$  and stored under  $\text{N}_2$  atmosphere. Cleaned substrates were exposed to UV/ozone (30 min) prior to use. Gold-coated QCM-D sensors (QSX301; Biolin Scientific), silicon wafers with a 100 nm gold coating and glass cover slips with a 5 nm gold coating (both from G. Albert PVD Beschichtungen, Silz, Germany) were used as substrates to create HA films on oligoethylene glycol (OEG) monolayers for QCM-D, ellipsometric and RICM measurements, respectively. The surfaces were cleaned by exposure to UV/ozone (30 min) prior to use.

### **Preparation of vesicles, and formation of supported lipid bilayers (SLBs) on silica or glass surfaces.**

1,2-dioleoyl-*sn*-glycero-3-phosphocholine (DOPC) and 1,2-dioleoyl-*sn*-glycero-3-phosphoethanolamine-N-(cap biotinyl) (DOPE-CAP-biotin) were purchased from Avanti Polar Lipids (Alabaster, AL, USA). A mixture of DOPC/DOPE-CAP-biotin (9:1 molar ratio) was dissolved in chloroform, dried, re-suspended in Hepes buffer without added calcium and

homogenized as described earlier<sup>124</sup>. Small unilamellar vesicles (SUVs) were formed by sonication<sup>166</sup>. 50 µg/ml biotinylated SUVs were exposed to cleaned silica or glass surfaces for 30 min, leading to the formation of an SLB (Fig. 2.1).

### **OEG-functionalization of gold surfaces.**

Clean gold surfaces were functionalized by overnight incubation in a solution of 1 mol % of a biotinylated oligo(ethylene glycol) disulfide (SS-OEG-biotin;  $M_w = 1540$  Da) and 99 mol % of a plain OEG disulfide (SS-OEG; 771 Da) (both Polypure, Oslo, Norway) with a total thiol concentration of 0.5 mM in spectroscopy grade ethanol rinsed and sonicated (15 min) in ethanol, blow-dried in  $N_2$ , and stored in the dark under  $N_2$  atmosphere at 4°C for no longer than one week before being used. This procedure leads to the formation of a dense OEG monolayer with a few nanometres in thickness<sup>167, 168</sup>.

### **Design of oHA films.**

HA<sub>9</sub><sup>AA</sup> (i.e. an HA monosaccharide with D-glucuronic acid (A) at the nonreducing and reducing termini) functionalized with a biotin group at the reducing end (b-HA<sub>9</sub>) was prepared and provided by Michael Haller (Hyalose, Oklahoma, USA)<sup>168</sup>.

### **Quartz crystal microbalance with dissipation monitoring.**

Measurements were performed with a Q-Sense E4 system (Q-Sense AB), in flow mode<sup>166</sup> with flow speeds between 5 and 20 µl/min and at a working temperature of 23°C. To avoid depletion of sample by adsorption to tubings or chamber walls, these were passivated by exposure to a 1% (w/v) solution of bovine serum albumin (BSA; Sigma) in Hepes buffer (30 min), rinsed with ultrapure water and blow-dried with  $N_2$  prior to each measurement. QCM-D data were collected at six overtones ( $n = 3, 5, 7, 9, 11, 13$ , corresponding to resonance frequencies of ~15, 25, 35, 45, 55, 65 MHz). Changes in dissipation and normalized frequency,  $\Delta f = \Delta f_n/n$ , of the fifth overtone ( $n = 5$ ) are presented.

For homogeneous and sufficiently rigid layers, the film thickness can be estimated, to within an error of typically < 20%, from  $d = \Delta m/\rho = -C/\rho \times \Delta f$ , where  $\Delta m$ ,  $\rho = 1.0$  g/cm<sup>3</sup> and  $C = 18.06$  ng/cm<sup>2</sup>/Hz are, respectively, the adsorbed mass (including coupled water), the density of the bulk solution, and the mass sensitivity constant for a sensor with a fundamental resonance frequency of 4.95 MHz<sup>132</sup>. For soft films (exhibiting high dissipation) this equation is not valid. To determine the film thickness of HA films, colloidal probe reflection interference contrast microscopy was used instead.

### **In situ combination of QCM-D and ellipsometry.**

An *in situ* combination of QCM-D and ellipsometry was used to correlate the surface density of pHA (58 kDa) films with the corresponding QCM-D response. Adsorption and interfacial properties were monitored simultaneously, by QCM-D and ellipsometry, on the same surface and in liquid environment, as described elsewhere<sup>169</sup>. For SLB-based model systems, specialized silica-coated QCM-D sensors (Qsx335, Biolin Scientific) were

employed. The Q-Sense closed fluid cell for combined QCM-D/ellipsometry measurements (Biolin Scientific) was attached to a Q-Sense E1 module, providing access to QCM-D data, and mounted on the sample stage of a rotating compensator ellipsometer (M2000V; Woollam, Lincoln, USA), providing ellipsometric data. QCM-D data were collected as described above. Ellipsometric data,  $\Delta$  and  $\Psi$ , were acquired over a spectrum of wavelengths, ranging from  $\lambda = 380$  to 1000 nm, simultaneously at  $65^\circ$  angle of incidence with a time resolution of  $\sim 5$  s. The working temperature was set to  $23^\circ\text{C}$ . To extract the areal mass density, the ellipsometric data was fitted as described elsewhere<sup>166, 169</sup>.

### **Drying/rehydration of pHA films.**

A stabilizing trehalose solution was prepared prior to use by solubilizing trehalose (Sigma, Aldrich) in ultrapure water at a concentration of 1% (w/v). Functionalized surfaces, immersed in trehalose solution, were dried under a gentle stream of nitrogen gas ( $\sim 100$  Pa). HA digestion assays were performed with hyaluronidase (HA-ase) to test for the presence of HA. Lyophilized *streptomyces* hyaluronidase (Sigma, Aldrich) was dissolved in ultrapure water at a concentration of 1 unit/ml, aliquoted and stored at  $-20^\circ\text{C}$ . Thawed HA-ase was stored at  $4^\circ\text{C}$  and used within 1 day. The stock solution was diluted in working buffer immediately before use, and HA films were incubated at a concentration of 0.01 U/ml.

## 2.3 Results

### 2.3.1 Design of well-defined HA films

We designed surface-confined films that present HA of selected molecular weights in a well defined supramolecular assembly (Fig. 2.1). Design features that are common to all films are (i) the use of a protein-repellent surface coating and (ii) end-grafting of HA with the aid of a biotin group at its reducing end.

On the one hand, polymeric hyaluronan (pHA) with a molecular weight of 58 kDa (this chapter and chapter 3), 837 kDa (chapters 4-5) and 1083 kDa (chapters 2-5) was used. The grafting density can be controlled and a highly hydrated film of partly stretched and interpenetrating HA chains with up to several 100 nm in thickness, a so-called HA brush, is formed<sup>124</sup>. Moreover, a large number of proteins (10s to 100s, depending on the molecular weight) can potentially bind simultaneously along the contour length of a given pHA chain. On the other hand, short oligomeric HA chains, comprising only 9 monosaccharides (oligoHA), were used. These chains are distinct in that they can only bind a single protein (e.g. TSG-6) at a time.

#### **HA films on supported lipid bilayers.**

Two different surface passivation strategies were employed. The first strategy, based on a silica-supported lipid bilayer (SLB), had previously been established<sup>124</sup>. Formation of the SLB and subsequent assembly of the HA film was followed by QCM-D (Fig. 2.1).

The two-phase behavior in the frequency and dissipation shifts upon incubation of 50 µg/ml small unilamellar vesicles (SUVs; containing 10 mol-% of biotinylated lipids (DOPE-CAP-biotin) and 90 mol-% inert lipids (DOPC)) is characteristic for the process of SLB formation in which vesicles first adsorb intact and then rupture and spread. The final value of  $\Delta f = -24 \pm 1$  Hz corresponds to an acoustic thickness of  $4.3 \pm 0.2$  nm, in good agreement with the thickness of a solvated lipid bilayer. In addition,  $\Delta D < 0.3 \times 10^{-6}$  indicates that the SLB is of good quality, i.e. the number of residual intact vesicles is small<sup>170</sup>.

The presence of biotin-functionalized lipids in the SLB enables immobilization of streptavidin (SAv). The additional frequency shift of  $-26 \pm 1$  Hz together with a small dissipation shift of  $(0.5 \pm 0.1) \times 10^{-6}$  upon exposure of the SLB to 20 µg/ml SAv is characteristic for the formation of a thin and densely packed protein monolayer<sup>171</sup>. SAv is a tetrameric protein with 4 biotin binding sites. For steric reasons, at most two of the four binding sites can bind simultaneously to the SLB, while the two other sites remain available for the capture of biotinylated molecules from the solution phase.

Polymeric HA with average molecular mass of 58 kDa (pHA) and with a biotin functionality at its reducing end, incubated at 1 µg/ml, assembled into a thick, soft and highly hydrated film, as shown by the pronounced increase in dissipation of  $(9.5 \pm 0.5) \times 10^{-6}$ <sup>124</sup>

(Fig. 2.1A). The thickness of the pHA (58 kDa) film could not be extracted from the QCM-D response. Instead, it was measured to be  $120 \pm 10$  nm by colloidal probe RICM (Chapters 3-5). For comparison, the contour length of pHA is about 150 nm.

When biotinylated oligomeric HA<sub>9</sub> (oHA) was used instead at comparable concentration, the QCM-D response was much smaller (Fig. 2.1B). The contour length of the oHA chain is 4.5 nm, and a linker of about 3 nm in length<sup>172</sup> was placed between the biotin and the reducing end of the oHA to enhance the conformational freedom of the surface-bound oHA chains. The QCM-D response for oHA is in agreement with the formation of a monolayer of short linear chains. A mean anchor spacing of  $5.8 \pm 0.8$  nm between adjacent oHA chains on the surface was calculated by ellipsometry, confirming that such short chains can form a dense monolayer on the surface (Fig. 2.5E). Given the available space on the surface and the flexible linker, it is likely that the chains sample many orientations with respect to the surface normal.

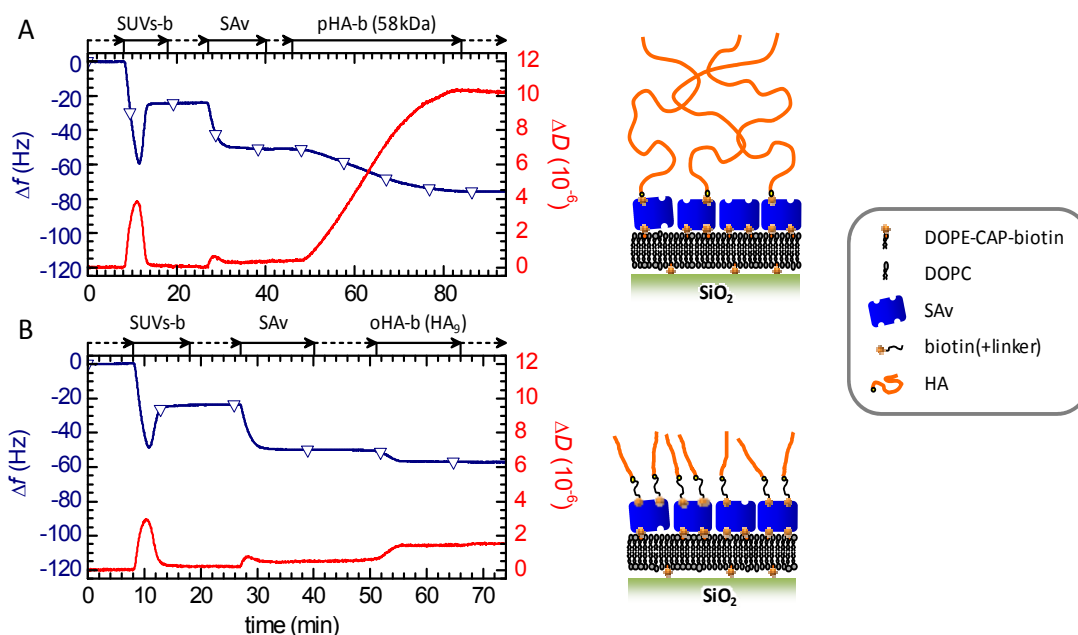


Fig. 2.1 **Build up of HA films on supported lipid bilayers (SLBs).** Film formation was monitored by QCM-D ( $\Delta f$  - blue curves with open triangles,  $\Delta D$  - red curves) for biotinylated pHA (58 kDa; A) and oHA (HA<sub>9</sub>; B), respectively. The start and duration of the incubation with different samples and buffer is indicated (solid arrows and dashed arrows, respectively). Schematic presentations of the design of the model systems are also shown (right). The size of the proteins, the thickness of the SLB, and the length of the oHA are drawn to scale; the thickness of the pHA films is compressed by about one order of magnitude.

### HA films on self-assembled monolayers.

The second passivation strategy is based on a self-assembled monolayer of oligoethylene glycols (OEGs). The mixed self-assembled monolayer was made from an ethanolic solution of 1 mol-% biotinylated OEG disulfide (b-OEG-SS) and 99 mol-% inert OEG disulfide



(OEG-SS). The chemical structure of these molecules is presented in Fig. 2.2A. As the substrate we used gold, well known for its strong interaction with thiols and disulfides. The OEG layer with a thickness of a few nanometers was formed *ex situ*, following a protocol established by Nilebäck et al.<sup>167</sup>. The surface morphology of the OEG layer, as observed by atomic force microscopy in air (Fig. 2.2C), was comparable to the underlying gold surface (Fig. 2.2B), indicating that a homogeneous monolayer was indeed formed.

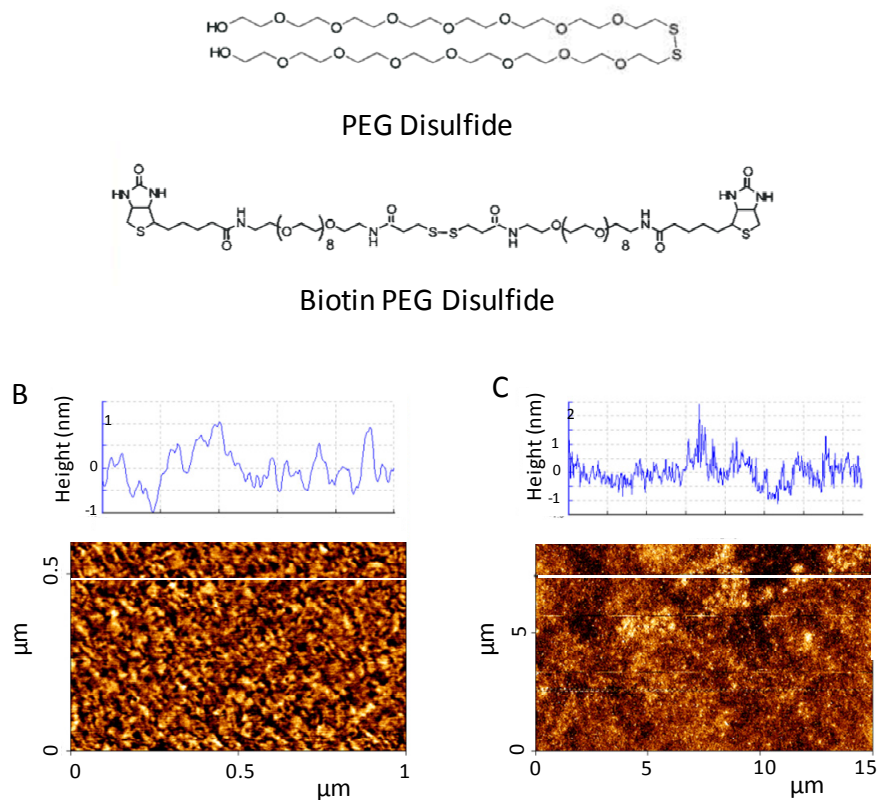


Fig. 2.2 (A) Chemical structure of OEG disulfides used for the preparation of mixed self-assembled monolayers. (B) Tapping mode atomic force microscopy image (phase) in air of a 5 nm thick gold film evaporated on a glass cover slip (*bottom*) with a representative topographic cross-section of the same surface (*top*). The roughness of the naked gold layer is on the order of 1 nm. (C) Tapping mode atomic force microscopy image (topography) for an OEG-coated gold layer (*bottom*) with a representative cross-section (*top*). The roughness and surface morphology are not significantly affected by the OEG film, suggesting that the OEG film is homogeneous. Images provided by S. Attili (CIC biomaGUNE).

Subsequent assembly of the HA film was followed by QCM-D (Fig. 2.3). Frequency shifts of  $\Delta f = -20 \pm 2$  Hz and small dissipation shifts of  $\Delta D = (0.3 \pm 0.15) \times 10^{-6}$  upon exposure of the OEG film to SAV indicate formation of a protein monolayer that is less dense than the SAV monolayer on SLBs (Fig. 2.1).

Binding curves for pHA (58 kDa; Fig. 2.3A) and oHA (Fig. 2.3B) were similar to those obtained on SLBs. The final frequency shift for oHA on the OEG layer ( $-7 \pm 1$  Hz), however, was slightly smaller than on the SLB ( $-8 \pm 2$  Hz; Fig. 2.1B), indicating somewhat lower coverage. By ellipsometry, we found typical oHA surface coverages of  $23 \pm 5$  ng/cm<sup>2</sup> on SLBs and around  $18 \pm 5$  ng/cm<sup>2</sup> on OEG layers, corresponding to a mean spacing between adjacent anchor points of  $5.1 \pm 0.6$  nm and  $5.8 \pm 0.8$  nm, respectively. By ellipsometry, we found also that 1.6 to 2.0 biotin-binding sites per SAv molecule were on average occupied with oHA (data not shown).

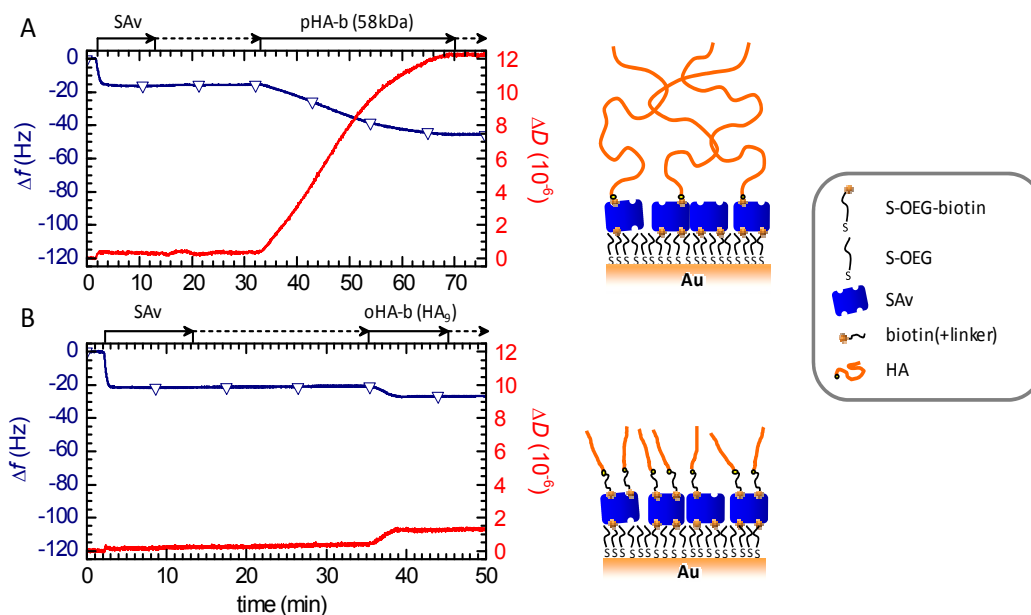


Fig. 2.3 **Build up of HA films on OEG layers.** Film formation was monitored by QCM-D ( $\Delta f$  - blue curves with open triangles,  $\Delta D$  - red curves) for biotinylated pHA (58 kDa; A) and oHA (HA<sub>9</sub>; B), respectively. The biotin-OEG layer was formed *ex situ* prior to the QCM-D measurement. The start and duration of the incubation with different samples and buffer is indicated (solid arrows and dashed arrows, respectively). Schematic presentations of the design of the model systems are also shown (right).

To test if the nature of the passivation layer affects the HA film morphology, parametric plots of  $\Delta D$  vs.  $\Delta f$  were generated for the QCM-D data that correspond to the formation of pHA (58 kDa; Fig. 2.4A) and oHA (Fig. 2.4B) films in Fig. 2.1 and Fig. 2.3. Such a plot provides insight into the evolution of the viscoelastic properties as the HA film grows. In this presentation, the curves for the respective HA films on the SLB and on the OEG layer were very similar, indicating that the morphology of the HA film was not affected by the choice of the immobilization platform.

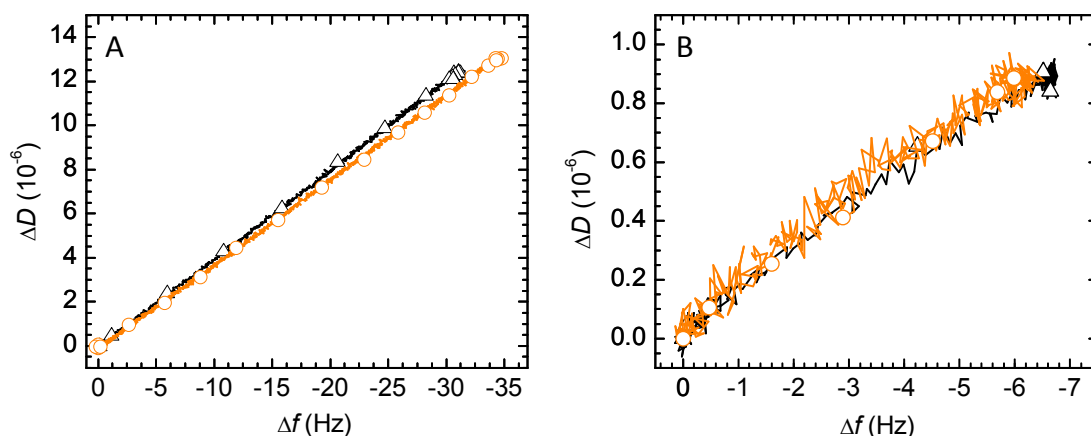


Fig. 2.4 Parametric plot of  $\Delta D$  vs.  $\Delta f$  for the QCM-D data that corresponds to the formation of pHA (58 kDa; A) and oHA (HA<sub>9</sub>; B) films in Fig. 2.1 and Fig. 2.3. The curves for the respective HA films on the SLB (black lines with open triangles) and on the OEG layer (orange lines with open circles) are very similar, indicating that the film morphology is the same on both immobilization platforms.

### 2.3.2 Surface density of pHA films – correlation between QCM-D and ellipsometry responses

The QCM-D frequency shift provides a relative measure for the surface density of HA in our model films, but not an absolute quantification. For future QCM-D studies, it would be useful to be able to control the absolute surface density based on the frequency response. To this end, we performed a measurement with an *in situ* combination of QCM-D and ellipsometry on the same surface (Fig. 2.5). In the combined measurement, the surface density of adsorbed HA chains, quantified through ellipsometry (Fig. 2.5A), can be correlated with the QCM-D frequency shift (Fig. 2.5B) response in a time (or coverage) resolved manner. With the aid of the resulting calibration curve (Fig. 2.5C), the surface density of pHA can be quantified from QCM-D frequency shifts for arbitrary coverages. It is notable that the dependence is linear over the entire range of surface densities investigated, with a slope of  $-0.46 \text{ Hz}/(\text{ng}/\text{cm}^2)$ .

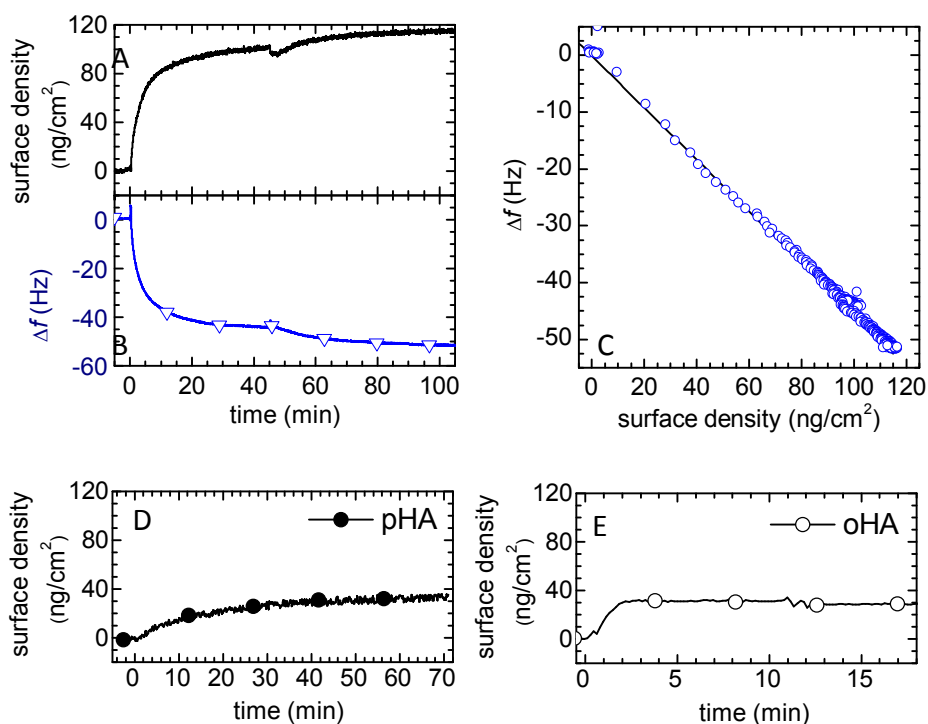
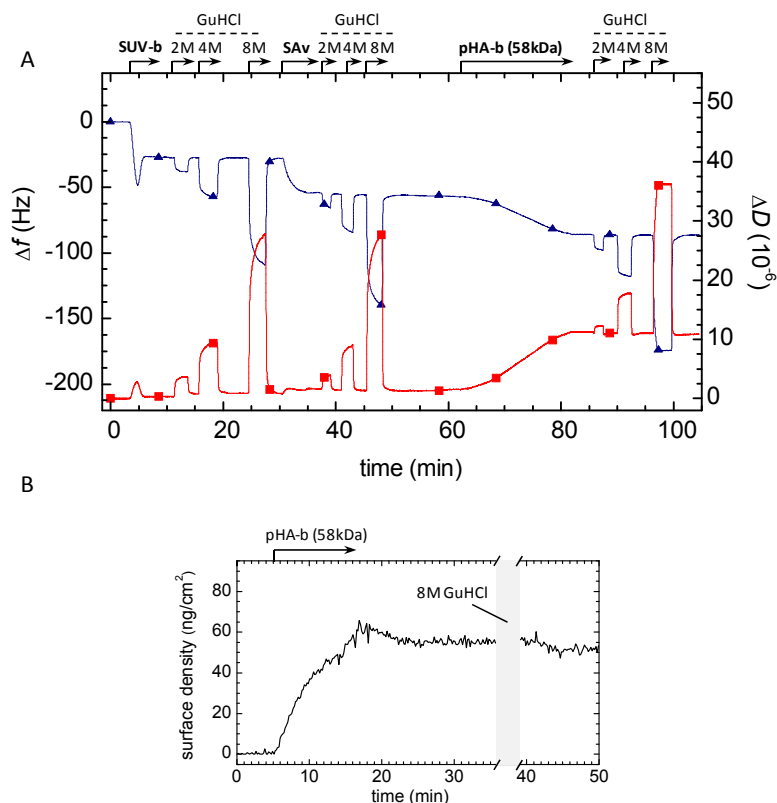


Fig. 2.5 **Correlation between the hyaluronan surface mass density and the QCM-D frequency shifts upon binding of 58 kDa pHA.** Data from a simultaneous measurement by QCM-D and ellipsometry on the same surface. (A) Surface mass densities upon incubation of pHA as determined by ellipsometry. (B) Corresponding QCM-D frequency shifts. At 0 min, pHA was injected at a concentration of 7.5  $\mu\text{g/ml}$ ; a second injection of equal concentration after 45 min led to renewed HA binding, indicating some depletion of HA in the solution phase. (C) Parametric plot of the frequency shifts vs. surface density for the data from (A) and (B). The data were acquired on SAV-coated SLBs. (D) Surface mass densities upon incubation of 25  $\mu\text{g/ml}$  1083 kDa pHA as determined by ellipsometry. The adsorption rate is very slow beyond one hour of incubation, consistent with the kinetic limitations that are associated with the densification of a polyelectrolyte brush in the ‘grafting-to’ method<sup>173</sup>. A maximal adsorbed amount of 35  $\text{ng/cm}^2$  is obtained after one hour of incubation, which is similar to, yet slightly below, a previously reported value<sup>173</sup>. The RICM measurements in this study were performed with 1083 kDa pHA, under similar incubation conditions as shown here. (E) Surface mass density of 29  $\text{ng/cm}^2$  of oHA film confirms that oHA can form a dense film. Absence of size constraints resulted in faster adsorption kinetics compare to HA 1083 kDa.

### 2.3.3 Resistance of HA films against the dissociating agent GuHCl

HA is known to be modified with HCs of I $\alpha$ I in covalent manner, with formation a so-called serum-derived hyaluronan associated protein (SHAP) complex<sup>174</sup>. On the other hand, proteins like TSG-6 bind non-covalently to HA. It would be useful to be able to differentiate between covalent and non-covalent interaction in our QCM-D or ellipsometric binding

assays. A dissociating agent such as guanidine hydrochloride (GuHCl) can be particularly useful here. By inducing the unfolding of proteins, it can trigger the selective release of non-covalently (i.e. biospecifically) bound material. Since we exploit the biospecific interaction between SAV and biotin to construct our model films, it was important to test if the films remain stable to treatment with GuHCl.



**Fig. 2.6 HA films are stable against treatment with the dissociating agent GuHCl.** (A) QCM-D response,  $\Delta f$  (blue curves with open triangles) and  $\Delta D$  (red curves), for the formation of a pHA (58 kDa) film on a SAV-coated SLB. After each incubation step, the biofunctionalized surface was sequentially exposed to 2, 4 and 8 M GuHCl. The start and duration of the incubation with different samples is indicated (solid arrows). Both  $\Delta f$  and  $\Delta D$  recovered their original value after GuHCl treatment, indicating that even 8 M GuHCl does not irreversibly alter the morphology of the surface-bound films. (B) Areal mass density, determined from ellipsometric data, for the incubation of pHA (58 kDa) on a SAV-covered OEG layer and subsequent exposure of 8 M GuHCl (incubation period shaded in grey was not monitored). The areal mass density is identical before and after GuHCl treatment, indicating that the anchorage of HA to this surface is also resistant to 8 M GuHCl.

We found that the SLB layer was completely stable to the exposure to increasing concentrations of 2, 4 and 8 M GuHCl (Fig. 2.6A): the responses in both frequency and dissipation before and after addition of GuHCl were identical. Changes in  $\Delta f$  and  $\Delta D$  during exposure to GuHCl are likely not to reflect any changes on the surface. Instead, they result predominantly from a change in the viscosity and/or density of the surrounding solution

owing to the presence of GuHCl. The same was observed after subsequent deposition of a SAV monolayer and after formation of the HA film. An *in situ* ellipsometry measurement on a pHA (58 kDa) film on the SAV-OEG platform did not reveal any measurable release of material upon exposure to 8 M GuHCl (Fig. 2.6B), confirming that this immobilization method does also produce stable films. Films made from pHA of a different molecular weight (1083 kDa) or from oHA at were also tested at various grafting densities, and showed full resistance to treatment with GuHCl (data not shown). The stability against GuHCl treatment is remarkable, considering that most proteins are completely denatured at 8 M GuHCl. Clearly, streptavidin (at least in its biotin-bound state) has an exceptional resistance against dissociating agents.

### 2.3.4 Drying and rehydration of OEG-based HA films

To broaden the range of applications for our HA films, it would be useful if these could be prepared and dried, then stored and/or shipped, and subsequently re-hydrated for use. HA films are osmotic because of the polyelectrolyte nature of the HA polymer. Thus, we first hypothesized that HA might be potent to provide additional hydration to the SAV layer. To test this, HA films, immersed in either standard buffer solution or in ultrapure water, were blow-dried under a stream of nitrogen gas, and then re-immersed in buffer solution. Unfortunately, we found that a substantial part of the biomolecular film was lost after a drying and re-hydration cycle (data not shown).

Trehalose, a natural disaccharide ( $\alpha$ -D-glucopyranosyl-(1 $\rightarrow$ 1)- $\alpha$ -D-glucopyranoside) is widely used for freeze-drying and rehydration of biological substances. The mechanism of action is stabilization of the folded state and thus activity of many proteins. It is also used to stabilize lipid membranes and liposomes<sup>175</sup>. Thus, we tested if trehalose can render the HA films stable to drying and rehydration.

First, the stability of the SAV monolayer was tested. Addition of a solution of 1% trehalose in ultrapure water to a SAV monolayer (Fig. 2.7A) led to minor changes in frequency and dissipation. Most likely, this response is predominantly or entirely due to differences in the viscosity and/or density of the buffer *vs.* trehalose solution. Importantly, trehalose did not permanently affect the SAV layer: the QCM-D responses before and after trehalose exposure were identical. After a second trehalose injection the sensor was dismantled from the QCM-D chamber and dried under a gentle N<sub>2</sub> stream.

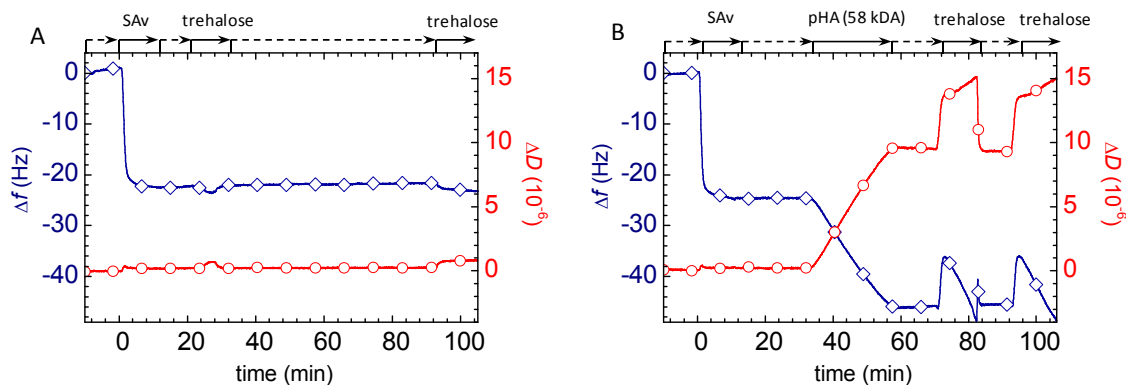
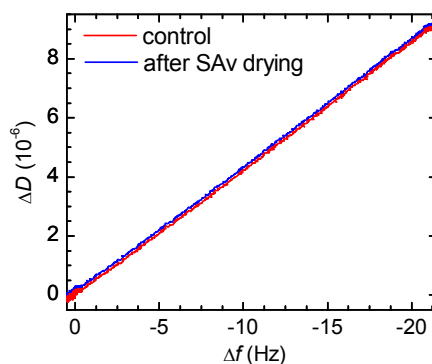


Fig. 2.7 **Preparation of a SAw-coated OEG film and a HA film for drying.** (A) A monolayer of SAw with typical frequency and dissipation shifts ( $\Delta f = -24 \pm 2.5$  Hz and  $\Delta D = 0.3 \pm 0.3 \times 10^{-6}$ ) was formed on an OEG-b functionalized gold-coated QCM-D sensor. Exposure to a 1% trehalose solution for 10 min did not permanently affect the film. Small shifts in dissipation and frequency during trehalose incubation are likely to be the result of differences in the viscosity and/or density of the trehalose solution compared to buffer. (B) SAw and subsequently pHA-b (58 kDa) was immobilized on an OEG-b functionalized gold-coated QCM-D sensor. HA binding was interrupted at  $\Delta f = -21$  Hz, corresponding to a surface density of  $40 \text{ ng/cm}^2$  (see Fig. 5B), and  $\Delta D = 9.2 \times 10^{-6}$ . Exposure to trehalose solution resulted in a complex response that indicates morphological changes in the HA film. Elution of trehalose by rinsing in buffer revealed no permanent effect of trehalose on the properties of the HA film: both frequency and dissipation recovered the values prior to trehalose treatment.

After drying and re-hydration, the HA-binding activity of the SAw layer remained unchanged. In particular it can be seen in the plot of dissipation vs. frequency for the HA binding process (Fig. 2.8). Thus drying and re-hydration cycles did not affect SAw properties, and the morphology of the subsequently formed HA film is not perturbed.

HA (58 kDa) films with a surface density of  $40 \text{ ng/cm}^2$  were subjected to a similar test. Interestingly, the presence of trehalose had a pronounced effect on the HA film (Fig. 2.7B). The QCM-D response revealed a two-phase behavior. Exposure to trehalose solution resulted initially in a rapid and pronounced simultaneous increase in frequency and dissipation. In the second phase, the frequency decreased slowly and the dissipation increased slowly, and equilibrium was not reached after 10 min. These responses indicate that the morphology of the HA film changes upon interaction with trehalose. However, the effect of trehalose on the HA film was not permanent: when replacing trehalose with buffer solution, the QCM-D response recovered to the values prior to trehalose incubation. After a second trehalose injection, the sensor was unmounted and dried as described for the SAw layer.



**Fig. 2.8 Rehydration of the OEG-bound SAV layer does not affect its b-HA binding properties.** The formation of pHA films (HA 58 kDa) on SAV monolayers that were either freshly prepared (*red line*) or dried in the presence of trehalose, stored dry for 30 min at room temperature, and then rehydrated (*blue line*) was followed by QCM-D. Plots of dissipation vs. frequency are identical, indicating that the morphology of the HA film is not affected by drying and rehydration of the OEG-bound SAV-layer.

It was important to check if all HA is retained upon drying and rehydration, and that the initial morphology of the HA film is recovered after re-hydration. To this end, we compared the QCM-D responses before and after digestion of HA films by *streptomyces hyaluronidase*, a HA-specific lyase (HA-ase) that is active at physiological ionic strength and pH 7.4. This method proved to be more accurate than a direct comparison of the QCM-D response before and after drying, because controlled drying requires unmounting of the HA-coated QCM-D sensor from the QCM-D chamber and re-mounting can significantly affect the baseline.

Fig. 2.9 shows the results of such an assay. To facilitate comparison, frequency and dissipation were offset by the shifts that were measured upon HA film formation (see Fig. 2.7B). Addition of HA-ase induced an increase in frequency accompanied with a decrease in dissipation, as expected for the desorption of HA as a result of degradation. Comparison revealed that the QCM-D response upon HA-ase treatment corresponds to approximately 90% of the response upon HA film formation.

Surface constraints might influence the degradation efficiency of HA-ase in our HA films. To test this, we performed a control measurement, where an HA film was digested immediately after formation, i.e. without intermediate drying (Fig. 2.9B). In this case, both frequency and dissipation recovered values that, within experimental error, were indistinguishable from the baseline. This indicates that the HA film can be close-to-completely digested and that HA-ase does not bind non-specifically to the SAV-coated OEG film.



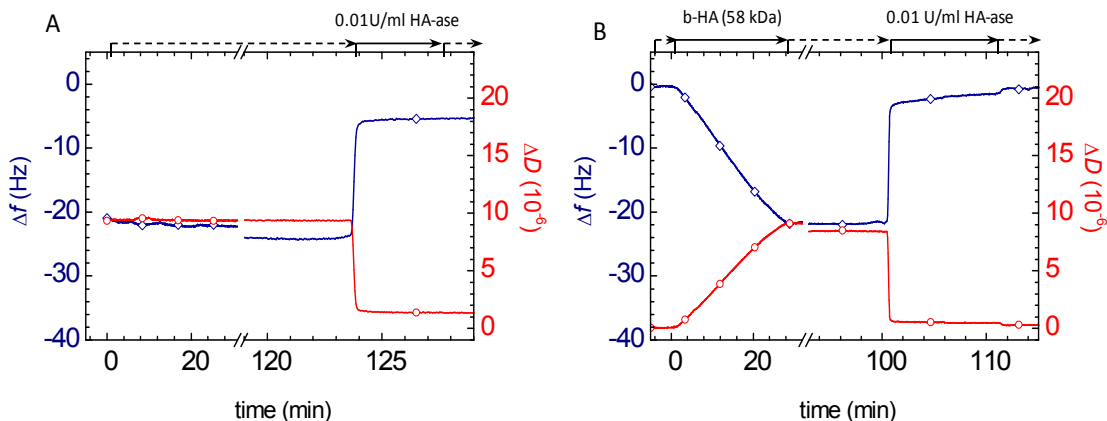


**Fig. 2.9 Quantification of the HA film after surface rehydration with an HA-ase degradation assay.** (A) The pHA (58 kDa) film shown in Fig. 2.7B was dried *ex situ*, stored dry for 30 min at room temperature, installed in the QCM-D chamber, rehydrated in buffer. The QCM-D response was left to stabilize for two hours, and frequency and dissipation were offset by the shifts that were measured upon HA film formation ( $\Delta f = -21$  Hz and  $\Delta D = 9.2 \times 10^{-6}$ , Fig. 2.7B). Addition of 10 U/ml HA-ase induced an increase in  $\Delta f$ , by  $19 \pm 0.5$  Hz, and a decrease in  $\Delta D$ , by  $-9.2 \times 10^{-6}$ , as expected for enzymatic degradation of approximately 90% HA. (B) A pHA (58 kDa) film of similar surface density was formed and directly incubated with HA-ase. After HA-ase treatment,  $\Delta f$  and  $\Delta D$  recover values close to the baseline (97%), indicating close-to-complete digestion.

Based on the results in Fig. 2.9, we can conclude that drying and rehydration induces a 10% loss in the initial QCM-D response for the HA film. Because of the linear dependence of the frequency shift on HA surface density (Fig. 2.5) we can translate this value into a HA loss of 10%, or  $4 \text{ ng/cm}^2$ . The enzymatic HA degradation assay confirmed that HA films on SAV-coated OEG layers can be dried in the presence of 1% trehalose, kept dry for at least 30 min, and then rehydrated with only minor losses in coverage and minor changes in film morphology. Further tests are required to establish if the films do also resist long-term storage in a dry environment.

## 2.4 Discussion

The end-grafted HA films can be used as a universal tool to study directly the relation between the supramolecular organization and dynamics of the PCC-like assemblies and their biological functions. This well-defined albeit simple platform provides a level of control which cannot be accessed by many other approaches, mentioned in the introduction (Chapter 1.7). The properties of the model system can be tuned to study even complex interactions of HA with one or several different proteins. Building on previously reported work of the group, this chapter highlights several further developments, namely:

- (i) the design of oligo HA films as a complement to polymeric HA films;
- (ii) the design of HA films on OEG monolayers as a complement to SLB-based HA films;
- (iii) demonstration that the HA films are resistant to the chaotropic agent GuHCl, even at very high concentration;
- (iv) development of a protocol for drying/rehydration of OEG-based HA films without substantial decrease in performance.

### 2.4.1 OEG- versus SLB-based model system.

Reconstitution of the COC matrix required the main modification of the established before model – replacement of SLB layer by OEG layer. The HA films formed in OEG-based model has similar morphology (Fig. 2.3A-B), but OEG/SAv layer showed better passivation properties for nonspecific binding of some proteins (see Chapter 3-5). Another advantage of the complementary model system is that by switching between OEG and SLB platforms, the anchor points can potentially be kept either laterally mobile or frozen.

### 2.4.2 Applications of oligo HA films.

All presented model system have in common that HA chains are end-grafted. The resulting films can be tuned to exhibit different densities and thicknesses, and the HA length can be chosen as desired<sup>124</sup>. Some hyaladherins have been suggested to bind cooperatively to HA, in such a way that the interaction between adjacent proteins along the HA chain facilitates binding<sup>22</sup>. This cooperative effect is expected to disappear, if the HA chain becomes so short that it can only accommodate a single protein at a time. Therefore, films of oligomeric and polymeric HA, respectively, are complementary to study binding mechanisms, as exemplified for TSG-6 in Chapter 3.

It should be noted that while the HA-binding site of TSG-6 corresponds to a hexasaccharide, other hyaladherins, including cartilage Link<sub>protein</sub>, the G1 domain of

aggrecan or versican have a footprint of HA<sub>10</sub><sup>65</sup>. Hence, to study the influence of cooperativity on the interaction of these proteins with HA, a longer oligo HA would be required (e.g. HA<sub>14</sub>). In addition, the packing density of oHA chains in our films was very high. In order to study interaction of high molecular weight proteins such as aggrecan or versican, lower surface concentrations might be required to prevent undesired effects of steric hindrance. These issues, however, are beyond the scope of this thesis.

### 2.4.3 Stability of HA films against GuHCl.

Another finding that proved to be particularly useful for this project was the resistance of HA films to harsh treatment with GuHCl (Fig. 2.6A-B), demonstrated for both SLB- and OEG-based films. The affinity of interaction between streptavidin and biotin is very high ( $K_D = 10^{-15}$  M). It was shown that biotin stabilizes the ternary structure of SAV and prevents its dissociation in 6.4 M GuHCl<sup>176</sup>. One of the proposed mechanisms of stabilization is prevention of penetration of GuHCl into the binding pocket by the bound biotin. We note that even plain SAV monolayers were completely resistant to 8 M GuHCl treatment<sup>176</sup>. This is remarkable if one considers that two of the four biotin binding sites per SAV in the monolayer are not occupied by the ligand in this case. We suggest that there is an allosteric stabilization of neighboring biotin-free subunits by the biotin-bound subunits.

### 2.4.4 Drying/rehydration of OEG-based pHA films.

Considering other possible applications of HA films, we established a protocol for its drying/rehydration without significant performance losses. Usage of 1% trehalose solution drastically increased the stability of the SAV and HA layers against drying and/or rehydration. Among all stabilizing agents, trehalose is known to be the most efficient to stabilize protein structure<sup>177</sup>. An increased surface tension of solution in the presence of trehalose leads to preferential hydration of the protein and supports its folded structure. Important to note, that drying/rehydration was tested only for the OEG-based model, though the use of trehalose solution for the stabilization of liposomes is well established<sup>175</sup>. It was also shown that trehalose can stabilize supported lipid bilayers<sup>178</sup>. Potentially SLB-based system model system can be reconstructed after drying in trehalose solution, though this requires further tests.

### 2.4.5 Potential applications of rehydrated HA films.

Drying/rehydration of OEG-based HA films may be used to produce surface plasmon resonance (SPR) chips to study activity and kinetics of hyaladherins binding to HA. SPR is a very popular surface sensitive technique among biologists. A main challenge in setting up SPR experiments is the immobilization of biomolecules on the sensor surface without

disrupting their activity. This issue is overcome with end-grafted HA. In addition HA films on their own, or modified with desired proteins, can be used in cell adhesion studies, as well by SPR imaging <sup>179</sup>. The use of pre-prepared HA films might help in enhancing the rate of data acquisition and thus more efficient understanding of numerous fundamental processes in the assembly of the HA-based cellular coats.



### 3 The inflammation-associated protein TSG-6 cross-links hyaluronan via hyaluronan-induced TSG-6 oligomers

---

Tumor necrosis factor-stimulated gene-6 (TSG-6) is a hyaluronan (HA)-binding protein that plays important roles in inflammation and ovulation. TSG-6 mediated cross-linking of HA has been proposed as a functional mechanism (e.g. for regulating leukocyte adhesion), but direct evidence for cross-linking is lacking, and we know very little about its impact on HA ultrastructure. Here we used films of polymeric and oligomeric HA chains, end-grafted to a solid support, and a combination of surface-sensitive biophysical techniques, to quantify the binding of TSG-6 into HA films, and to correlate binding to morphological changes. We find that full length TSG-6 binds with pronounced positive cooperativity, and demonstrate that it can cross-link HA at physiologically relevant concentrations. Our data indicates that cooperative binding of full length TSG-6 arises from HA-induced protein oligomerization, and that the TSG-6 oligomers act as cross-linkers. In contrast, the HA-binding domain of TSG-6 (the Link module) alone binds without positive cooperativity, and weaker than the full-length protein. Both Link module and full length TSG-6 condensed and rigidified HA films, and the degree of condensation scaled with the affinity between the TSG-6 constructs and HA. We propose that condensation is the result of protein-mediated HA cross-linking. Our findings firmly establish that TSG-6 is a potent HA cross-linking agent and might hence have important implications for the mechanistic understanding of the biological function of TSG-6, e.g. in inflammation.

The contents of this chapter was reproduced from Baranova N. S., Nileback E., Haller F. M., Briggs D. C., Svedhem S., Day A. J. and Richter R. P. *JBC* 2011 286, 29:25675

### 3.1 Introduction

Hyaluronan (HA) is a structurally simple and linear polysaccharide. It is ubiquitous in the extracellular matrix of vertebrates and plays important roles in numerous physiological and pathological processes, such as inflammation, fertilization, embryogenesis, tumor development, osteoarthritis and atherosclerosis<sup>64, 180</sup>. HA is considered a ‘pericellular cue’<sup>181</sup>, i.e. it serves as a versatile scaffold within which other molecules are organized and regulated. A number of proteins, called hyaladherins<sup>65</sup>, can bind to the flexible HA chains and engender self-assembly into large and hydrated multimolecular complexes<sup>2, 22, 26</sup>.

The secreted product of tumor necrosis factor-stimulated gene-6 (TSG-6)<sup>182, 183</sup>, is of particular importance for the formation and remodeling of HA-rich pericellular coats<sup>184, 185</sup> and extracellular matrices<sup>41</sup>. There is little or no constitutive expression of TSG-6 in most adult tissues (with the exception of bone marrow<sup>186</sup> and epidermis<sup>187</sup>). Expression is elevated in response to stimulation with pro-inflammatory mediators or certain growth factors<sup>71, 182, 183, 188-190</sup>, and TSG-6 is detected in the context of many inflammatory diseases<sup>191, 192</sup> and in inflammation-like processes such as ovulation<sup>120, 121</sup>.

TSG-6 is composed mainly of two contiguous domains, a Link module and a CUB module<sup>77, 182, 190, 193</sup>. The Link module is conserved among members of the hyaladherin family<sup>65</sup>, and essential for binding to HA<sup>77</sup>. Administration of recombinant human TSG-6 Link module (Link\_TSG6) *in vivo* or in cell culture has frequently been found to elicit biological responses comparable to those of endogenously produced TSG-6<sup>186, 194-197</sup>, suggesting that Link\_TSG6 is a useful model for full length TSG-6. Indeed, most of our current knowledge about the interaction between HA and TSG-6 comes from structural studies and *in vitro* binding assays on Link\_TSG6. In contrast, only a few plate-based HA-binding assays have been reported for full length TSG-6<sup>165, 198, 199</sup>.

Little is known about the function of the TSG-6 CUB module, although the fact that it is highly conserved between species suggests that it is important for at least some activities of TSG-6<sup>182, 199</sup>. A case in point is that the TSG-6 mediated covalent transfer of heavy chains of inter- $\alpha$ -inhibitor (I $\alpha$ I) on to HA requires the full-length protein<sup>98, 195</sup>. Furthermore, Kuznetsova et al. have recently identified that the CUB\_C domain of TSG-6 (i.e. the CUB module together with the C-terminal region) mediates the binding of TSG-6 to fibronectin<sup>193</sup>.

Some of the functions of TSG-6 are clearly related to its ability to bind to HA. Moreover, TSG-6 and HA were reported to form stable complexes in solution that enhance or induce binding of HA to the cell surface receptor CD44 on lymphocyte cell lines<sup>194</sup>. Based on this observation, it was proposed that either Link\_TSG6 or full length TSG-6 alone can cross-link HA and that cross-linking is functionally important in the regulation of inflammation<sup>26, 194</sup>.

TSG-6 has a wide range of binding partners. Apart from HA, the protein interacts with the glycosaminoglycans chondroitin-4-sulfate, dermatan sulfate, heparin/heparan sulfate, with the G1 domains of the proteoglycans aggrecan and versican, and with a number of other extracellular proteins, including, inter- $\alpha$ -inhibitor (I $\alpha$ I), pentraxin 3 (PTX3) and thrombospondin 1<sup>37, 195-197, 200-203</sup> (reviewed in<sup>26, 182, 183</sup>). Simultaneous binding of TSG-6 to HA and to either of these latter proteins has been suggested as alternative routes for HA cross-linking<sup>26, 197</sup>.

To obtain direct evidence for and to understand the mechanisms behind TSG-6 mediated cross-linking, it would be desirable to be able to study the interaction between TSG-6 and a well-defined supramolecular assembly of HA. Here, we present a novel experimental approach that realizes this goal. The method is based on the immobilization of either polymeric or oligomeric HA *via* their reducing end to protein-repellent planar solid supports. With a combination of several surface-sensitive biophysical techniques, namely quartz crystal microbalance with dissipation monitoring (QCM-D), ellipsometry, and colloidal probe reflection interference contrast microscopy (RICM), we have quantified the binding kinetics of both recombinant human full-length TSG-6 (rhTSG-6) and Link\_TSG6 to HA, and correlated the binding to morphological changes of HA films. Our results provide novel insights into the molecular mechanism of HA cross-linking by TSG-6, and the properties of the ensuing HA supramolecular complexes, which have far-reaching implications for the potential effect of TSG-6 *in vivo*.



## 3.2 Experimental procedures

### Protein and hyaluronan preparations.

Wild type human TSG-6 Link module (Link\_TSG6, 10.9 kDa<sup>204</sup>) was expressed in *Escherichia coli* as described previously<sup>204, 205</sup>. Full length recombinant human TSG-6 (rhTSG-6; 30.1 kDa<sup>199</sup>) was expressed in *Drosophila* Schneider 2 cells and purified as described previously<sup>199</sup>. Lyophilized streptavidin (SAv; Sigma) was taken up in ultrapure water. Stock solutions of all proteins, typically at 1 mg/ml, were aliquoted and stored at -20°C.

Lyophilized polymeric HA (pHA), biotinylated at its reducing end and with well-defined molecular weights of 58±3 kDa (Select-HA B50) and 1083±53 kDa (Select-HA B1000) was purchased from Hyalose (Oklahoma City, OK, USA), as well as non-biotinylated HA of 262±13 kDa (Select-HA 250). For reconstitution, HA was taken up in ultrapure water at a stock concentration of 1 mg/ml, gently shaken over night, aliquoted, and stored at -20°C. HA<sub>9</sub> oligomers (oHA) with D-glucuronic acid at both termini, and with a ~3 nm spacer and a biotin moiety at their reducing end as described elsewhere<sup>168</sup>.

A ‘hepes’ buffer (150 mM NaCl, 10 mM HEPES at pH 7.4, 3 mM NaN<sub>3</sub>, 2 mM CaCl<sub>2</sub> in ultrapure water) was used throughout all measurements, and protein and HA solutions at their final concentrations were prepared in this buffer, except where otherwise stated.

### Preparation of protein repellent, biotin-functionalized surface coatings.

Supported lipid bilayers (SLBs) on silica or glass surfaces were formed by the method of vesicle spreading<sup>170</sup>, using small unilamellar vesicles that contained dioleoylphosphatidylethanolamine-cap-biotin (DOPE-CAP-biotin) and dioleoylphosphatidylcholine (DOPC) (both Avanti Polar Lipids, Alabaster, AL, USA) at a molar ratio of 1:9. Gold surfaces were functionalized with a dense oligoethylene glycol (OEG) monolayer by incubation in an ethanolic solution of a biotin-OEG disulfide (SS-OEG-biotin) and plain OEG disulfide (SS-OEG; both Polypure, Oslo, Norway) at a molar ratio of 1:99 (see Chapter 2 for the details).

### Assembly of HA films on SLBs and OEG layers.

HA films were prepared as described previously for SLBs<sup>173</sup>. Briefly, a dense SAv monolayer was formed by exposure of 10 µg/ml SAv (30 min) to a biotinylated SLB or OEG layer. Biotinylated HA was then grafted to the SAv monolayer by incubation of 1 to 10 µg/ml HA solution (Fig. 2.1 and Fig. 2.3). Samples were kept wet at all times.

Tuning of HA concentration and incubation time allowed for the HA density on the surface to be controlled in a quantitative manner (Fig. 2.5). The grafting density was set to 65±5 ng/cm<sup>2</sup> for 58 kDa HA in QCM-D measurements, and to approximately 35 ng/cm<sup>2</sup> for 1083 kDa HA in RICM measurements (Fig. 2.5D), corresponding to mean anchor distances of 13 and 77 nm between neighboring chains, respectively. For ellipsometric measurements,

densities of 58 kDa HA from 20 to 75 ng/cm<sup>2</sup> were used, corresponding to mean distances of 24 to 12 nm, respectively. The surface density of oHA ranged between 13 and 28 ng/cm<sup>2</sup>, corresponding to mean distances of 6.6 to 4.5 nm (Chapter **Error! Reference source not found.**).

### Quartz crystal microbalance with dissipation monitoring.

QCM-D measures changes in resonance frequency,  $\Delta f$ , and dissipation,  $\Delta D$ , of a sensor crystal upon interaction of (soft) matter (e.g. biomolecules) with its surface<sup>206</sup>. The QCM-D response is sensitive to the mass (including coupled water) and the viscoelastic properties of the surface adlayer. Adsorption and interfacial processes on silica or gold-coated QCM-D sensors were monitored *in situ* with sub-second time resolution under continuous flow of sample solution<sup>166</sup> (Chapters 1.7.1).

### In situ ellipsometry.

Ellipsometry measures changes in the polarization of light upon reflection at a planar surface. We employed ellipsometry *in situ* on silica or gold-coated silicon wafers as substrates that were installed in a custom-built open cuvette with a continuously stirred sample solution, to quantify adsorbed biomolecular masses in a time-resolved manner<sup>166</sup> (Chapter 1.7.3).

### Quantification of binding constants.

The binding constant,  $K_{0.5}$ , and the saturation limit,  $\Gamma_{\max}$ , for the binding of TSG-6 to HA films was obtained from the surface densities at equilibrium,  $\Gamma_{\text{eq}}$ , as a function of the TSG-6 bulk concentrations, by numerical fitting to the Hill equation:

$$\Gamma_{\text{eq}} = \Gamma_{\max} \frac{[\text{TSG} - 6]^n}{K_{0.5}^n + [\text{TSG} - 6]^n} \quad 3.1$$

with the Hill coefficient  $n$  being a measure for the cooperativity of binding<sup>207</sup>.  $K_{0.5}$  corresponds to the bulk concentration at which half-maximal binding occurs. For non-cooperative binding ( $n = 1$ ), it equals the dissociation constant  $K_D$ . [TSG-6] relates to the concentrations of either Link\_TSG6 or rhTSG-6. Dissociation rate constants,  $k_{\text{off}}$ , were derived from an exponential fit:

$$\Gamma = \Gamma_r e^{-k_{\text{off}} \Delta t} + \Gamma_{\text{ir}}, \Gamma_{\text{eq}} \quad 3.2$$

or from a double exponential fit:

$$\Gamma = \Gamma_r^{(1)} e^{-k_{\text{off}}^{(1)} \Delta t} + \Gamma_r^{(2)} e^{-k_{\text{off}}^{(2)} \Delta t} + \Gamma_{\text{ir}} \quad 3.3$$

to the desorption curve upon rinsing in pure buffer solution. Here,  $\Gamma$  is the TSG-6 surface density, and  $\Delta t$  is the rinsing time.  $\Gamma_r$  and  $\Gamma_{ir}$  are the surface density of reversibly and irreversibly bound TSG-6, respectively.

### **Colloidal probe reflection interference contrast microscopy (RICM).**

This micointerferometric technique measures the height at which a colloidal probe hovers above a transparent planar substrate with a resolution of a few nanometers (see Chapter 1.7.3 for details). The thickness of surface-bound HA films was determined by triple wavelength colloidal probe RICM, as described previously {Richter, 2007 #6;{Wolny, #24}}. Naked polystyrene microspheres of  $\sim 25 \mu\text{m}$  diameter (Polysciences, Eppelheim, Germany) were used as colloidal probes. The HA films were assembled on bare or gold-coated glass cover slips, using custom-built liquid flow cells with an internal volume of a few  $\mu\text{l}$ . Protein solutions at desired concentrations were injected with a flow rate of  $20 \mu\text{l}/\text{min}$  until equilibrium was reached (typically within 5 to 20 min). At the end of each titration step, colloidal probes were mixed into the protein solution and applied at a flow rate of  $5 \mu\text{l}/\text{min}$ . Presented thickness values correspond to the increase in the total measured film thickness upon the addition of HA, or of HA and TSG-6. From the analysis of the microspheres' lateral mobility, we estimate that interactions between the microspheres and the HA films did not perturb the samples appreciably <sup>21</sup>.

## 3.3 Results

To analyze the interaction of TSG-6 with HA, we designed surface-confined films that present HA of selected molecular weights in a well-defined supramolecular assembly. The construction of the films was monitored and controlled by QCM-D (Fig. 2.1-Fig. 2.3).

In a first model system, polymeric hyaluronan (pHA) with a molecular weight of either 58 kDa or 1083 kDa was immobilized *via* a biotin-tag at its reducing end to solid supports that were previously functionalized with a protein-repellent coating and a dense monolayer of streptavidin (Fig. 3.1A). The grafting density can be controlled and a highly hydrated film of partly stretched and entangled HA chains with up to several 100 nm in thickness, a so-called HA brush, is formed<sup>173</sup>. Assuming a footprint of HA<sub>10</sub> per TSG-6 protein<sup>198, 208</sup>, each pHA chain of 58 and 1083 kDa can accommodate up to 30 and 571 TSG-6 molecules, respectively.

In a second approach, short oligomeric HA chains, comprising only 9 monosaccharides (oHA), were grafted to the surface (Fig. 3.1 B). Grafting was again mediated by a biotin-tag. A linker of about 3 nm in contour length<sup>172</sup> was placed between the biotin and the reducing end of HA to enhance the conformational freedom of the surface-bound oHA chains. Each oHA chain is 4.5 nm long and can interact with only one TSG-6 molecule at a time, where previous studies have shown that ~5 sugar monomers likely fill its HA-binding site<sup>75</sup>.

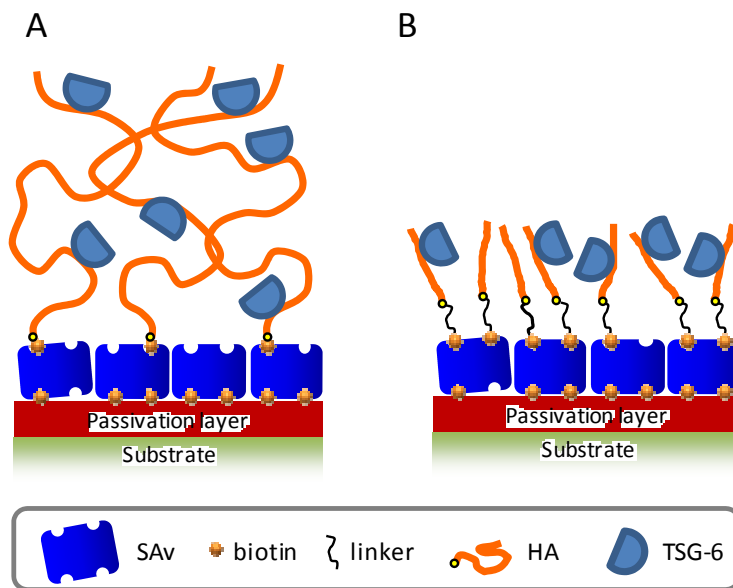


Fig. 3.1 **Architecture of hyaluronan (HA) films.** A dense streptavidin (SAV) monolayer was formed on a biotin-functionalized passivation layer. The passivation layer - either a silica-supported lipid bilayer or a gold-supported OEG layer (Fig. 2.1 Fig. 2.3) – was designed to inhibit non-specific binding of TSG-6. HA chains were grafted through a biotin functionality at their reducing end to the SAV layer. (A) Polymeric HA (pHA) with molecular weights of 58 or 1083 kDa exposes up to several hundred binding sites for TSG-6 on each individual polymer chain. (B) Only one TSG-6 molecule can bind to an HA9 oligomer (oHA). The size of the proteins, the thickness of the passivation layer and the length of oHA are drawn to scale; the thickness of the pHA films is compressed by up to 20-fold.

Two different primary surface functionalizations were employed: (i) silica-supported lipid bilayers (SLBs) exposing biotin groups (Fig. 2.1) and (ii) gold-supported oligo-ethylene glycol (OEG) films exposing biotin groups (Fig. 2.3). The properties of the HA films were not affected by the choice of the primary surface-layer (Fig. 2.4). SLBs were used for all studies related to Link\_TSG6. OEG-covered surfaces were used for rhTSG-6 as they were found to exhibit better passivation against nonspecific binding of this protein (Fig. 3.2).

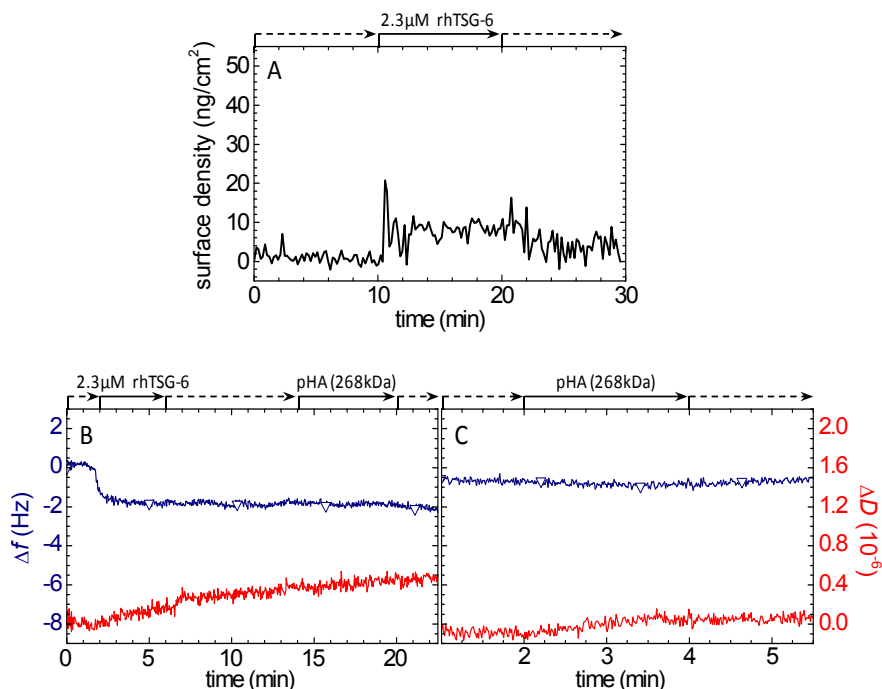


Fig. 3.2 **Controls for the binding of rhTSG-6 to SAV-covered OEG layers.** (A) Ellipsometric data for the exposure of 2.3  $\mu\text{M}$  rhTSG-6 to a SAV-covered OEG layer that was formed as described in Chapter 2. The start and duration of the incubation with different samples and buffer is indicated (solid arrows and dashed arrows, respectively). The bound amount is very small ( $<10 \text{ ng/cm}^2$ ). (B) QCM-D responses,  $\Delta f$  (blue curves with open triangles) and  $\Delta D$  (red curves) are shown for the sequential exposure of 2.3  $\mu\text{M}$  rhTSG-6 and 50  $\mu\text{g/ml}$  biotin-free polymeric HA (268 kDa) to a SAV-covered OEG layer. Exposure to rhTSG-6 induces a small frequency response of -2 Hz, indicating minor unspecific binding. Non-specifically bound rhTSG-6 does not have detectable pHA binding activity. (C) QCM-D responses for the exposure of 50  $\mu\text{g/ml}$  biotin-free polymeric HA (268 kDa) to a SAV-covered OEG layer that had been incubated with biotinylated oHA; no binding was observed

### 3.3.1 Binding of full length TSG-6 to HA films.

To obtain quantitative insight into the kinetics of rhTSG-6 binding, we performed titration assays on oHA and pHA films using *in situ* ellipsometry (Fig. 3.3). The titration curves (Fig. 3.3 C) exhibited a pronounced sigmoidal shape. The curves could be fitted well by the Hill equation (equation 3.1) with exponents above 2, indicating that binding is cooperative. The exponents for pHA and oHA ( $2.7 \pm 0.8$  and  $2.8 \pm 0.5$ , respectively) coincided within experimental error (Table 3.1). The  $K_{0.5}$  for pHA was similar to although slightly lower than for oHA (Table 3.1). On oHA, we found a stoichiometry of  $2.7 \pm 0.8$  rhTSG-6 molecules per oHA chain (Table 3.1), indicating that more than one rhTSG-6 molecule can on average associate with a single oHA chain.

What is the origin of the cooperative binding? One possibility that has been proposed previously<sup>22, 198</sup> is that cooperativity arises from facilitated binding of a several proteins to

adjacent binding sites on the same HA chain. In light of the similar Hill coefficients and  $K_{0.5}$  for pHA (with many binding sites per chain) and oHA (with a single binding site) this scenario is unlikely. Facilitated binding of a second (or more) rhTSG-6 molecules must hence occur either on another HA chain (or distant binding sites on the same pHA chain), or on the HA-bound rhTSG-6, or both. In fact, the supra-stoichiometric binding of rhTSG-6 to oHA provides strong indications that the binding of one rhTSG-6 molecule to HA is sufficient to induce the formation of protein dimers (or even larger oligomers). In this regard, our collaborators Day et al. have observed previously that rhTSG-6 forms elongated end-to-end dimers in the presence of excess HA<sub>8</sub>, as well as larger species<sup>81</sup>.

The dissociation of rhTSG-6 from HA films was generally slow. Only double exponentials (Fig. 3.3) provided a good fit to the desorption curves upon rinsing of close-to-saturated HA films with buffer (Fig. 3.3A-B; Table 3.1). The fit did not reveal a significant fraction of irreversibly bound rhTSG-6 ( $\Gamma_{ir} = 0$ ). The first dissociation rate constant was approximately  $4 \times 10^{-3} \text{ s}^{-1}$  for oHA, and slightly smaller for pHA ( $\sim 3 \times 10^{-3} \text{ s}^{-1}$ ). Notably, almost 50% of the protein on oHA but less than 10% on pHA desorbed with the faster dissociation rate. The second dissociation rate constant was at least one order of magnitude smaller than the first, and slightly larger for pHA. One might be tempted to attribute the two apparent rate constants to two discrete unbinding events. The numbers are, however, also consistent with the presence of a spectrum of dissociation rates. The latter would be expected for the formation of a wide range of HA/TSG-6 complexes where the different interactions (e.g. HA/protein and protein/protein) likely have different stabilities.

Given the slow dissociation, not all rhTSG-6 could be unbound within experimentally accessible time scales. However, the remaining fraction could readily be eluted by 8 M of the dissociating agent guanidine hydrochloride (GuHCl; Fig. 3.4). In contrast, the attachment of HA to our passivation layers *via* biotin and streptavidin was not disrupted by GuHCl (Fig. 2.6). rhTSG-6 hence does not form covalent complexes with HA, as had been suggested based on microtiter plate-based HA-binding assays<sup>165</sup>.

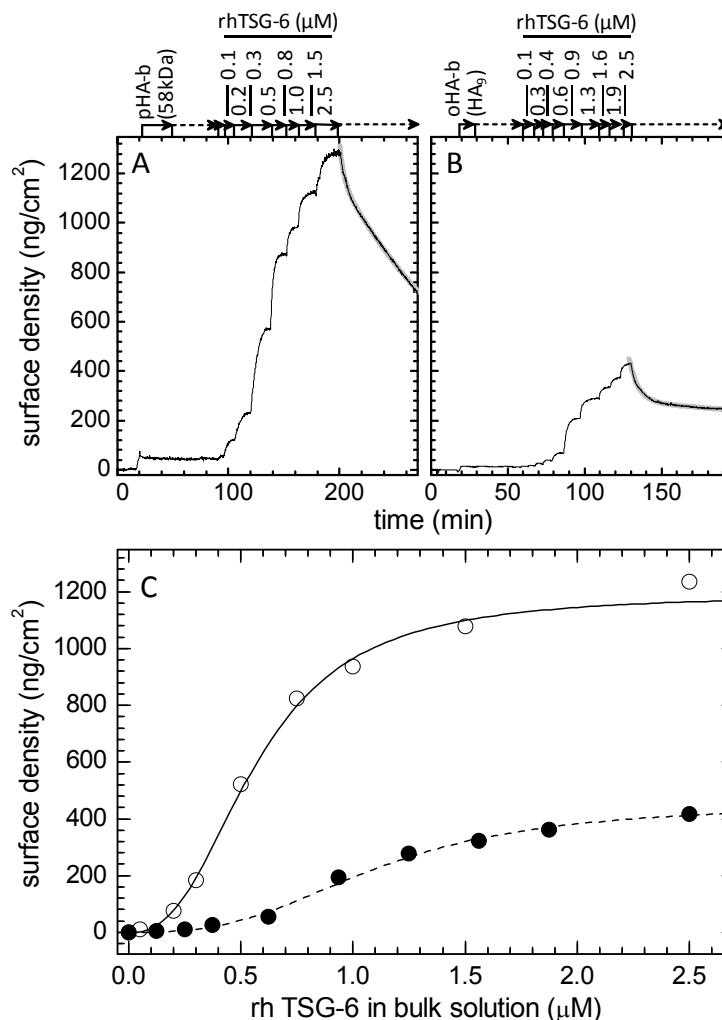


Fig. 3.3 **Binding of full length TSG-6 into HA films.** (A-B) Representative titration curves by ellipsometry for the binding of rhTSG-6 to a pHA (58 kDa) and an oHA (HA9) film, respectively. The start and duration of the incubation with different samples and buffer is indicated (solid arrows and dashed arrows, respectively). Fits with Eq. 2b to the desorption curves upon rinsing in buffer (thick grey solid lines) provide estimates for the dissociation rate constants  $k_{\text{off}}(1)$  and  $k_{\text{off}}(2)$ . Binding of rhTSG-6 to HA-free surfaces was negligible (Fig. 3.2). (C) Adsorbed amounts of rhTSG-6 at equilibrium in films of pHA (58 kDa; ○) and oHA (HA9; ●), determined from A and B. Both curves have pronounced sigmoidal shapes and can be fitted well by Eq. 1. Measurements were performed two to three times; determined  $K_{0.5}$ ,  $k_{\text{off}}$ ,  $n$  and binding stoichiometries are given in Table 3.1 Hill exponents above  $n = 2$  indicate strong positive cooperativity.



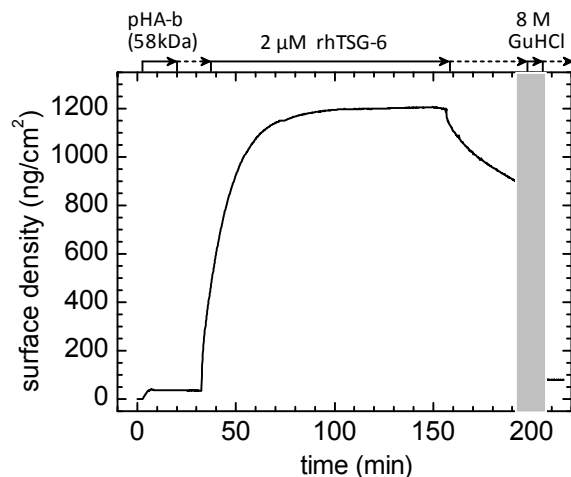


Fig. 3.4 **Full-length TSG-6 can be fully eluted with dissociating agents.** (A) A pHA (58 kDa) film that was previously close-to-saturated with rhTSG-6 and rinsed with hepes buffer was exposed to 8 M guanidine hydrochloride (GuHCl). All of the protein is rapidly diluted in the dissociating agent and, hence, rhTSG-6 does not bind covalently to HA. All processes, except the incubation with GuHCl (*shaded in grey*), were monitored by ellipsometry. The HA film was stable in GuHCl (Fig. S7A). The measurement was repeated twice, and the displayed data is representative.

### 3.3.2 Full-length TSG-6 oligomers can cross-link HA.

To test if rhTSG-6 that is bound to HA films can still bind additional HA, a “sandwich” assay by QCM-D was designed (Fig. 3.5). rhTSG-6 was first exposed to an oHA film. The total frequency shift for the oHA/rhTSG-6 film was -34 Hz. The corresponding thickness of approximately 6 nm and the minor changes in dissipation are consistent with the formation of a rather dense layer of rhTSG-6; a control measurement on an HA-free surface did not show measurable binding of active rhTSG-6 (i.e. the small amount of non-specifically bound rhTSG-6 was not able to bind to HA; (Fig. 3.2B). This confirms that the rhTSG-6 protein was indeed immobilized *via* its binding to oHA and that rinsing in buffer induced a slow release of TSG-6 (between 62 and 67 min in 3.5A).

Subsequent rapid incubation with pHA (262 kDa) resulted in a two-phase response (Fig. 3.5A). Initially, the frequency decreased rapidly, together with a pronounced increase in dissipation. Such a response is typical for the formation of a soft layer, as would be expected for the binding of pHA on top of the TSG-6 covered oHA film. For comparison, no pHA binding was observed on a rhTSG-6 free surface (Fig. 3.2C). Clearly, full length TSG-6 dimers (or higher oligomers) that had already bound to oHA retained the ability to bind additional HA. In the second phase, both the frequency and the dissipation shift increased slowly, suggesting remodeling of the surface-bound film. The rate of frequency increase changed after removal of pHA from the solution phase, indicating that supply of unbound HA must be involved in this process. A plausible explanation for the observed response would be that pHA captures some of the rhTSG-6 that is slowly released from the oHA film,

and thanks to the cross-linking activity of rhTSG-6 a multilayer of pHA is formed on top of the oHA film (Fig. 3.5B).

The cooperative binding of rhTSG-6, and its ability to cross-link HA have interesting implications with respect to the stability of rhTSG-6 dimers (or oligomers) in the absence of HA. If rhTSG-6 alone would form stable dimers (or oligomers), their binding into the HA matrix would correspond to a multivalent interaction. Although multivalent binding would most likely exhibit an increased avidity, as compared to monovalent binding, it would not be cooperative. The observed cooperativity hence implies that the oligomeric state of rhTSG-6 is induced (or stabilized) by HA.

With respect to cross-linking, the binding behavior of rhTSG-6 to oHA films merits detailed consideration. The average spacing between neighboring oHA strands, 4 to 7 nm, is comparable to the size of TSG-6; TSG-6 can be estimated to be ~6-7 nm in length from the  $D_{\max} = 13 \pm 1$  nm determined from small angle X-ray scattering<sup>209</sup>, which is consistent with the structures of the Link module<sup>75</sup> and CUB module domains (Protein Data Bank code 2WNO)<sup>210</sup>. rhTSG-6 oligomers are hence sufficiently large to interconnect neighboring oHA chains. The immobilization of oHA to a surface, on the other hand, imposes constraints with respect to the exact distance between and orientation of oHA chains, which may hamper cross-linking. These steric constraints might explain, why the binding stoichiometry at saturation is significantly larger than 1.0, as expected if the surface-confined rhTSG-6 oligomers would mostly connect to only a single oHA chain. This is also consistent with the finding that immobilized TSG-6 is still able to bind pHA from the solution phase (Fig. 3.5A).

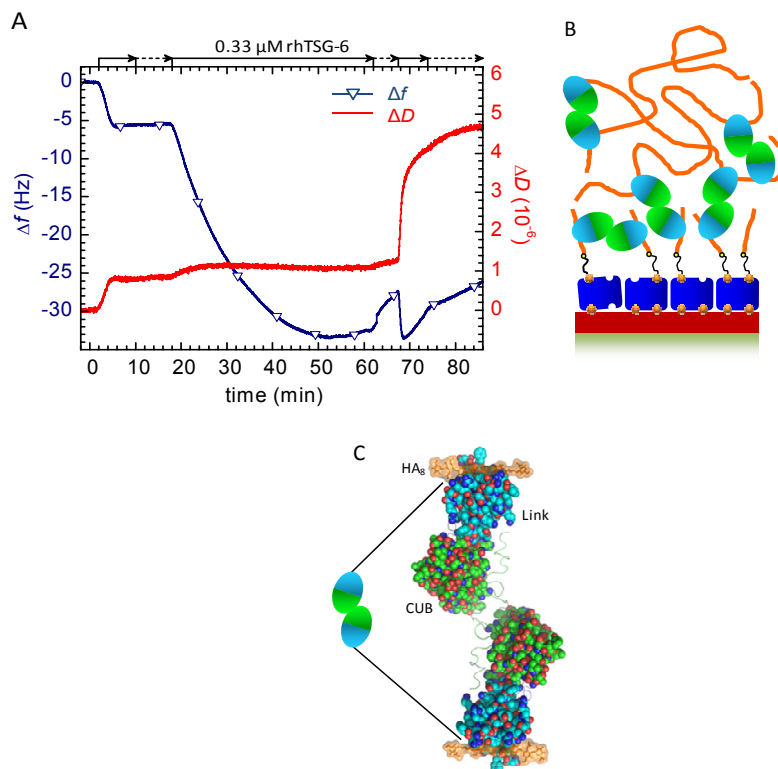


**Fig. 3.5 Full length TSG-6 cross-links HA.** (A) Sandwich assay, monitored by QCM-D. The start and duration of the incubation with different samples and buffer is indicated (solid arrows and dashed arrows, respectively). A film of surface-bound oHA was incubated with rhTSG-6 until equilibrium, reaching a frequency shift of  $\Delta f = -34$  Hz and a dissipation shift of  $\Delta D = 1.1 \times 10^{-6}$ , indicating the formation of a rather dense and rigid film of about 6 nm in thickness. The frequency increase upon subsequent rinsing with buffer indicates slow desorption of some rhTSG-6. Rapid addition of pHA (262 kDa) without biotin linker resulted in a two-phase response that is indicative of two overlapping processes. The initial decrease in frequency indicates binding of pHA to the oHA-bound rhTSG-6. The concomitant strong increase in dissipation is characteristic for the formation of a soft and highly hydrated film. The subsequent increase in frequency is likely a result of desorption of rhTSG-6 and/or migration of rhTSG-6 inside the pHA film. This process continues, albeit at slower pace, after rinsing in buffer. The measurement was performed twice, and the shown data is representative. (B) Schematic illustration of the final sandwich structure. Our data indicates that HA cross-linking is mediated by rhTSG-6 oligomers (e.g. dimers). The Link module and the CUB\_C module of TSG-6 are schematically indicated in light blue and pink, respectively. (C) For comparison, a molecular model of a TSG-6 dimer with two bound HA octasaccharides derived from small angle X-ray scattering data<sup>209</sup> is also shown; the Link module structure (blue) in its HA-bound conformation<sup>75</sup>, docked HA oligomers (orange) and CUB module model (green) are shown in space filling representations, while the N- and C-terminal regions of TSG-6 (for which no structural data are available) are represented as protein backbone traces predicted from the scattering data<sup>209</sup>. Image C was provided by D.C. Briggs & A.J. Day (Manchester University).

### 3.3.3 Full-length TSG-6 induces strong condensation of HA films.

Next, we investigated how the influx of rhTSG-6, and the ensuing cross-linking, affect the overall morphology of pHA films. Exposure of rhTSG-6 to a pHA (58 kDa) film induced a monotonous and strong decrease in the QCM-D frequency response (Fig. 3.6A). In contrast, the dissipation initially increased and then decreased. The decrease in particular is indicative of a rigidification of the pHA film.

We employed colloidal probe RICM to quantify the variations in film thickness upon rhTSG-6 addition (Fig. 3.6B). To extend the range of potential thicknesses, we used HA of larger molecular weight (1083 kDa), while maintaining the total mass of HA per surface area comparable to the previously described pHA films (Fig. 2.5D). Titration of rhTSG6 initially resulted in a gradual decrease in film thickness. Significant film condensation was already observed at 0.16  $\mu\text{M}$  rhTSG-6 in the bulk solution, and the film thickness decreased by more than twofold, from 400 to 180 nm, upon exposure to 0.34  $\mu\text{M}$  rhTSG-6 protein. Based on the kinetic data that we had obtained by ellipsometry (Table 3.1), a bulk concentration of 0.34  $\mu\text{M}$  would result in an average occupancy of one rhTSG-6 molecule per 44 HA<sub>2</sub> segments (one every HA<sub>88</sub>; Fig. 3.6B, *inset*), which is equivalent to one protein every 44 nm of HA contour length), or  $\sim 65$  TSG-6 molecules per HA chain.

How can this rather low occupancy induce such a strong condensation of the HA films? In the absence of TSG-6, the surface-grafted pHA films form a so-called polymer brush<sup>173</sup>. Such a brush can be pictured as a strongly hydrated and highly dynamic meshwork of entangled polymer chains that are weakly stretched in the direction perpendicular to the surface<sup>211, 212</sup> (Fig. 3.7A). The water content in the 1083 kDa pHA films that we used in the RICM measurements, for example, is approximately 99.9%, as can be calculated from the grafting density (35 ng/cm<sup>2</sup>) and the film thickness (400 nm). Polymer theory<sup>211, 212</sup> predicts that the size of the meshes (or ‘holes’) in the pHA meshwork is comparable to the mean distance between the anchor points of neighboring HA chains ( $\sim 80$  nm for 1083 kDa pHA films). The introduction of cross-linkers will force neighboring HA chains closer together and decrease the mesh size (Fig. 3.7B). As a result, the film’s thickness will decrease while its rigidity will increase. Given that the films have a large mesh-size to start with, a rather small amount of cross-linkers can already have an appreciable effect on the film thickness. The above considerations illustrate that cross-linking is an efficient route for the condensation of HA films, and rationalize the increase in rigidity and the decrease in thickness that we have observed upon introduction of rhTSG-6 in pHA films (Fig. 3.6).

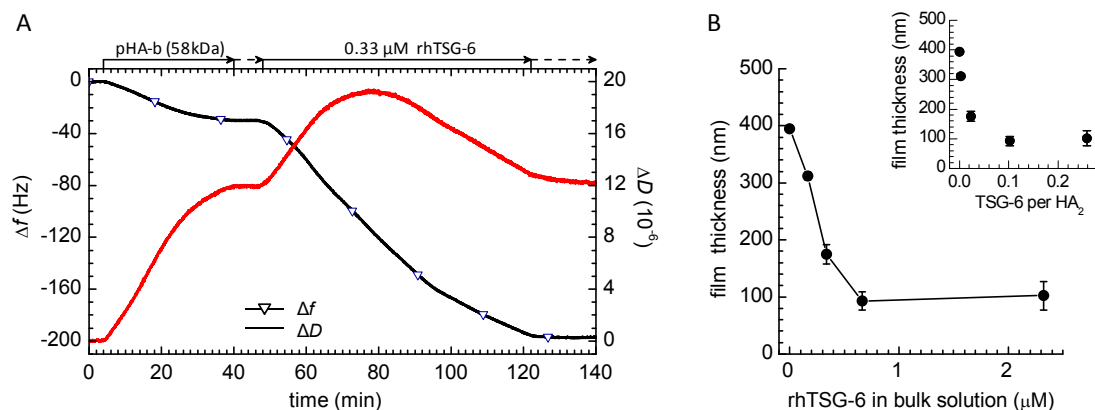


**Fig. 3.6 Rigidification and condensation of HA films upon influx of full-length TSG-6.** (A) Binding of rhTSG-6 to a pHA (58 kDa) film was monitored by QCM-D. The strong decrease in frequency upon exposure to rhTSG-6 is initially accompanied by an increase, followed by a decrease, in dissipation. The latter indicates rigidification of the HA film. (B) Variations in the thickness of a pHA (1083 kDa) film as a function of increasing rhTSG-6 concentration, quantified by colloidal probe RCM. The film retained its collapsed state upon rinsing in buffer (*data not shown*). The *inset* shows the thickness as a function of the occupancy of HA (calculated from *B*, using Eq. 1 and the data for pHA in Table 3.1). Error bars are standard deviations for 10 independent measurements on the same surface.

Maximal film collapse, to about 100 nm, was induced at a protein concentration of 0.7  $\mu\text{M}$  in the bulk solution. This corresponds to an occupancy of one rhTSG-6 per about 10  $\text{HA}_2$  segments (one every  $\text{HA}_{20}$ ), and a protein concentration inside the film of around 1.0 mM, or 30 mg/ml. Notably, the film thickness did not decrease further, but instead slightly increased upon further increasing the rhTSG-6 bulk concentration to 2.3  $\mu\text{M}$ . At this point, the rhTSG-6 concentration inside the HA film reached a value of approximately 2.3 mM, or 70 mg/ml, i.e. TSG-6 occupied a significant fraction (about 5%) of the total volume in the HA film. We propose that crowding of rhTSG-6 prevents further film condensation. The thickness of the maximally collapsed film did not change over a period of at least one hour following removal (by rinsing) of the remaining rhTSG-6 in solution, confirming that release of rhTSG-6 is slow and that the protein/HA complexes are rather stable, as previously observed by ellipsometry Fig. 3.3A).

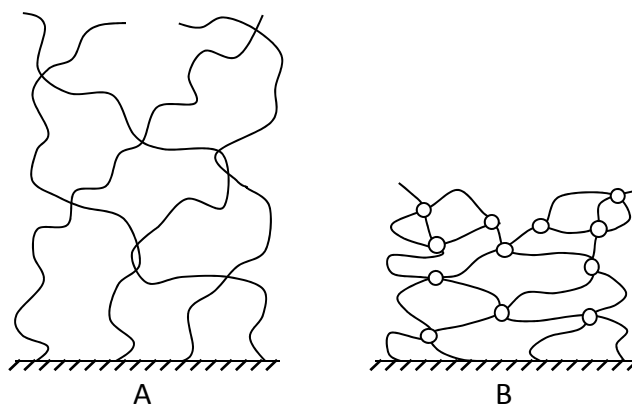


**Fig. 3.7 Schematic presentation of the mechanism behind condensation of pHA brushes upon cross-linking with full length TSG-6.** (A) In the absence of TSG-6, HA forms a strongly hydrated meshwork of entangled polymer chains; the size of individual meshes is comparable to the distance between anchor points of HA chains on the surface. (B) The introduction of cross-linkers (open circles) forces neighboring HA chains closer together; this leads to smaller mesh sizes, film condensation and rigidification.

### 3.3.4 Binding of Link\_TSG6 to HA films.

To compare the HA-binding behavior of full-length TSG-6 with that of the Link module, Link\_TSG6 was titrated into both oHA and pHA (58 kDa) films, and the binding kinetics were quantified by ellipsometry (Fig.3.9). The titration curves (Fig.3.9C) could be fitted well with Eq. 1 and a Hill coefficient of  $\sim 1$ , revealing dissociation constants of approximately 5  $\mu\text{M}$  (Table 3.1). The Hill coefficient of unity, and similar  $K_D$  values for oHA and pHA, indicate that interactions between adjacent binding sites along a given polymeric HA chain do not affect binding. Furthermore, Link\_TSG6 bound stoichiometrically to oHA at saturation (Table 3.1). All these findings are consistent with a simple one-site model, i.e. in which all binding sites are identical (as also found in recent confocal-FRAP analysis of the binding of Link\_TSG6 to pHA in solution phase<sup>213</sup>, in stark contrast to rhTSG-6.

Overall, the observed simple, non-cooperative binding, and the micromolar affinities for Link\_TSG6 are consistent with earlier solution-phase studies by calorimetry on HA oligosaccharides<sup>75, 198, 208, 214</sup> and by confocal fluorescence recovery after photobleaching on polymeric HA<sup>213</sup>. However, it should be noted that these measurements were performed at different pH and ionic strength to those used here, and that both parameters have been found to significantly affect the binding affinity<sup>198, 201, 213, 214</sup>. A detailed quantitative comparison of the binding affinities is hence far from trivial.

For polymeric HA, we found a stoichiometry of  $2.9 \pm 0.3$  HA disaccharides per Link\_TSG6 at saturation (Table 3.1). This number is similar to the minimum size of HA oligomer that binds with maximal affinity to Link\_TSG6 (HA<sub>7</sub> with D-glucuronic acid at both termini<sup>75</sup>), but it is smaller than the decameric footprint that has been reported based on calorimetric binding studies with HA oligosaccharides of different size<sup>198</sup>.

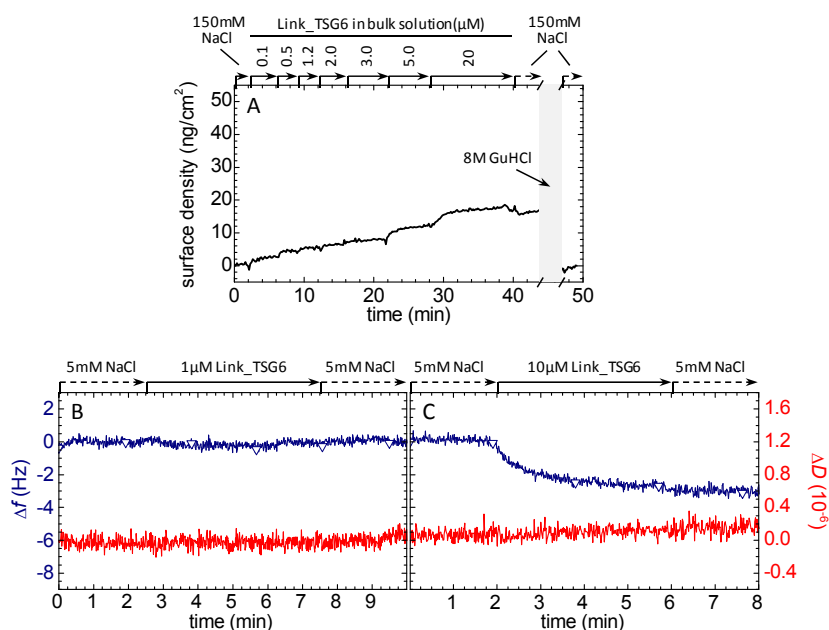


Fig. 3.8 **Controls for binding of Link\_TSG6 to SAv-covered SLBs.** (A) Ellipsometric response for the titration of Link\_TSG6 on a SAv-covered SLB that was formed as described in Fig. S1. The start and duration of the incubation with different samples and buffer is indicated (solid arrows and dashed arrows, respectively). Minor but significant amounts of Link\_TSG6 bind non-specifically in a concentration-dependent manner. Bound Link\_TSG6 could not be eluted in buffer, but in 8 M GuHCl (GuHCl incubation period shaded in grey). (B-C) QCM-D responses,  $\Delta f$  (blue curves with open triangles) and  $\Delta D$  (red curves), for the exposure of Link\_TSG6 to SAv-covered SLBs in 5 mM NaCl. At 1  $\mu\text{M}$  concentration, Link\_TSG6 showed no detectable binding:  $|\Delta f| < 0.5$  Hz and  $\Delta D < 0.1 \times 10^{-6}$  (B). A small frequency shift of -3 Hz was detected at 10  $\mu\text{M}$  concentration in 5 mM NaCl, indicating some minor unspecific binding (C).

The desorption curves upon rinsing of close-to-saturated HA films with buffer could be fitted well by simple exponential fits (Fig.3.9A-B). The dissociation rate constants (

Table 3.1) for Link\_TSG6 were similar for oHA and pHA films, but more than 5-fold larger than the fastest desorption rates observed for rhTSG-6. Most Link\_TSG6 could be readily dissociated within experimental time scales, although a proportion of the protein could not be removed by rinsing in hepes buffer, i.e.  $\sim 10\%$  and  $\sim 25\%$  for the oHA and pHA films, respectively (Fig.3.9A-B). Control measurements with Link\_TSG6 on HA-free surfaces (Fig. 3.8) revealed minor nonspecific binding that was comparable in magnitude to the irreversibly bound amounts on oHA films. It remains unclear if the significantly larger amount of irreversibly bound Link\_TSG6 protein in pHA films is specifically bound to HA. It might also reflect some tendency of the protein to aggregate at the high concentrations reached in the HA film. In this regard, Link\_TSG6 has been found to be stable at concentrations in solution phase up to at least 2 mM in the presence of a 1:1 molar ratio of HA<sub>8</sub><sup>75</sup>, although precipitation has been reported under some conditions in the presence of a

larger HA oligomer<sup>198</sup>. However, the protein fraction that remained bound upon rinsing in buffer could readily be eluted in 8 M GuHCl (Fig.3.9) i.e. Link\_TSG6, as rhTSG-6, did not engage in a covalent interaction with HA.

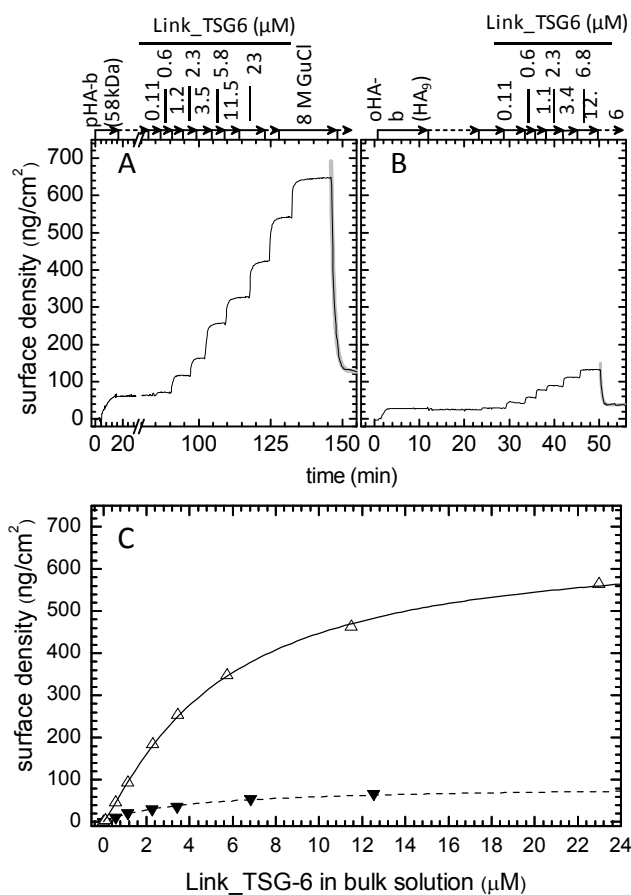


Fig. 3.9 **Binding of Link\_TSG6 into HA films.** (A-B) Representative titration curves by ellipsometry for a pHA (58 kDa) and an oHA (HA<sub>9</sub>) film, respectively. Fits with Eq. 2a to the desorption curves upon rinsing in buffer (*thick grey solid lines*) provide estimates for the dissociation rate constant  $k_{\text{off}}$ . The irreversibly bound protein fraction could be fully eluted in GuHCl (A; incubation period *shaded in grey*), and is hence non-covalently bound. (C) Adsorbed amounts of Link\_TSG6 at equilibrium in films of pHA (Δ) and oHA (▼); minor amounts of nonspecific binding, observed on HA-free surfaces (Fig. 3.8), were subtracted from the data in A and B. Fits by Eq. 1 (*solid line* and *dashed line*, respectively) provide a Hill exponent close to unity. Measurements were performed two to three times; determined  $K_{0.5}$ ,  $k_{\text{off}}$ ,  $n$  and binding stoichiometries are given in (Table 3.1).



### 3.3.5 Condensation of HA films by Link\_TSG6.

Next, we tested how Link\_TSG6 affects the morphology of pHA films, as compared to rhTSG-6. Titration of Link\_TSG6 at bulk concentrations ranging from 0.05 to 5  $\mu\text{M}$  into pHA (58 kDa) films was monitored by QCM-D (Fig. 3.10A). A remarkable decrease in dissipation, concomitant with a decrease in frequency, occurred at concentrations above 3  $\mu\text{M}$ , indicating rigidification of the film<sup>139, 166, 215</sup>; in comparison, we had observed a similar decrease in dissipation already at a 8-fold lower concentration of rhTSG-6 (Fig. 3.6A). The QCM-D responses reversed upon gradually decreasing the Link\_TSG6 concentration in solution. Compared to the responses at increasing protein concentrations, a hysteresis was observed, i.e. the process was only partly reversible.

Colloidal probe RICM revealed a gradual decrease in thickness upon titration of Link\_TSG6 into pHA (1083 kDa) films (Fig. 3.10B), from  $427\pm 4$  nm in the absence of proteins to  $66\pm 16$  nm in the presence of 10  $\mu\text{M}$  Link\_TSG6. Stepwise elution of Link\_TSG6 resulted in a gradual thickness increase. A hysteresis in thickness between adsorption and desorption processes (Fig. 3.10B) was consistent with QCM-D data (Fig. 3.10A) and the irreversibly bound protein fraction observed by ellipsometry (Fig. 3.9A).

In order to compare the potency of rhTSG-6 and Link\_TSG6 to condense HA films, it is useful to consider the degree of condensation as a function of occupancy of HA chains with proteins, rather than the bulk protein concentration (Fig. 3.10 C). At low occupancies, full length TSG-6 was considerably more potent in condensing HA than Link\_TSG6. To reach a twofold decrease in thickness, for example, only one rhTSG-6 per 44 HA<sub>2</sub> segments (HA<sub>88</sub>), but more than one Link\_TSG6 per 6 HA<sub>2</sub> segments (HA<sub>12</sub>), were required.

Within experimental error, the film thickness decreased linearly with the occupancy for Link\_TSG6. At the maximal experimentally assessed protein uptake, one Link\_TSG6 per 4.0 HA<sub>2</sub> segments (HA<sub>8</sub>) (which is somewhat higher than the stoichiometry at saturation predicted from the Hill equation, Table 1), the film thickness had attained approximately 15% of its original value, and the concentration of Link\_TSG6 inside the film was approximately 3.2 mM, or 35 mg/ml.

Several mechanisms might be considered for the rigidification and condensation of pHA films by Link\_TSG6. In analogy with our arguments for rhTSG-6, cross-linking is one possible driving force. It would be probable that Link\_TSG6 dimers (or larger oligomers), rather than monomers, act as cross-linkers: only about 6 carbohydrate monomers are on average available per Link\_TSG6 at saturation in pHA films (

Table 3.1); if a monomer was sufficient for cross-linking, then the average footprint per HA chain would need to be an HA trimer unless two Link\_TSG6 molecules can simultaneously bind to the same part of the HA chain. Based on the structure of the HA binding site<sup>75, 216</sup>, this is unlikely. Furthermore, it should be noted that previous studies on Link\_TSG6 by analytical ultracentrifugation<sup>208</sup> and NMR spectroscopy<sup>217</sup> indicated that, in solution phase, this protein domain is monomeric in both the absence and presence of HA<sub>8</sub>.

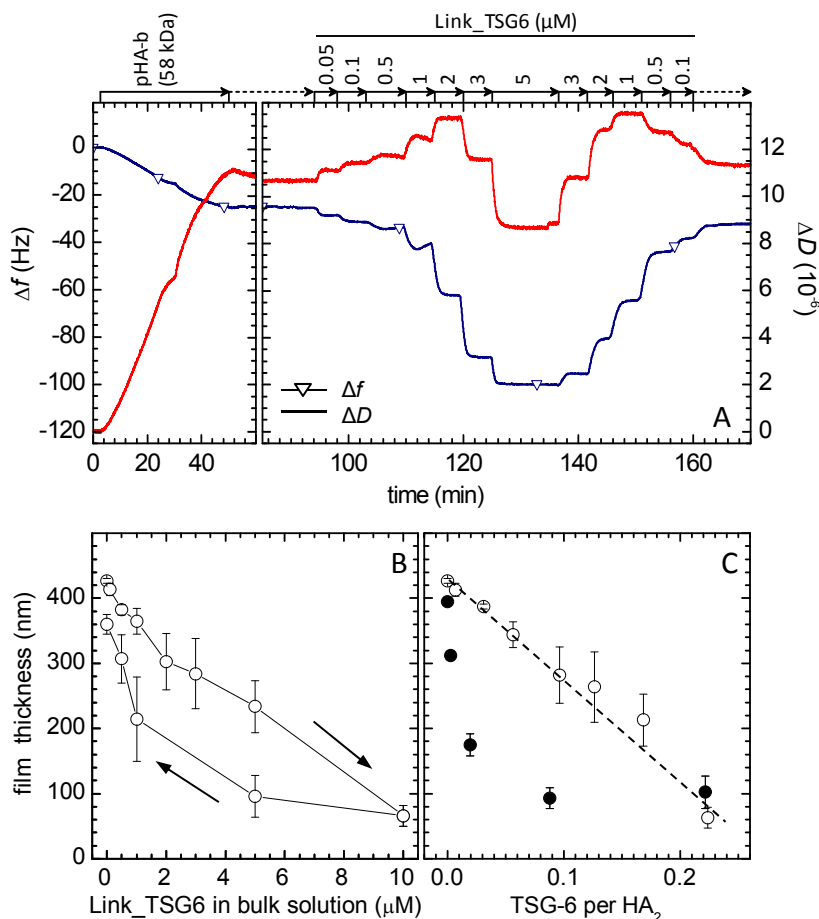


Fig. 3.10 **Rigidification and condensation of pHA films upon influx of Link\_TSG6.** (A) Titration curve by QCM-D on a pHA (58 kDa) film. Incorporation of Link\_TSG6 at bulk concentrations above 3  $\mu\text{M}$  results in a pronounced decrease in dissipation while the frequency continues to decrease, indicating rigidification of the film. A comparison of the responses upon increasing and decreasing bulk concentrations of Link\_TSG6, respectively, reveals hysteresis between the adsorption and desorption process. (B) Variations in the thickness of a pHA (1083 kDa) film as a function of Link\_TSG6 bulk concentration, determined by colloidal probe RICM. The Link\_TSG6 concentration was first increased and then decreased (indicated by *arrows*). The film thickness decreases with increasing Link\_TSG6 concentrations, in a partly reversible manner. Error bars are standard deviations for 10 independent measurements on the same surface. (C) Comparison of the condensation of 1083 kDa pHA films by rhTSG-6 (●; from Fig. 4B *inset*) and Link\_TSG6 (○; calculated from B, using Eq. 1 and the data for pHA in Table 3.1) as a function of the occupancy of HA. The film thickness scales approximately linearly with the Link\_TSG6/ $\text{HA}_2$ -ratio (*dashed line*). At equal occupancy, rhTSG-6 is a more potent cross-linker than Link\_TSG6.

An alternative route towards condensation and rigidification of HA films would be *via* the condensation and/or rigidification of individual HA chains. Recent molecular modelling studies on Link\_TSG6 suggest that HA chains bend locally in order to fit into the HA-binding site<sup>217</sup>, as is the case for CD44<sup>218</sup>, and such bending might induce an apparent chain shortening. The bending is pronounced; however, it is unclear at present whether alone it could explain the more than 6-fold decrease in film thickness that we have observed. It has

also been proposed that the dense coverage of an HA chain with many hyaladherins, like beads on a string, induces or stabilizes distinct HA conformations<sup>22</sup>, that are more condensed and/or more rigid than the free HA chain. An increase in chain rigidity would decrease the entropically driven stretching of the individual chains in the HA brush in the direction perpendicular to the surface<sup>211, 212</sup>, and might thereby induce re-arrangement into a thinner but more densely packed film. The final film density and the linear relationship between film thickness and occupancy would be consistent with such a scenario. Based on the present experimental data, it appears difficult to exclude any of the above mechanisms, which might even act jointly.

### 3.3.6 Link\_TSG6 induces total film collapse at low ionic strength.

Previous studies have shown that the affinity of Link\_TSG6 increases strongly with decreasing ionic strength, with sub- $\mu\text{M}$  affinities being reached at 5 mM sodium ions<sup>75, 214</sup>. To test how such an increase in affinity can influence the morphology of HA assemblies, we analyzed the Link\_TSG6 induced remodeling of films made from 58 kDa and 1083 kDa HA by QCM-D and by RICM, respectively, at low salt strength (Fig. 3.11).

Upon addition of 1  $\mu\text{M}$  Link\_TSG6 to a pHA film (58 kDa) in 5 mM NaCl, both frequency and dissipation decreased (Fig. 3.11 A). The decrease in dissipation, from  $9.3 \times 10^{-6}$  to  $1.5 \times 10^{-6}$ , was dramatic, and revealed total brush collapse, into a rigid and most likely very dense film. From the frequency response for the collapsed film, we can estimate a thickness of approximately 8 nm. Only minor responses were observed on a pHA free surface (Fig. 3.8B-C), confirming that the collapse is the result of the interaction between Link\_TSG6 and pHA. The dramatic film condensation and rigidification suggests that some form of cross-linking might be at play, although the exact mechanism remains obscure. The film remained fully collapsed after rinsing with 5 mM NaCl buffer. It recovered a swollen conformation at physiological ionic strength, confirming that the strong interaction and film collapse is salt dependent and at least partly reversible.

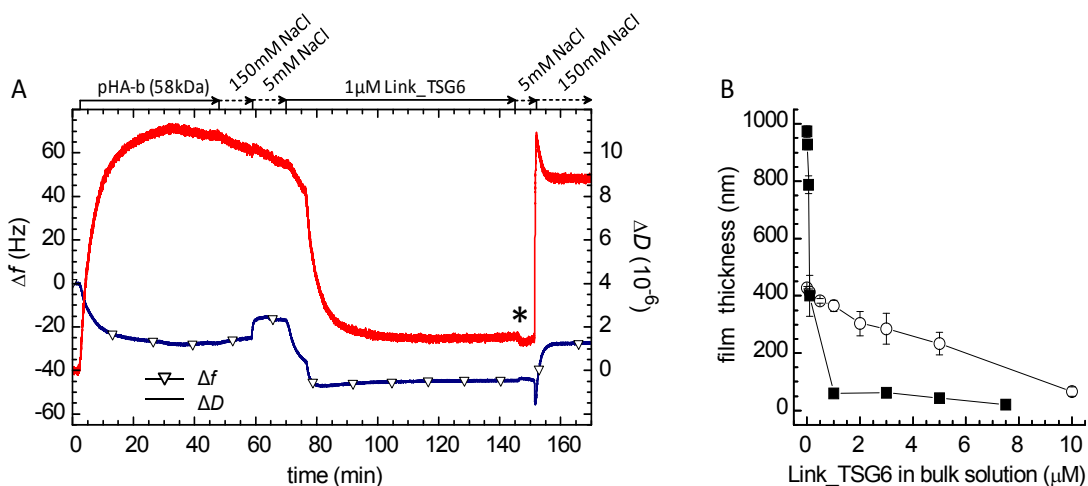


Fig. 3.11 **Link\_TSG6 induces total pHA film collapse at low ionic strength.** (A) Interaction assay by QCM-D on a pHA (58 kDa) film. The dramatic decrease in dissipation upon exposure to 1  $\mu\text{M}$  Link\_TSG6 in 5 mM NaCl indicates complete film collapse and rigidification. The film remains collapsed after rinsing in 5 mM NaCl (marked by an asterisk), but recovers partly in 150 mM NaCl. (B) Variations in the thickness of a pHA (1083 kDa) film as a function of the Link\_TSG6 concentration in solution at 5 mM NaCl, determined by colloidal probe RICM (■). A more than twofold decrease in film thickness was already observed at Link\_TSG6 concentrations of 0.1  $\mu\text{M}$ , and close to complete collapse is attained at 1  $\mu\text{M}$ . Data acquired in 150 mM NaCl under otherwise identical conditions is shown for comparison (○, from Fig. 7B). Note that the decrease in ionic strength induced a swelling of the protein free HA film, from  $450 \pm 20$  nm at physiological ionic strength to about 1  $\mu\text{m}$  in 5 mM NaCl, as a result of electrostatic repulsion between HA chains. Error bars are standard deviations for 10 independent measurements on the same surface.

Upon addition of 1  $\mu\text{M}$  Link\_TSG6 to a pHA film (58 kDa) in 5 mM NaCl, both frequency and dissipation decreased (Fig. 3.11 A). The decrease in dissipation, from  $9.3 \times 10^{-6}$  to  $1.5 \times 10^{-6}$ , was dramatic, and revealed total brush collapse, into a rigid and most likely very dense film. From the frequency response for the collapsed film, we can estimate a thickness of approximately 8 nm. Only minor responses were observed on a pHA free surface (Fig. 3.8B-C), confirming that the collapse is the result of the interaction between Link\_TSG6 and pHA. The dramatic film condensation and rigidification suggests that some form of cross-linking might be at play, although the exact mechanism remains obscure. The film remained fully collapsed after rinsing with 5 mM NaCl buffer. It recovered a swollen conformation at physiological ionic strength, confirming that the strong interaction and film collapse is salt dependent and at least partly reversible.

The results by RICM (Fig. 3.11 B) on pHA (1083 kDa) films correlated with the QCM-D data. Addition of a small concentration (0.1  $\mu\text{M}$ ) of Link\_TSG6 already decreased the thickness of the pHA (1083 kDa) film by more than 2-fold, and concentrations of 1  $\mu\text{M}$  induced a 15-fold reduction. Again, in 150 mM NaCl the brush thickness was partly restored, to about 65% of the thickness at that salt strength in the absence of protein.

These findings indicate that the affinity of Link\_TSG6 for HA at different salt strengths affects its ability to rigidify and condense HA films. Interestingly, the potency of Link\_TSG6 to condense HA at low ionic strength exceeds that of rhTSG-6 at physiological salt concentration. There is hence a notable correlation between the degree of pHA film condensation on the one hand, and the affinity between the TSG-6 constructs and HA on the other.

Table 3.1 Binding parameters for the incorporation of Link\_TSG6 and rhTSG-6 into oHA and pHA films, determined from titration curves as in Figs. 2 and 7.

	$K_{0.5}$ ( $\mu\text{M}$ )	$k_{\text{off}}$ ( $10^{-3}\text{s}^{-1}$ )	$f_r^{\text{a)}$	$k_{\text{on}}^{\text{b)}$ ( $10^3\text{M}^{-1}\text{s}^{-1}$ )	$n$	stoichiometry at $e^{\text{c)}$ maximal binding
in oHA films ( $\text{HA}_9$ )						
Link_TSG6	$6.1 \pm 2.5$	$28 \pm 3^{\text{c)}$	$\sim 86 \pm 3\%$	$4.6 \pm 2.4$	$0.9 \pm 0.2$	$1.3 \pm 0.3$ per $\text{HA}_9$
rhTSG-6	$1.2 \pm 0.4$	$4.3 \pm 1.7^{\text{d)}$ $0.052 \pm 0.018$	$43 \pm 9\%$ $57 \pm 9\%$	-	$2.7 \pm 0.8$	$2.7 \pm 0.8$ per $\text{HA}_9$
in pHA films (58 kDa HA)						
Link_TSG6	$5.5 \pm 0.6$	$23 \pm 8^{\text{c)}$	$\sim 79 \pm 4\%$	$4.2 \pm 1.9$	$1.2 \pm 0.2$	1 per $2.9 \pm 0.3$ $\text{HA}_2$
rhTSG-6	$0.79 \pm 0.17$	$2.8 \pm 2.0^{\text{d)}$ $0.14 \pm 0.07$	$8 \pm 1\%$ $92 \pm 1\%$	-	$2.8 \pm 0.5$	1 per $3.7 \pm 1.0$ $\text{HA}_2$

<sup>a)</sup>  $f_r = \Gamma_r / \Gamma_{\text{total}}$  with  $\Gamma_{\text{total}} = \Gamma_r^{(1)} + \Gamma_r^{(2)} + \Gamma_{\text{ir}}$  is the fraction of TSG-6 that was found to dissociate with the respective  $k_{\text{off}}$  (see Eqs. 2a-b); <sup>b)</sup> Determined from  $K_{0.5} = K_D = k_{\text{off}}/k_{\text{on}}$  for non-cooperative binding ( $n \approx 1$ ); <sup>c)</sup> Determined with Eq. 2a; <sup>d)</sup> Determined with Eq. 2b for desorption processes of 1 h duration and with  $\Gamma_{\text{ir}}$  set to 0; <sup>e)</sup> Determined from  $\Gamma_{\text{max}}$  in Eq. 1, and the surface density of immobilized HA. Errors correspond to experimental uncertainties and variations across two to three measurements.

## 3.4 Discussion

Using a novel experimental platform, based on films of end-grafted HA, in conjunction with a toolbox of surface-sensitive characterization techniques, we have investigated the interaction of TSG-6 with HA in an ultrastructural context.

The experimental platform is interesting for several reasons. First, the morphology and quantity of immobilized HA is well-controlled and non-specific binding to the underlying surface is low. These are prerequisites for detailed and quantitative binding studies. Second, the binding behavior on both oligomeric and polymeric HA can be interrogated on the same immobilization platform and directly compared. Third, with a toolbox of surface-sensitive characterization techniques, the amount and kinetics of protein binding can be correlated with changes in the physicochemical properties, such as the dimensions, mechanical properties and morphology, of the resulting HA ultrastructures.

Key results of our study are the direct experimental evidence that full-length TSG-6 alone can cross-link HA (Fig. 3.5), and that the cross-linking induces condensation of HA at what are likely to be physiologically relevant concentrations (Fig. 3.6). Furthermore, our study provides novel and quantitative insights into the interaction between TSG-6 and HA. The cooperative binding of rhTSG-6 to both oHA and pHA (Fig. 3.3), and its supra-stoichiometric binding to oHA (Table 3.1) provide evidence for HA-induced protein oligomerization.

The HA-binding behavior of Link\_TSG6 at physiological ionic strength is distinctly different from that of rhTSG-6: binding is both simpler and weaker. The lack of positive cooperativity might well explain the weaker binding of Link\_TSG6. We can though not rule out that, in addition to the Link module, some other part of the TSG-6 protein makes a contribution to HA binding. This could occur in a number of ways, for instance, via a direct interaction of a neighboring region of the protein with the bound HA (e.g. an extension of the Link module binding groove<sup>75, 216</sup> or via an allosteric effect on the affinity of the Link module (e.g. stabilizing the Link module in its bound conformation<sup>75, 217</sup>).

Although less potent than rhTSG-6, Link\_TSG6 retains the ability to condense and rigidify HA films. At present, the structures of the HA-induced rhTSG-6 oligomers and the mechanism underlying Link\_TSG6-mediated HA-film condensation and rigidification remain unclear. The observed Hill coefficients above 2 on oHA and pHA films, and the maximal binding stoichiometry above 2 on oHA films (Table 3.1) indicate that rhTSG-6 must form oligomers that are larger than dimers. Small angle X-ray scattering data suggested the formation of rhTSG-6 dimers (Fig. 3.5C) as well as larger species in the presence of HA octasaccharides in solution<sup>209</sup>, and it is possible that a spectrum of oligomer sizes is also present in our HA films.

Our observations that rhTSG-6 binds HA more strongly than Link\_TSG6 (Table 3.1), and that both protein constructs can be fully released from HA by a dissociating agent (Fig. 3.4 and

Fig.3.9A-B) contrast an earlier study<sup>165</sup> that had reported similar binding properties and non-dissociable HA-TSG-6 complexes for full length TSG-6 and the TSG-6 Link module in plate binding assays with immobilized HA. These assays, however, were performed at a non-physiological ionic strength of 500 mM NaCl. This, and the limited control on the immobilization of analytes in these plate binding assays, might explain the discrepancies with our study.

### 3.4.1 Implications for the function of TSG-6 in vivo.

For pHA films containing a concentration of approximately 1 mg/ml HA, we observed significant condensation already at 0.16  $\mu$ M rhTSG-6, and maximal condensation was attained at 0.7  $\mu$ M (Fig. 3.6). These concentrations are likely to be physiologically relevant. For example, HA is present in synovial fluid and umbilical cord at  $>1$  mg/ml<sup>219</sup> and is also found at high concentrations in other tissues such as skin ( $\sim 0.2$  mg/ml<sup>219</sup>) and the expanded cumulus matrix surrounding the mature oocyte ( $\sim 0.2$ - $0.5$  mg/ml<sup>220</sup>). While it has been suggested that TSG-6 is present at up to  $\sim 0.6$   $\mu$ M in synovial fluids from patients with inflammatory arthritis (i.e. based on data from Western blots<sup>71</sup>), more recent ELISA analysis suggests a maximum of  $\sim 3$  nM<sup>221</sup>. However, given that the likely source of this protein is synovium and cartilage<sup>222</sup>, its local concentration in certain regions of these tissues is likely to be much higher than this (e.g. in the HA-containing pericellular matrix of chondrocytes that are synthesizing TSG-6). Similarly, there is likely to be a high local concentration of TSG-6 in the HA-rich cumulus matrix formed during cumulus-oocyte-complex (COC) expansion, prior to ovulation<sup>120, 121</sup>. Thus, the effects that we observed *in vitro* may have physiological relevance. The TSG-6 mediated cross-linking has two major consequences, condensation and rigidification, where both might be functionally important.

The high affinity of TSG-6 for HA and the ensuing cross-linking, might lead to the formation of rather dense and spatially confined HA matrices. For example, Simpson et al.<sup>185</sup> have shown that the coordinated expression of HA and TSG-6 during fibroblast to myofibroblast differentiation is necessary for the formation of a pericellular coat during normal wound healing and that this diminishes with age. Furthermore, it might be envisaged that a TSG-6-mediated contraction of the chondrocyte pericellular matrix during inflammation might serve to promote matrix remodeling that could contribute to its chondroprotective properties<sup>213</sup>. Such dense matrices could not only locally sequester TSG-6, but might also enhance the retention of HA and matrix-associated molecules. Since the cross-links formed between TSG-6 and HA are reversible, and the HA chains flexible, it is likely that such matrices can dynamically adopt various shapes as a function of external cues. Upon uniaxial stretching, for example, highly elongated ‘fiber like’ assemblies with particular mechanical properties might form<sup>26</sup>. Extracellular matrix rigidity has emerged as an important regulator of cellular behavior<sup>223-225</sup>. Thus, TSG-6 induced modulation of the

local mechanical properties of the extracellular space might directly affect the phenotype of adjacent cells.

### 3.4.2 Relevance of the cross-linking of HA-rich pericellular coats for leukocyte homing.

Lesley and coworkers have shown that decoration of HA with either Link\_TSG6 or rhTSG-6 promotes adhesion and rolling of CD44+ T-lymphocytes, and suggested that cross-linked HA/TSG-6 complexes might be the adhesion-promoting agent<sup>26, 194</sup>. Our direct evidence for TSG-6 mediated cross-linking and condensation (i.e. the formation of dense HA-networks) supports this hypothesis. Cross-linking likely increases the valency of interactions between HA and the cell surface. For example, rigidifying HA might reduce the entropic cost of cell surface receptor binding<sup>226</sup>. It might also trigger a re-distribution/clustering of cell surface receptors<sup>227</sup>, or promote their conformational up-regulation<sup>218</sup>. Interestingly, condensation occurs gradually with increasing rhTSG-6 concentration, from 0.1 to 0.7  $\mu$ M (Fig. 3.6), and local cross-linking of HA in the endothelial matrix by TSG-6 might hence be a dynamic regulator of the inflammatory response<sup>26, 194</sup>.

It should be noted that other hyaladherins or TSG-6 binding proteins<sup>37, 201</sup> might alter the HA cross-linking activity of TSG-6, in subtle ways that remain to be elucidated (Chapter 4-5). A case in point is the catalytic action of TSG-6 in mediating covalent transfer of heavy chains from inter- $\alpha$ -inhibitor (I $\alpha$ I) onto HA, which leads to a different mechanism of HA cross-linking to that described here<sup>26, 94, 98</sup>. In this regard, the heavy chain transfer activity of TSG-6, but not the formation TSG-6/HA complexes, leads to a pro-migratory phenotype of proximal tubular epithelial cells<sup>184</sup>. Also, the cross-linking of HA in the COC matrix was shown to involve at least two proteins, I $\alpha$ I and PTX3, in addition to TSG-6<sup>20, 37, 41, 102, 122, 220</sup>, in a way that remains only partly understood.

On the other hand, the binding of TSG-6 to other glycosaminoglycans (chondroitin-4-sulfate, heparin/heparan sulfate) and highly hydrated proteoglycans, such as aggrecan and versican<sup>182, 196, 200, 201, 203</sup> suggests that TSG-6's cross-linking activity might not be restricted to HA. In this regard, it was shown previously that TSG-6 could promote the interaction of fibronectin with thrombospondin-1, likely by bridging between these two proteins via interactions mediated by its CUB\_C domain and Link module, respectively<sup>193</sup>. By simultaneously interacting with and cross-linking various components of pericellular and extracellular matrices, TSG-6 might play a central role as a matrix re-organizer.





## 4 Inter- $\alpha$ -inhibitor impairs TSG-6 induced hyaluronan cross-linking

---

Under inflammatory conditions and in the matrix of the cumulus-oocyte complex (COC), the polysaccharide hyaluronan (HA) becomes decorated covalently with heavy chains (HCs) of the serum glycoprotein inter- $\alpha$ -inhibitor (I $\alpha$ I). This alters the functional properties of the HA as well as its structural role within extracellular matrices. The covalent transfer of HCs from I $\alpha$ I to HA is catalyzed by tumor necrosis factor-stimulated gene-6 (TSG-6) but TSG-6 is also known as a HA cross-linker that induces condensation of the HA matrix. Here, we investigate the interplay of these two distinct functions of TSG-6 by studying the ternary interactions of I $\alpha$ I and TSG-6 with well defined films of end-grafted HA chains. We demonstrate that TSG-6 mediated cross-linking of HA films is impaired in the presence of I $\alpha$ I, and that this effect suppresses the TSG-6-mediated enhancement of HA binding to CD44 positive cells. Furthermore, we find that the interaction of TSG-6 and I $\alpha$ I in the presence of HA gives rise to two types of complexes that independently promote the covalent transfer of heavy chains to HA. One type of complex interacts very weakly with HA and is likely to correspond to the previously reported covalent HC•TSG-6 complexes. The other type of complex is novel and binds stably but non-covalently to HA. Prolonged incubation with TSG-6 and I $\alpha$ I leads to HA films that contain, in addition to covalently HA-bound HCs, several tightly but non-covalently bound molecular species. These findings have important implications for understanding how the biological activities of TSG-6 are regulated, such that the presence or absence of I $\alpha$ I will dictate its function.

## 4.1 Introduction

Hyaluronan (HA) is the main non-protein component of the extracellular matrix of vertebrates, and plays an important role in many physiological and pathological processes, such as inflammation and ovulation<sup>57, 228</sup>. HA is a high molecular weight glycosaminoglycan composed of repeating disaccharides of N-acetylglucosamine (GlcNAc) and glucuronic acid. The linear polysaccharide is flexible and can adopt various conformations.

Proteins that bind to hyaluronan can drive conformational changes and thereby remodel the morphology and physico-chemical properties of HA-rich extracellular matrices<sup>26, 210, 229</sup>. For example, HA can be modified with heavy chains (HCs) of inter- $\alpha$ -inhibitor (I $\alpha$ I). The ensuing covalent HA•HC complex is also known as serum-derived hyaluronan-associated protein (SHAP) complex<sup>96, 97</sup>.

This modification is the only naturally occurring covalent modification of HA known to date. It was shown to be critical for the expansion of the cumulus-oocyte complex (COC) matrix around oocytes<sup>35, 43</sup>. Correct assembly of the HA matrix around oocytes is crucial for successful ovulation and fertilization<sup>35, 37, 38, 43, 109, 115</sup>. HA•HC complexes were also found under inflammatory conditions in synovial fluid of arthritis patients<sup>97, 230</sup>. HA•HC extracts from rheumatoid synovial fluid can undergo gelation at pH 4.5<sup>231</sup>, and can form macromolecular aggregates that are more adhesive for leukocytes via their enhanced interaction with CD44<sup>97, 232</sup>. Airway smooth muscle cells in response to poly(I:C) were also demonstrated to produce HA•HC cable like complexes with enhanced leukocyte binding<sup>233</sup>. It has been hypothesized that HCs mediate cross-linking of HA and thereby induce the observed changes in the morphology, rheological and cell-binding properties of HA assemblies<sup>82, 97, 234</sup>.

HCs are subunits of I $\alpha$ I, a serum proteoglycan that consists of heavy chain 1 (HC1), heavy chain 2 (HC2) and bikunin, a serine protease inhibitor, held together by a chondroitin-4-sulphate (C4S) chain<sup>83</sup>. Each HC is linked to C4S *via* an ester bond between the C-terminal Asp residue of the HC and the C-6 of N-acetylgalactosamine in C4S, which is itself attached to the bikunin core protein through a standard glycosaminoglycan linkage<sup>235</sup>.

The transfer of HCs from I $\alpha$ I onto HA is mediated by tumor necrosis factor-stimulated gene-6 (TSG-6) in two sequential transesterification reactions<sup>98</sup>. Firstly a covalent complex is formed between TSG-6 and either HC1 or HC2<sup>86, 236, 237</sup> followed by the transfer of the HC from this HC•TSG-6 intermediate onto the C-6 hydroxyl of GlcNAc of HA<sup>96</sup>. Here TSG-6 acts as a catalyst since its release from the HC1•TSG-6 or HC2•TSG-6 complexes allows it to be recycled for a new reaction with I $\alpha$ I<sup>236</sup>.

There is evidence that intact I $\alpha$ I (or I $\alpha$ I-related species that contain at least one ester bond<sup>238</sup>) is required for this reaction<sup>35, 239</sup>. Bikunin null mice, which have impaired female fertility<sup>35, 40</sup>, while expressing HCs did not assemble an I $\alpha$ I molecule and failed to form HA•HC complexes<sup>35</sup>; ovulation/fertilization was rescued by intraperitoneal administration of

purified IaI, but not bikunin alone<sup>35</sup>. Furthermore, partial proteolysis of bikunin did not influence the transfer of HCs onto TSG-6<sup>239</sup>, indicating that the function of bikunin is to provide the C4S chain where ester bonds with HCs can be formed; the energy stored in the ester bonds (during biosynthesis) is used to drive subsequent transfer of HCs onto TSG-6, and ultimately their attachment to HA<sup>236</sup>. Both of these transesterification steps require the presence of divalent cations<sup>236, 239</sup>, for which Ca<sup>2+</sup> and Mg<sup>2+</sup>/Mn<sup>2+</sup> ions have been implicated as being involved<sup>189, 236</sup>.

In addition to its enzymatic function, TSG-6 is well established as an HA-binding protein<sup>68, 77</sup>. It is composed mainly of two contiguous domains<sup>240</sup>: a Link module, where the HA-binding groove is located<sup>76, 241, 242</sup>, and a CUB module (Protein Data Bank ID: 2WNO)<sup>80</sup>. Recently, we have shown that full length TSG-6 alone can cross-link HA, and that TSG-6 oligomers that are induced by the binding of TSG-6 to HA constitute the cross-linking entities<sup>210</sup>. We also showed that the TSG-6-mediated cross-linking can induce a drastic condensation of an HA network.

Considering that both TSG-6 and HA can participate in two distinct processes – HC transfer on the one hand and TSG-6 mediated HA cross-linking on the other – raises the question of how these two processes influence each other. This is perhaps of particular relevance for COC matrix expansion. Here the expression of TSG-6 mRNA is detectable within 2 hours after the induction of ovulation, in cumulus and granulosa cells in ovarian follicles harbouring an oocyte<sup>31, 32</sup>, which is a similar timescale to the initiation of HA biosynthesis<sup>28</sup>. IaI is thought to diffuse into the follicle only after initiation of ovulation. COC matrix-associated IaI was reported to increase over time, and HA•HC complexes are typically detected after 6 hours<sup>116-119</sup>. *TSG-6*<sup>-/-</sup> mice (like bikunin null animals<sup>35, 40</sup>) were unable to assemble a functional COC matrix and had a phenotype that correlates with the total absence of HA•HC complexes<sup>43</sup>; however, administration of recombinant TSG-6 was able to rescue COC matrix expansion.

To directly study, how the presence of IaI affects the binding of TSG-6 to HA, and to understand how the HA-cross-linking and enzymatic activities of TSG-6 influence each other, we designed *in vitro* binding assays in which TSG-6 and/or IaI can interact with well-defined films of HA in controlled sequence and concentrations. We demonstrate that the HA-binding properties of TSG-6 are impaired in the presence of IaI, and as a consequence the TSG-6-mediated condensation of HA does not occur. We also provide novel insight into the kinetics of the TSG-6-mediated enzymatic transfer of HCs from IaI to HA, and show that HA•HC complex formation is accompanied by the incorporation of tightly but non-covalently bound protein material into the HA matrix.

## 4.2 Experimental procedures

### **Protein and hyaluronan preparations.**

I $\alpha$ I was purified from human serum as described previously<sup>83</sup>. Full length recombinant human TSG-6 (rhTSG-6; 30.1 kDa) was expressed in *Drosophila* Schneider 2 cells and purified as described previously<sup>243</sup>.

Recombinant human heavy chains 1, 2 and 3 (rHC1, rHC2, rHC3) were expressed by David Briggs (University of Manchester) in *E. coli* “SHuffle” cells (New England Biolabs). Codon optimized genes encoding the mature protein sequences (rHC1 – Uniprot P19827 amino acid residues 35-672; rHC2 – Uniprot P19823 55-702; rHC3 – Uniprot Q06033 35-651) were cloned into pET-45b+, using BamHI and HindIII restriction sites, by Genscript USA, Inc. Transformed cells were cultured in Terrific Broth at 30°C and protein expression was induced by addition of IPTG to 0.5 mM at an OD<sub>600</sub> of 0.6. Cells were harvested at 16 h post-induction, at either 30°C (rHC1 and rHC3) or 20°C (rHC2), and lysed by sonication. Protein purification was achieved by Ni<sup>2+</sup> ion affinity chromatography, followed by HiTrap Heparin affinity chromatography (rHC1 and rHC2) or anion exchange (rHC3), and size exclusion chromatography on a Superdex-200 column. Purity was assayed by SDS-PAGE, and electrospray ionization mass spectrometry (see Fig. S6).

Lyophilized HA, biotinylated at its reducing end and with well-defined molecular masses of 1083±53 kDa or 837±54 kDa (i.e. two different batches of Select-HA B1000) was purchased from Hyalose (Oklahoma City, OK, USA). For reconstitution, HA was taken up in ultrapure water at a stock concentration of 1 mg/ml, gently shaken over night, aliquoted, and stored at -20°C.

A ‘hepes’ buffer (150 mM NaCl, 10 mM HEPES at pH 7.4, 3 mM NaN<sub>3</sub>, 2 mM CaCl<sub>2</sub>, 5 mM MgCl<sub>2</sub>, in ultrapure water) was used throughout all measurements. Protein and HA solutions at their final concentrations were prepared in this buffer.

### **Assembly of films of end-grafted HA on a biotin-functionalized surface coating.**

HA films were prepared as described previously<sup>210</sup> (Fig. 1A). Briefly, a dense streptavidin (SAv) monolayer was formed by exposure of 50 µg/ml SAv (30 min) to a gold surface that had been functionalized with a biotinylated oligoethylene glycol (OEG) monolayer. Biotinylated HA was then grafted to the SAv monolayer by incubation of 10 µg/ml HA solution.

The HA grafting density was set to 30±10 ng/cm<sup>2</sup> by adjusting the incubation time in ellipsometry measurements. This corresponds to a mean anchor distance of 81±14 nm between neighboring HA grafting points. End-grafted HA at this grafting density forms a so-called brush of entangled HA chains that are weakly stretched in the direction normal to the surface<sup>60, 163</sup>. For polymer brushes, the mesh size in the film is predicted to be as large as the

mean anchor distance<sup>244</sup>. Therefore, molecules such as TSG-6 and IαI should be able to diffuse rapidly in and out of the HA film.

In the measurements by colloidal probe reflection interference contrast microscopy (RICM), the incubation time was kept at two hours. From the measured film thickness, we estimate the areal surface density to be  $50 \pm 15 \text{ ng/cm}^2$ <sup>60</sup>. To release non-covalently bound material, the HA film was treated with 2 or 8 M guanidine hydrochloride (GuHCl) for 5 min. The HA films are stable to this treatment<sup>210</sup>.

#### **Co-incubation assay.**

IαI and TSG-6 were pre-mixed at concentrations of  $9.8 \mu\text{M}$  and  $3.3 \mu\text{M}$ , respectively, at  $23^\circ\text{C}$  for desired times (1 to 120 min). The pre-mixed solution was then injected into the measurement cell that contained buffer and the HA film. Rapid mixing generated final concentrations in the soluble phase of  $1 \mu\text{M}$  IαI and  $0.3 \mu\text{M}$  TSG-6. Alternatively, IαI and TSG-6 were sequentially injected into the measurement cell at the same final concentrations. In this case, we refer to 0 min of pre-mixing time. In all co-incubation assays, the HA grafting density was fixed to  $33 \pm 10 \text{ ng/cm}^2$ .

#### **In situ ellipsometry.**

Ellipsometry measures changes in the polarization of light upon reflection at a planar surface. We employed ellipsometry *in situ* on gold-coated silicon wafers as substrates that were installed in a custom-built open cuvette with continuously stirred sample solution ( $\sim 150 \mu\text{l}$ ), to quantify adsorbed biomolecular masses in a time-resolved manner<sup>245</sup>.

#### **Surface plasmon resonance (SPR).**

SPR data were acquired by David Briggs (University of Manchester) using a BiaCore 3000 (GE Healthcare). rHC1, rHC2 or rHC3 was immobilized at a concentration of  $10 \mu\text{g/ml}$  in either 10 mM Na-Acetate pH 5.5 (rHC1 and rHC2) or pH 4.0 (rHC3) to a C1 chip (GE Healthcare) using Sulfo-NHS/EDC amine coupling. Immobilization contact times were adjusted to give approximately 1000 response units (RU) for all 3 proteins. Experiments were conducted in HEPES-buffered Saline with 0.5% (v/v) Tween-20 (HBS-T) either with 10 mM EDTA added or 1 mM each of  $\text{CaCl}_2$  and  $\text{MgCl}_2$ . All experiments were conducted with a flow rate of  $50 \mu\text{l/min}$ . TSG-6 was used as analyte at concentrations ranging from 6.25 to 200 nM. Data were fitted to a 1:1 Langmuir model using BiaEval software.

#### **Colloidal probe reflection interference contrast microscopy (RICM).**

This microinterferometric technique measures the height at which a colloidal probe hovers above a transparent planar substrate with a resolution of a few nanometers over a range of about  $1 \mu\text{m}$ . RICM was used to measure the thickness of HA films that were assembled on gold-coated glass cover slips, using a custom-built measurement cell<sup>210, 246</sup>.

### **Western blotting.**

Western blot analysis was performed by Viranga Tilakaratna (University of Manchester). Samples of ~150  $\mu$ l volume were extracted from the ellipsometry cuvette, and stored frozen in aliquots of 50  $\mu$ l until further use. One aliquot per lane was used for Western blot analysis; protein was recovered using 10  $\mu$ l of StrataClean resin (Agilent Technologies) according to manufacturer's instructions, and following a wash with water the resin was analyzed by SDS-PAGE on 4-12% (w/v) NuPAGE Bis-Tris polyacrylamide gels (Life Technologies) after boiling in SDS loading buffer containing  $\beta$ -mercaptoethanol. A rabbit anti-human polyclonal antibody against I $\alpha$ I (DAKO), 1:20,000 dilution, was used to screen for I $\alpha$ I and its subunits, and the anti-TSG-6 antibody RAH-1<sup>247</sup> at 1:1000 was used to detect TSG-6; bands were visualized with a goat-anti-rabbit LI-COR Odyssey Infrared (IR) secondary antibody using a Li-Cor Odyssey imaging system. As a control 2  $\mu$ g TSG-6 was incubated with 8  $\mu$ g I $\alpha$ I and 1  $\mu$ g HA<sub>14</sub> in 20 mM HEPES-HCl (pH 7.5), 150 mM NaCl and 5 mM MgCl<sub>2</sub> in a total volume of 25  $\mu$ l for 2 h at 4°C. For TSG-6 blots 1.25  $\mu$ l of the reaction mix was used per lane (to get approximately 100 ng of TSG-6), and for I $\alpha$ I blots the reaction mix was diluted 1:10 and 0.78  $\mu$ l was used per lane (to get approximately 25 ng of I $\alpha$ I).

### **Fluoresceinamine labeling of HA.**

Fluorescently labeled HA was produced by Simon Foulcer (University of Manchester) as essentially as described by De Belder and Wik<sup>248</sup>. In brief, 10 mg of polymeric HA (HyluMed Medical Grade; Genzyme Corporation; ~1.5 MDa) was resuspended in 8 ml of H<sub>2</sub>O by incubating at 4°C overnight and then added to 4 ml DMSO. Fluoresceinamine (5 mg) was combined with 5  $\mu$ l acetaldehyde, 5  $\mu$ l cyclohexyl isocyanide and 300  $\mu$ l DMSO and then combined with the HA solution, and gently stirred at room temperature for 5 h. The reaction mixture was transferred to 160 ml of ice cold ethanol and the labelled HA precipitated by adding ~2 ml saturated NaCl solution. The precipitate was collected by centrifugation (3000 g, 10 min), resuspended in 10 ml H<sub>2</sub>O and the ethanol precipitation and centrifugation steps repeated. The fluorescein-labelled HA (fl-HA) was resuspended in 20 ml H<sub>2</sub>O and dialysed overnight against 2 l H<sub>2</sub>O containing 0.05% (w/v) sodium azide.

### **Flow cytometry of HA-binding to CD44+ cells.**

All flow cytometry experiments were performed by Simon Foulcer (University of Manchester) with a CyAn ADP analyser coupled with Summit v4.3 software (Beckman Coulter, Fullerton, CA). Forward scatter gain was set to 3.5 and the FITC voltage gate set to 530 V. The level of fluorescence was quantified as the mean fluorescence intensity of ~10000 cells.

AKR1 and AKR1/CD44+ cell lines were used for all experiments<sup>249, 250</sup>. The AKR1 cell line is a CD44-negative T lymphoma (purified from the AKR/J mouse) that does not bind

HA. The AKR1/CD44+ cells are a transfectant of the AKR1 cells containing cDNA encoding the CD44.1 allele resulting in CD44 expression and constitutive HA binding properties.

The expression of CD44 was confirmed here using FITC-conjugated IM7 antibody (1:1000; Abcam); all incubations were performed at 37°C and cells ( $0.5 \times 10^6$ ) were washed 2-3 times with PBS between incubations and prior to flow cytometric analysis. Binding of fl-HA to AKR1/CD44+ cells (and AKR1 cells) was assessed by incubating them together with increasing concentrations of fl-HA for 120 min; competition with unlabelled HA showed that there was only ~4% internalization of fl-HA (at 1 µg/ml) by AKR1/CD44+ cells after 120 min incubation (data not shown). The enhancing effect of TSG-6 on HA binding to CD44 (reported in <sup>251</sup>) was confirmed by co-incubating 0-10 µg/ml fl-HA with 0.25 µM TSG-6 prior to adding to the CD44+ cells.

AKR1/CD44+ cells were also incubated with 1 µg/ml fl-HA in the absence or presence of 1 µM IαI and/or 0.3 µM TSG-6, where these incubations were done in various orders/combinations; i.e. to test the effect of IαI on the TSG-6-mediated enhancement of HA binding to CD44.



## 4.3 Results

### 4.3.1 I $\alpha$ I partially impairs TSG-6 binding to HA

To understand how the HA-binding properties of TSG-6 correlate with its ability to form a covalent complex with the HCs of I $\alpha$ I and transfer these onto HA, we designed a sequential incubation assay (Fig.4.1). Firstly, a film of end-grafted HA of molecular mass of either 1083 or 837 kDa was assembled on a solid support (Fig.4.1A), as described earlier<sup>210</sup>. Secondly, the film was loaded with TSG-6, excess TSG-6 was removed by rinsing in buffer and then I $\alpha$ I was exposed to the film. Changes in the areal surface density of HA and proteins during the assay were monitored by *in situ* ellipsometry.

We exposed the HA film to TSG-6 at a bulk concentration of 0.3  $\mu$ M (Fig.4.1B, at 36 min) until equilibrium was attained. The dissociation rate of TSG-6 after removal of excess TSG-6 from solution was relatively slow, and in good quantitative agreement with the dissociation rate that we had previously reported for TSG-6 in a saturated film<sup>210</sup>.

Importantly, subsequent addition of 1  $\mu$ M I $\alpha$ I (Fig.4.1B, at 122 min) strongly enhanced TSG-6 desorption: comparison of the release rates just before and after I $\alpha$ I injection revealed an 11-fold enhancement. A control measurement showed that I $\alpha$ I alone does not bind to HA (Fig.4.1C). Hence, the formation of a complex between I $\alpha$ I and TSG-6 must be responsible for the displacement of TSG-6 from HA.

The I $\alpha$ I-induced displacement of TSG-6 was found to terminate within 10 min (Fig.4.1B). Remarkably, a sizeable amount of protein, corresponding to about one third of the maximally incorporated TSG-6 mass, remained bound to the HA film after exposure to I $\alpha$ I. In a similar experiment (not shown), we incubated with 0.5 instead of 1  $\mu$ M I $\alpha$ I, yet found the remaining fraction to be similar; in addition, a subsequent increase of the I $\alpha$ I concentration to 1  $\mu$ M did not lead to any further release of material. This indicates that the protein remaining in the film is not simply the result of an equilibrium distribution of TSG-6 between surface-bound HA and I $\alpha$ I in the solution phase. Further controls showed that neither TSG-6 alone<sup>210</sup> nor TSG-6 in a mixture with I $\alpha$ I (Fig. S1) bound in appreciable amounts to the SAV-coated passivation layer on which the HA films were immobilized. The retained protein fraction, therefore, must be the result of a genuine interaction of TSG-6 with HA, and possibly even with I $\alpha$ I, that is distinct from the HA/TSG-6 interaction that can be impaired by I $\alpha$ I.

In yet another similar experiment (Fig. S2), we found that the protein fraction that was retained 10 min after the start of incubation with I $\alpha$ I could be completely eluted with GuHCl. Because the HA film itself is resistant to GuHCl<sup>210</sup>, we conclude that all bound protein was non-covalently bound at this stage. At present, we do not know if this non-covalently bound material contains exclusively TSG-6 or also I $\alpha$ I (or its subunits).

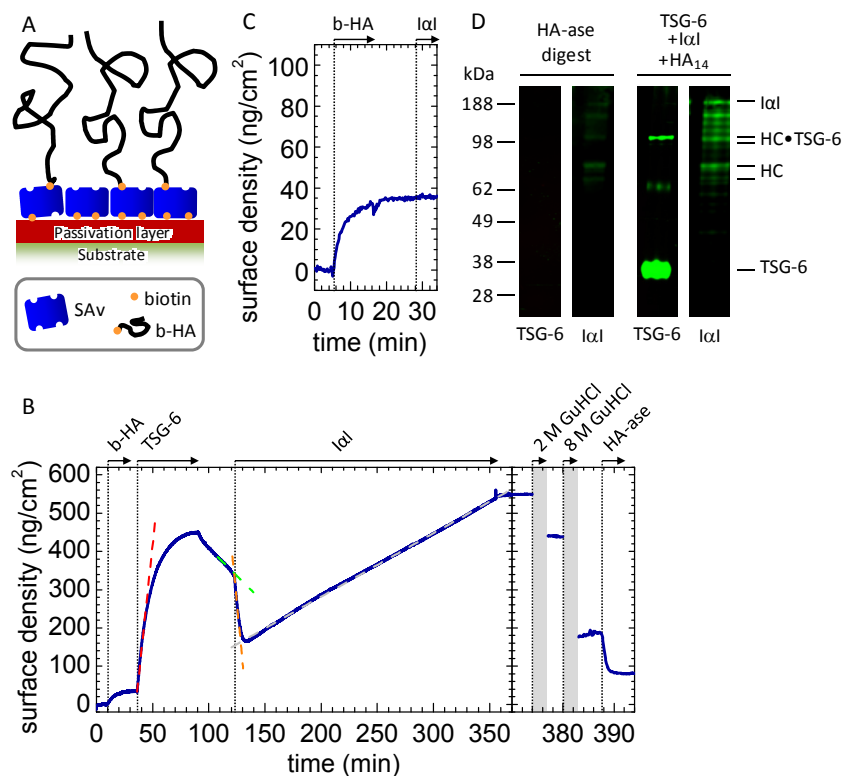


**Fig. 4.1 IαI partially impairs TSG-6 binding to HA.** (A) Architecture of end-grafted hyaluronan films. A biotin-functionalized passivation layer was immobilized on a gold support, followed by the formation of a dense streptavidin (SAv) layer. HA chains were grafted via a biotin functionality at their reducing end to SAv. The thickness of the passivation layer and the size of SAv are drawn to scale; the thickness of the HA brush and the mean distance between HA anchors are reduced by 10 to 20-fold for illustrative purposes. (B) Sequential incubation assay by ellipsometry. The start and duration of each incubation step with different samples are indicated with solid arrows; after each incubation step, the solution phase was replaced by buffer. First, a biotinylated HA (b-HA, 837 kDa) film was formed and incubated with 0.3 μM TSG-6. After binding equilibrium had been established, excess TSG-6 was removed from the bulk solution. Addition of IαI at 1 μM strongly enhanced TSG-6 displacement from the HA film (dashed lines are linear fits to the data at selected times). A fraction of 38% of the TSG-6 mass was not displaced by IαI, and prolonged incubation led to renewed incorporation of protein material at a constant rate. Proteins were eluted by sequential incubation with 2 and 8 M GuHCl (shaded in grey, elution process not monitored by ellipsometry), and the remainder of the film digested with HA-ase. (C) Control showing that 1 μM IαI does not bind to HA films. (D) Western blots of the HA-ase digest. No TSG-6 was detected. The strongest bands for IαI, at around 80 kDa, are assigned to HC1 and HC2. Based on the ellipsometry data, the amount of total digested protein material used per lane was estimated to be around 10 ng. The control reaction mix of TSG-6, HA14 and IαI is expected to contain a total amount of 100 ng TSG-6 and 25 ng IαI,

and the detection limits are estimated to be around 5 ng for TSG-6 and 0.5 ng for I $\alpha$ I. Western blots were provided by V. Tilakaratna & A. J. Day (Manchester University).

### 4.3.2 Retained TSG-6 promotes slow incorporation of I $\alpha$ I (or its subunits).

Remarkably, the areal surface density increased again upon prolonged incubation with I $\alpha$ I (Fig.4.1B, beyond 132 min), at a rate of 1.7 ng/cm<sup>2</sup>/min. Compared to the initial binding of TSG-6 alone (Fig.4.1B, at 36 min), the increase was about 20-fold slower. Moreover, the binding rate was constant throughout the remaining incubation time of almost 4 h.

All incorporated protein material was stably bound: no desorption was observed after rinsing in buffer (

Fig. 4.1B, at 355 min). In the presence of 2 M GuHCl (at 374 min), about 20% of the total protein mass could be eluted, whereas exposure to 8 M GuHCl (at 380 min), resulted in the release of another 55%. This indicates that a large fraction of the protein material was very tightly bound albeit not covalently. A significant fraction resisted even 8 M GuHCl, suggesting that some material ultimately becomes covalently incorporated. The remaining film could be partially digested with *Streptomyces* hyaluronidase (HA-ase;

Fig. 4.1B, at 388 min), confirming that (at least the major proportion of) the GuHCl resistant material is bound to HA.

The amount of non-covalently bound material at the end of the incubation process was larger than the total amount of bound material shortly after the start of incubation with I $\alpha$ I. This implies that at least two different interactions must contribute to the linear adsorption rate, one leading to covalently and the other to tightly but non-covalently incorporated material.

TSG-6 is known to catalyze the transfer of HCs from the C4S moiety of I $\alpha$ I to HA chains via two sequential transesterification reactions<sup>236, 237</sup>. We hypothesized that the covalently incorporated material corresponds to HA•HC complexes. To test this, we subjected the GuHCl eluates (not shown) and the HA-ase digest to Western blotting (Fig.4.1D). Indeed, the strongest bands revealed with an anti-I $\alpha$ I antibody for the digest ran at about 80 kDa, consistent with the sizes of HC1 and/or HC2 plus a short HA stub<sup>236</sup>. In contrast, no bands could be detected upon staining of the digest with the anti-TSG-6 antibody RAH1, indicating that TSG-6 is not covalently incorporated into the HA films.

The areal surface density of HA-ase digestible material after the 230 min incubation process was 105 ng/cm<sup>2</sup>, or 35 ng/cm<sup>2</sup> HA and 70 ng/cm<sup>2</sup> HCs, if we assume that all HA was digested and consider that the protein fraction consists exclusively of HCs. This corresponds to an occupancy of one HC per 105 HA disaccharides, or 21 HCs per HA chain of 837 kDa. The average transfer rate would be 0.06 fmol/cm<sup>2</sup>/s.

Considering the surface density of TSG-6 prior to incubation with I $\alpha$ I (310 ng/cm<sup>2</sup>) and the total functional surface area in our assay (0.5 cm<sup>2</sup>), one can estimate the total available amount of the enzyme (i.e. TSG-6) throughout the HC transfer reaction to be 5 pmol. In comparison, the substrate I $\alpha$ I was incubated at 150 pmol, i.e. in a large excess. Under these conditions, a constant rate for the enzymatic transfer would be expected, as long as TSG-6 maintains a constant enzymatic activity. In this context, the constant binding rate observed throughout the HA•HC complex formation process (Fig. 4.1B, from 132 to 355 min) receives particular significance. It implies that, if the incorporation of covalently bound material (HA•HC complexes) indeed occurs at a constant rate, then the concomitant incorporation of non-covalently bound material (of currently unknown composition) must also occur at a constant rate. A simple explanation for such a response would be that both binding processes are interdependent, i.e. a protein (or protein complex) is incorporated into the HC•HA film through its non-covalent interaction with the covalently attached HCs.

### 4.3.3 TSG-6 can bind tightly but non-covalently to HCs.

To better understand the possible interactions between the involved proteins David Briggs (University of Manchester) analyzed binding of recombinantly produced HC1, HC2 and HC3 (rHC1, rHC2 and rHC3; see Fig. S6), individually immobilized on a C1 chip, to TSG-6 (the analyte) by surface plasmon resonance (Fig.4.2). Analysis of the binding data revealed that all three HCs interact rapidly and strongly with TSG-6, in a divalent cation-independent manner (i.e. in the presence of either Ca<sup>2+</sup>/Mg<sup>2+</sup> or EDTA), each with a dissociation constant of  $K_D \approx 10$  nM. On-rates and off-rates for the binding of the 3 HCs to TSG-6 were all very similar ( $k_{on} \approx 1 \times 10^5$  M<sup>-1</sup>s<sup>-1</sup>,  $k_{off} \approx 7 \times 10^{-4}$  s<sup>-1</sup>), suggesting that they all bind (via conserved residues) to a common interaction site on TSG-6.

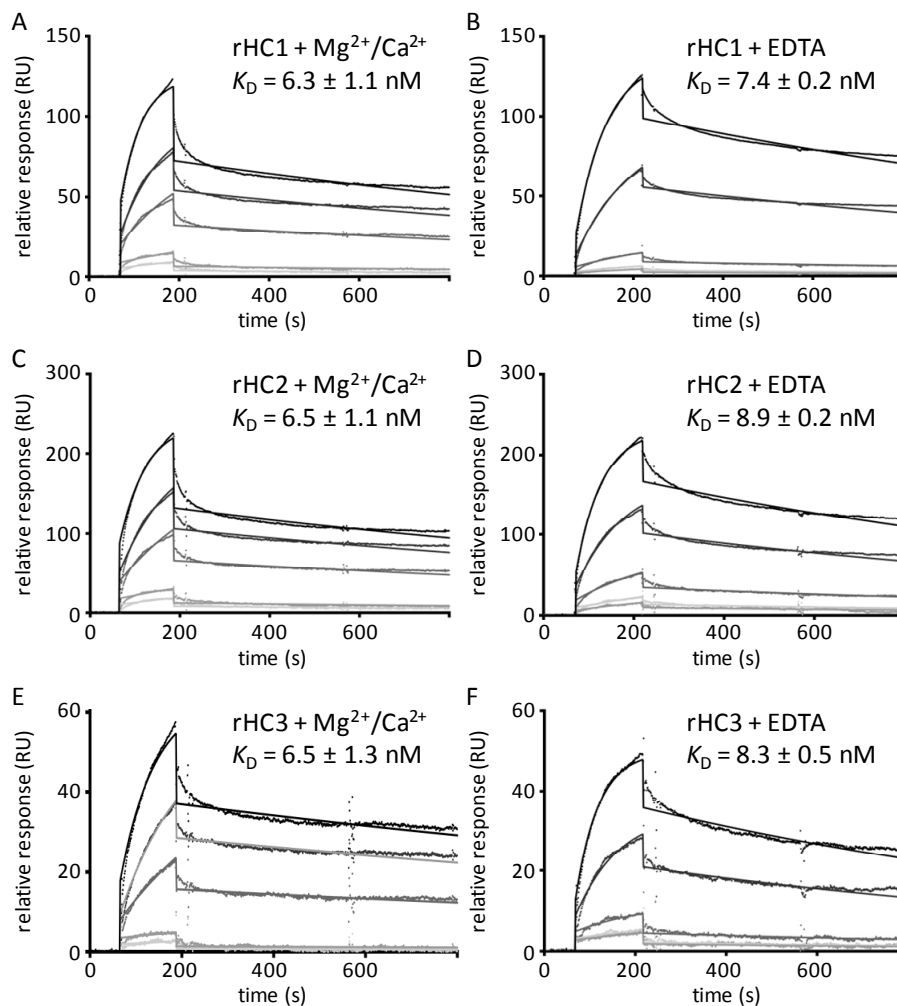
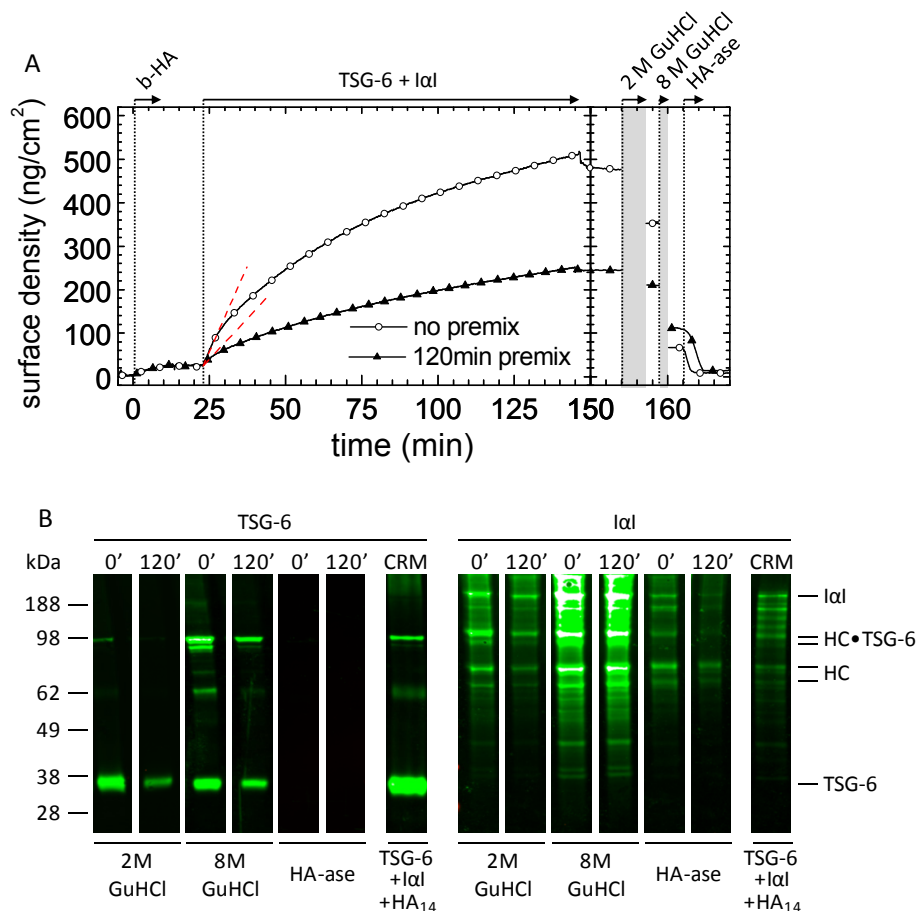


Fig. 4.2 **TSG-6 interacts with high affinity with HC1, HC2 and HC3.** Representative figures of TSG-6 (analyte) interacting with immobilized rHC1 (A, B), rHC2 (C, D) and rHC3 (E, F) shown by surface plasmon resonance in HBS-T with 1 mM  $\text{MgCl}_2$  and 1 mM  $\text{CaCl}_2$  (A, C, E) or in HBS-T with 10 mM EDTA (B, D, F). Raw data and curve fits (with a 1:1 Langmuir model) are shown for TSG-6 concentrations of 6.25 nM, 12.5 nM, 25 nM, 50 nM and 100 nM.  $K_D$  values were determined from the mean of 3 experiments  $\pm$  standard deviation. Stepwise changes in response at the end of sample injection are due to RI changes upon solution exchange, modeled by BiaEval 1:1 Langmuir model fitting. Other binding models tested did not improve the fit significantly. SPR data from D.C. Briggs (Manchester University).

#### 4.3.4 Pre-mixing of TSG-6 and I $\alpha$ I affects protein incorporation into HA films

To further assess the ternary interaction between HA, TSG-6 and I $\alpha$ I, we performed assays in which the HA film was co-incubated with TSG-6 and I $\alpha$ I (Fig. 4.3A). In one assay, TSG-6 and I $\alpha$ I were first pre-mixed for 120 min at room temperature, and the mixture was then added to the HA film (Fig. 4.3A, filled triangles). In another assay, the pre-mixing time

was minimized. To this end, we first incubated the HA film with IαI, because these two species do not interact (Fig. 4.1C), and then added TSG-6 (4.3A, open circles).



**Fig. 4.3 Pre-mixing of TSG-6 and IαI affects protein incorporation.** (A) Co-incubation assay by ellipsometry. TSG-6 and IαI were pre-mixed for 120 min prior to exposure to the HA (837 kDa) film at final concentrations of 0.3 and 1.0 μM, respectively (filled triangles). Alternatively, first IαI and then TSG-6 were added to the HA film (open circles). The two pre-mixing scenarios led to distinctly different binding and unbinding responses. Dashed lines are linear fits to the data at the start of incubation, giving initial binding rates of 1.8 and 1.1 ng/cm<sup>2</sup>/min, respectively. (B) *Western blots of the fractions eluted with 2 and 8 M GuHCl, and of HA-ase digests.* Numbers at the top of the lanes correspond to the pre-mixing time in minutes; assignments of the strongest bands are indicated. Western blots for the control reaction mix (CRM) of TSG-6, HA<sub>14</sub> and IαI are also shown. Western blots were prepared by V. Tilakaratna & A. J. Day (Manchester University).

In both assays, a steady increase in the amount of adsorbed material was observed. Comparison of the initial binding rates in Fig. 4.3 (at 23 min) and Fig. 4.1B (at 36 min) reveals that binding from the pre-mixed IαI/TSG-6 solutions is slowed down significantly, by 2 to 4-fold, compared to TSG-6 alone. This means that in a mixture with IαI, the HA binding

properties of TSG-6 are impaired, which is in agreement with the (partial) displacement that we had observed in the sequential incubation assay (Fig.4.1).

Comparison of the two curves in Fig. 4.3A shows that the 120 min pre-mixing of TSG-6 and I $\alpha$ I has an appreciable effect on the subsequent interaction with HA. Firstly, the binding rates in the 120 min pre-mix scenario were significantly slower than without pre-mixing throughout the entire binding process. Secondly, the stability of binding was different. Following 120 min pre-mixing, binding was completely stable to rinsing in buffer whereas a small but significant fraction was released without pre-mixing. As in the sequential binding assay, sizeable fractions could be eluted by exposure to 2 and 8 M GuHCl. The remainder of the film could be completely removed by digestion with HA-ase, confirming that all remaining protein material was covalently bound to HA. If the covalently bound protein fraction consists exclusively of HCs, then the maximal occupancy after 2 h of incubating HA with the protein mixture is 35 HCs per HA chain.

To shed light on the molecular species present in the film, the fractions eluted through exposure to 2 and 8 M GuHCl or digestion by hyaluronidase were subjected to Western blot analysis with anti-TSG-6 and anti-I $\alpha$ I antibodies (Fig. 4.3B). All samples eluted in GuHCl showed a band with an apparent Mw of  $\sim$ 36 kDa, identical to TSG-6 protein in a control sample taken from a pre-mixed solution of TSG-6, HA<sub>14</sub> and I $\alpha$ I<sup>236</sup>. Two bands at around 100 kDa were detected by both antibodies in the GuHCl-eluted fractions and the control, consistent with the presence of covalent complexes of TSG-6 with HC1 or HC2<sup>236</sup>. In addition, a minor band at  $\sim$ 65 kDa was detected with RAH-1, which we suggest is a disulfide-linked TSG-6 dimer, since we know this sometime forms during electrophoresis when TSG-6 is reduced with  $\beta$ -mercaptoethanol. In addition to HC•TSG-6 complexes, a rather large number of bands were stained exclusively with the anti-I $\alpha$ I antibody. In particular, bands for intact I $\alpha$ I and isolated heavy chains are clearly visible at around 190 and 80 kDa, respectively. Notably, the same bands were detected regardless of the pre-mixing time of I $\alpha$ I and TSG-6, albeit at different intensities. Apparently, the pre-mixing time does not affect the identity, but rather the quantity, of material incorporated into the HA film.

As already observed in the sequential binding assay, no bands were detected with the anti-TSG-6 antibody in HA-ase digests, whereas the strongest band visible with anti-I $\alpha$ I antibody ran at about 80 kDa. This suggests that the major, and perhaps only, covalently incorporated species are heavy chains. Our findings provide evidence that while TSG-6 is always active to transfer HC into HA films, the efficiency of HC transfer and/or incorporation of other protein species depends on the conditions of co-incubation.

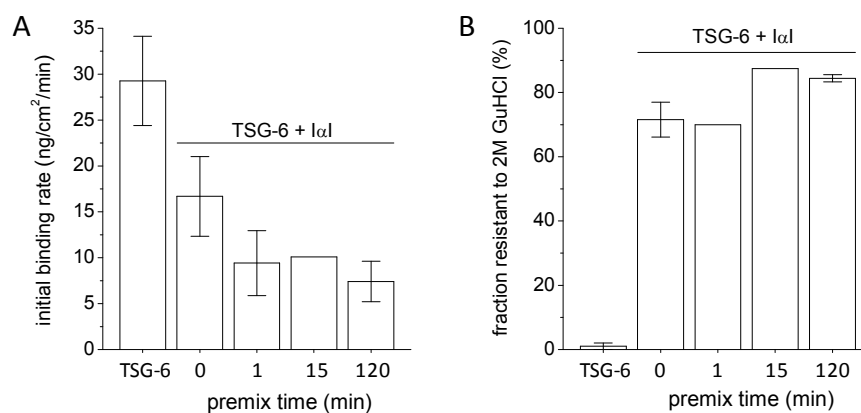


**Fig. 4.4 Ternary interaction of HA, TSG-6 and IαI as a function of TSG-6/IαI pre-mixing time.** TSG-6 at 0.3  $\mu$ M was exposed to HA (837 kDa) films either alone or in a mixture with 1  $\mu$ M IαI for 2 h. Proteins were pre-mixed ex situ for different periods of time (0 to 120 min). (A) Initial rate of binding to the HA film. (B) Protein fractions that were resistant to elution in 2 M GuHCl, in percent of total bound protein. Data plotted correspond to one measurement, or to the mean of two or three independent measurements (with error bars indicating maximal/minimal measured values).

Intrigued by the large differences observed between the co-incubation assays with 120 min and those without pre-mixing (Fig. 4.3A), we tested how the pre-mixing time influences the initial binding rate of protein into the HA film (Fig. 4.4). With increasing pre-mixing time, the initial binding rate of the TSG-6/IαI mixture decreased rapidly (Fig. 4.4A). Already after 1 min of pre-mixing, the initial binding rate had reached levels comparable to those observed for 120 min. The fraction of very tightly bound material (i.e. stable to 2 M GuHCl), on the other hand, was only influenced to a small extent; i.e. with ~70% bound at 0 and 1 min pre-mixing time and ~85% at 15 and 120 min (Fig. 4.4B). Apparently, there is a short time window for pre-mixing, not longer than a few minutes that influences the amount of incorporation of material into HA films.

#### 4.3.5 IαI-binding and HC transfer activity are retained, albeit reduced, in the absence of TSG-6 in the soluble phase.

To test if HC transfer is exclusively driven by TSG-6 in the soluble phase, an HA film was first exposed to a pre-mixed (1 min) solution of IαI and TSG-6 (Fig. 4.5, at 15 in) for 210 min. IαI and TSG-6 were then removed from the bulk solution by rinsing in buffer, and 1  $\mu$ M IαI was subsequently added without TSG-6 (Fig. 4.5, at 240 min). Despite the absence of TSG-6 in the solution phase, we observed a significant increase in the areal surface density, confirming binding of IαI into the HA film. Over 2 h of incubation, the areal surface density continued to increase. Except for a faster initial phase of about 15 min, the areal



surface density increased linearly, at a rate of  $0.6 \text{ ng/cm}^2/\text{min}$ , i.e. somewhat lower than the rates observed in

Fig. 4.1B and Fig. 4.3.

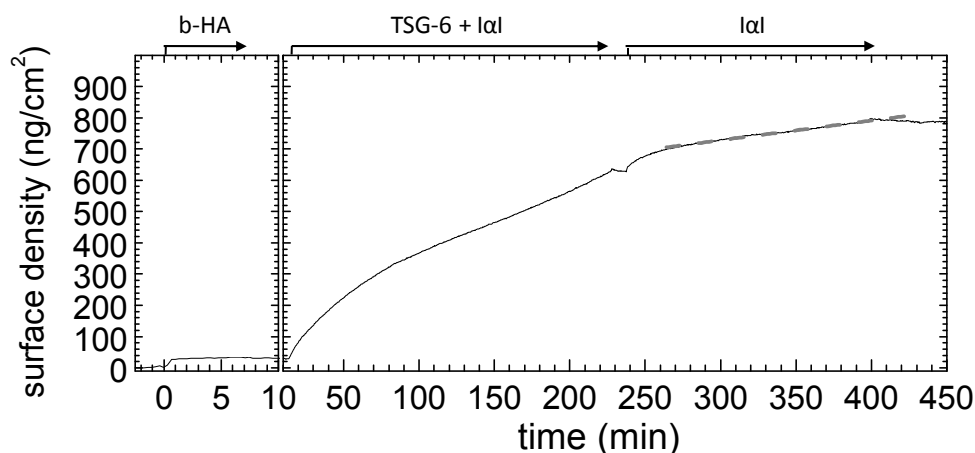


Fig. 4.5 **HA-bound material is catalytically active.** An HA (1083 kDa) film was first exposed to  $0.3 \mu\text{M}$  TSG-6 and  $1 \mu\text{M}$  I $\alpha$ I (1 min pre-mixing) for 4 h, and residual proteins in the soluble phase were then removed by buffer exchange. All incorporated material remained stably bound in the HA film. Addition of  $1 \mu\text{M}$  I $\alpha$ I, without TSG-6, induced significant binding. Beyond 15 min of incubation and for at least 2 h, the adsorbed mass increased linearly at a slow rate (the dashed line is a fit), suggesting HC transfer.

The linear trend and the low rate suggest that this phase corresponds to enzymatic transfer of HCs, implying that HA-bound TSG-6 material has a catalytic function on its own. This and the significantly lower rate in the absence of TSG-6 in solution indicate that HC transfer can occur via two different pathways, i.e. from HC•TSG-6 complexes in solution that interact very weakly with HA, and *via* protein/complexes (presumably TSG-6 and/or HC•TSG-6) that interact stably yet in a non-covalent manner with HA or with HCs that are covalently attached to HA.

#### 4.3.6 Effect of I $\alpha$ I incubation on the thickness of the HA film.

Next, we studied how the covalent modification of HA films by HCs influences the morphology of HA. We had reported earlier that TSG-6, when presented alone, cross-links HA and induces HA film shrinkage<sup>210</sup>. Indeed, addition of TSG-6 at  $0.3 \mu\text{M}$  resulted in a strong decrease of the film thickness, by more than 60% (Fig.4.6.). In contrast, the thickness of the HA film decreased only about 20%, when TSG-6 was co-incubated with  $1 \mu\text{M}$  I $\alpha$ I. Apparently, the cross-linking properties of TSG-6 are impaired in the presence of I $\alpha$ I. Beyond 30 min of incubation, the thickness remained virtually constant (Fig. 4.6.A). The TSG-6/I $\alpha$ I pre-mixing time had no significant influence on the film thickness in the co-

incubation assays. However, the film only partially recovered, to 65% of its original thickness, when an already TSG-6 cross-linked HA film was exposed to I $\alpha$ I (Fig.4.6B).

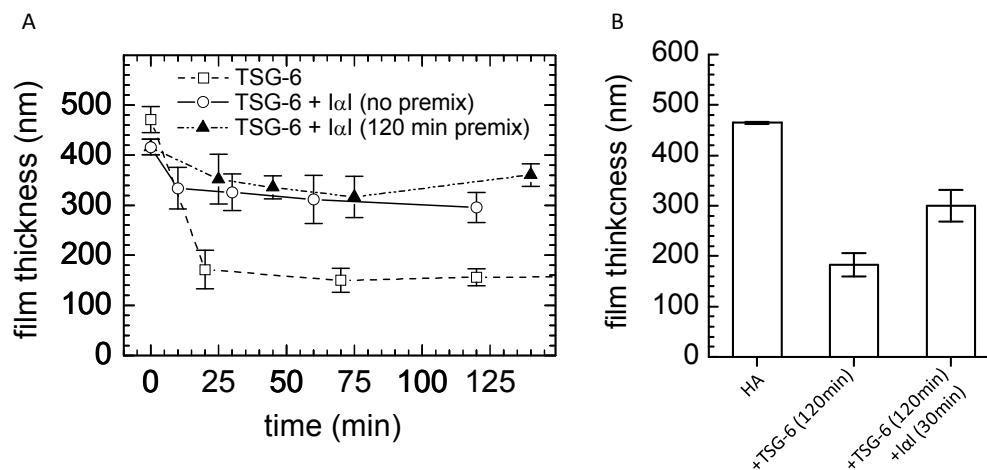


**Fig. 4.6 Changes in the thickness of HA films upon incubation with TSG-6 and I $\alpha$ I.** Variations in the thickness of a HA (1083 kDa) film as a function of incubation time were quantified by colloidal probe RICM. (A) Incubation with a mixture of 0.3  $\mu$ M TSG-6 and 1  $\mu$ M I $\alpha$ I (no pre-mixing – open circles, 120 min pre-mixing – filled triangles) resulted in a minor decrease in film thickness during the first 25 min after incubation. In contrast, incubation with TSG-6 alone, at the same concentration, induced pronounced condensation of the film within the same time (open squares). Film thicknesses remained virtually unaltered throughout the subsequent 2 h of incubation. (B) Addition of 1  $\mu$ M I $\alpha$ I to the TSG-6 loaded film led to a partial recovery of the original film thickness. Data are plotted as mean values of 10 independent measurements on the same surface ( $\pm$  S.E.M).

### 4.3.7 Effect of I $\alpha$ I on TSG-6-enhanced HA cell coats.

Lesley et al.<sup>251</sup> have shown that TSG-6 can act as a strong enhancer of HA binding to the surface of CD44 positive cells. In light of the drastic impact of I $\alpha$ I on the binding of TSG-6 to HA (Figs. 1 and 3), and on the morphology of the HA films (Fig.4.6), we hypothesized that I $\alpha$ I would also affect the enhanced binding of HA to cells. To test this, Simon Foulcer adapted the assay by Lesley et al.<sup>251</sup> using a CD44+ cell line (Fig. S3) which constitutively binds HA (Fig. S4) and quantified the influence of TSG-6 and I $\alpha$ I on the binding of fluorescently labeled HA (fl-HA) to AKR1/CD44+ cells (Fig. 4.7).

The presence of TSG-6 alone strongly enhanced HA binding to AKR1/CD44+ cells (compare sample (i) and (ii) in Fig. 4.7B), which is in good agreement with Lesley et al.<sup>251</sup>. This effect of TSG-6 was HA dose dependent (Fig. S5). In contrast, when fl-HA was incubated with a pre-mixed solution of TSG-6 and I $\alpha$ I, and then added to the cells (iii), the mean fluorescence intensity was comparable to that observed for fl-HA alone (i). Hence, co-incubation with I $\alpha$ I is sufficient to inhibit any enhancement of the CD44/HA interaction by TSG-6. Following addition of I $\alpha$ I to TSG-6/HA-coated cells (iv), a 35% decrease was

observed in the mean fluorescence, indicative of a partial reversal of the enhancement of the CD44/HA interaction induced by TSG-6. The mean fluorescence intensity of cells exposed to pre-formed TSG-6/fl-HA complexes that had been pre-mixed with I $\alpha$ I (v) was intermediate between fl-HA alone and TSG-6/fl-HA, giving a clear indication that I $\alpha$ I is able to partially reverse the TSG-6/HA complex formation. Taken together, the effect of I $\alpha$ I on the TSG-6-enhanced binding of HA to CD44<sup>+</sup> cells mirrors very closely the I $\alpha$ I-mediated impairment of TSG-6 binding into HA brushes.

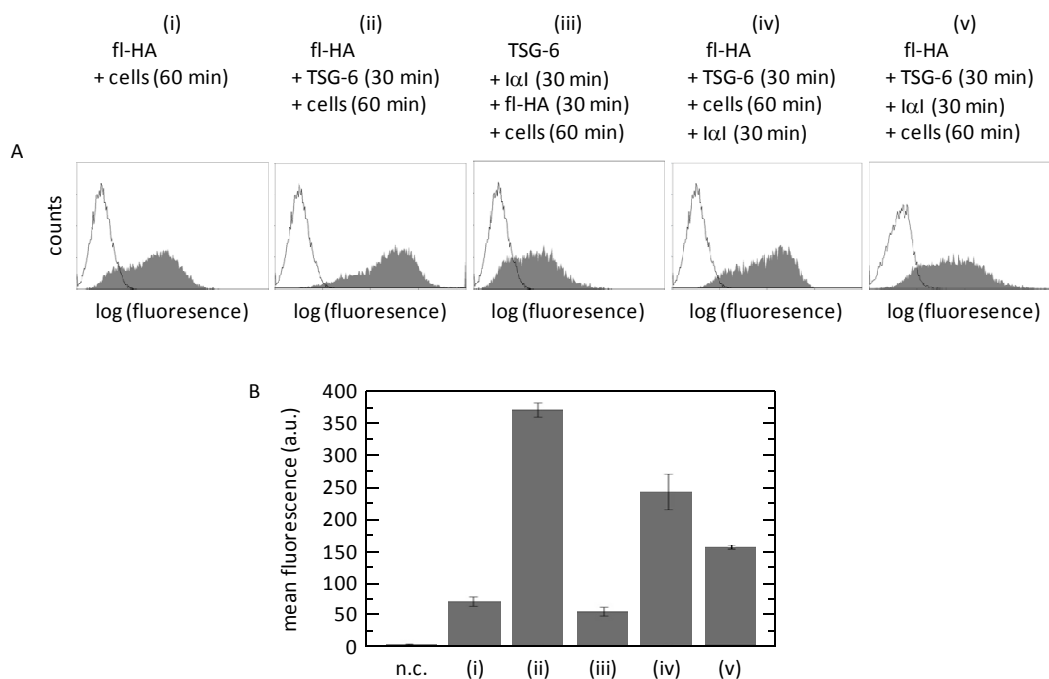


**Fig. 4.7 The effect of I $\alpha$ I on TSG-6 enhancement of HA binding to CD44.** (A) Representative histograms showing the distribution of the fluorescence of 10000 cells for fl-HA binding to CD44 in the absence of TSG-6 (i), in the presence of TSG-6 (ii), and in the presence of TSG-6 together with I $\alpha$ I (iii-v). TSG-6 and I $\alpha$ I in samples (iii-v) were incubated together at different sample preparation stages. In sample (iii) the TSG-6 was incubated with I $\alpha$ I prior to the addition of fl-HA and cells. In samples (iv and v), TSG-6 was incubated with HA. I $\alpha$ I was subsequently added after the addition of cells in (iv), i.e. after the formation of a TSG-6 enhanced film, and before the addition of cells in (v). Final concentrations of 1  $\mu$ g/ml fl-HA, 0.3  $\mu$ M TSG-6 and 1  $\mu$ M I $\alpha$ I, and  $\sim 5 \times 10^5$  AKR1/CD44<sup>+</sup> positive cells were used throughout; fl-HA, TSG-6 and I $\alpha$ I were incubated for 30 min, cells for 60 min, all at 37°C. (B) Mean fluorescence intensity for the negative control sample (i.e. PBS alone) and for each sample (i-v; defined above). I $\alpha$ I reverses the enhancement of the CD44/HA interaction induced by TSG-6 in all assays, yet the degree of reversal depends on the incubation sequence. Data are plotted as mean of 3 independent experiments performed in triplicate ( $\pm$  S.E.M). Data and images from S. Foulcer & A.J. Day (University of Manchester).

## 4.4 Discussion

The ternary interactions between HA, TSG-6 and IαI were investigated in an ultrastructural context by using films of end-grafted HA and surface-sensitive analysis techniques. The HA films are well-defined in that their surface density and thickness can be controlled. Time-resolved measurements by *in situ* ellipsometry and RICM provided quantitative information about the kinetics of protein incorporation/release and concomitant changes in film thickness, respectively. A combination of several purpose-designed assays, sequential addition and co-incubation, revealed several different interactions and provided novel insight into the interaction mechanisms at play. The key findings of this study are:

- i. In the presence of IαI, TSG-6 is partially displaced from HA films (Fig. 4.1) and HA cross-linking through HA-induced TSG-6 oligomers is impaired (Fig.4.6). In particular, this effect leads to impairment of TSG-6 enhanced binding of HA to CD44 positive cells.
- iii. Long-term incubation of HA with TSG-6 and IαI leads to films that contain, in addition to covalently HA-bound HCs, several tightly but non-covalently bound molecular species. A likely route of incorporation is through the strong non-covalent interaction of TSG-6 (or HC•TSG-6) with HC1 and HC2 (Fig.4.2.). The timing of the encounter between TSG-6, IαI and HA has an appreciable effect on the ultimate film composition (Fig. 4.3-Fig. 4.4).
- iv. TSG-6, or TSG-6 related species, can drive the formation of HA•HC complexes both from the soluble phase and when stably bound in the HA film (Fig. 4.5).

### 4.4.1 A hierarchy of interactions determines protein function.

The present study, together with previously published work from ourselves and others, provides compelling evidence that a variety of different complexes can be generated upon interaction of TSG-6, IαI (or its subunits) and HA. Among them are two covalent complexes, namely HC•HA<sup>96</sup> and HC•TSG-6<sup>86, 236</sup>, and many non-covalent complexes of varying affinity, including HA-TSG-6<sup>76, 77, 242</sup>, HC-TSG-6 (this manuscript), HC-HC<sup>97</sup>, TSG-6-TSG-6<sup>210</sup>, C4S-TSG-6<sup>239, 252-254</sup>, and TSG-6-bikunin<sup>237, 239, 255, 256</sup>.

Here, we show that many of these complexes can be present at the same time, giving rise to supramolecular matrices of complex composition. Remarkably, the presence of IαI switches the function of TSG-6, from being an HA cross-linker to being an enzyme and in part a stably incorporated matrix component, where the sequence of encounter between the different molecular species has an appreciable effect on matrix composition.

Based on these observations, we propose that there is a hierarchy of interactions between the molecular players that ultimately determines protein functions as well as matrix assembly. This concept may not be restricted to the three molecules investigated here, but

can perhaps be extended to additional molecular species. For example, pentraxin 3 (PTX3) is known to be crucial for COC matrix assembly in addition to HA, TSG-6 and I $\alpha$ I, and interacts with TSG-6 and I $\alpha$ I<sup>37, 38, 115</sup>, so will likely add further complexity/regulation to this system.

Future studies that aim at mapping the hierarchy of interactions will be needed to gain a full mechanistic understanding of the regulation of matrix assembly. Based on currently available data, we hypothesize that HC•HA complexes play a central role in matrix assembly, because (i) they serve as docking sites for the attachment of other proteins and protein complexes to HA chains and (ii) may also be involved in matrix stabilization.

#### 4.4.2 Possible mechanisms for the I $\alpha$ I-induced displacement of TSG-6 from HA.

It was demonstrated before that the interaction between TSG-6 and I $\alpha$ I proceeds in two-steps: first the non-covalent binding of TSG-6 to bikunin- chondroitin sulfate and second the cation-dependent transesterification in which the ester bond between HC and C4S in I $\alpha$ I is transferred to Ser 28 of TSG-6 located in the N-terminal region, next to the Link module, with generation of a covalent HC•TSG-6 complex<sup>237, 239</sup>. In contrast, the recombinant Link module of TSG-6, lacking the N-terminal region, was found to bind to I $\alpha$ I (and to potentiate the bikunin chain's anti-plasmin activity), but without formation of a covalent complex with HC<sup>255, 256</sup>. Notably, the Link module of TSG-6 has binding sites for both HA and bikunin•C4S, which are likely to overlap based on data from competition experiments and their mapping by site directed mutagenesis<sup>252, 255</sup>. Thus, it appears possible that the competition between HA and bikunin•C4S for the Link module drives, or contributes to, the release of TSG-6 from HA through I $\alpha$ I (

Fig. 4.1).

Here, we show that TSG-6 can also bind non-covalently to HC1, HC2 and HC3 (Fig.4.2). These interactions occur with higher affinity ( $K_D \approx 10$  nM) than its binding to HA ( $K_{0.5} \approx 1$   $\mu$ M<sup>210</sup>) or bikunin•C4S binding ( $K_D = 180$  nM<sup>239</sup>). It is possible, therefore, that TSG-6 may be able to bind simultaneously to bikunin•C4S and a HC within I $\alpha$ I, which would lead to the formation of a very stable complex (e.g. with a combined affinity of up to  $K_D \approx 2$  fM). However, preliminary results indicate that I $\alpha$ I binds with a similar affinity to that of the HCs ( $\sim 10$  nM); this indicates that TSG-6 can form a number of different complexes with I $\alpha$ I via individual interactions with HC1, HC2 or bikunin•CS. If any of these interactions occlude the HA binding site on TSG-6 (or perhaps stabilize it in its closed conformation, see refs.<sup>76, 242</sup>), this could provide a mechanism as to why the presence of I $\alpha$ I so rapidly inhibits TSG-6-HA binding.

Based on the tight interaction of HCs with TSG-6, we propose a new two-stage model for HC•TSG-6 formation: the first stage would involve the metal-ion independent interaction of TSG-6 with HC1 or HC2 (and perhaps even bikunin•CS) into a very stable I $\alpha$ I-TSG-6

complex; this would then be followed by metal-ion dependent transesterification step leading to HC•TSG-6.

### 4.4.3 The nature and physiological relevance of non-covalently HA-bound material.

The finding that the interaction between IαI and TSG-6 in the presence of HA can give rise to TSG-6 that is stably but non-covalently bound to HA, and that some of this material can interact with IαI and most likely also transfer HCs to HA, is novel.

Colon et al.<sup>257</sup> had previously reported that HA-bound TSG-6 can mediate transfer of HCs to HA, using a sequential incubation plate binding assay with immobilized HA. In that study, however, TSG-6 was found to form non-dissociable complexes with HA, i.e. these complexes are likely to be different from the non-covalently HA-bound material in our study. The non-dissociable TSG-6•HA complexes were formed at a non-physiological ionic strength of 500 mM NaCl even in the absence of IαI<sup>165</sup>, whereas we found all TSG-6 that was incorporated into HA films under physiological ionic strength to be dissociable (Fig. 4.4B)<sup>210</sup>. It is therefore unlikely that the HC transfer pathway reported by Colon et al.<sup>257</sup> occurs in our HA films.

Our data indicate that the extent of non-covalently HA-bound material is highly sensitive to the abundance of HA at the moment when IαI and TSG-6 encounter each other. By extension, the presence of this fraction *in vivo* should depend on the spatial and temporal localization of IαI, TSG-6 and HA. In this context, it is interesting to note that IαI/TSG-6 were reported to be non-covalently bound into the matrix of mouse COCs expanded *in vitro* but not in COCs extracted from murine ovulating follicles<sup>31, 118</sup> (see also ref.<sup>32</sup>). This might suggest that the temporal expression of HA is different in these two systems. Electrostatic attraction between IαI and HA was postulated as a mechanism for retention of IαI in the COC matrix<sup>101</sup>. However, under the conditions that we used here, we did not observe any binding of IαI alone into HA films (Fig. 4.1C), i.e. the presence of TSG-6 was required for the formation of a non-covalently bound fraction<sup>32</sup>.

### 4.4.4 Covalent modification of HA with HCs.

In our 2 h co-incubation assays (Fig. 4.3), the amount of covalently incorporated material reached values corresponding to up to 35 HCs per HA chain. For comparison, 3 to 5 HCs per HA chain were found in the synovial fluid of arthritis patients<sup>97</sup>. The size of HA in synovial fluid is about double the size in our HA films, i.e. the HC coverage in our films is 14 to 24-fold higher than in this *in vivo* situation.

Given that both HA and IαI are present in synovial fluid of arthritis patients, and that the HA concentration in synovial fluid (between 1 and 4 mg/ml<sup>67</sup>) is comparable to our HA films (1 mg/ml<sup>60</sup>), a plausible explanation for the difference could be that the extent of

covalent modification correlates with TSG-6 concentration. In this case, a concentration of 16 nM TSG-6 would be enough to transfer 4 HCs per HA chain in 2 h. This number correlates rather well with the concentrations of TSG-6 (up to 3 nM) recently reported for synovial fluids of patients with inflammatory arthritis<sup>70</sup>.

Also, the time required for expansion of mouse COC matrix during ovulation is around 12-14 h after hormonal stimulation<sup>28</sup>. To obtain the level of transfer found in synovial fluid within this time, as little as 2 nM TSG-6 would be sufficient.

#### 4.4.5 Is an HA film exposed to I $\alpha$ I/TSG-6 cross-linked?

In earlier work, we demonstrated that TSG-6 alone can cross-link and induce condensation of HA into dense matrices<sup>210</sup>. Here, we show that TSG-6 mediated condensation does not occur in the presence of I $\alpha$ I, and can even be reversed upon addition of I $\alpha$ I to HA/TSG-6 complexes.

*In vivo*, the ternary interaction of I $\alpha$ I, TSG-6 and HA is regulated by the temporal expression and localization of reactants. The synthesis of HA and TSG-6 is often coordinated and occurs in tissue extracellular matrix during inflammation. In contrast, I $\alpha$ I is constitutively present in the blood. It can only diffuse into tissue extracellular space when the permeability barriers that separate different tissues from blood become leaky, for instance during ovulation or vasodilatation. This raises the possibility that a dense TSG-6/HA matrix that may form in the absence of I $\alpha$ I undergoes substantial swelling as soon as I $\alpha$ I penetrates into the tissue. Such a regulatory mechanism could be particularly relevant for the expansion of the COC matrix, where HA and TSG-6 are produced in the matrix, and the ingress of I $\alpha$ I increases over time after the induction of ovulation.

It should be noted, however, that even the expanded COC matrix remains cohesive, i.e. some cross-links must remain upon expansion. Cross-linking *via* HCs has been proposed as another possible cross-linking mechanism (either via HC-HC interactions between HC•HA<sup>97</sup> and/or via interactions between HC•HA and PTX3<sup>38, 115</sup>). In general, one would expect the introduction of (sufficiently stable) cross-linkers to force neighboring HA chains in an expanded meshwork closer together, leading to condensation. Our measurements of the film thickness (Fig.4.6) indicate only a minor condensation in the presence of I $\alpha$ I. Moreover, the thickness decrease occurred within less than 30 min (Fig.4.6) whereas HC incorporation continued over many hours (Figs. 4.1, 4.3 and 4.5). The small decrease in thickness and the limited correlation between thickness decrease and HC incorporation suggest that cross-linking through HCs, if present at all, is rather weak. We can though not exclude that the presence of non-covalently bound material somehow prevents cross-linking. For example, COCs extracted from the ovulating follicles of mice, which were more resistant to shear stress than COCs in culture, contained no detectable non-covalently incorporated material<sup>118</sup>, in contrast to cultured COCs. Further studies are clearly required to fully elucidate the mechanism behind COC matrix stabilization.

#### 4.4.6 Role of HC•HA in leukocyte adhesion.

Here we have found that TSG-6-mediated transfer of HCs onto HA counteracts the enhancement of binding seen with TSG-6/HA complexes and does not promote the binding of HA to CD44+ cells. This is in stark contrast to a previous finding that HC•HA binds better to CD44+ leukocyte cell lines when compared to unmodified HA<sup>232</sup>. One major difference between the two studies is that whereas we formed HC•HA *in vitro* (with purified human IαI<sup>83</sup>, recombinant TSG-6<sup>243</sup> and medical grade HA) the material used by Zhou *et al.*<sup>232</sup> was isolated from the synovial fluids of patients with rheumatoid arthritis. Thus, while the HC•HA used in the present study will only contain HC1 and HC2 (and possibly non-covalently bound TSG-6/HC•TSG-6 species), the native material<sup>232</sup> is likely to contain HC3<sup>96</sup> along with HA-binding proteins, such as PTX3, which is known to be present in rheumatoid synovial fluid<sup>258</sup>; interestingly, the purified HC•HA was found to be free of any associated TSG-6<sup>232</sup>. It seems likely therefore that compositional differences may explain the distinct adhesive properties of these two different HC•HA preparations. This raises the exciting possibility that the exact composition of the inflammatory milieu can regulate HA-receptor interactions and hence determine the extent of cell adhesion and HA-mediated signaling.

Taken together, this study strikingly illustrates how hyaluronan, although structurally a very simple molecule, can promote many different processes and functions, depending on the microenvironment or availability of particular binding partners. Thus, our results provide an important new insight as to how the broad range of HA biology arises from the complexity and diversity of HA-protein interaction



## 4.5 Supplemental Data

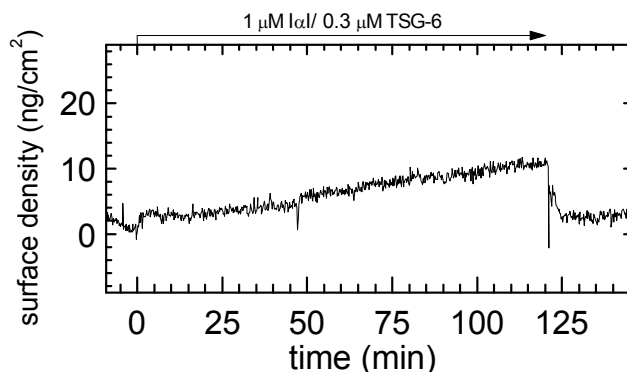


Figure S1. Control for binding of pre-mixed I $\alpha$ I/TSG-6 to SAv-covered OEG surfaces, monitored by ellipsometry. 1  $\mu$ M I $\alpha$ I and 0.3  $\mu$ M TSG-6 were pre-mixed for 1 min prior to exposure to the SAv layer (at 0 min). The bound amount over 2 h of incubation, measured by ellipsometry, was small (10 ng/cm<sup>2</sup>), and could be fully eluted by rinsing in buffer (at 120 min). Also, TSG-6 alone does not bind appreciably to the SAv-coated OEG surface, as we have previously shown (Fig. S5 in ref. <sup>210</sup>).

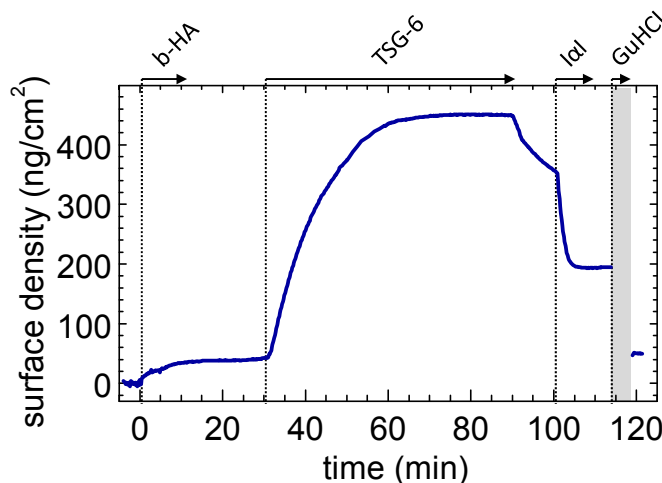


Figure S2. The protein fraction retained after brief exposure of a TSG-6-loaded HA films to I $\alpha$ I is non-covalently bound. A sequential incubation assay was performed similar to Fig. 1B, i.e. a biotinylated HA (b-HA, 837 kDa) film was formed and incubated with 0.3  $\mu$ M TSG-6; after binding equilibrium had been established, excess TSG-6 was removed from the bulk solution, and 1  $\mu$ M I $\alpha$ I was added. Here, the incubation with I $\alpha$ I was kept short (10 min). After incubation with 6 M GuHCl (shaded in grey, elution process not monitored by ellipsometry), the surface density returned to the same level as for a pure HA film, indicating that essentially all protein was stably but non-covalently bound.

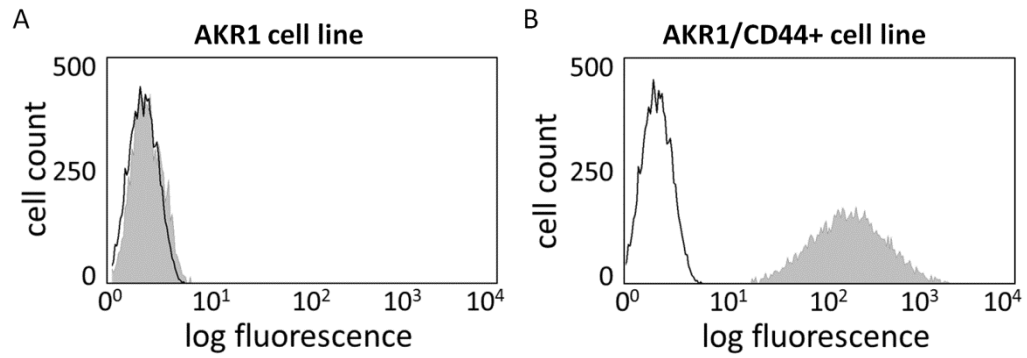


Figure S3. Flow cytometry analysis of CD44 expression on AKR1 and AKR1/CD44+ cells. AKR1 cells (A) and AKR1/CD44+ (B) cells were incubated with anti-CD44 FITC-conjugated IM7 antibody (grey); ~10000 cells were analysed. The negative control (rat IgG isotype matched antibody; Abcam) is shown as a black outline. Data are representative of 3 experiments. Data from S. Foulcer & A.J. Day (University of Manchester).

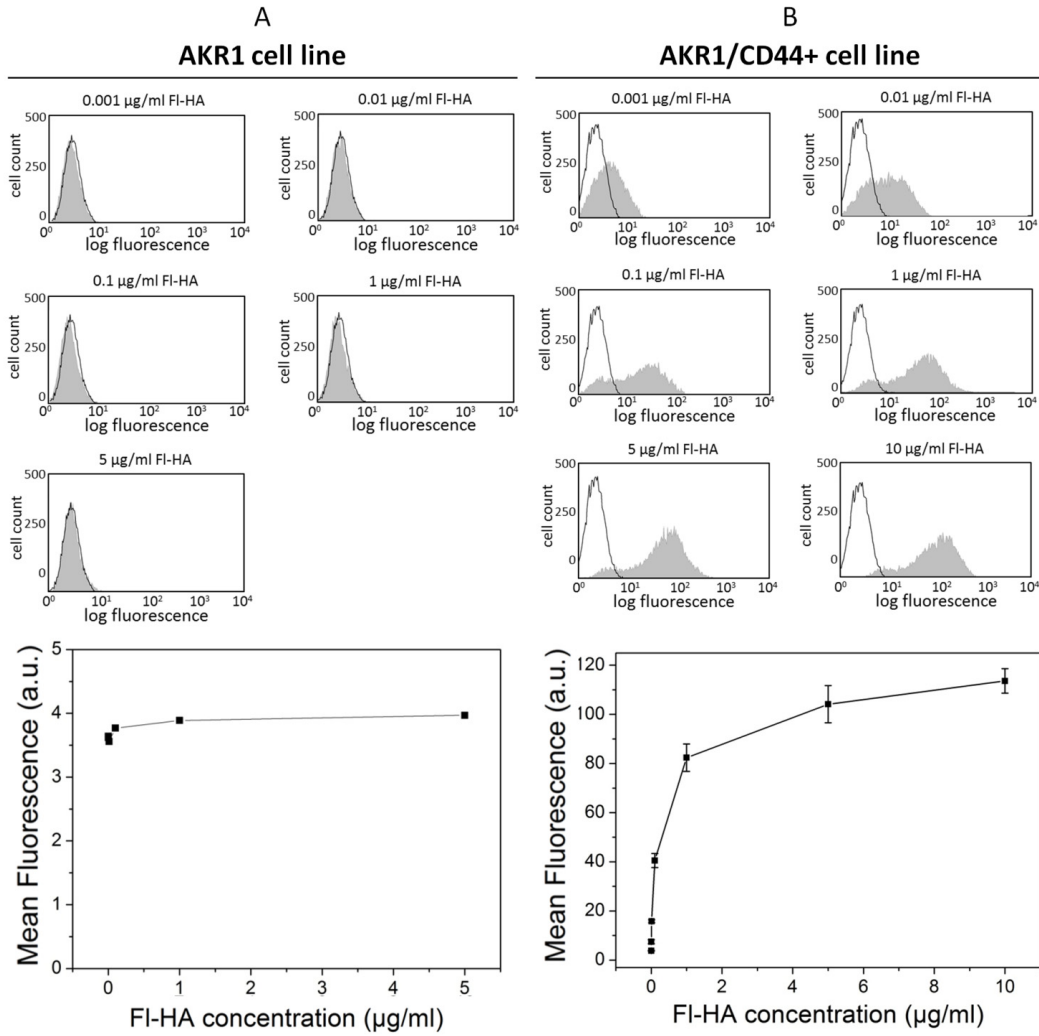


Figure S4. Binding of fl-HA to AKR1 and AKR1/CD44+ cells. AKR1 cells (A) and AKR1/CD44+ cells (B) were incubated with various concentrations (0-10  $\mu\text{g/ml}$ ) of fl-HA and the fluorescence intensity of  $\sim 10000$  cells was analyzed; representative HA binding data are shown (in grey) and the no fl-HA (negative control) is depicted as a black outline. Mean fluorescence values (in arbitrary units) were calculated from 3 independent experiments performed in triplicate and plotted ( $\pm$  S.E.M.) in the lower panel. Data from S. Foulcer & A.J. Day (University of Manchester).

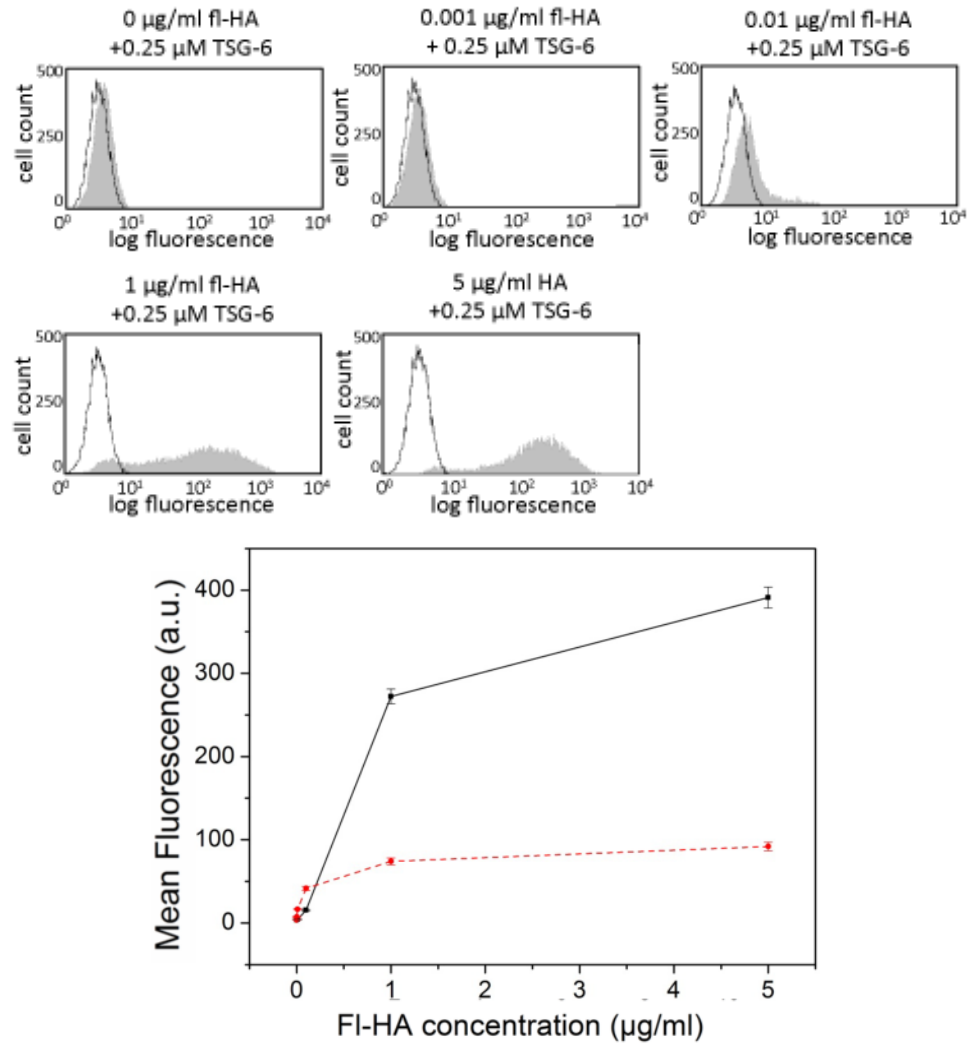


Figure S5. TSG-6-mediated enhancement of fl-HA binding to CD44. AKR1/CD44<sup>+</sup> cells were incubated with 0-5 µg/ml fl-HA in the absence or presence of 0.25 µM TSG-6 and the fluorescence intensity of ~10000 cells was analysed. Representative HA binding data are shown (in grey) and the no fl-HA (negative control) is depicted as a black outline. Mean fluorescence values were calculated for fl-HA incubated in the absence (dashed red line) and presence (solid black line) of TSG-6 from 3 independent experiments performed in triplicate and plotted ( $\pm$  S.E.M.) in the lower panel. Data from S. Foulcer & A.J. Day (University of Manchester).

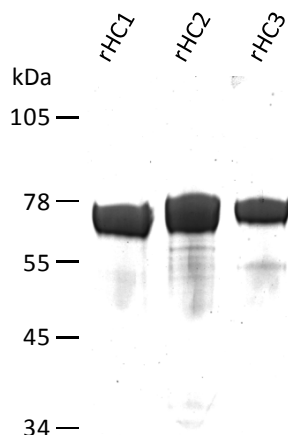


Figure S6. SDS-PAGE analysis of purified recombinant heavy chains (rHC1, rHC2 and rHC3, each with an N-terminal His-tag (MAHHHHHHVGTGSNDDDDKSPDP)). 3 mg of rHC1, rHC2 and rHC3, respectively, were loaded per lane and run under reducing conditions, indicating that these preparations are > 95% pure; rHC1 has been crystallized and its structure determined to 2.5Å (Briggs, D. C., Milner, C. M., and Day, A. J. *unpublished data*) indicating that the method of HC expression used here leads to folded protein. Electrospray ionization mass spectrometry analysis of the rHCs gave molecular masses of 73,802.8 Da (rHC1), 74,842.4 Da (rHC2) and 71,754.4 Da (rHC3). The theoretical masses expected for these constructs in a non-reduced (i.e. disulphide bonded) form, and missing the N-terminal methionine residue are 73,805.4 Da, 74,842.7 Da and 71,752.5 Da, respectively. The masses are consistent, i.e. they agree within 3 Da. SDS-PAGE was performed by D.C. Briggs (University of Manchester).

## 5 PTX3 incorporation into HA-rich matrices

---

Mammalian oocytes are surrounded by several layers of cumulus granulosa cells embedded in a thick cellular coat - the cumulus cell-oocyte complex (COC) matrix. A main component of the COC matrix is the high molecular weight linear polysaccharide hyaluronan (HA). The polyanionic nature of HA promotes formation of a highly hydrated matrix directly after induction of ovulation. The stability and mechanical properties of the matrix depend on the interaction between HA and specific HA-binding proteins, hyaladherins. The presence of TSG-6, IaI and PTX3 proteins is critical for successful ovulation and fertilization. The proteins' expression is temporally regulated and the spatial distribution is likely to be heterogeneous: HA, TSG-6 and PTX3 are synthesized by cumulus cells, while IaI is derived from the serum. The supramolecular organization of the COC matrix as well as the mechanism of matrix stabilization remain unknown. It is difficult to probe the architecture of HA matrices by conventional biological approaches. Here, we use a surface-based model system – films of end-grafted HA – to investigate the mechanism of COC matrix assembly. We found that PTX3 neither binds to HA alone nor to HA films preformed with TSG-6, or a combination of IaI (or its subunits) and TSG-6. Instead, encounter of PTX3 with IaI before interaction with HA is required for incorporation of PTX3. In the presence of all proteins, the HA film appears cross-linked but not collapsed. Based on these results, we propose that the spatio-temporal regulation of HA/protein interactions *in vivo* is responsible for the balance between effective expansion of the COC matrix during ovulation on one hand and matrix stabilization through cross-linking on the other.

## 5.1 Introduction

Just a few hours before ovulation, an extended visco-elastic coat grows around the oocyte and cumulus cells, forming the cumulus cell-oocyte complex (COC) matrix. The COC matrix surrounds the oocyte during ovulation and fertilization in the oviduct and was shown to be particularly important for successful fertilization *in vivo*<sup>29, 37</sup>. The expansion of the coat is supported by production of hyaluronan (HA)<sup>228</sup>. It was suggested that HA in the matrix is organized in a mesh-like network<sup>259</sup>. In order to maintain a stable structure, the gel-like matrix requires stabilization by proteins. Three proteins have been indentified to be essential for the correct assembly of COC matrix: the secreted product of tumor necrosis factor-stimulated gene-6 (TSG-6<sup>43</sup>), inter- $\alpha$ -inhibitor (I $\alpha$ I<sup>35</sup>) and pentraxin 3 (PTX3<sup>37</sup>). Currently we have limited understanding of how HA and the proteins interact with each other to stabilize the COC matrix.

TSG-6 is a multifunctional protein expressed under inflammatory conditions and by cumulus cells in the preovulatory follicle<sup>32, 260-263</sup>. It has numerous ligands among which are HA<sup>68, 77</sup>, I $\alpha$ I<sup>236</sup> and PTX3<sup>37</sup>. TSG-6 is composed of two domains: the Link module with its HA binding domain<sup>76, 241, 242</sup> and the CUB module (pdb: 2WNO). The Link module, at least in some cases, has biological responses comparable to full length TSG-6<sup>70, 251, 255</sup>. However, this is not the case for the interaction with HA: Link module alone binds to HA in a simple manner, while full length binds to HA cooperatively, because of HA-induced TSG-6 oligomerization<sup>210</sup>(Chapter 3).

I $\alpha$ I is a complex proteoglycan constitutively present in serum; it consists of two heavy chain subunits (HC1 and HC2), covalently linked via a chondroitin sulphate linker to a light chain, bikunin<sup>84</sup>. The interaction between I $\alpha$ I, TSG-6 and HA results in the formation of covalent HA•HCs, TSG-6•HC complexes and numerous non-covalent complexes (Chapter 4). In the presence of I $\alpha$ I, the HA binding and cross-linking properties of TSG-6 are impaired (Chapter 4). Instead, TSG-6 acts as a catalyst for the transfer of HCs to HA<sup>236</sup>. In the COC matrix, TSG-6 was found in two distinct populations: as a TSG-6•HC complex and in its native state<sup>32</sup>. The covalent modification of the COC matrix with HCs has a particular implication for the assembly of the matrix - bikunin deficient mice (which cannot assemble intact I $\alpha$ I) were unable to form a stable matrix<sup>35, 40</sup>. However, the functional interplay between TSG-6 and I $\alpha$ I is not enough to stabilize COC matrix assembly, because mice deficient in PTX3 show cumulus matrix instability and lack of fertility<sup>38</sup>.

PTX3, the soluble pattern recognition receptor pentraxin 3, also called TSG-14, is a member of the pentraxin family<sup>104, 264</sup>. The protein assembles into a multimeric complex of 8 identical subunits (MW ~42.5 kDa) stabilized by disulfide bonds. Each protomer of PTX3 consists of a C-terminal pentraxin domain, sharing homology with a classical short pentraxin, and a unique N-terminal region<sup>109, 113</sup>. PTX3 is an extracellular matrix protein, its synthesis is upregulated by monocytes, endothelial cells and smooth muscle cells in response to primary

inflammatory signals<sup>103, 104, 264, 265</sup>. PTX3 fulfils important functions in fertility, angiogenesis and innate immunity<sup>264, 266</sup>. Its diverse functionality can be related to its complex structure. PTX3 has an elongated and asymmetric shape. It is composed of two differently sized globular lobes connected by a short stalk<sup>113</sup> in which the N- and C- terminal regions of PTX3 mediate binding to multiple ligands. Cumulus cells from of PTX3<sup>-/-</sup> mice are unable to organize into a functional matrix, although the covalent modification of HA with HC (HA•HC) remains unperturbed<sup>37</sup>. Exogenous addition of PTX3 rescued COC matrix formation. Although PTX3 does not interact with HA, it was suggested that its incorporation can be mediated by TSG-6 via its Link module domain through two distinct binding sites for HA and PTX3<sup>37</sup>. The coordinated expression of PTX3 and TSG-6 was found in leukocytes and endothelial cells under inflammatory conditions<sup>267</sup> as well as in ovulation, suggesting that these proteins are co-localized.

More recently, by immuno-co-precipitation *in vivo*, PTX3 was shown to be also colocalized with HCs, but not with bikunin of IaI<sup>38</sup>. Solid phase binding assays confirmed that there is a direct interaction between the N-terminal domain of PTX3 and HCs<sup>38, 115</sup>. The oligomeric state of PTX3 is known to be functionally important: PTX3 mutants that form dimers were unable to rescue the COC matrix assembly, while mutants that form tetramers support the formation of thick HA matrices<sup>115</sup>. PTX3 has been suggested to act as an HA cross-linker, which stabilizes the COC matrix<sup>37, 38, 260</sup>. It was proposed that direct interaction of PTX3 with TSG-6 or HCs (or both) is critical for proper COC matrix assembly<sup>38</sup>.

Moreover, *in vivo* data suggest the importance of spatio-temporal regulation in the organization of the COC matrix. In particular, it was established that the expressions of TSG-6, PTX3 and HA synthases have similar temporal profiles<sup>28, 32, 37, 102</sup>. TSG-6 was found to be co-localized with HA throughout the matrix from the periphery of the cumulus cells to the zona pellucida<sup>31</sup>. IaI is constitutively present in the blood and enters the follicle after hormonal activation of ovulation, when the permeability barrier becomes leaky, and with time diffuses towards the oocyte<sup>116, 268</sup>. PTX3 is expressed by the inner cumulus corona radiata i.e. the cumulus cells in close proximity to the oocyte. A gradient of PTX3 within the COC matrix is retained after 6 h of ovulation induction<sup>38</sup>. Such spatio-temporal organization may be crucial for the regulation of HA/protein interaction and correct assembly of the COC matrix.

Despite numerous data *in vivo*, a complete mechanistic understanding of matrix formation and stabilization remains elusive. It is our long term goal to reconstruct the assembly of the COC matrix. Here, by varying the sequence of protein addition and by using a range of surface-sensitive techniques, we provide new insights on how TSG-6, IaI and PTX3 integrate their actions. We show that TSG-6 alone cannot mediate PTX3 incorporation into HA films and neither do HA films that result from the ternary interaction of IaI, TSG-6 and HA. Our data indicate, that simultaneous encounter between proteins is a requirement for successful PTX3 incorporation. The final quaternary complex assembled by proteins can



cross-link HA, in a way that is different from cross-linking with TSG-6 alone: HA films are not collapsed but retain a soft and swollen state.

## 5.2 Experimental procedures

### **Protein and hyaluronan preparations.**

Wild type human TSG-6 Link module (Link\_TSG6, 10.9 kDa<sup>269</sup>) was expressed in *Escherichia coli* as described previously<sup>269, 270</sup>. The biotinylated Link\_TSG6 was kindly provided by Anthony Day and biotinylation of PTX3 was performed by Antonio Inforzato. Full-length recombinant human TSG-6 (rhTSG-6, 30.1 kDa) was expressed in *Drosophila Schneider 2* cells and purified as described previously<sup>243</sup>. Recombinant human PTX3 (rhPTX3, MW 344 ± 7 kDa) was purified from a Chinese hamster ovary 3.5 cell line as described previously<sup>271</sup>. Anti-human PTX3 monoclonal antibody (MNB4) was made as previously described<sup>105, 109</sup>. Stock solutions of all proteins were aliquoted and stored at -20 °C. Protein solution were defrosted shortly before use and diluted in buffer at desired concentrations.

Lyophilized HA, biotinylated at its reducing end and with well-defined molecular masses of 1083±53 kDa or 837±54 kDa (i.e. two different batches of Select-HA B1000) was purchased from Hyalose (Oklahoma City, OK, USA). For reconstitution, HA was taken up in ultrapure water at a stock concentration of 1 mg/ml, gently shaken over night, aliquoted, and stored at -20°C. Films of end-grafted HA on protein-repellent surfaces were assembled as described in Chapters 3 and 4.

A ‘hepes’ buffer (150 mM NaCl, 10 mM HEPES at pH 7.4, 3 mM NaN<sub>3</sub>, 2 mM CaCl<sub>2</sub>, 5 mM MgCl<sub>2</sub>, in ultrapure water) was used throughout all measurements. Proteins and HA solutions at their final concentrations were prepared in this buffer.

### **Quartz crystal microbalance with dissipation monitoring.**

QCM-D measurements were performed as described in detail elsewhere<sup>166, 173</sup>. The QCM-D response is sensitive to the mass (including coupled water) and the viscoelastic properties of the surface adlayer. Measurements were performed with a Q-Sense E4 system (Biolin Scientific) in flow mode<sup>245</sup> with flow speeds of typically 20 µl/min and at a working temperature of 23°C. QCM-D data were collected at six overtones ( $n = 3, 5, 7, 9, 11, 13$ , corresponding to resonance frequencies of ~15, 25, 35, 45, 55, 65 MHz). Changes in dissipation and normalized frequency,  $\Delta f = \Delta f_n/n$ , of the fifth overtone ( $n = 5$ ) are presented. Adsorption and interfacial processes on gold-coated QCM-D sensors (QX301, Biotin Scientific) were monitored *in situ* with sub-second time resolution<sup>154</sup>.

For homogeneous and sufficiently rigid layers, the film thickness can be estimated, to within an error of typically < 20%, from  $d = \Delta m/\rho = -C/\rho \times \Delta f$ , where  $\Delta m$  is the adsorbed mass per unit surface area,  $\rho = 1.0 \text{ g/cm}^3$  is the density of bulk solution and  $C = 18.06 \text{ ng/cm}^2/\text{Hz}$

the mass sensitivity constant for a sensor with a fundamental resonance frequency of 4.95 MHz<sup>135</sup>.

### ***In situ* ellipsometry.**

In situ ellipsometry measures changes in the polarization of light upon reflection from a planar surface, and was used to quantify adsorbed biomolecular masses on gold-coated silicon wafers (G. Albert PVD Beschichtungen, Silz, Germany) in a time-resolved manner. A custom-built small volume (150  $\mu$ l) open glass cuvette was used and passivated through exposure to a 10 mg/mL BSA solution for 30 min to prevent non-specific adsorption of samples to the cuvette walls. The surface density of adsorbed material was determined by numerical fitting of acquired data, as described in detail earlier<sup>166</sup>. Unbinding rates were approximated by exponential fits to the region of interest in desorption curves.

### **Western blotting.**

Samples of  $\sim$ 150  $\mu$ l volume were extracted from the ellipsometry cuvette, and stored frozen in aliquots of 30  $\mu$ l until further use. A part of collected material was analyzed for the presence of TSG-6 and subunits of IaI by Viranga Tilakaratno by western blot stained with LI-COR as described previously (Chapter 4). The presence of PTX3 in the elutes was analyzed by Antonio Inforzato by western blot with X-ray detection. Briefly, proteins in the elutes were recovered using 15  $\mu$ l of StrataClean resin (Agilent Technologies) and incubated for 15 min at room temperature under agitation, followed by a water wash. To denature and reduce the proteins they were heated at 70°C for 10 min in a sample loading buffer containing DTT (Invitrogen). The resin was analyzed by 10% Bis-Tris gel (Invitrogen) SDS-PAGE, using MOPS SDS running buffer, and transferred onto 0.45  $\mu$ m PVDF membranes. To screen for PTX3, rat anti-human PTX3 monoclonal antibody (500 ng/ml) was used, followed by addition of secondary anti-rat IgG HRP-conjugate (1:5000 dilution, GE Healthcare). Immunoreactive bands were revealed using ECL substrate (Millipore) and a Chemidoc system (Bio-Rad).

### **Colloidal probe reflection interference contrast microscopy.**

The thickness of surface-bound HA films was determined by triple-wavelength colloidal probe RICM, as described previously<sup>173, 226</sup>. Naked polystyrene microspheres of  $\sim$ 25  $\mu$ m diameter (Polysciences, Eppelheim, Germany) were used as colloidal probes. The HA films were assembled on bare or gold-coated glass cover slips, using custom-built open cells with an internal volume of 50  $\mu$ l. Protein solutions at desired concentrations were added, and the incubation time was set to 5h. Colloidal probes were added shortly before acquisition of RICM images.

### **Functionalization of colloidal beads with HA films.**

Streptavidin-functionalized polystyrene microspheres (SAv-PS) with a nominal diameter of 22.7  $\mu$ m (SPHERO, USA) were used. The stock solution at 0.5% (w/v) concentration was

washed by 3 cycles of adding a 5-fold volume excess of ultrapure water, centrifugation at 10000 rpm for 10 min, and removal of the supernatant. End-biotinylated HA (837 kDa) was added to 0.5% (w/v) of particles at a final concentration of 50  $\mu\text{g/ml}$  (the ratio corresponds to a bead surface area of 1  $\text{nm}^3$  per HA chain) and incubated under agitation for 30 min at room temperature. Unbound HA was eluted by 5 cycles of washing as described before. The HA-functionalized beads were used immediately after preparation.

### **Quantification of the mobility of colloidal probes by RICM.**

The motion of microspheres was monitored by RICM imaging at a wavelength of 490 nm, at a rate of 8 frames per second and an exposure time of 100 ms, for 12.5 s. From the images, variations in the bead position were quantified in all three spatial directions ( $x$ ,  $y$ ,  $z$ ) with a resolution on the order of 1 nm through custom-made image analysis software (Ralf Richter). From the evolution of the spatial position as a function of time  $t$ , the mean square displacement (MSD) was calculated. Typically, the microspheres were found to undergo a directed motion parallel to the surface in addition to random stochastic motion, presumably driven by convection or by gravity on a slightly tilted sample. To correct for the directed motion, we subtracted a linear fit from the  $x(t)$  and  $y(t)$  data sets before computing the MSD. Only the MSD at a lag time  $\tau = 0.125\text{s}$  was considered for further analysis. Based on the number of data points per trace, we estimate a statistical uncertainty of 10% for the MSDs at  $\tau = 0.125\text{s}$ .

## 5.3 Results

### 5.3.1 PTX3 interacts with Link\_TSG6, rhTSG-6 and I $\alpha$ I in the absence of HA.

PTX3 does not interact directly with HA (Fig. 5.1). The incorporation of the protein into HA-rich matrices (in particular into the COC matrix) must hence be mediated by other molecular players that interact with HA. TSG-6<sup>37</sup> and the heavy chains (HCs) of I $\alpha$ I<sup>122</sup> have been proposed to be involved in this interaction. First, we tested the interaction of PTX3 with these binding partners in the absence of HA.

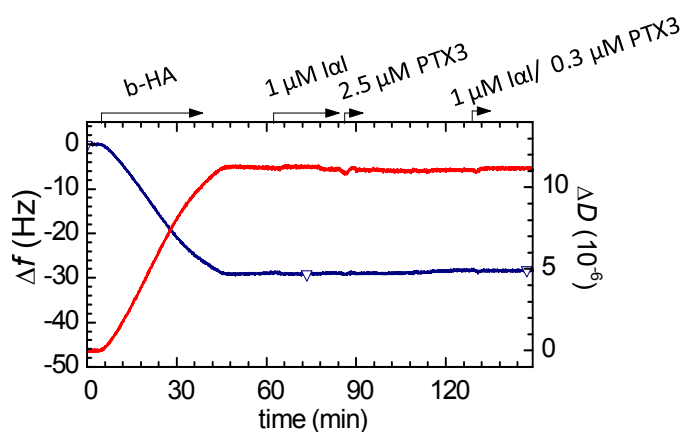


Fig. 5.1 **Interaction between HA and I $\alpha$ I, PTX3 or PTX3/I $\alpha$ I.** The start and duration of the incubation with different samples is indicated (*solid arrows*). After each incubation step, the solution phase was replaced by buffer. QCM-D did not show any significant interaction between the HA film (58 kDa) and I $\alpha$ I, PTX3 or a PTX3/I $\alpha$ I mixture.

All interactions were assessed through solid-phase binding assays using gold-coated surfaces as supports; QCM-D and *in situ* ellipsometry were utilized to monitor the binding events. The gold-coated surfaces were functionalized with a protein-repellent oligoethylene glycol (OEG) coating exposing biotin groups and a dense monolayer of streptavidin (SAv), as described earlier<sup>210</sup>. The SAv layer provides sites for the stable immobilization of biotinylated biomolecules. The underlying OEG ensures that only biotinylated species can bind directly to the surface, i.e. the binding is specific.

The binding of PTX3 to biotinylated Link\_TSG6 (b-Link\_TSG6) was first tested by QCM-D (Fig. 5.2A). The final responses after incubation of the surface with b-Link\_TSG6 were  $\Delta f = -14$  Hz and  $\Delta D = 0.3 \times 10^{-6}$ . This response indicates formation of a protein layer of approximately 2 nm in thickness, consistent with the dimensions of Link\_TSG6<sup>210, 242</sup>. No desorption was observed upon rinsing in buffer, i.e. b-Link\_TSG6 was firmly immobilized.

Addition of PTX3 resulted in rapid binding with an additional frequency shift of  $\Delta f = -42.5$  Hz and a strong increase in dissipation by  $\Delta D = 2.1 \times 10^{-6}$ . The interaction between Link\_TSG6 and PTX3 was rather stable: only a minor fraction of proteins desorbed within 10 min after rinsing in buffer. From the frequency shift, a thickness of the PTX3 film of 7 to 8 nm can be estimated. PTX3 forms an octamer<sup>113</sup> of approximately cuboid shape with a size of  $9.6 \times 14.3 \times 26$  nm<sup>3</sup>, i.e. PTX3 binds predominantly side-on to the Link\_TSG6 monolayer.

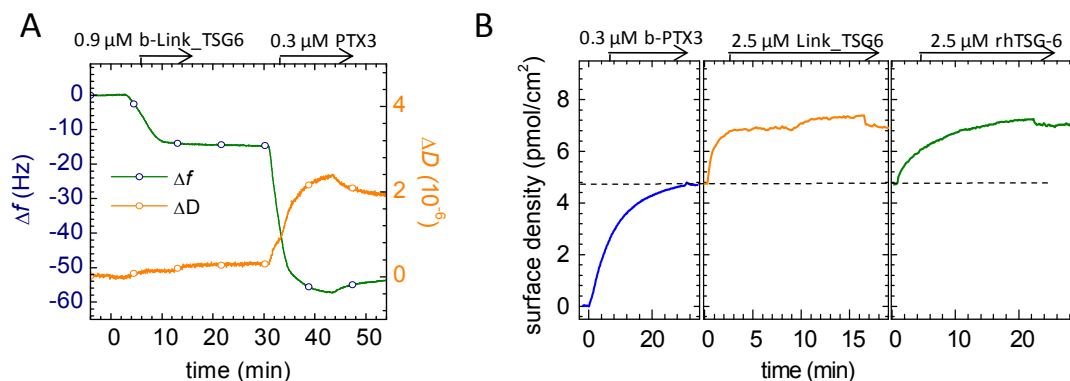


Fig. 5.2 **Interaction between PTX3 and TSG-6.** *A.* Interaction of surface-bound Link\_TSG6 with PTX3, measured by QCM-D. Biotinylated Link\_TSG6 (b-Link\_TSG6) was immobilized to a streptavidin monolayer and binding of native PTX3 was monitored. The bulk PTX3 concentration refers to PTX3 monomers. *B.* Interaction of surface-bound PTX3 with Link\_TSG6 and rhTSG-6 measured by *in situ* ellipsometry. Biotinylated PTX3 (b-PTX3) was immobilized and binding of Link\_TSG6 and rhTSG-6 monitored. Start and duration of each incubation step with different samples are indicated with solid arrows. After each incubation step, the solution phase was replaced by buffer.

A reverse approach was used in a complementary *in situ* ellipsometry assay, that is, biotinylated PTX3 (b-PTX3) was first immobilized (Fig. 5.2B). Binding of b-PTX3 was interrupted at a monomer surface density of 4.8 pmol/cm<sup>2</sup>, corresponding to 1 PTX3 octamer per 280 nm<sup>2</sup>. Here, binding of both Link\_TSG6 and rhTSG-6 (which is not available in a biotinylated form) could be tested (Fig. 2B). Addition of both TSG-6 constructs at identical molar bulk concentrations yielded comparable molar surface densities corresponding to approximately 50% of the PTX3 monomer surface density. Most of the bound protein could not be eluted by rinsing in buffer indicating that binding is rather tight. Even though Link\_TSG6 and rhTSG-6 bound in similar amounts and with similar stability, they differ distinctly in the adsorption kinetics: Link\_TSG6 bound rapidly with an initial binding rate that suggests mass-transport limited binding, whereas rhTSG-6 binding was much slower. The distinctly different binding kinetics might well reflect differences in the mode of binding of both TSG-6 constructs, such as previously reported for the binding to HA (see Chapter 2). We can though not fully exclude that the decreased binding rate for rhTSG-6 is due to steric effects: the solid support and crowding might partially mask TSG-6 binding

sites in the PTX3 monolayer rendering binding of the rather large rhTSG-6 (30.5 kDa) more difficult than the smaller Link\_TSG6 (10.9 kDa).

### 5.3.2 Ternary interaction between TSG-6 constructs, PTX3 and HA.

Next, we tested how the interaction of PTX3 and TSG-6 is affected by the presence of HA. The ternary interaction between HA, PTX3 and TSG-6 could lead to incorporation of PTX3 into HA matrices only if the HA and PTX3 binding sites on TSG-6 do not interfere with each other. To test if this is the case, we performed a sequential binding assay (Fig 5.3). First, the HA film was incubated with Link\_TSG6 at a bulk concentration of 5  $\mu\text{M}$ . The surface density of adsorbed material at equilibrium was  $215 \pm 16 \text{ ng/cm}^2$ , corresponding to an occupancy of 1 Link\_TSG6 per 5 HA disaccharides, in a good agreement with previous work (Chapter 3, Table 3.1). An excess of Link\_TSG6 was kept in the bulk solution without rinse to avoid desorption of Link\_TSG6, which could occur rapidly<sup>210</sup>. Addition of PTX3 at a bulk monomer concentration of 0.3  $\mu\text{M}$  revealed a large increase in the adsorbed mass. The surface density of incorporated material was  $418 \pm 55 \text{ ng/cm}^2$ . Since PXT3 alone does not interact with HA (Fig. 5.1) we conclude that incorporation is Link\_TSG6 mediated, as proposed before<sup>37, 272</sup>. Hence, the binding sites for HA and PTX3 on Link\_TSG6 do not overlap, allowing Link\_TSG6 to act as a linker for PTX3 incorporation into HA matrices.

In addition to the sequential binding assay, we performed co-incubation of 0.3  $\mu\text{M}$  PTX3 with gradually increasing concentrations of Link\_TSG6 (Fig. 5.4A). For comparison, Link\_TSG6 was titrated into the HA film in the absence of PTX3 (Fig. 5.4B). Both assays were performed one after the other on the same HA film. Consistent with the sequential binding assay, the amount of adsorbed material in the presence of PTX3 was larger than with Link\_TSG6 alone. It is notable that enhanced binding was observed for 3.5  $\mu\text{M}$  and more Link\_TSG6 in solution, but not for smaller Link\_TSG6 concentrations.

The dissociation rate of Link\_TSG6 alone from the HA film was  $(31 \pm 2) \times 10^{-3} \text{ s}^{-1}$  (Fig. 5.4B), comparable with previously reported rates on polymeric HA and oligo HA films (Chapter 3, Table 3.1). The dissociation rate in the presence of PTX3 was  $(14.7 \pm 0.6) \times 10^{-3} \text{ s}^{-1}$ , i.e. two times lower than for Link\_TSG6 alone. The decrease in the desorption rate might indicate that PTX3/Link\_TSG6 complex binds to the films in a multivalent manner.

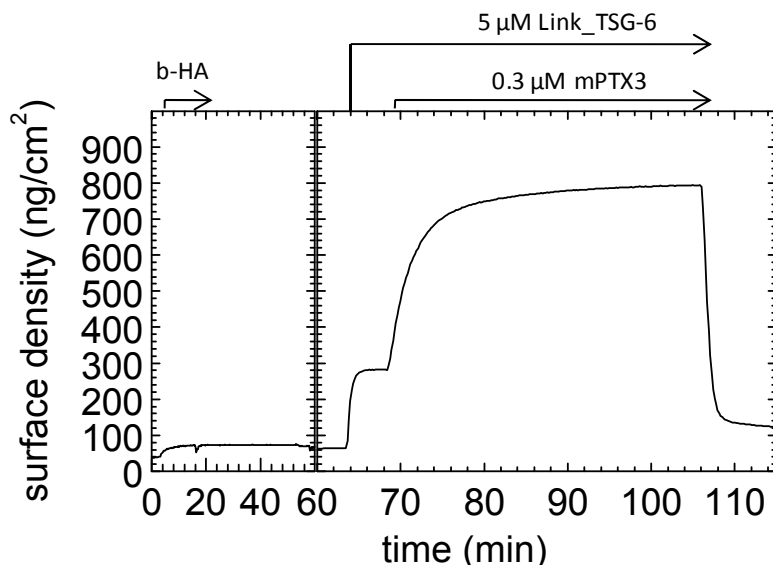


Fig. 5.3 **Incorporation of PTX3 into HA film via Link\_TSG-6.** The HA film (837 kDa) was first exposed to Link\_TSG6. After equilibrium was established, free Link\_TSG6 remained in solution. Addition of PTX3 revealed fast adsorption to the surface confirming incorporation into the HA film.

The binding isotherm in the presence of PTX3 (Fig. 5.5) exhibited a pronounced sigmoidal shape. A fit with the Hill equation (Chapter 3, Fig. 3.3) to the data in Fig. 5.5 gave an exponent of  $3.6 \pm 0.5$ , indicative for cooperativity, with  $K_{0.5} = 2.9 \pm 0.2 \mu\text{M}$  and  $\Gamma_{\text{max}} = 945 \pm 42 \text{ ng/cm}^2$ . In contrast, the data for Link\_TSG6 alone could be fitted by a Langmuir isotherm ( $K_{0.5} = K_D = 4.6 \pm 0.6 \mu\text{M}$ ), in agreement with previous reports (Chapter 3, Table 3.1). Thus, the cooperative binding must somehow originate from the interaction of Link\_TSG-6 with PTX3.

Next, we tested the ternary interaction between full-length TSG-6, PTX3 and HA. In contrast to Link\_TSG6, the interaction between rhTSG-6 and HA is characterized by a pronounced positive cooperativity (Chapter 3, Fig. 3.3), and  $K_{0.5}$  is about five-fold lower than for Link\_TSG6<sup>210</sup>.

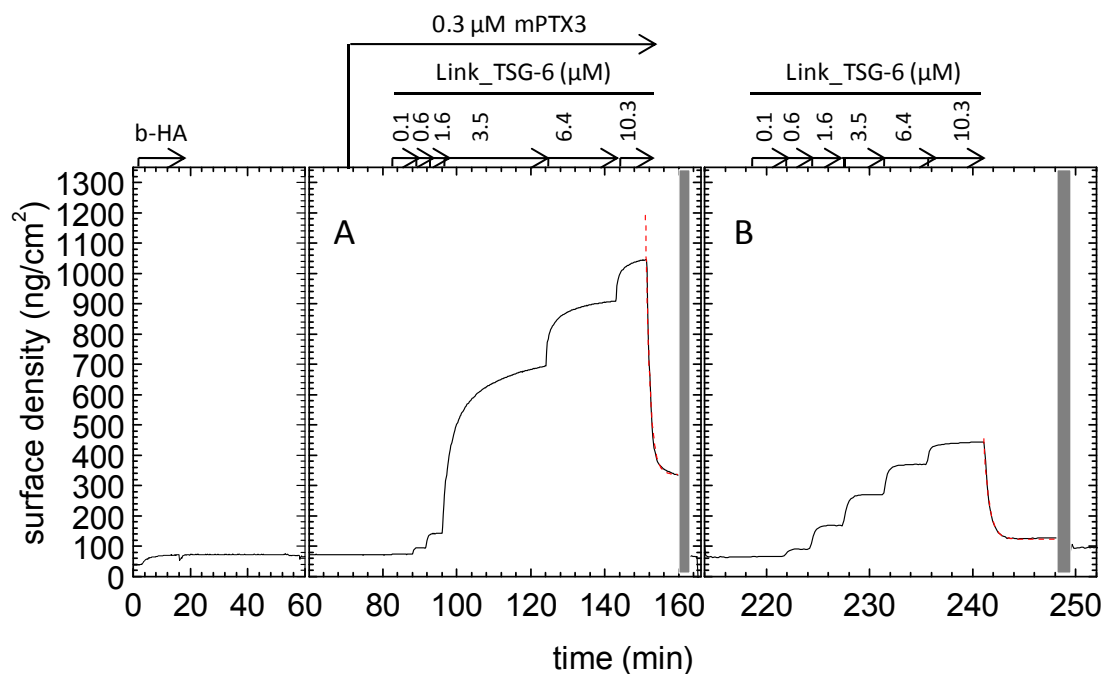


Fig. 5.4 **Titration of Link\_TSG-6 into an HA film in the presence of PTX3 in solution phase.** *A.* PTX3 at a bulk concentration of  $0.3 \mu\text{M}$  was kept in solution throughout Link\_TSG6 titration. The bulk concentration of Link\_TSG6 was increased stepwise (indicated with arrows). *B.* For comparison, Link\_TSG6 was titrated into the HA film in the absence of PTX3. Co-incubation of Link\_TSG6 with PTX3 resulted in a pronounced increase in the surface density. The desorption rate after removal of proteins from the bulk solution was fitted by an exponential. Washes with 8 M GuHCl after the titrations (not monitored, indicated as grey shaded areas), confirmed that the stably bound fraction could be fully eluted under denaturing conditions.



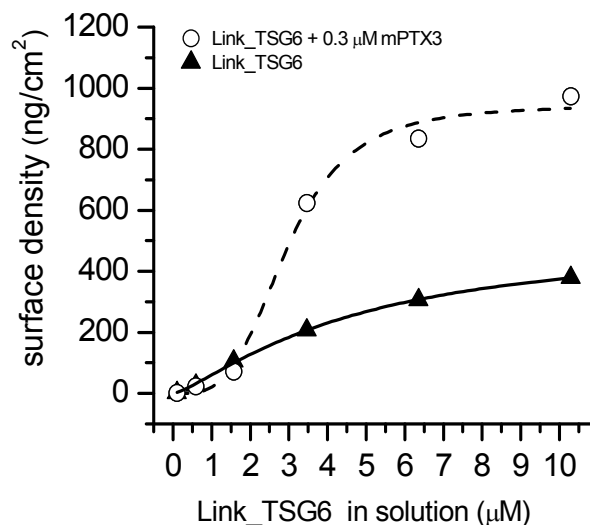


Fig. 5.5 **PTX3 modulates Link\_TSG6 interaction with HA.** The titration curve for Link\_TSG6 can be approximated well with a simple Langmuir isotherm (filled triangles/solid line). In the presence of PTX3 the interaction is more complex, The sigmoidal shape indicates cooperative binding (empty circles/dashed line).

Analogous to our approach described above (Fig 5.3), we performed a sequential incubation assay where PTX3 at 0.3  $\mu\text{M}$  bulk concentration was added to an HA film that had previously been incubated with rhTSG-6 (Fig. 5.6A). PTX3 did not show any significant binding to the rhTSG-6 loaded HA film when incubated at 0.3 and 1  $\mu\text{M}$ . Subsequent addition of an anti-PTX3 antibody did not lead to any response either, confirming the absence of PTX3 binding. In a modified assay, excess rhTSG-6 was removed from the bulk solution prior to addition of PTX3 (Fig. 5.6B). In this case, PTX3 induced a minor yet significant increase in the dissociation rate of TSG-6. Apparently, PTX3 and HA compete for rhTSG6, although the competing capacity of PTX3 is rather weak at concentrations as high as 0.3  $\mu\text{M}$  (which is already 1000-fold higher than the PTX3 concentrations found *in vivo*, in particular in follicular fluid)<sup>37</sup>.

The absence of rhTSG-6 mediated incorporation of PTX3 into HA films is in stark contrast to our observation for Link\_TSG6 (Fig. 5.3-5.4). From Fig. 5.2B, as well as previous reports in the literature<sup>37, 114</sup> we know that rhTSG6 can interact with PTX3 in the absence of HA. Somehow, this interaction must be perturbed by HA. To further investigate the interplay between the binding of rhTSG-6 to HA and PTX3, we performed titrations of rhTSG6 to HA films in the presence of selected concentrations of PTX3 in the solution phase (Fig. 5.7).

Within the experimentally accessible range of rhTSG-6 concentrations (up to 2  $\mu\text{M}$ ), PTX3 inhibited protein binding to HA in a dose-dependent manner. Addition of a polyclonal anti-PTX3 antibody to the protein-loaded HA films at the end of the titration assays did not result in any significant response (Fig. 5.7A), confirming that the bound protein material

consisted exclusively of rhTSG-6. Apparently, PTX3 competes with HA for the binding of rhTSG-6. As a consequence, we conclude that PTX3 cannot be incorporated into HA matrices through rhTSG-6 alone at physiologically relevant protein concentrations, contrary to what has been proposed in the literature<sup>37</sup>, based on experimental data with Link\_TSG6.

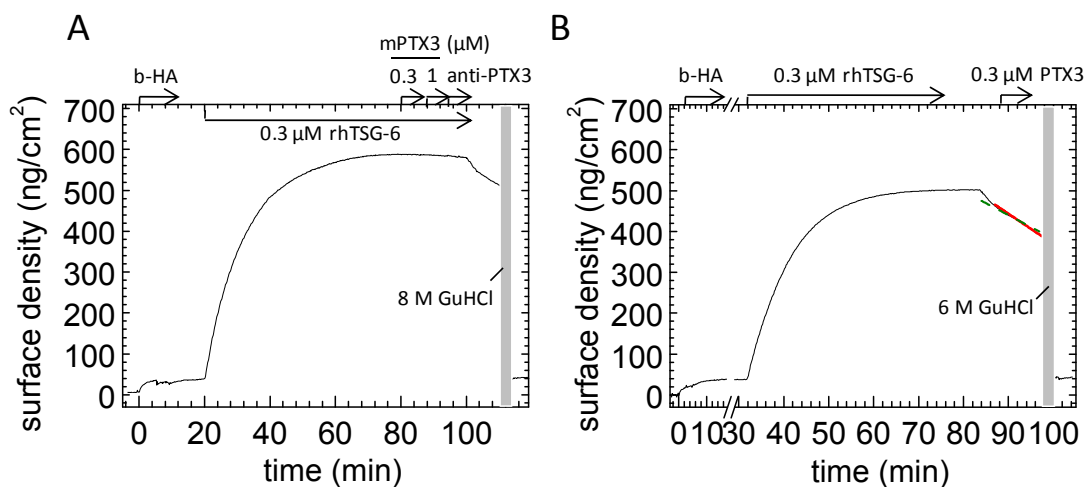


Fig. 5.6 **Sequential incubation assays with TSG-6 and PTX3 by ellipsometry.** *A.* The HA film was loaded with rhTSG-6. After binding equilibrium was established and without an additional rinsing step, PTX3 was added. No significant binding upon PTX3 exposure was observed. Absence of anti-PTX3 binding confirmed that there is no PTX3 incorporation into the rhTSG-6 loaded film. *B.* rhTSG-6 was added to an HA film at a final concentration of 0.3 μM. After binding equilibrium had been established, excess TSG-6 was removed from the solution. Addition of 0.3 μM PTX3 induced a minor increase in the desorption rate (red and olive dashed lines indicate the slope shortly before and after addition of PTX3, respectively). All bound protein material could be eluted with 6 M GuHCl, i.e. it was non-covalently bound.

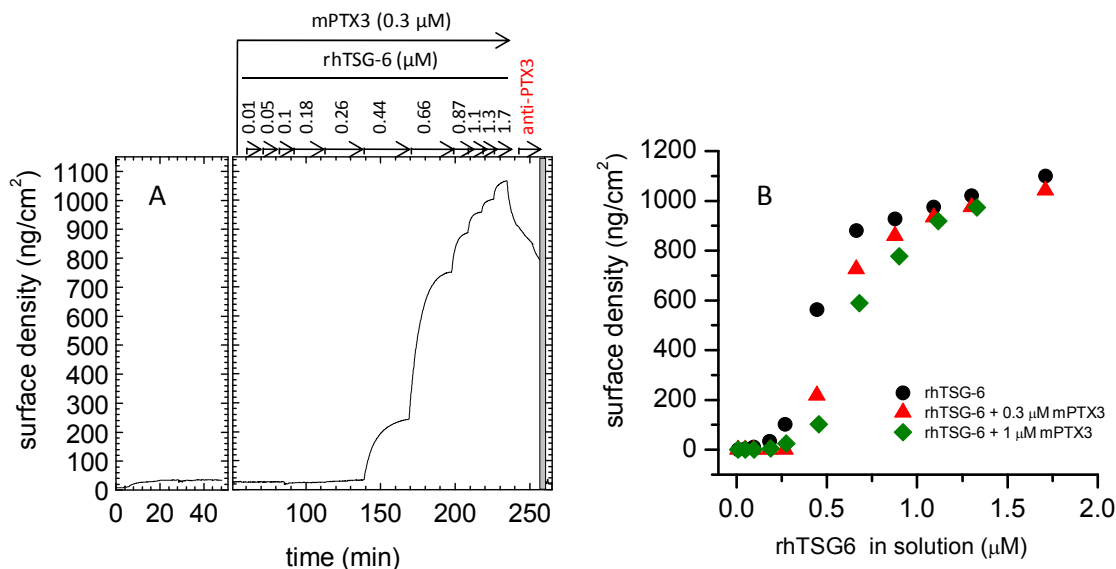


Fig. 5.7 **Competition of PTX3 and HA for TSG-6 binding.** (A) Representative titration assay by ellipsometry of rhTSG-6 into HA films in the presence of 0.3  $\mu\text{M}$  PTX3 (B) Binding isotherms from the measurement in A, and two other measurements performed at different PTX3 concentrations. At a bulk rhTSG-6 concentration of 0.45  $\mu\text{M}$ , an approximately 3-fold decrease in the surface density of adsorbed rhTSG-6 can be detected in the presence of 0.3  $\mu\text{M}$  PTX3. At 1  $\mu\text{M}$  PTX3, the decrease in binding becomes even more pronounced.

### 5.3.3 Interaction of PTX3 with HA films that were pre-exposed to TSG-6 and I $\alpha$ I.

PTX3 is also known to bind to intact I $\alpha$ I<sup>38, 115</sup>, and it has been proposed that PTX3 incorporates into HA matrices through interaction with heavy chains (HCs)<sup>38</sup>. The latter can be covalently transferred from I $\alpha$ I to HA via a reaction that is catalyzed by TSG-6. To test this hypothesis, we first exposed HA films to a mixture of TSG-6 and I $\alpha$ I and then studied PTX3 binding (Fig. 5.8).

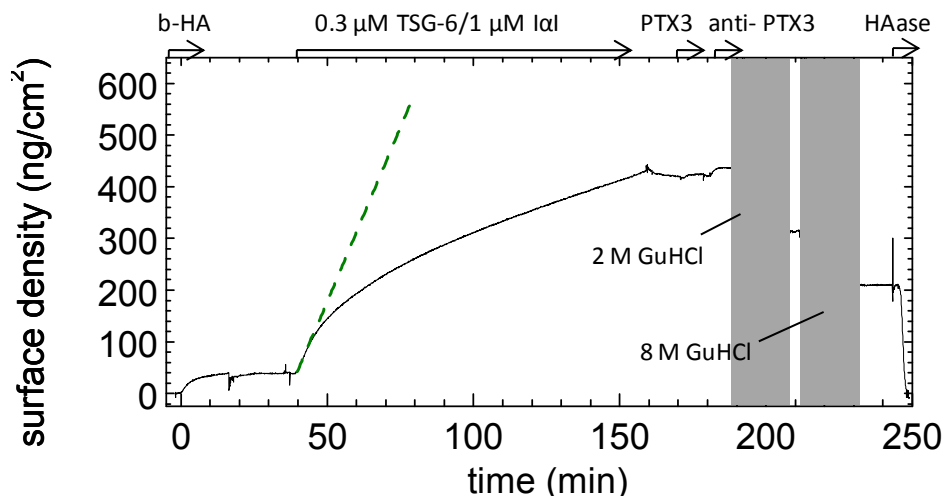


Fig. 5.8 **PTX3 does not bind to HA films that had been exposed to a mixture of I $\alpha$ I/TSG-6.** 1  $\mu$ M I $\alpha$ I and 0.3  $\mu$ M TSG-6 were sequentially added to the HA film (no pre-mixing). In this case, the film contains an additional fraction of non-covalently but stably bound protein (see Chapter 4). Incubation with 0.3  $\mu$ M PTX3 does not affect the surface density of the film. The lack of a significant response upon incubation with 0.08  $\mu$ M anti-PTX3 antibody (MNB4) confirms the absence of PTX3 binding.

Incubation of the film with 0.3  $\mu$ M PTX3 revealed that it does not bind significant amounts of PTX3. This unexpected finding seems to indicate that none of the HA-bound material that arises from ternary interactions between TSG-6, I $\alpha$ I and HA is able to bind PTX3. Alternatively, one may argue that PTX3 binding is simply limited by the access of the protein to the interior of the HA film. We recall that PTX3 forms octamers in solution<sup>113</sup> that are significantly larger than TSG-6 or I $\alpha$ I.

#### 5.3.4 Permeability of HA films for PTX3.

In order to test if PTX3 is sterically excluded from our HA films, we performed permeation assays using b-PTX3 (Fig. 5.9). The assay exploits the fact that only a small fraction ( $\sim$ 1%) of the biotin binding sites on the SA<sub>v</sub> monolayer that accommodates the HA film are occupied by b-HA<sup>173</sup>. Biotinylated PTX3 that diffuses through the HA film should hence find plenty of sites to bind through its biotin group.

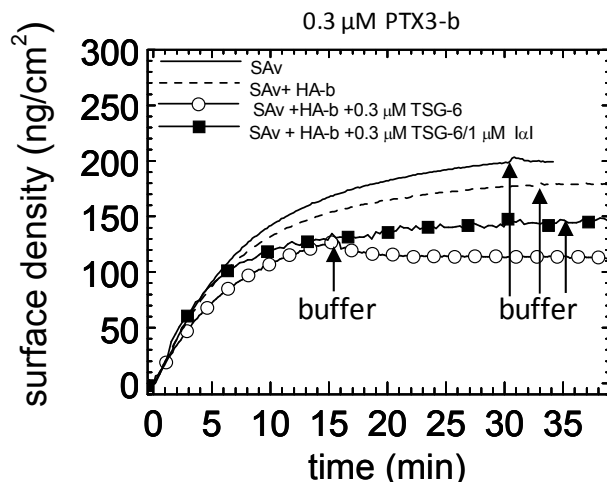


Fig. 5.9 **Permeability of HA films to PTX3.** b-PTX3 was added to SAV-covered surfaces without any further functionalization (solid line), and in the presence of HA (837 kDa) films with a surface density of  $35 \pm 5$  ng/cm<sup>2</sup>. HA films were presented pure (dashed line), or they had previously been exposed to 0.3  $\mu$ M rhTSG-6 (solid line with filled squares) or to a mixture of 1  $\mu$ M I $\alpha$ I and 0.3  $\mu$ M TSG-6 (pre-mixed for 1 min before addition to the HA film; solid line with empty circles). Only initial binding is shown. Binding with similar rates is observed for all surfaces. Since PTX3 alone did not show binding on any of these surfaces, the binding of b-PTX3 must occur via the biotin moiety to SAV, indicating that all HA films are permeable to PTX3.

When added at a bulk concentration of 0.3  $\mu$ M to a plain SAV monolayer, b-PTX3 bound with a maximal surface density of  $190 \pm 10$  ng/cm<sup>2</sup>. Final adsorbed amounts of similar magnitude, although slightly smaller, were also observed for HA films with a surface density of  $35 \pm 5$  ng/cm<sup>2</sup> that were pure or had been incubated with 0.3  $\mu$ M rhTSG-6, alone or in a mixture with 1  $\mu$ M I $\alpha$ I (data not shown). Importantly, the initial PTX3 binding rates through all HA films did not differ significantly from the initial rate on the plain SAV surface (Fig. 5.9), indicating that the different HA films do not significantly delay the access of b-PTX3 to SAV. Clearly, all HA films of interest retained good permeability to PTX3. Therefore, we must conclude that neither pure HA films nor HA films that were treated with TSG-6 or with a mixture of TSG-6 and I $\alpha$ I present appropriate PTX3 ligands.

### 5.3.5 How to incorporate PTX3 into HA films?

The absence of PTX3 binding in the above-described assays disproves existing hypotheses about the mechanism by which PTX3 is incorporated into HA matrices<sup>37, 38</sup>. On the other hand, PTX3 has been shown to be an essential component of some HA matrices. Then how to incorporate PTX3 into HA film? We hypothesized that the encounter between PTX3 on the one hand and I $\alpha$ I and/or TSG-6 on the other prior to their interaction with HA is required to incorporate PTX3 into HA assemblies.

To test this hypothesis, we first added a mixture of PTX3 and I $\alpha$ I at bulk concentrations of 0.3  $\mu$ M and 1  $\mu$ M, respectively, to an HA film. This mixture did not show any HA binding activity (Fig. 5.1). Second, TSG-6 was added at a bulk concentration of 0.3  $\mu$ M. This protein did start a binding reaction (Fig. 5.10). After 2 h of incubation, all proteins in the soluble phase were removed. Subsequent incubation with MBN4, an antibody that recognizes to the N-terminal domain of PTX3, induced additional binding. In contrast, the same antibody did not bind to an HA film that had been incubated with TSG-6 (Fig. 5.6B). This confirms that the antibody recognizes PTX3 specifically, and demonstrates that the co-incubation of PTX3 in a ternary mixture with I $\alpha$ I and TSG-6 promotes PTX3 incorporation into the HA film.

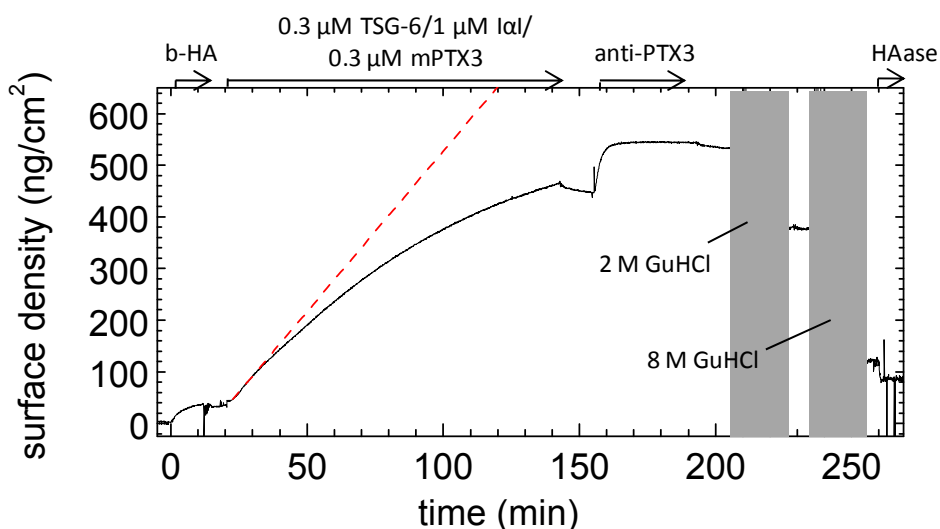


**Fig. 5.10 PTX3 incorporates into HA films when presented in a ternary mixture with TSG-6 and I $\alpha$ I.** Binding assay by ellipsometry. HA films were first briefly incubated with 0.3  $\mu$ M PTX3 mixed with 1  $\mu$ M I $\alpha$ I added to HA sequentially within one minute and 0.3  $\mu$ M TSG-6 was subsequently added within 30 seconds. The graph shows the binding reaction that ensues immediately after addition of TSG-6 (at 22 min). The protein mixtures were incubated with the HA films for 2 h. Binding of anti-PTX3 antibody, incubated at 0.08  $\mu$ M, indicates successful incorporation of PTX3.

It is difficult to use the antibody test to quantify the amount of incorporated PTX3: the accessibility of PTX3 inside the HA film might be limited and it is also not clear if the antibody can bind simultaneously to all monomers in the PTX3 octamer. By assuming a stoichiometry of 1 antibody per PTX3, and using a molecular weight of the antibody of 150 kDa, a lower limit for the amount of incorporated PTX3 can be estimated as 0.6 pmol/cm<sup>2</sup>. For comparison, the density of TSG-6 when incubated alone at the same concentration would be about 20-fold higher.

More generally, our data do not provide full information about the exact composition of the polysaccharide-protein assembly that forms upon interaction of the ternary protein mixture with HA. Considering that the four starting molecules can engage in a variety of

homotypic and heterotypic interactions, it is also difficult to suggest what type of molecule/molecular complex acts as ligand for PTX3. However, we can extract some information about the functional role of PTX3 by analyzing the kinetics of the binding reaction and the stability of binding from the ternary protein mixture.

The initial rate of the binding reaction with the ternary protein mixture (Fig. 5.10) was much smaller than the initial binding rates of TSG-6 alone (Fig. 5.6B) and about 2 times smaller than the reaction rate for the binary mixture of TSG-6 and I $\alpha$ I (Fig. 5.8). This indicates that the propensity of I $\alpha$ I to (partially) impair the binding of TSG-6 to HA (see Chapter 4) is retained and perhaps even enhanced in the presence of PTX3.

To test if PTX3 influences the competition between I $\alpha$ I and HA for TSG-6 (see Chapter 4), we performed another sequential incubation assay (Fig. 5.11): I $\alpha$ I and PTX3 were pre-mixed and exposed to a TSG-6 loaded HA film. Linear fits allowed us to approximate the unbinding rates just before ( $3.70 \pm 0.03$  ng/cm<sup>2</sup>/min) and after addition of I $\alpha$ I and PTX3 ( $26.6 \pm 0.3$  ng/cm<sup>2</sup>/min). Comparison with the displacement induced by I $\alpha$ I alone (Fig. 4.1B in Chapter 4) did not reveal any significant difference. Also, the fraction of stably but non-covalently bound material that persisted after incubation with I $\alpha$ I and PTX3 was comparable to the fraction displaced by I $\alpha$ I alone (30% and 35%, respectively). Hence, PTX3 does not affect the propensity of I $\alpha$ I to displace TSG-6 from HA. More generally, this finding would indicate that PTX3 does not influence the initial interaction between TSG-6 and I $\alpha$ I.

Approximately 10 min after the start of incubation with I $\alpha$ I and PTX3 (Fig. 5.11), at 107 min), an increase in the surface density was observed. We had already seen a similar effect with I $\alpha$ I alone (Fig. 4.1B, Chapter 4) and concluded that this response relates to transfer of HCs to HA, accompanied by the incorporation of several non-covalently bound protein material into the HA film. The overall similarity in the rates and magnitudes of binding suggests that similar processes occur also in the presence of PTX3. Yet, a detailed comparison of the binding curves reveals distinct shapes: the curve for I $\alpha$ I alone (Fig. 4.1B of Chapter 4) was linear over more than 3 h of incubation, whereas the binding curve for the mixture of I $\alpha$ I and PTX3 (Fig. 5.11) is well approximated by an exponential with a half time of 3 h. In Chapter 4, we had proposed that the linear response is a signature for the transfer of HCs from I $\alpha$ I to HA with TSG-6 acting as a catalyst. In this context, the exponentially decaying binding rate in Fig. 5.11 might indicate that, in the presence of PTX3, TSG-6 is consumed in the HC transfer reaction. In other words, we hypothesize that PTX3 inhibits recycling of TSG-6.

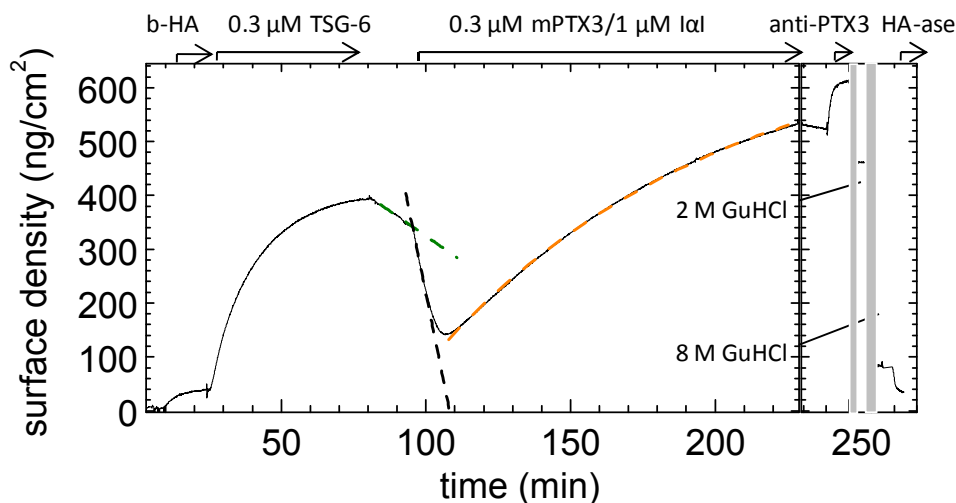


Fig. 5.11 **PTX3 incorporation into TSG-6 loaded HA film.** The HA film first was loaded with  $0.3 \mu\text{M}$  TSG-6, excess protein was removed from the solution phase, and a mixture of  $0.3 \mu\text{M}$  PTX3/ $1 \mu\text{M}$  I $\alpha$ I was added. Addition of the PTX3/I $\alpha$ I mixture first enhanced desorption until a mass fraction of 35% remained, and thereafter incorporation of material into the HA film started. Addition of anti-PTX3, after removal of excess protein in the solution phase, confirmed PTX3 incorporation into the film. Only a small fraction of about 12% could be eluted with 2 M GuHCl, while most material was eluted with 8 M GuHCl. A fraction of 10% remained bound in 8 M GuHCl but could be largely digested by hyaluronidase. The increase in the desorption rate upon addition of I $\alpha$ I/PTX3 can be appreciated from the linear fits to the data shortly before (green dashed line) and after (black dashed line) the start of protein incubation. The adsorption process setting in 10 min after incubation with I $\alpha$ I/PTX3 was fitted by an exponential (orange dashed line). The fit revealed a maximal surface density of  $690 \text{ ng/cm}^2$  and a half time of about 93 min.

### 5.3.6 Stability of PTX3 incorporation and effect of PTX3 on HA film composition.

To analyze the composition of the HA film after protein incubation Viranga Tilakaratna and Antonio Inforzato performed Western blot analyses with anti-PTX3, anti-TSG-6, anti-I $\alpha$ I antibodies of material collected from the incubation assays in Fig. 5.8 and Fig. 5.10 after exposure to 2 M GuHCl, 8 M GuHCl and hyaluronidase, respectively. The anti-PTX3 antibody (Fig. 5.12A) revealed the two strongest bands for the 8 M GuHCl elute that was retrieved from the ternary protein mixture. The apparent molecular weights of about 50 and 100 kDa were identical to PTX3 monomers and dimers in a control. No bands were found at these positions for the 2 M GuHCl elutes, the HA-ase digests, and the 8 M GuHCl elute retrieved from the binary mixture. This indicates that most, if not all, PTX3 is very tightly yet non-covalently bound into the HA matrix. Some anti-PTX3 mAb immunoreactive bands were observed at 28 and 55 kDa in samples from 2M GuHCl washes (Fig. 5.12A, labeled as (a -b)). These bands might correspond to the antibody leftovers from the injections



performed in Fig. 5.8 and Fig. 5.10, light chain and heavy chain of IgG respectively. Also a band about 65 kDa (Fig. 5.12A, labeled as (c)) is present due to the contaminant of the samples with BSA, that are recognized by rabbit polyclonal antibody.

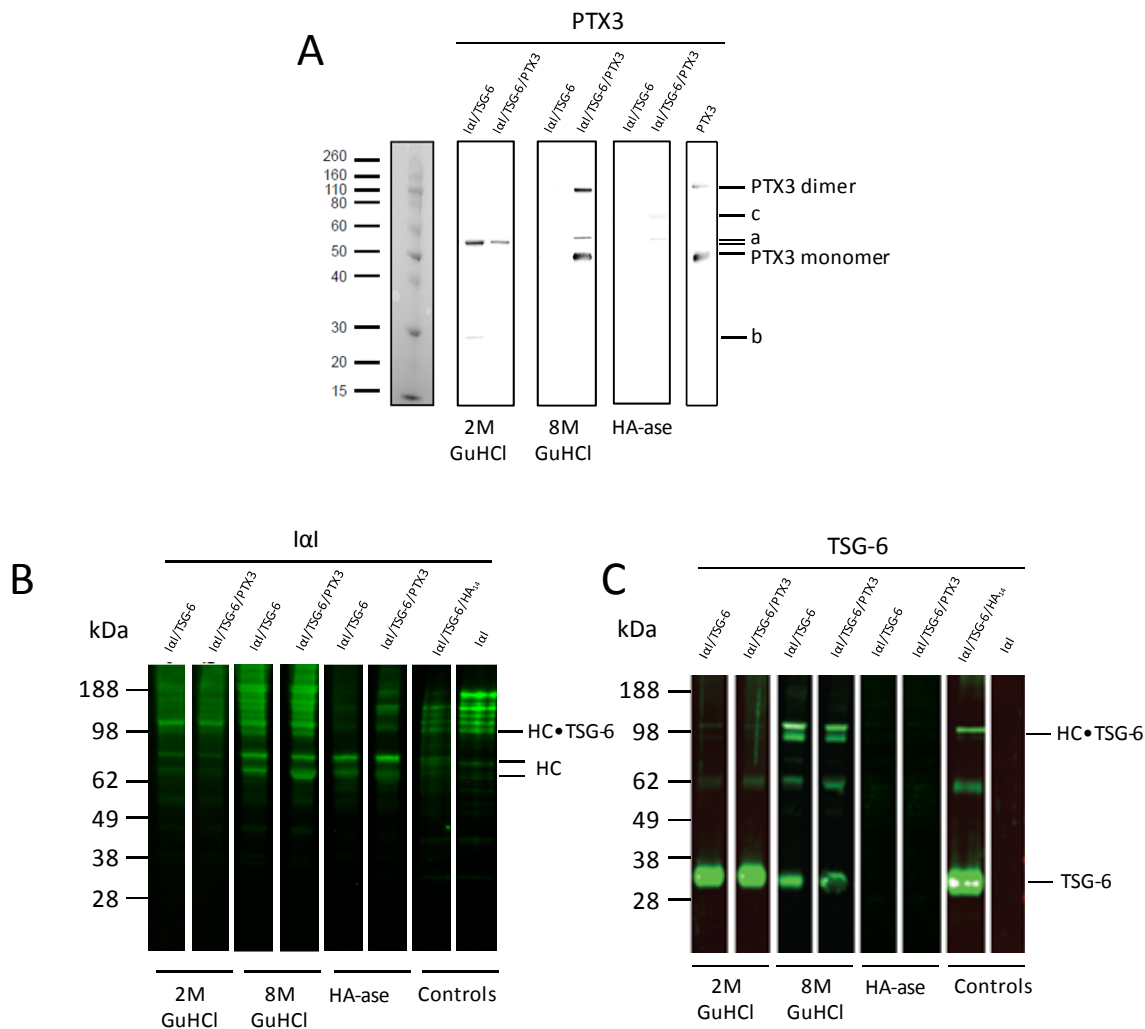


**Fig. 5.12 Western blot analysis of protein material incorporated into HA films.** HA films were incubated with proteins in binary (IαI/TSG-6) and ternary (IαI/TSG-6/PTX3) mixtures, as shown in Figs. 8 and 10, respectively. Western blots were made from fractions obtained by stepwise elution with 2 and 8 M GuHCl, and by digestion with HA-ase. Collected material was analyzed by Western blots with anti-PTX3 (A), anti-IαI (B) and anti-TSG-6 (C) antibodies. The control reaction mix of TSG-6, HA<sub>14</sub> and IαI is expected to contain a total amount of 100 ng TSG-6 and 25 ng IαI, and the detection limits are estimated to be around 5 ng for TSG-6 and 0.5 ng for IαI. Western Blots were prepared by A. Inforzato (Istituto Clinico Humanitas, IRCCS) and V. Tilakaratna & A.J. Day (University of Manchester).

The staining patterns with the anti-TSG-6 and anti-IαI antibodies (Fig. 5.12B-C) were consistent with the results already reported in Chapter 4 (Figs. 4.1D and 4.3B), i.e. rhTSG-6

protein and TSG-6•HC were found in all GuHCl elutes but not in the HA-ase digest, while HC was also found in the HA-ase digest. Notably, the blots of elutes and digests that were retrieved from the PTX3-containing HA film were very similar to corresponding blots from the PTX3-free HA film. Apparently, the presence of PTX3 does not appreciably affect the incorporation of TSG-6, (subunits of) I $\alpha$ I, and its complexes into the HA film.

### 5.3.7 Structural role of PTX3.

PTX3 has been suggested to act as a HA cross-linker, which stabilizes the COC matrix<sup>37, 38</sup>. Furthermore, the oligomeric state of PTX3 is known to be functionally important: PTX3 mutants that form dimers were unable to rescue the COC matrix assembly, while mutants that form tetramers did support the formation of thick HA matrices<sup>115</sup>. To assess how PTX3 affects the morphology of HA films, we quantified the variations in film thickness upon protein incorporation by colloidal probe RCM. In initial assays, we employed plain polystyrene beads as colloidal probes. HA films (1083 kDa) with a surface density of approximately 40 ng/cm<sup>2</sup> were constructed on functionalized glass cover slips, as described earlier<sup>210</sup>. The thickness of the HA film alone was compared to the thickness of the film after addition of selected proteins. The duration of incubation with all proteins was fixed to 5 h. The results are displayed in Fig. 5.13.

Addition of rhTSG-6 at a bulk concentration of 0.3  $\mu$ M resulted in a pronounced condensation of the film. This is in agreement with previous studies (Chapter 3, Fig 3.6). The thickness after co-incubation with 0.3  $\mu$ M PTX3 and 0.3  $\mu$ M TSG-6 did not differ significantly from the film exposed to TSG-6 alone. This correlates with the result by ellipsometry (Fig. 5.6A-B, Fig. 5.7), confirming that PTX3 does hardly affect the interaction between TSG-6 and HA films at the chosen concentrations. Co-incubation (1 min) of 0.3  $\mu$ M I $\alpha$ I and 0.3  $\mu$ M TSG-6 only produced a minor decrease in thickness as compared to HA alone, in good agreement with previous results (Chapter 4, Fig. 4.6). Interestingly, the ternary protein mixture did not show any further decrease in thickness, even though we know that PTX3 is present in the film (Fig. 5.10-Fig. 5.12).

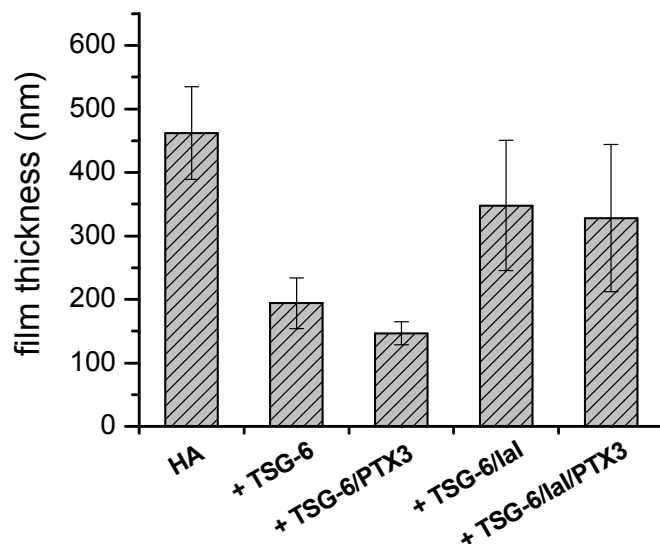


**Fig. 5.13 HA film thickness changes upon protein incorporation.** Thicknesses of the HA (1083 kDa) films were measured by colloidal probe RICM. All proteins were incubated for 5 h. rhTSG-6 and PTX3 were incubated at monomer concentrations of 0.3  $\mu$ M, and IaI at 1  $\mu$ M. Proteins were pre-mixed for 1 min and then added to the HA film. Error bars correspond to S.E.M. of 10 measurements with different colloidal probes on the same sample.

In general, one would expect the introduction of cross-linkers to force neighboring HA chains in an expanded meshwork closer together, leading to condensation, such as it is observed with TSG-6 alone. Clearly, the incorporation of PTX3 does not produce such a collapse. However, the effect of cross-linkers on the film morphology might be small, if the density of cross-linkers is low. Therefore, the above findings do not exclude PTX3-mediated cross-linking.

To address this question further, the assay was modified. Now, polystyrene beads with a SAV coating were used as colloidal probes, and incubated with b-HA (1083 kDa) to form a second HA film. The interaction between a planar HA film on the glass cover slip and the HA film on the colloidal probe was then monitored by RICM, in the absence and in the presence of selected proteins. The distance between the bead and the glass cover slip now represents the interaction range across two films and is displayed in Fig. 5.14.

The interaction range in the case of pure HA films was 680 nm. i.e. about 1.5-fold larger than the thickness of the planar HA film. To a first approximation, a factor of 2 would be expected for the encounter of two identical HA films, because the two films are unlikely to interpenetrate. The results therefore suggest that the grafting density on the colloidal probe is smaller than on the planar surface. Lower grafting density is expected on the PS beads, because their functionalization was performed in water, where the radius of gyration for flexible HA chain is much higher than in 150 mM NaCl buffer. The higher radius of gyration slows down the kinetics of HA film formation and results in a less dense HA film.

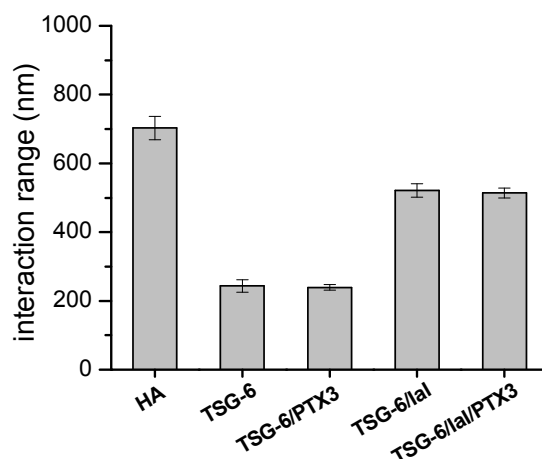


Fig. 5.14 **Interaction range between a polystyrene bead and a glass cover slip both covered with a HA (1083 kDa) film, measured by RICM.** All proteins were incubated for 5 hr. TSG-6 and PTX3 were incubated at monomer concentrations of 0.3  $\mu$ M, and I $\alpha$ I at 1  $\mu$ M. Proteins were pre-mixed for 1 min and then added to the HA film. Error bars correspond to S.E.M. of 5 measurements with different colloidal probes on the same sample.

In the presence of TSG-6, the interaction range decreased drastically, to  $245 \pm 18$  nm. The same interaction range was obtained for the mixture of TSG-6 and PTX3. In the presence of I $\alpha$ I and TSG-6, the interaction range was  $521 \pm 20$  nm, and this number did not change significantly for the ternary mixture. A detailed comparison reveals that the interaction ranges in Fig. 14 are always 1.5-fold larger than the thicknesses in Fig. 5.13, irrespective of the incubated proteins. The measurement of film thicknesses with bare beads on the one hand and interaction ranges with HA-coated beads on the other hence provided consistent results.

The latter assay, however, can provide additional insight into the interaction between HA films. To this end, we tracked the in-plane motion of HA coated beads in the presence of selected proteins. Fig. 5.15A-D reveals that the beads' thermally driven random motion depends sensitively on the presence of proteins. For example, for a pure HA film (Fig. 5.15A), the motion trace covered a surface area of  $200 \times 200$  nm<sup>2</sup> while it was confined to a 100-fold smaller area in the presence of TSG-6 alone (Fig. 5.15B).

For quantitative comparison, we also computed the mean square displacement (MSD; Fig. 5.15E). The binary mixture of I $\alpha$ I and TSG-6 decreased the MSD slightly, compared to HA alone (additional measurements are required to test if this difference is significant, because the variation in the MSD on pure HA films was large). The presence of PTX3 in the mixture reduced the MSD further, by approximately twofold. The strongest reduction, by another 75-fold, occurred with TSG-6 alone. Clearly, protein-mediated interactions between the two apposed HA films reduced the mobility of the beads. We propose that the reduced mobility results predominantly from the transient cross-linking of the two HA films. The

strong effect of TSG-6, which we had previously established to be a potent cross-linker of HA, supports this hypothesis. The significant decrease in the MSD in the ternary protein mixture compared to the binary mixture indicates that the incorporated PTX3 enhances cross-linking, even though it did not induce an appreciable condensation of the HA film (Fig. 5.13-Fig. 5.14).

It should be noted that the reduction in the mobility of the beads might in part be caused by protein-induced changes in the morphology of the interface between the two HA films. The mobility of a bead becomes reduced as a bead approaches a wall, because the wall limits the motion of the adjacent fluid. Therefore, a bead that hovers atop a fuzzy interface is likely to diffuse faster than a bead atop a sharp interface, even if the net interfacial interaction is repulsive in both cases. At present, we have now direct information about the effect of the proteins on the fuzziness of the interface. The fact that the binary and ternary protein mixtures affected the thickness of the HA films only marginally, however, seems to suggest that the fuzziness of the interface is not drastically affected, and that the effect of morphology on mobility is therefore minor. A rigorous evaluation of the magnitude of this effect will be the subject of a future study.

Taken together, the RICM assays indicate that the binary and ternary protein mixtures have only a moderate condensing effect on HA matrices. Furthermore, they suggest that, when incubated together with  $\text{I}\alpha\text{I}$  and TSG-6, PTX3 enhances the cross-linking of the matrix.

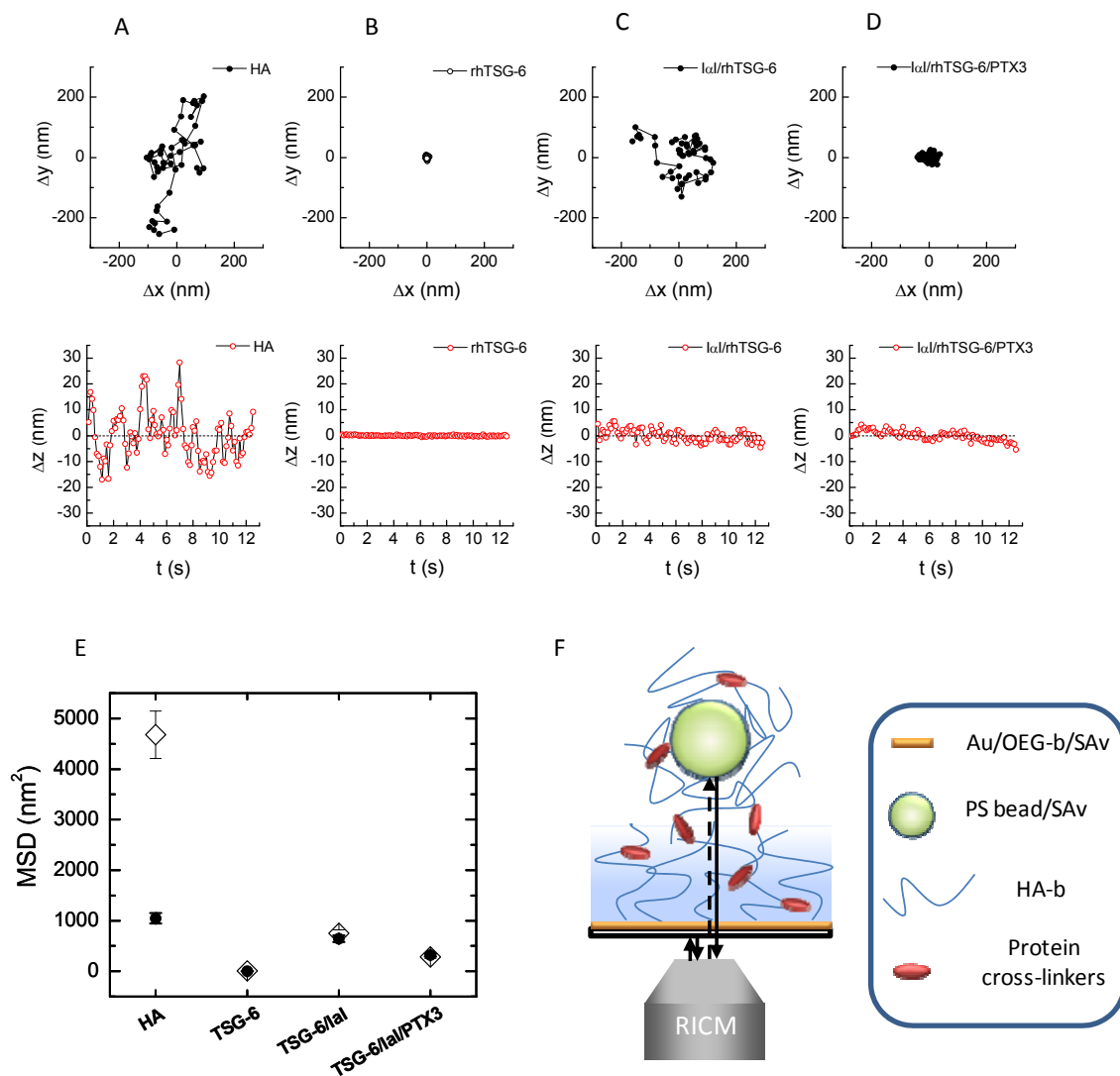


Fig. 5.15 **Mean square lateral displacement of HA-coated colloidal probes.** *A-D.* Typical traces of the thermally driven random in-plane movement of a bead's center over a period of 12.5 s for pure HA films (*A*), in the presence of 0.3  $\mu\text{M}$  TSG-6 (*B*), 1  $\mu\text{M}$  I $\alpha$ I/0.3  $\mu\text{M}$  TSG-6 (*C*) and 1  $\mu\text{M}$  I $\alpha$ I/0.3  $\mu\text{M}$  TSG-6/0.3  $\mu\text{M}$  PTX3 (*D*). *E.* Lateral mean square displacement (MSD) over a time interval of 0.125 s, extracted from traces such as those shown in *A-D*. For each protein incubation scenario, the MSD of two different beads was calculated independently, corresponding to two different data points. *F.* Sketch of the experimental setup.

## 5.4 Discussion

In this chapter we investigated the interactions between well-defined HA films and an ensemble of three proteins that are essential for the integrity of the COC matrix: TSG-6, IαI and PTX3. By varying the sequence of protein addition to HA, and by use of a range of surface-sensitive techniques, we provide new insights on how these proteins integrate their actions in matrix assembly. We have shown that TSG-6 alone cannot mediate PTX3 incorporation into HA films. Neither does PTX3 bind to HA films that contain the products of the ternary interaction between IαI, TSG-6 and HA, among which are the covalent HC•HA and TSG-6•HC complexes. Our data indicate that simultaneous encounter between all three proteins leads to successful PTX3 incorporation into HA matrices and suggest that PTX3 together with TSG-6 and IαI can create a cross-linked HA matrix. The morphology of such a matrix is distinct from HA matrices that are cross-linked by TSG-6 alone, i.e. the matrices are less collapsed.

### 5.4.1 TSG-6-mediated binding of PTX3 to HA.

Salustri et al. (2007) hypothesized that TSG-6 mediates the incorporation of PTX3 into HA matrices. More recently, surface plasmon resonance assays demonstrated that the binding of TSG-6 to PTX3 is mediated by its Link module and that the binding sites for PTX3 and HA binding are different<sup>114</sup>. Our data on the incorporation of PTX3 into HA films via Link\_TSG6 are consistent with these findings (Fig.5.3-5.4).

However, even though Leali et al. reported similar affinities of Link\_TSG6 and rhTSG-6 for PTX3 (0.3 and 0.6 μM, respectively) and even though we confirmed that both TSG-6 constructs can bind PTX3 rather tightly (Fig. 5.2), we could not find any evidence for the incorporation of PTX3 into HA films via full length TSG-6 (Fig. 5.6B)<sup>114</sup>. On the contrary, PTX3 even inhibited TSG-6 binding to HA at some TSG-6 concentrations (Fig. 5.7B). What is the reason for this discrepancy? In Chapter 3, we had provided evidence that HA induces oligomerization of rhTSG-6 but not Link\_TSG6, and proposed that the CUB\_C domains of rhTSG-6 associate during oligomerization (Chapter 3, Fig.3.5C). Although the CUB\_C domain does not seem to be directly involved in the interaction between TSG-6 and PTX3 interaction<sup>114</sup>, it would be possible that oligomerization creates steric constraints that impair PTX3 binding. According to this model, the binding of PTX3 to full length TSG-6 would directly compete with TSG-6 oligomerization. In Chapter 3, we had also proposed that oligomerization is responsible for the enhanced binding of rhTSG-6 to HA, as compared to Link\_TSG6. Thus, PTX3 could indirectly weaken the interaction between TSG-6 and HA. The ensemble of the data presented in Fig. 5.4 - Fig. 5.7 would be consistent with such a scenario.

We stress in particular that the Link\_TSG6 concentrations required to promote efficient incorporation of PTX3 into HA films exceeded those experimentally accessible for our *in vitro* assays with rhTSG-6. They also exceeded the reported *in vivo* concentrations of TSG-6 by far <sup>273</sup>. Therefore, we conclude that rhTSG-6 alone is unlikely to serve as an efficient linker for the binding of PTX3 to HA under physiologically relevant conditions.

### 5.4.2 The display of PTX3 binding sites in HA matrices appears to be tightly regulated.

In Chapter 4 we demonstrated that the co-incubation of HA films with a binary mixture of IαI and TSG-6 leads to the formation of covalent HA•HC complexes but also to the stable but non-covalent incorporation of several other molecules and molecular complexes, including (presumably HC-bound) TSG-6 or covalent TSG-6•HC complexes, into the matrix (Chapter 4, Fig. 4.3). Considering that PTX3 is known to engage in rather strong binary interactions with TSG-6 as well as with HCs <sup>37, 114, 115</sup>, it is quite remarkable that such a matrix is inert to PTX3 binding (Fig 8). Scharchilli et al. suggested that TSG-6 might favor the interaction of PTX3 with HCs in TSG-6•HC complexes. We indeed found TSG-6•HC being incorporated into HA films (Fig. 5.12), but apparently the inter-molecular interactions and the local arrangement of the molecules and their complexes in the matrix are organized such that all PTX3 binding sites are obscured.

PTX3 incorporated into HA films only if all three proteins were pre-mixed prior to their addition to HA (Fig. 5.10), or if PTX3 and IαI were pre-mixed and then added to a TSG-6 containing HA matrix (Fig. 5.11). Clearly, the encounter of proteins, and perhaps the encounter between PTX3 and IαI in particular, plays a critical role for PTX3 incorporation. Moreover, our observation that the TSG-6 displacement rate in sequential incubation assays did not depend on PTX3 (Fig. 4.1A in Chapter 4 and Fig. 5.11) suggests that the initial interaction between IαI and TSG-6 is not influenced by PTX3.

The presence of PTX3 did not have a detectable impact on the qualitative composition of species detected in HA films. This result is consistent with an *in vivo* study where HCs transfer was found to be unaffected in PTX3 *-/-* mice <sup>37</sup>. The comparison of the putative HC transfer kinetics in the sequential incubation assays (Fig. 4.1B in Chapter 4 and Fig. 5.11) suggested that TSG-6 is not recycled as an HC-transfer enzyme in the presence of PTX3. A plausible explanation for the inhibition of the enzymatic function of TSG-6 could be that TSG-6 is not released upon HCs transfer, but remains in a tightly PTX3-bound state. More specifically, we propose that the formation of TSG-6•HC complexes and subsequent transfer of HCs to HA takes place in the context of a non-covalent complex of TSG-6 and IαI (or its subunits) with PTX3, and that the reorganization of this complex upon HC transfer leads to the integration of PTX3 into the HA matrix.

Even though the specific interaction through which PTX3 integrates into the HA matrix remains elusive, it is clear from our data that the sequence of encounter between proteins and



HA is determinant for the correct assembly of a matrix that contains PTX3, I $\alpha$ I, TSG-6 and HA. A remote analogy between the formation of HA-based extracellular matrices and intracellular signaling pathways can be drawn - both processes exhibit spatio-temporal regulation and involve a hierarchy of interactions. In Chapter 4, we already proposed the concept of hierarchy of interactions for the assembly of HA matrices, and proposed HC•HA complexes as a central player in matrix assembly. Here, it appears that PTX3 has an elevated status in the sense that its incorporation into the matrix is only realized under very specific conditions.

### 5.4.3 Structural role of PTX3 in the assembly of COC matrix.

In Chapter 3 we presented evidence that TSG-6 alone can cross-link, and hence stabilize, HA matrices. Why then are the expression of PTX3 and the presence of I $\alpha$ I essential for the assembly of a functional COC matrix? Here, we demonstrate that the addition of proteins at different compositions results in HA films with different morphologies (Fig. 5.13-Fig. 5.15). This finding might have a particular implication for the structure and the formation mechanism of the COC matrix.

HA films with incorporated PTX3 do not become strongly collapsed (Fig. 5.14), in contrast to HA films containing TSG-6 alone. The moderate decrease in HA film thickness upon incubation with the I $\alpha$ I/TSG-6/PTX3 (Fig. 5.13-5.15), and the elevated MSD of HA-coated colloidal probes as compared to incubation with TSG-6 alone (Fig. 5.15E), suggest that HA-matrices exposed to the ternary protein mixture remain rather soft and are relatively weakly cross-linked. Direct measurements of the interaction forces between an HA-coated bead and an HA-coated planar film, for example by AFM or optical tweezers, should in the future provide direct and quantitative information about the cross-linking strength. The presence of weak cross-linking should have a particular relevance in the process of COC matrix expansion: opening of transient cross-links can support the integration of newly synthesized HA chains into the matrix and thereby facilitate matrix growth. Given the large size of individual HA chains, a rather low concentration of cross-linkers would be required to stabilize the assembly.

We find that the incorporation of PTX3 requires I $\alpha$ I (Fig. 5.9-Fig. 5.11). In the COC matrix, the ingress of I $\alpha$ I increases over time after the induction of ovulation. Therefore, it appears possible that the expanding COC matrix is initially cross-linked by TSG-6 alone whereas later the interaction with I $\alpha$ I/PTX3 complexes impairs these cross-links, leading to expansion and stabilization through another type of cross-link that contains PTX3. In agreement with this conjecture, the TSG-6•HC complex, but not TSG-6 alone, was found in the COC matrix just some hours before ovulation<sup>33</sup>. This implies that ternary I $\alpha$ I/TSG-6/PTX3 interactions, perhaps jointly with binary I $\alpha$ I/TSG-6 interactions, determine the actual morphology of the mature matrix.

To summarize, we propose that weak, transient cross-linking by the products of the quaternary HA/I $\alpha$ I/TSG-6/PTX3 interactions can simultaneously support two processes – matrix stabilization and matrix expansion. Furthermore, orchestration of the encounter between the different protein species in time and space may lead to spatio-temporal modulation of HA matrix morphology. These processes should be of prime importance in the formation of COC matrix, but they may also be relevant in other inflammatory processes that are accompanied by the expression of TSG-6 and PTX3.







## 6 Conclusions and perspectives

---

The goal of this PhD thesis was to understand the mechanisms underlying the assembly and stabilization of HA-rich matrices. In particular, we focused on the investigation of the interactions between proteins that are crucial for the assembly of the COC matrix, and HA. The main results, listed below, provide novel mechanistic insights into the assembly and remodeling of HA-rich matrices under inflammation and inflammation like conditions.

Several methodological developments in the design and manipulation of films of end-grafted HA were required for the thesis. In particular, polymeric HA can be replaced by oligomeric HA, thus affording control over the number of binding sites per HA chain. By switching between OEG and SLB platforms, the anchor points can potentially be kept either laterally mobile or frozen. Both SLB- and OEG-based models were remarkably resistant to treatment with GuHCl. Last but not least, we established a protocol for drying/rehydration of OEG-based HA films without significant performance losses, thereby facilitating the use of HA films outside the laboratory in which they have been produced. These modifications highlight that the properties of the HA films can be easily tuned for desired applications.

The quantitative data from the model systems demonstrate that full length TSG-6 forms oligomers upon interaction with HA which act as effective HA cross-linkers. At concentrations that might be physiologically relevant, full length TSG-6 is able to remodel HA films from a highly expanded state into a condensed and rather rigid coat. Such remodeling may occur locally in the endothelial glycocalyx and serve as a primary signal for leukocyte attraction. Extracellular matrix remodeling by TSG-6 may also affect mechanical properties of cells and significantly change their phenotype. In arthritis, HA retention by TSG-6 cross-linking in the coat of chondrocytes may contribute to its chondroprotective function.

I $\alpha$ I dictates TSG-6 activity and remodels HA matrix properties. TSG-6 induced cross-linking and compaction of HA films is impaired in the presence of I $\alpha$ I. This leads to the inhibition of the TSG-6-mediated HA binding to CD44 positive cells. Prolonged incubation with TSG-6 and I $\alpha$ I results in HA films that contain, in addition to covalently HA-bound HCs, several tightly but non-covalently bound molecular species. The non-covalently bound material, which included TSG-6, has the ability to transfer HCs onto HA.

We also demonstrated that the encounter between the proteins TSG-6, I $\alpha$ I and PTX3 determines the structural and morphological properties of the HA matrix. PTX3 was inert to binding to an HA matrix that results from the ternary interaction of I $\alpha$ I, TSG-6 and HA, even

though such matrices contain HA•HC complexes which have previously suggested as a potential PTX3 ligand. Moreover, PTX3 cannot be incorporated into an HA matrix via TSG-6 alone. Instead, we showed that the interaction of PTX3 with IαI and TSG-6 prior to encounter with HA is required for efficient incorporation into the matrix. PTX3 seems to be involved in the formation of cross-links. Even though we succeeded to incorporate all proteins that have been found to be crucial for COC matrix stability into HA films, the exact structure of the cross-linking nodes in the HA matrix remains unknown. Further studies with selected protein domains (in particular recombinant HCs) or mutant forms (for instance PTX3 that forms dimers or tetramers) using the assays developed in this thesis should allow to shed further light onto this question.

Based on the above-listed findings, we hypothesize that there is a functional interplay of different cross-linking mechanisms in the assembly of the COC matrix. In particular, TSG-6 induced cross-linking might play a role at the early stages of COC matrix assembly, when the synthesis of HA and TSG-6 is elevated. TSG-6 could help to retain overproduced HA in the matrix of cumulus cells before the follicle wall becomes permeable for another TSG-6 ligand - IαI. When IαI enters the follicle, TSG-6 cross-linking would be impaired. To stabilize the entire structure, PTX3 incorporates into the HA matrix at regions where all proteins (or their subunits) encounter each other. This would lead to the formation of cross-links which are transient and thus allow incorporation of new HA chains and ultimately COC matrix expansion.

In the future, this hypothesis can be verified in three-dimensional (3D) model systems. To this end, HA-coated microbeads could be embedded into an HA matrix by external addition of proteins and HA. The mechanical properties of the artificial matrices at different compositions can then be probed and compared to a real COC matrix. The reconstitution of such an extended 3D material should provide a valuable test if HA, TSG-6, IαI and PTX3 together can indeed compose a minimal system required for the assembly, expansion and stabilization of COC matrix.

## 7 Annex I

### Polymer theory concepts for HA characterization

#### 7.1. Estimate of HA dimension in solution.

A polymeric HA chain can be characterized by two parameters: the persistence length  $l_p$  and the contour length  $L_c$ . Basically, the persistence length defines the characteristic contour length over which the polymer chain cannot be bent and this is the measure of the polymer's flexibility. The relations between  $l_p$  and  $L_c$  are following:

$$2l_p = a, \quad 4$$

$$L_c = aN, \quad 5$$

where  $a$  is the Kuhn segment length, and  $N$  is the number of Kuhn segments in the polymer chain<sup>212</sup>. The persistence length can be quantified empirically by determination of the radius of gyration,  $R_g$ , which corresponds to the root mean square distance between the polymer segments and the polymer chain's center of mass. Under physiological ionic strength, an HA chain behaves like a so-called real chain in a good solvent. The conformational states of a real chain are well-described by a so-called self-avoiding random walk, because there is no formation of stable intermolecular interactions and two segments of one chain cannot occupy the same volume.  $R_g$  is a measure of the extension of the isolated polymer chain. For ideal chains, the radius of gyration becomes<sup>274</sup>:

$$\begin{aligned} R_g &\approx aN^{3/5} \\ &= (2l_p)^{2/5} L_c^{3/5} \end{aligned} \quad 6$$

Equations 6 nicely demonstrates that the dimension of HA coil in solution can be determined based on the molecular weight (proportional to  $L_c$ ) and the persistence length of the polymer. The persistence length of HA was calculated by Takahashi et al. based on the determination of the  $R_g$  by light scattering and low shear viscosimetry according to equations 6 and 7. In 0.2 M salt solution the persistence length of HA was estimated to 4.2 nm or 7 nm<sup>66, 275</sup>.



$$R_g = 0.021\text{nm} \times \left(\frac{M}{\text{Da}}\right)^{0.6} \quad 7$$

At very low concentrations, HA chains can indeed be treated as isolated chains. As the HA concentration increases, the chains start to meet each other and to fill the entire volume (Fig. 7.1). The concentration at which the solution volume is completely filled with polymers is called the overlap concentration:

$$c^* \approx \frac{M}{N_A} (R_g)^{-3} \quad 8$$

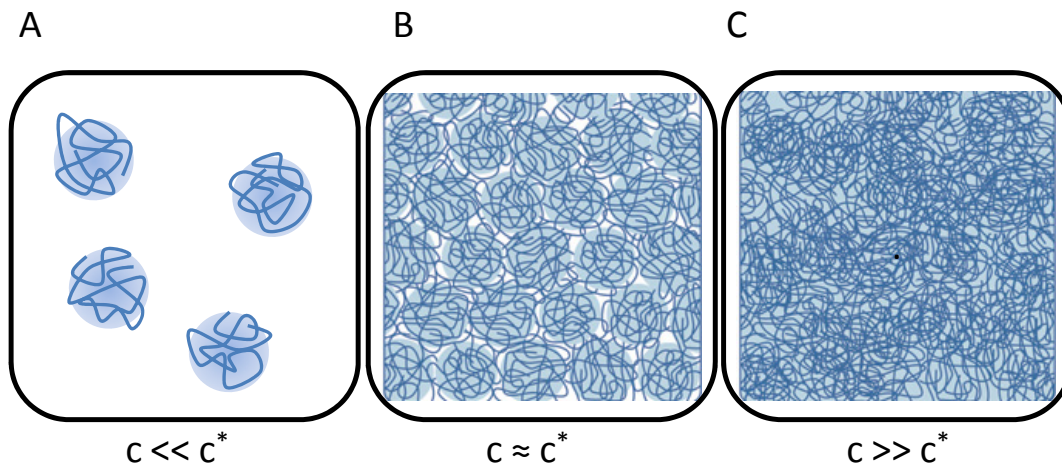


Fig. 7.1 The concentration regimes that can be defined for HA as a flexible polymer in solution. *A*. Dilute regime - the polymer chains of individual coils do not overlap. *B*. At the overlap concentration,  $c^*$ , chain start to interact with each other. *C*. In the semi-diluted regime, the chains are entangled.

From the equations 7-8 and assuming an average molecular weight for HA of 1 MDa, the overlap concentration for HA solution is determined to be  $c^* \approx 0.6$  mg/ml.

## 7.2. End-grafted polymers

When polymers are end-grafted to a surface, two conformational regimes are possible: the “mushroom” and the “brush” (Fig. 7.2). The mushroom conformation corresponds to the regime when the chains do not overlap and the distance between two grafting points  $D$  is larger than the dimension of the chain coil  $R_g$ . The thickness of the film in the mushroom regime corresponds to the dimension of the individual chains ( $h \approx R_g$ ). When the distance between two coils becomes smaller than  $R_g$ , HA chains become stretched because of steric and repulsive interactions between chains, and form a so-called polymer brush.

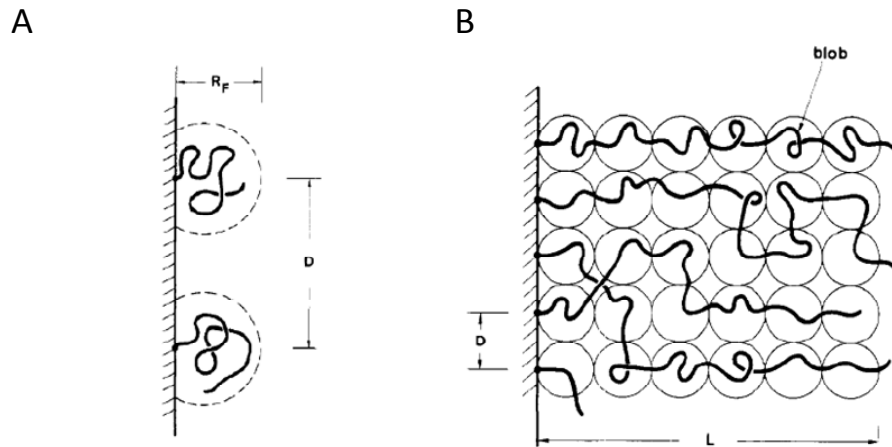


Fig. 7.2 Different conformation of end-grafted polymers, presented according to the blob model. *A.* Mushroom regime. *B.* Brush regime. Adapted from <sup>244</sup>.

The simplest model to describe a HA brush is the Alexander-de Gennes model, where polymer chains are virtually divided into a number of spheres, so-called “blobs” <sup>244, 276</sup>. Within a given blob, the HA chain behaves as an unperturbed real chain. At length scales larger than the blob size, the conformation of the HA chain is determined by the external force: in the case of a brush, the inter-chain repulsion leads to chain stretching. The degree of stretching depends on the polymer size,  $N$ , and the grafting density,  $\sigma$ , which can be expressed via the distance between grafting points,  $D$ :

$$\sigma = \left(\frac{a}{D}\right)^2 \quad 9$$

The thickness of the brush can then be estimated by:

$$h \approx aN\sigma^{1/3} \quad 10$$

### 7.3. The mesh size of an entangled polymer meshwork

The “mesh size”, or the characteristic distance between segments in a polymer solution can be described by the correlation length  $\xi$ :

$$\xi \approx R_g \left(\frac{c^*}{c}\right)^{3/4} \quad 11$$

For the concentration of HA in the COC matrix (0.5 -1 mg/ml), equation 1.8 gives a correlation length of 50 to 100 nm



## 8 References

---

1. Alberts B, J. A., Walter P, Lewis J, Raff M and Roberts K. (2008) *Molecular Biology of the Cell*, 5th edition ed., Taylor and Francis.
2. Evanko, S. P., Tammi, M. I., Tammi, R. H., and Wight, T. N. (2007) Hyaluronan-dependent pericellular matrix, *Adv Drug Deliv Rev* 59, 1351-1365.
3. Hedman, K., Kurkinen, M., Alitalo, K., Vaheri, A., Johansson, S., and Hook, M. (1979) Isolation of the pericellular matrix of human fibroblast cultures, *J Cell Biol* 81, 83-91.
4. Knudson, C. B. (1993) Hyaluronan receptor-directed assembly of chondrocyte pericellular matrix, *J Cell Biol* 120, 825-834.
5. Cohen, M., Klein, E., Geiger, B., and Addadi, L. (2003) Organization and adhesive properties of the hyaluronan pericellular coat of chondrocytes and epithelial cells, *Biophys J* 85, 1996-2005.
6. Ricciardelli, C., Russell, D. L., Ween, M. P., Mayne, K., Suwivat, S., Byers, S., Marshall, V. R., Tilley, W. D., and Horsfall, D. J. (2007) Formation of hyaluronan- and versican-rich pericellular matrix by prostate cancer cells promotes cell motility, *J Biol Chem* 282, 10814-10825.
7. Sabri, S., Soler, M., Foa, C., Pierres, A., Benoliel, A., and Bongrand, P. (2000) Glycocalyx modulation is a physiological means of regulating cell adhesion, *J Cell Sci* 113 ( Pt 9), 1589-1600.
8. Smith, M. L., Long, D. S., Damiano, E. R., and Ley, K. (2003) Near-wall micro-PIV reveals a hydrodynamically relevant endothelial surface layer in venules in vivo, *Biophys J* 85, 637-645.
9. Constantinescu, A. A., Vink, H., and Spaan, J. A. (2003) Endothelial cell glycocalyx modulates immobilization of leukocytes at the endothelial surface, *Arterioscler Thromb Vasc Biol* 23, 1541-1547.
10. Kultti, A., Rilla, K., Tiihonen, R., Spicer, A. P., Tammi, R. H., and Tammi, M. I. (2006) Hyaluronan synthesis induces microvillus-like cell surface protrusions, *J Biol Chem* 281, 15821-15828.
11. McLane, L. T., Chang, P., Granqvist, A., Boehm, H., Kramer, A., Scrimgeour, J., and Curtis, J. E. (2013) Spatial organization and mechanical properties of the pericellular matrix on chondrocytes, *Biophys J* 104, 986-996.
12. Clarris, B. J., and Fraser, J. R. (1968) On the pericellular zone of some mammalian cells in vitro, *Exp Cell Res* 49, 181-193.
13. Toole, B. P. (2001) Hyaluronan in morphogenesis, *Semin Cell Dev Biol* 12, 79-87.

14. Cohen, M., Kam, Z., Addadi, L., and Geiger, B. (2006) Dynamic study of the transition from hyaluronan- to integrin-mediated adhesion in chondrocytes, *EMBO J* 25, 302-311.
15. Siegelman, M. H., DeGrendele, H. C., and Estess, P. (1999) Activation and interaction of CD44 and hyaluronan in immunological systems, *J Leukoc Biol* 66, 315-321.
16. Evanko, S. P., Angello, J. C., and Wight, T. N. (1999) Formation of hyaluronan- and versican-rich pericellular matrix is required for proliferation and migration of vascular smooth muscle cells, *Arterioscler Thromb Vasc Biol* 19, 1004-1013.
17. Brecht, M., Mayer, U., Schlosser, E., and Prehm, P. (1986) Increased hyaluronate synthesis is required for fibroblast detachment and mitosis, *Biochem J* 239, 445-450.
18. Itano, N., Atsumi, F., Sawai, T., Yamada, Y., Miyaishi, O., Senga, T., Hamaguchi, M., and Kimata, K. (2002) Abnormal accumulation of hyaluronan matrix diminishes contact inhibition of cell growth and promotes cell migration, *Proc Natl Acad Sci U S A* 99, 3609-3614.
19. Macri, L., Silverstein, D., and Clark, R. A. (2007) Growth factor binding to the pericellular matrix and its importance in tissue engineering, *Adv Drug Deliv Rev* 59, 1366-1381.
20. Russell, D. L., and Salustri, A. (2006) Extracellular matrix of the cumulus-oocyte complex, *Semin. Reprod. Med.* 24, 217-227.
21. Wolny, P. M., Banerji, S., Gounou, C., Brisson, A. R., Day, A. J., Jackson, D. G., and Richter, R. P. Analysis of CD44-hyaluronan interactions in an artificial membrane system: insights into the distinct binding properties of high and low molecular weight hyaluronan, *J Biol Chem* 285, 30170-30180.
22. Day, A. J., and Sheehan, J. K. (2001) Hyaluronan: polysaccharide chaos to protein organisation, *Curr. Opin. Struct. Biol.* 11, 617-622.
23. Rilla, K., Tiihonen, R., Kultti, A., Tammi, M., and Tammi, R. (2008) Pericellular hyaluronan coat visualized in live cells with a fluorescent probe is scaffolded by plasma membrane protrusions, *J Histochem Cytochem* 56, 901-910.
24. Lee, G. M., Johnstone, B., Jacobson, K., and Caterson, B. (1993) The dynamic structure of the pericellular matrix on living cells, *J Cell Biol* 123, 1899-1907.
25. Horwitz, A. R., and Parsons, J. T. (1999) Cell migration--movin' on, *Science* 286, 1102-1103.
26. Day, A. J., and de la Motte, C. A. (2005) Hyaluronan cross-linking: a protective mechanism in inflammation?, *Trends Immunol.* 26, 637-643.
27. de la Motte, C. A., Hascall, V. C., Drazba, J., Bandyopadhyay, S. K., and Strong, S. A. (2003) Mononuclear leukocytes bind to specific hyaluronan structures on colon mucosal smooth muscle cells treated with polyinosinic acid:polycytidylic acid: inter-alpha-trypsin inhibitor is crucial to structure and function, *Am. J. Pathol.* 163, 121-133.
28. Salustri, A., Yanagishita, M., and Hascall, V. C. (1989) Synthesis and accumulation of hyaluronic acid and proteoglycans in the mouse cumulus cell-oocyte complex

- during follicle-stimulating hormone-induced mucification, *J Biol Chem* 264, 13840-13847.
29. Salustri A., F. C. (1998) Role of Hyaluronan during Ovulation and Fertilization.
  30. Cherr, G. N., Yudin, A. I., and Katz, D. F. (1990) Organization of the Hamster Cumulus Extracellular Matrix: A Hyaluronate-Glycoprotein Gel which Modulates Sperm Access to the Oocyte, *Development, Growth & Differentiation* 32, 353-365.
  31. Carrette, O., Nemade, R. V., Day, A. J., Brickner, A., and Larsen, W. J. (2001) TSG-6 is concentrated in the extracellular matrix of mouse cumulus oocyte complexes through hyaluronan and inter-alpha-inhibitor binding, *Biol Reprod* 65, 301-308.
  32. Mukhopadhyay, D., Hascall, V. C., Day, A. J., Salustri, A., and Fulop, C. (2001) Two distinct populations of tumor necrosis factor-stimulated gene-6 protein in the extracellular matrix of expanded mouse cumulus cell-oocyte complexes, *Arch Biochem Biophys* 394, 173-181.
  33. Ochsner, S. A., Russell, D. L., Day, A. J., Breyer, R. M., and Richards, J. S. (2003) Decreased expression of tumor necrosis factor-alpha-stimulated gene 6 in cumulus cells of the cyclooxygenase-2 and EP2 null mice, *Endocrinology* 144, 1008-1019.
  34. Russell, D. L., Ochsner, S. A., Hsieh, M., Mulders, S., and Richards, J. S. (2003) Hormone-regulated expression and localization of versican in the rodent ovary, *Endocrinology* 144, 1020-1031.
  35. Zhuo, L., Yoneda, M., Zhao, M., Yingsung, W., Yoshida, N., Kitagawa, Y., Kawamura, K., Suzuki, T., and Kimata, K. (2001) Defect in SHAP-hyaluronan complex causes severe female infertility. A study by inactivation of the bikunin gene in mice, *J Biol Chem* 276, 7693-7696.
  36. Kobayashi, H., Sun, G. W., Hirashima, Y., and Terao, T. (1999) Identification of link protein during follicle development and cumulus cell cultures in rats, *Endocrinology* 140, 3835-3842.
  37. Salustri, A., Garlanda, C., Hirsch, E., De Acetis, M., Maccagno, A., Bottazzi, B., Doni, A., Bastone, A., Mantovani, G., Beck Peccoz, P., Salvatori, G., Mahoney, D. J., Day, A. J., Siracusa, G., Romani, L., and Mantovani, A. (2004) PTX3 plays a key role in the organization of the cumulus oophorus extracellular matrix and in in vivo fertilization, *Development* 131, 1577-1586.
  38. Scarchilli, L., Camaioni, A., Bottazzi, B., Negri, V., Doni, A., Deban, L., Bastone, A., Salvatori, G., Mantovani, A., Siracusa, G., and Salustri, A. (2007) PTX3 interacts with inter-alpha-trypsin inhibitor: implications for hyaluronan organization and cumulus oophorus expansion, *J Biol Chem* 282, 30161-30170.
  39. Familiari, G., Heyn, R., Relucenti, M., Nottola, S. A., and Sathanathan, A. H. (2006) Ultrastructural dynamics of human reproduction, from ovulation to fertilization and early embryo development, *Int Rev Cytol* 249, 53-141.
  40. Sato, H., Kajikawa, S., Kuroda, S., Horisawa, Y., Nakamura, N., Kaga, N., Kakinuma, C., Kato, K., Morishita, H., Niwa, H., and Miyazaki, J. (2001) Impaired fertility in female mice lacking urinary trypsin inhibitor, *Biochem Biophys Res Commun* 281, 1154-1160.
  41. Fülöp, C., Szanto, S., Mukhopadhyay, D., Bardos, T., Kamath, R. V., Rugg, M. S., Day, A. J., Salustri, A., Hascall, V. C., Glant, T. T., and Mikecz, K. (2003) Impaired

- cumulus mucification and female sterility in tumor necrosis factor-induced protein-6 deficient mice, *Development* 130, 2253-2261.
42. Hess, K. A., Chen, L., and Larsen, W. J. (1999) Inter-alpha-inhibitor binding to hyaluronan in the cumulus extracellular matrix is required for optimal ovulation and development of mouse oocytes, *Biol Reprod* 61, 436-443.
  43. Fulop, C., Szanto, S., Mukhopadhyay, D., Bardos, T., Kamath, R. V., Rugg, M. S., Day, A. J., Salustri, A., Hascall, V. C., Glant, T. T., and Mikecz, K. (2003) Impaired cumulus mucification and female sterility in tumor necrosis factor-induced protein-6 deficient mice, *Development* 130, 2253-2261.
  44. Varani, S., Elvin, J. A., Yan, C., DeMayo, J., DeMayo, F. J., Horton, H. F., Byrne, M. C., and Matzuk, M. M. (2002) Knockout of pentraxin 3, a downstream target of growth differentiation factor-9, causes female subfertility, *Mol Endocrinol* 16, 1154-1167.
  45. Rodgers, R. J., and Irving-Rodgers, H. F. Formation of the ovarian follicular antrum and follicular fluid, *Biol Reprod* 82, 1021-1029.
  46. Brown, H. M., Dunning, K. R., Robker, R. L., Boerboom, D., Pritchard, M., Lane, M., and Russell, D. L. ADAMTS1 cleavage of versican mediates essential structural remodeling of the ovarian follicle and cumulus-oocyte matrix during ovulation in mice, *Biol Reprod* 83, 549-557.
  47. Lam, X., Gieseke, C., Knoll, M., and Talbot, P. (2000) Assay and importance of adhesive interaction between hamster (*Mesocricetus auratus*) oocyte-cumulus complexes and the oviductal epithelium, *Biol Reprod* 62, 579-588.
  48. Talbot, P., Shur, B. D., and Myles, D. G. (2003) Cell adhesion and fertilization: steps in oocyte transport, sperm-zona pellucida interactions, and sperm-egg fusion, *Biol Reprod* 68, 1-9.
  49. Hong, S. J., Chiu, P. C., Lee, K. F., Tse, J. M., Ho, P. C., and Yeung, W. S. (2004) Establishment of a capillary-cumulus model to study the selection of sperm for fertilization by the cumulus oophorus, *Hum Reprod* 19, 1562-1569.
  50. Tesarik, J., Pilka, L., Drahorad, J., Cechova, D., and Veselsky, L. (1988) The role of cumulus cell-secreted proteins in the development of human sperm fertilizing ability: implication in IVF, *Hum Reprod* 3, 129-132.
  51. Drahorad, J., Tesarik, J., Cechova, D., and Vilim, V. (1991) Proteins and glycosaminoglycans in the intercellular matrix of the human cumulus-oophorus and their effect on conversion of proacrosin to acrosin, *J Reprod Fertil* 93, 253-262.
  52. Ball, G. D., Leibfried, M. L., Lenz, R. W., Ax, R. L., Bavister, B. D., and First, N. L. (1983) Factors affecting successful in vitro fertilization of bovine follicular oocytes, *Biol Reprod* 28, 717-725.
  53. Toole, B. P. (2004) Hyaluronan: from extracellular glue to pericellular cue, *Nat Rev Cancer* 4, 528-539.
  54. Meyer, K., Palmer, J W. (1934) The polysaccharide of the vitreous humor., *J Biol Chem* 107, 629-634.
  55. Weissmann, B. M., K. . (1954) The structure of hyalobiuronic acid and of hyaluronic acid from umbilical cord, *J. Am. Chem. Soc.* 76, 1753-1757.

56. Laurent, T. (1998) *The chemistry, biology and medical application of hyaluronan and its derivatives*, Portland Pr.
57. Tammi, M. I., Day, A. J., and Turley, E. A. (2002) Hyaluronan and homeostasis: a balancing act, *J Biol Chem* 277, 4581-4584.
58. Albersdörfer, A., and Sackmann, E. (1999) Swelling behavior and viscoelasticity of ultrathin grafted hyaluronic acid films, *European Physical Journal B* 10, 663-672.
59. Cleland, R. L. (1984) Viscometry and sedimentation equilibrium of partially hydrolyzed hyaluronate: Comparison with theoretical models of wormlike chains, *Biopolymers* 23, 647-666.
60. Attili, S., Borisov, O. V., and Richter, R. P. (2012) Films of end-grafted hyaluronan are a prototype of a brush of a strongly charged, semi-flexible polyelectrolyte with intrinsic excluded volume. , *Biomacromolecules* 13, 1466-1477.
61. Hascall, V. C. L., T.C. (1997) Hyaluronan: Structure and Physical Properties, *Hyaluronan Today*.
62. Sheehan, J. K., and Atkins, E. D. T. (1983) X-ray fibre diffraction study of conformational changes in hyaluronate induced in the presence of sodium, potassium and calcium cations, *International Journal of Biological Macromolecules* 5, 215-221.
63. Cleland, R. L., and Wang, J. L. (1970) Ionic polysaccharides. 3. Dilute solution properties of hyaluronic acid fractions, *Biopolymers* 9, 799-810.
64. Tammi, M. I., Day, A. J., and Turley, E. A. (2002) Hyaluronan and homeostasis: a balancing act, *J. Biol. Chem.* 277, 4581-4584.
65. Day, A. J., and Prestwich, G. D. (2002) Hyaluronan-binding proteins: tying up the giant, *J. Biol. Chem.* 277, 4585-4588.
66. Takahashi, R., Kubota, K., Kawada, M., and Okamoto, A. (1999) Effect of molecular weight distribution on the solution properties of sodium hyaluronate in 0.2M NaCl solution, *Biopolymers* 50, 87-98.
67. Fraser, J. R., Laurent, T. C., and Laurent, U. B. (1997) Hyaluronan: its nature, distribution, functions and turnover, *J Intern Med* 242, 27-33.
68. Lee, T. H., Wisniewski, H. G., and Vilcek, J. (1992) A novel secretory tumor necrosis factor-inducible protein (TSG-6) is a member of the family of hyaluronate binding proteins, closely related to the adhesion receptor CD44, *J Cell Biol* 116, 545-557.
69. Maier, R., Wisniewski, H. G., Vilcek, J., and Lotz, M. (1996) TSG-6 expression in human articular chondrocytes. Possible implications in joint inflammation and cartilage degradation, *Arthritis Rheum* 39, 552-559.
70. Mahoney, D. J., Swales, C., Athanasou, N. A., Bombardieri, M., Pitzalis, C., Kliskey, K., Sharif, M., Day, A. J., Milner, C. M., and Sabokbar, A. TSG-6 inhibits osteoclast activity via an autocrine mechanism and is functionally synergistic with osteoprotegerin, *Arthritis Rheum* 63, 1034-1043.
71. Wisniewski, H. G., Maier, R., Lotz, M., Lee, S., Klampfer, L., Lee, T. H., and Vilcek, J. (1993) TSG-6: a TNF-, IL-1-, and LPS-inducible secreted glycoprotein associated with arthritis, *J. Immunol.* 151, 6593-6601.
72. Glant, T. T., Kamath, R. V., Bardos, T., Gal, I., Szanto, S., Murad, Y. M., Sandy, J. D., Mort, J. S., Roughley, P. J., and Mikecz, K. (2002) Cartilage-specific constitutive



- expression of TSG-6 protein (product of tumor necrosis factor alpha-stimulated gene 6) provides a chondroprotective, but not antiinflammatory, effect in antigen-induced arthritis, *Arthritis Rheum* 46, 2207-2218.
73. Mindrescu, C., Dias, A. A., Olszewski, R. J., Klein, M. J., Reis, L. F., and Wisniewski, H. G. (2002) Reduced susceptibility to collagen-induced arthritis in DBA/1J mice expressing the TSG-6 transgene, *Arthritis Rheum* 46, 2453-2464.
  74. Szanto, S., Bardos, T., Gal, I., Glant, T. T., and Mikecz, K. (2004) Enhanced neutrophil extravasation and rapid progression of proteoglycan-induced arthritis in TSG-6-knockout mice, *Arthritis Rheum* 50, 3012-3022.
  75. Blundell, C. D., Mahoney, D. J., Almond, A., DeAngelis, P. L., Kahmann, J. D., Teriete, P., Pickford, A. R., Campbell, I. D., and Day, A. J. (2003) The link module from ovulation- and inflammation-associated protein TSG-6 changes conformation on hyaluronan binding, *Journal of Biological Chemistry* 278, 49261-49270.
  76. Blundell, C. D., Almond, A., Mahoney, D. J., DeAngelis, P. L., Campbell, I. D., and Day, A. J. (2005) Towards a structure for a TSG-6-hyaluronan complex by modeling and NMR spectroscopy: insights into other members of the link module superfamily, *J Biol Chem* 280, 18189-18201.
  77. Kohda, D., Morton, C. J., Parkar, A. A., Hatanaka, H., Inagaki, F. M., Campbell, I. D., and Day, A. J. (1996) Solution structure of the link module: a hyaluronan-binding domain involved in extracellular matrix stability and cell migration, *Cell* 86, 767-775.
  78. Mahoney, D. J., Blundell, C. D., and Day, A. J. (2001) Mapping the hyaluronan-binding site on the link module from human tumor necrosis factor-stimulated gene-6 by site-directed mutagenesis, *J. Biol. Chem.* 276, 22764-22771.
  79. Blundell, C. D., Kahmann, J. D., Perczel, A., Mahoney, D. J., Cordell, M. R., Teriete, P., Campbell, I. D., and Day, A., J. (2002) Getting to grips with HA-protein interactions, In *Hyaluronan 2000* (Kennedy, Ed.).
  80. Kuznetsova, S. A., Mahoney, D. J., Martin-Manso, G., Ali, T., Nentwich, H. A., Sipes, J. M., Zeng, B., Vogel, T., Day, A. J., and Roberts, D. D. (2008) TSG-6 binds via its CUB\_C domain to the cell-binding domain of fibronectin and increases fibronectin matrix assembly, *Matrix Biol* 27, 201-210.
  81. Day, A. J., Wright, A. J., Blanc, G., Konarev, P., Svergun, D. I., and Hulmes, D. J. S. . (2004) Small angle X-ray scattering reveals TSG-6 to be an end-to-end dimer in the presence of excess hyaluronan., in *HASYLAB DESY Annual Report 2004*
  82. Day, A. J., and de la Motte, C. A. (2005) Hyaluronan cross-linking: a protective mechanism in inflammation? *Trends Immunol* 26, 637-643.
  83. Enghild, J. J., Thogersen, I. B., Pizzo, S. V., and Salvesen, G. (1989) Analysis of inter-alpha-trypsin inhibitor and a novel trypsin inhibitor, pre-alpha-trypsin inhibitor, from human plasma. Polypeptide chain stoichiometry and assembly by glycan, *J Biol Chem* 264, 15975-15981.
  84. Salier, J. P., Rouet, P., Raguenez, G., and Daveau, M. (1996) The inter-alpha-inhibitor family: from structure to regulation, *Biochem J* 315 ( Pt 1), 1-9.
  85. Enghild, J. J., Thogersen, I. B., Cheng, F., Fransson, L. A., Roepstorff, P., and Rahbek-Nielsen, H. (1999) Organization of the inter-alpha-inhibitor heavy chains on

- the chondroitin sulfate originating from Ser(10) of bikunin: posttranslational modification of I $\alpha$ I-derived bikunin, *Biochemistry* 38, 11804-11813.
86. Sanggaard, K. W., Karring, H., Valnickova, Z., Thogersen, I. B., and Enghild, J. J. (2005) The TSG-6 and I  $\alpha$  I interaction promotes a transesterification cleaving the protein-glycosaminoglycan-protein (PGP) cross-link, *J Biol Chem* 280, 11936-11942.
  87. Blom, A. M., Morgelin, M., Oyen, M., Jarvet, J., and Fries, E. (1999) Structural characterization of inter-alpha-inhibitor. Evidence for an extended shape, *J Biol Chem* 274, 298-304.
  88. Steinbuch, M. (1976) The inter-alpha-trypsin inhibitor, *Methods Enzymol* 45, 760-772.
  89. Potempa, J., Kwon, K., Chawla, R., and Travis, J. (1989) Inter-alpha-trypsin inhibitor. Inhibition spectrum of native and derived forms, *J Biol Chem* 264, 15109-15114.
  90. Blom, A., Pertoft, H., and Fries, E. (1995) Inter-alpha-inhibitor is required for the formation of the hyaluronan-containing coat on fibroblasts and mesothelial cells, *J Biol Chem* 270, 9698-9701.
  91. Bost, F., Diarra-Mehrpour, M., and Martin, J. P. (1998) Inter-alpha-trypsin inhibitor proteoglycan family--a group of proteins binding and stabilizing the extracellular matrix, *Eur J Biochem* 252, 339-346.
  92. Pratt, C. W., and Pizzo, S. V. (1986) In vivo metabolism of inter-alpha-trypsin inhibitor and its proteinase complexes: evidence for proteinase transfer to alpha 2-macroglobulin and alpha 1-proteinase inhibitor, *Arch Biochem Biophys* 248, 587-596.
  93. Sugiki, M., Sumi, H., Maruyama, M., Yoshida, E., and Mihara, H. (1989) Clearance and distribution of acid-stable trypsin inhibitor (ASTI), *Enzyme* 42, 31-38.
  94. Yingsung, W., Zhuo, L., Morgelin, M., Yoneda, M., Kida, D., Watanabe, H., Ishiguro, N., Iwata, H., and Kimata, K. (2003) Molecular heterogeneity of the SHAP-hyaluronan complex. Isolation and characterization of the complex in synovial fluid from patients with rheumatoid arthritis, *J. Biol. Chem.* 278, 32710-32718.
  95. Jessen, T. E., Odum, L., and Johnsen, A. H. (1994) In vivo binding of human inter-alpha-trypsin inhibitor free heavy chains to hyaluronic acid, *Biol Chem Hoppe Seyler* 375, 521-526.
  96. Zhao, M., Yoneda, M., Ohashi, Y., Kurono, S., Iwata, H., Ohnuki, Y., and Kimata, K. (1995) Evidence for the covalent binding of SHAP, heavy chains of inter-alpha-trypsin inhibitor, to hyaluronan, *J Biol Chem* 270, 26657-26663.
  97. Yingsung, W., Zhuo, L., Morgelin, M., Yoneda, M., Kida, D., Watanabe, H., Ishiguro, N., Iwata, H., and Kimata, K. (2003) Molecular heterogeneity of the SHAP-hyaluronan complex. Isolation and characterization of the complex in synovial fluid from patients with rheumatoid arthritis, *J Biol Chem* 278, 32710-32718.
  98. Rugg, M. S., Willis, A. C., Mukhopadhyay, D., Hascall, V. C., Fries, E., Fülöp, C., Milner, C. M., and Day, A. J. (2005) Characterization of Complexes Formed between TSG-6 and Inter- $\alpha$ -inhibitor That Act as Intermediates in the Covalent Transfer of Heavy Chains onto Hyaluronan, *Journal of Biological Chemistry* 27, 25674-25686.

99. Wisniewski, H. G., Burgess, W. H., Oppenheim, J. D., and Vilcek, J. (1994) TSG-6, an arthritis-associated hyaluronan binding protein, forms a stable complex with the serum protein inter-alpha-inhibitor, *Biochemistry* 33, 7423-7429.
100. Mukhopadhyay, D., Asari, A., Rugg, M. S., Day, A. J., and Fulop, C. (2004) Specificity of the tumor necrosis factor-induced protein 6-mediated heavy chain transfer from inter-alpha-trypsin inhibitor to hyaluronan: implications for the assembly of the cumulus extracellular matrix, *J Biol Chem* 279, 11119-11128.
101. Chen, L., Mao, S. J., McLean, L. R., Powers, R. W., and Larsen, W. J. (1994) Proteins of the inter-alpha-trypsin inhibitor family stabilize the cumulus extracellular matrix through their direct binding with hyaluronic acid, *J Biol Chem* 269, 28282-28287.
102. Jessen, T. E., and Odum, L. (2003) Role of tumour necrosis factor stimulated gene 6 (TSG-6) in the coupling of inter-alpha-trypsin inhibitor to hyaluronan in human follicular fluid, *Reproduction* 125, 27-31.
103. Breviario, F., d'Aniello, E. M., Golay, J., Peri, G., Bottazzi, B., Bairoch, A., Saccone, S., Marzella, R., Predazzi, V., Rocchi, M., and et al. (1992) Interleukin-1-inducible genes in endothelial cells. Cloning of a new gene related to C-reactive protein and serum amyloid P component, *J Biol Chem* 267, 22190-22197.
104. Lee, G. W., Lee, T. H., and Vilcek, J. (1993) TSG-14, a tumor necrosis factor- and IL-1-inducible protein, is a novel member of the pentaxin family of acute phase proteins, *J Immunol* 150, 1804-1812.
105. Bottazzi, B., Vouret-Craviari, V., Bastone, A., De Gioia, L., Matteucci, C., Peri, G., Spreafico, F., Pausa, M., D'Ettore, C., Gianazza, E., Tagliabue, A., Salmons, M., Tedesco, F., Inrona, M., and Mantovani, A. (1997) Multimer formation and ligand recognition by the long pentraxin PTX3. Similarities and differences with the short pentraxins C-reactive protein and serum amyloid P component, *J Biol Chem* 272, 32817-32823.
106. Fazzini, F., Peri, G., Doni, A., Dell'Antonio, G., Dal Cin, E., Bozzolo, E., D'Auria, F., Praderio, L., Ciboddo, G., Sabbadini, M. G., Manfredi, A. A., Mantovani, A., and Querini, P. R. (2001) PTX3 in small-vessel vasculitides: an independent indicator of disease activity produced at sites of inflammation, *Arthritis Rheum* 44, 2841-2850.
107. Bottazzi, B., Garlanda, C., Cotena, A., Moalli, F., Jaillon, S., Deban, L., and Mantovani, A. (2009) The long pentraxin PTX3 as a prototypic humoral pattern recognition receptor: interplay with cellular innate immunity, *Immunol Rev* 227, 9-18.
108. Garlanda, C., Bottazzi, B., Bastone, A., and Mantovani, A. (2005) Pentraxins at the crossroads between innate immunity, inflammation, matrix deposition, and female fertility, *Annu Rev Immunol* 23, 337-366.
109. Inforzato, A., Riviaccio, V., Morreale, A. P., Bastone, A., Salustri, A., Scarchilli, L., Verdoliva, A., Vincenti, S., Gallo, G., Chiapparino, C., Pacello, L., Nucera, E., Serlupi-Crescenzi, O., Day, A. J., Bottazzi, B., Mantovani, A., De Santis, R., and Salvatori, G. (2008) Structural characterization of PTX3 disulfide bond network and its multimeric status in cumulus matrix organization, *J Biol Chem* 283, 10147-10161.
110. Presta, M., Camozzi, M., Salvatori, G., and Rusnati, M. (2007) Role of the soluble pattern recognition receptor PTX3 in vascular biology, *J Cell Mol Med* 11, 723-738.

111. Goodman, A. R., Cardozo, T., Abagyan, R., Altmeyer, A., Wisniewski, H. G., and Vilcek, J. (1996) Long pentraxins: an emerging group of proteins with diverse functions, *Cytokine Growth Factor Rev* 7, 191-202.
112. Inforzato, A., Peri, G., Doni, A., Garlanda, C., Mantovani, A., Bastone, A., Carpentieri, A., Amoresano, A., Pucci, P., Roos, A., Daha, M. R., Vincenti, S., Gallo, G., Carminati, P., De Santis, R., and Salvatori, G. (2006) Structure and function of the long pentraxin PTX3 glycosidic moiety: fine-tuning of the interaction with C1q and complement activation, *Biochemistry* 45, 11540-11551.
113. Inforzato, A., Baldock, C., Jowitt, T. A., Holmes, D. F., Lindstedt, R., Marcellini, M., Riviaccio, V., Briggs, D. C., Kadler, K. E., Verdoliva, A., Bottazzi, B., Mantovani, A., Salvatori, G., and Day, A. J. (2010) The angiogenic inhibitor long pentraxin PTX3 forms an asymmetric octamer with two binding sites for FGF2, *J Biol Chem* 285, 17681-17692.
114. Leali, D., Inforzato, A., Ronca, R., Bianchi, R., Belleri, M., Coltrini, D., Di Salle, E., Sironi, M., Norata, G. D., Bottazzi, B., Garlanda, C., Day, A. J., and Presta, M. (2012) Long pentraxin 3/tumor necrosis factor-stimulated gene-6 interaction: a biological rheostat for fibroblast growth factor 2-mediated angiogenesis, *Arterioscler Thromb Vasc Biol* 32, 696-703.
115. Ievoli, E., Lindstedt, R., Inforzato, A., Camaioni, A., Palone, F., Day, A. J., Mantovani, A., Salvatori, G., and Salustri, A. (2011) Implication of the oligomeric state of the N-terminal PTX3 domain in cumulus matrix assembly, *Matrix Biol* 30, 330-337.
116. Powers, R. W., Chen, L., Russell, P. T., and Larsen, W. J. (1995) Gonadotropin-stimulated regulation of blood-follicle barrier is mediated by nitric oxide, *Am J Physiol* 269, E290-298.
117. Hess, K. A., Chen, L., and Larsen, W. J. (1998) The ovarian blood follicle barrier is both charge- and size-selective in mice, *Biol Reprod* 58, 705-711.
118. Chen, L., Zhang, H., Powers, R. W., Russell, P. T., and Larsen, W. J. (1996) Covalent linkage between proteins of the inter-alpha-inhibitor family and hyaluronic acid is mediated by a factor produced by granulosa cells, *J Biol Chem* 271, 19409-19414.
119. Chen, L., Mao, S. J., and Larsen, W. J. (1992) Identification of a factor in fetal bovine serum that stabilizes the cumulus extracellular matrix. A role for a member of the inter-alpha-trypsin inhibitor family, *J Biol Chem* 267, 12380-12386.
120. Mukhopadhyay, D., Hascall, V. C., Day, A. J., Salustri, A., and Fulop, C. (2001) Two distinct populations of tumor necrosis factor-stimulated gene-6 protein in the extracellular matrix of expanded mouse cumulus cell-oocyte complexes, *Arch. Biochem. Biophys.* 394, 173-181.
121. Carrette, O., Nemade, R. V., Day, A. J., Brickner, A., and Larsen, W. J. (2001) TSG-6 is concentrated in the extracellular matrix of mouse cumulus oocyte complexes through hyaluronan and inter-alpha-inhibitor binding, *Biol. Reprod.* 65, 301-308.
122. Scarchilli, L., Camaioni, A., Bottazzi, B., Negri, V., Doni, A., Deban, L., Bastone, A., Salvatori, G., Mantovani, A., Siracusa, G., and Salustri, A. (2007) PTX3 interacts with inter-alpha-trypsin inhibitor: implications for hyaluronan organization and cumulus oophorus expansion, *J. Biol. Chem.* 282, 30161-30170.

123. Kasemo, B. (2002) Biological surface science, *Surface Science* 500, 656-677.
124. Richter, R. P., Hock, K. K., Burkhartsmeier, J., Boehm, H., Bingen, P., Wang, G. L., Steinmetz, N. F., Evans, D. J., and Spatz, J. P. (2007) Membrane-grafted hyaluronan films: A well-defined model system of glycoconjugate cell coats, *Journal of the American Chemical Society* 129, 5306-+.
125. Morra, M. (2005) Engineering of biomaterials surfaces by hyaluronan, *Biomacromolecules* 6, 1205-1223.
126. Delpech, B., Bertrand, P., and Maingonnat, C. (1985) Immunoenzymoassay of the hyaluronic acid-hyaluronectin interaction: application to the detection of hyaluronic acid in serum of normal subjects and cancer patients, *Anal Biochem* 149, 555-565.
127. Picart, C., Mutterer, J., Richert, L., Luo, Y., Prestwich, G. D., Schaaf, P., Voegel, J. C., and Lavallo, P. (2002) Molecular basis for the explanation of the exponential growth of polyelectrolyte multilayers, *Proc Natl Acad Sci U S A* 99, 12531-12535.
128. Burke, S. E., and Barrett, C. J. (2003) pH-responsive properties of multilayered poly(L-lysine)/hyaluronic acid surfaces, *Biomacromolecules* 4, 1773-1783.
129. Joester, D., Klein, E., Geiger, B., and Addadi, L. (2006) Temperature-sensitive micrometer-thick layers of hyaluronan grafted on microspheres, *J Am Chem Soc* 128, 1119-1124.
130. Benz, M., Chen, N., and Israelachvili, J. (2004) Lubrication and wear properties of grafted polyelectrolytes, hyaluronan and hylan, measured in the surface forces apparatus, *J Biomed Mater Res A* 71, 6-15.
131. Sengupta, K., Schilling, J., Marx, S., Fischer, M., Bacher, A., and Sackmann, E. (2003) Mimicking Tissue Surfaces by Supported Membrane Coupled Ultrathin Layer of Hyaluronic Acid, *Langmuir* 19, 1775-1781.
132. Wolny, P. M., Spatz, J. P., and Richter, R. P. (2010) On the adsorption behavior of biotin-binding proteins on gold and silica, *Langmuir* 26, 1029-1034.
133. Knudson, C. B., and Toole, B. P. (1985) Changes in the pericellular matrix during differentiation of limb bud mesoderm, *Dev Biol* 112, 308-318.
134. Boehm, H., Mundinger, T. A., Boehm, C. H. J., Hagel, V., Rauch, U., Spatz, J. P., and Curtis, J. E. (2009) Mapping the mechanics and macromolecular organization of hyaluronan-rich cell coats, *Soft Matter* 5, 4331-4337.
135. Reviakine, I., Johannsmann, D., and Richter, R. P. (2011) Hearing what you cannot see and visualizing what you hear: interpreting quartz crystal microbalance data from solvated interfaces, *Anal Chem* 83, 8838-8848.
136. Muratsugu, M., Ohta, F., Miya, Y., Hosokawa, T., Kurosawa, S., Kamo, N., and Ikeda, H. (1993) Quartz crystal microbalance for the detection of microgram quantities of human serum albumin: relationship between the frequency change and the mass of protein adsorbed, *Anal Chem* 65, 2933-2937.
137. Caruso, F., Furlong, D. N., and Kingshott, P. (1997) Characterization of Ferritin Adsorption onto Gold, *J Colloid Interface Sci* 186, 129-140.
138. Hook, F., Kasemo, B., Nylander, T., Fant, C., Sott, K., and Elwing, H. (2001) Variations in coupled water, viscoelastic properties, and film thickness of a Mefp-1 protein film during adsorption and cross-linking: a quartz crystal microbalance with

- dissipation monitoring, ellipsometry, and surface plasmon resonance study, *Anal Chem* 73, 5796-5804.
139. Höök, F., Kasemo, B., Nylander, T., Fant, C., Scott, K., and Elwing, H. (2001) Variations in Coupled Water, Viscoelastic Properties, and Film Thickness of a Mefp-1 Protein Film during Adsorption and Cross-Linking: A Quartz Crystal Microbalance with Dissipation Monitoring, Ellipsometry, and Surface Plasmon Resonance Study, *Anal. Chem.* 73, 5796-5804.
  140. Höök, F., Ray, A., Norden, B., and Kasemo, B. (2001) Characterization of PNA and DNA Immobilization and Subsequent Hybridization with DNA Using Acoustic-Shear-Wave Attenuation Measurements, *Langmuir* 17, 8305-8312.
  141. Larsson, C., Rodahl, M., and Hook, F. (2003) Characterization of DNA immobilization and subsequent hybridization on a 2D arrangement of streptavidin on a biotin-modified lipid bilayer supported on SiO<sub>2</sub>, *Anal Chem* 75, 5080-5087.
  142. Pope, L. H., Allen, S., Davies, M. C., Roberts, C. J., Tendler, S. J. B., and Williams, P. M. (2001) Probing DNA Duplex Formation and DNA-Drug Interactions by the Quartz Crystal Microbalance Technique, *Langmuir* 17, 8300-8304.
  143. Fredriksson, C., Kihlman, S., Rodahl, M., and Kasemo, B. (1998) The Piezoelectric Quartz Crystal Mass and Dissipation Sensor: A Means of Studying Cell Adhesion, *Langmuir* 14, 248-251.
  144. Reiss, B. r., Janshoff, A., Steinem, C., Seebach, J., and Wegener, J. (2002) Adhesion Kinetics of Functionalized Vesicles and Mammalian Cells: A Comparative Study, *Langmuir* 19, 1816-1823.
  145. Svedhem, S., Pfeiffer, I., Larsson, C., Wingren, C., Borrebaeck, C., and Hook, F. (2003) Patterns of DNA-labeled and scFv-antibody-carrying lipid vesicles directed by material-specific immobilization of DNA and supported lipid bilayer formation on an Au/SiO<sub>2</sub> template, *Chembiochem* 4, 339-343.
  146. Svedhem, S., Dahlborg, D., Ekeröth, J., Kelly, J., Höök, F., and Gold, J. (2003) In Situ Peptide-Modified Supported Lipid Bilayers for Controlled Cell Attachment, *Langmuir* 19, 6730-6736.
  147. Janshoff, A., Galla, H. J., and Steinem, C. (2000) Piezoelectric Mass-Sensing Devices as Biosensors-An Alternative to Optical Biosensors?, *Angew Chem Int Ed Engl* 39, 4004-4032.
  148. Domack, A., et al. (1997) Swelling of a polymer brush probed with a quartz crystal resonator, *Physical Review E* 56, 680-689.
  149. Voinova, M. V., et al. (1999) Viscoelastic Acoustic Response of Layered Polymer Films at Fluid-Solid Interfaces: Continuum Mechanics Approach, *Physica Scripta* 59, 391-396.
  150. Eisele, N. B., Andersson, F. I., Frey, S., and Richter, R. P. (2012) Viscoelasticity of thin biomolecular films: a case study on nucleoporin phenylalanine-glycine repeats grafted to a histidine-tag capturing QCM-D sensor, *Biomacromolecules* 13, 2322-2332.
  151. Richter, R. P., Mukhopadhyay, A., and Brisson, A. (2003) Pathways of lipid vesicle deposition on solid surfaces: a combined QCM-D and AFM study, *Biophys. J.* 85, 3035-3047.

- 
152. Bingen, P., Wang, G., Steinmetz, N. F., Rodahl, M., and Richter, R. P. (2008) Solvation effects in the quartz crystal microbalance with dissipation monitoring response to biomolecular adsorption. A phenomenological approach, *Analytical Chemistry* 80, 8880-8890.
  153. Reimhult, E., Larsson, C., Kasemo, B., and Hook, F. (2004) Simultaneous surface plasmon resonance and quartz crystal microbalance with dissipation monitoring measurements of biomolecular adsorption events involving structural transformations and variations in coupled water, *Anal Chem* 76, 7211-7220.
  154. Carton, I., Brisson, A. R., and Richter, R. P. (2010) Label-free detection of clustering of membrane-bound proteins, *Anal. Chem.* 82, 9275-9281.
  155. Fujiwara, H. (2007) *Spectroscopic Ellipsometry: Principles and Applications*, Wiley Interscience
  156. Goncalves, D. b., and Irene, E. A. (2002) Fundamentals and applications of spectroscopic ellipsometry, *Quimica Nova* 25, 794-800.
  157. De Feijter, J. A., Benjamins, J., and Veer, F. A. (1978) Ellipsometry as a tool to study the adsorption behavior of synthetic and biopolymers at the air–water interface, *Biopolymers* 17, 1759-1772.
  158. Salamon, Z., and Tollin, G. (2001) Optical Anisotropy in Lipid Bilayer Membranes: Coupled Plasmon-Waveguide Resonance Measurements of Molecular Orientation, Polarizability, and Shape, *Biophysical journal* 80, 1557-1567.
  159. Curtis, A. S. (1964) The Mechanism of Adhesion of Cells to Glass. A Study by Interference Reflection Microscopy, *J Cell Biol* 20, 199-215.
  160. Kuhner, M., and Sackmann, E. (1996) Ultrathin Hydrated Dextran Films Grafted on Glass: Preparation and Characterization of Structural, Viscous, and Elastic Properties by Quantitative Microinterferometry, *Langmuir* 12, 4866-4876.
  161. Radler, J., and Sackmann, E. (1997) Functionalization of solids by ultrathin soft polymer films and polymer/lipid film composites: modeling of cell surfaces and cell recognition processes, *Current Opinion in Solid State and Materials Science* 2, 330-336.
  162. Schilling, J. r., Sengupta, K., Goennenwein, S., Bausch, A. R., and Sackmann, E. (2004) Absolute interfacial distance measurements by dual-wavelength reflection interference contrast microscopy, *Physical Review E* 69, 021901.
  163. Attili, S., and Richter, R. P. (2012) Combining colloidal probe atomic force and reflection interference contrast microscopy to study the compressive mechanics of hyaluronan brushes, *Langmuir* 28, 3206-3216.
  164. Limozin, L., and Sengupta, K. (2009) Quantitative Reflection Interference Contrast Microscopy (RICM) in Soft Matter and Cell Adhesion, *ChemPhysChem* 10, 2752-2768.
  165. Wisniewski, H.-G., Snitkin, E. S., Mindrescu, C., Sweet, M. H., and Vilcek, J. (2005) TSG-6 Protein Binding to Glycosaminoglycans, *J. Biol. Chem.* 280, 14476-14484.
  166. Eisele, N. B., Frey, S., Piehler, J., Görlich, D., and Richter, R. P. (2010) Ultrathin nucleoporin FG repeat films and their interaction with nuclear transport receptors, *EMBO Rep.* 11, 366-372.

167. Nilebäck, E., Westberg, F., Deinum, J., and Svedhem, S. (2010) Viscoelastic Sensing of Conformational Changes in Plasminogen Induced upon Binding of Low Molecular Weight Compounds, *Anal. Chem.* *82*, 8374–8376.
168. Baranova, N. S., Nileback, E., Haller, F. M., Briggs, D. C., Svedhem, S., Day, A. J., and Richter, R. P. The inflammation-associated protein TSG-6 cross-links hyaluronan via hyaluronan-induced TSG-6 oligomers, *J Biol Chem* *286*, 25675-25686.
169. Carton, I., Brisson, A. R., and Richter, R. P. Label-free detection of clustering of membrane-bound proteins, *Anal Chem* *82*, 9275-9281.
170. Richter, R. P., Bérat, R., and Brisson, A. R. (2006) The formation of solid-supported lipid bilayers - an integrated view, *Langmuir* *22*, 3497-3505.
171. Bingen, P., Wang, G., Steinmetz, N. F., Rodahl, M., and Richter, R. P. (2008) Solvation effects in the QCM-D response to biomolecular adsorption - a phenomenological approach, *Anal. Chem.* *80*, 8880-8890.
172. Steinmetz, N. F., Bock, E., Richter, R. P., Spatz, J. P., Lomonossoff, G. P., and Evans, D. J. (2008) Assembly of multilayer arrays of viral nanoparticles via biospecific recognition: a quartz crystal microbalance with dissipation monitoring study., *Biomacromolecules* *9*, 456-462.
173. Richter, R. P., Hock, K. K., Burkhartsmeier, J., Boehm, H., Bingen, P., Wang, G., Steinmetz, N. F., Evans, D. J., and Spatz, J. P. (2007) Membrane-Grafted Hyaluronan Films: a Well-Defined Model System of Glycoconjugate Cell Coats, *J. Am. Chem. Soc.* *127*, 5306-5307.
174. Zhuo, L., Hascall, V. C., and Kimata, K. (2004) Inter-alpha-trypsin inhibitor, a covalent protein-glycosaminoglycan-protein complex, *J Biol Chem* *279*, 38079-38082.
175. Crowe, J. H., Crowe, L. M., Wolkers, W. F., Oliver, A. E., Ma, X., Auh, J. H., Tang, M., Zhu, S., Norris, J., and Tablin, F. (2005) Stabilization of dry Mammalian cells: lessons from nature, *Integr Comp Biol* *45*, 810-820.
176. Green, N. M., and Toms, E. J. (1972) The dissociation of avidin-biotin complexes by guanidinium chloride, *Biochem J* *130*, 707-711.
177. Kaushik, J. K., and Bhat, R. (2003) Why is trehalose an exceptional protein stabilizer? An analysis of the thermal stability of proteins in the presence of the compatible osmolyte trehalose, *J Biol Chem* *278*, 26458-26465.
178. Bennun, S. V., Faller, R., and Longo, M. L. (2008) Drying and Rehydration of DLPC/DSPC Symmetric and Asymmetric Supported Lipid Bilayers: a Combined AFM and Fluorescence Microscopy Study, *Langmuir* *24*, 10371-10381.
179. Peterson, A. W., Halter, M., Tona, A., Bhadriraju, K., and Plant, A. L. (2009) Surface plasmon resonance imaging of cells and surface-associated fibronectin, *BMC Cell Biol* *10*, 16.
180. Hascall, V. C., Majors, A. K., De La Motte, C. A., Evanko, S. P., Wang, A., Drazba, J. A., Strong, S. A., and Wight, T. N. (2004) Intracellular hyaluronan: a new frontier for inflammation?, *Biochim. Biophys. Acta* *1673*, 3-12.
181. Toole, B. P. (2004) Hyaluronan: from extracellular glue to pericellular cue, *Nat. Rev. Cancer* *4*, 528-539.



182. Milner, C. M., and Day, A. J. (2003) TSG-6: a multifunctional protein associated with inflammation, *J. Cell. Sci.* 116, 1863-1873.
183. Milner, C. M., Higman, V. A., and Day, A. J. (2006) TSG-6: a pluripotent inflammatory mediator?, *Biochem. Soc. Trans.* 34, 446-450.
184. Selbi, W., Day, A. J., Rugg, M. S., Fulop, C., de la Motte, C. A., Bowen, T., Hascall, V. C., and Phillips, A. O. (2006) Overexpression of hyaluronan synthase 2 alters hyaluronan distribution and function in proximal tubular epithelial cells, *J. Am. Soc. Nephrol.* 17, 1553-1567.
185. Simpson, R. M., Meran, S., Thomas, D., Stephens, P., Bowen, T., Steadman, R., and Phillips, A. (2009) Age-related changes in pericellular hyaluronan organization leads to impaired dermal fibroblast to myofibroblast differentiation, *Am. J. Pathol.* 175, 1915-1928.
186. Mahoney, D. J., Mikecz, K., Ali, T., Mabileau, G., Benayahu, D., Plaas, A., Milner, C. M., Day, A. J., and Sabokbar, A. (2008) TSG-6 regulates bone remodeling through inhibition of osteoblastogenesis and osteoclast activation, *J. Biol. Chem.* 283, 25952-25962.
187. Tan, K. T., McGrouther, D. A., Day, A. J., Milner, C. M., and Bayat, A. (2011) Characterization of hyaluronan and TSG-6 in skin scarring: differential distribution in keloid scars, normal scars and unscarred skin, *J. Eur. Acad. Dermatol. Venereol.* 25, 317-327.
188. Wisniewski, H. G., Hua, J. C., Poppers, D. M., Naime, D., Vilcek, J., and Cronstein, B. N. (1996) TNF/IL-1-inducible protein TSG-6 potentiates plasmin inhibition by inter-alpha-inhibitor and exerts a strong anti-inflammatory effect in vivo, *J. Immunol.* 156, 1609-1615.
189. Jessen, T. E., and Odum, L. (2004) TSG-6 and calcium ions are essential for the coupling of inter-alpha-trypsin inhibitor to hyaluronan in human synovial fluid, *Osteoarthritis Cartilage* 12, 142-148.
190. Lee, T. H., Wisniewski, H. G., and Vilcek, J. (1992) A novel secretory tumor necrosis factor-inducible protein (TSG-6) is a member of the family of hyaluronate binding proteins, closely related to the adhesion receptor CD44, *J. Cell. Biol.* 116, 545-557.
191. Wisniewski, H. G., and Vilcek, J. (1997) TSG-6: an IL-1/TNF-inducible protein with anti-inflammatory activity, *Cytokine Growth Factor Rev.* 8, 143-156.
192. Forteza, R., Casalino-Matsuda, S. M., Monzon, M. E., Fries, E., Rugg, M. S., Milner, C. M., and Day, A. J. (2007) TSG-6 potentiates the antitissue kallikrein activity of inter-alpha-inhibitor through bikunin release, *Am. J. Respir. Cell Mol. Biol.* 36, 20-31.
193. Kuznetsova, S. A., Mahoney, D. J., Martin-Manso, G., Ali, T., Nentwich, H. A., Sipes, J. M., Zeng, B., Vogel, T., Day, A. J., and Roberts, D. D. (2008) TSG-6 binds via its CUB\_C domain to the cell-binding domain of fibronectin and increases fibronectin matrix assembly, *Matrix Biol.* 27, 201-210.
194. Lesley, J., Gal, I., Mahoney, D. J., Cordell, M. R., Rugg, M. S., Hyman, R., Day, A. J., and Mikecz, K. (2004) TSG-6 modulates the interaction between hyaluronan and cell surface CD44, *Journal of Biological Chemistry* 279, 25745-25754.
195. Getting, S. J., Mahoney, D. J., Cao, T., Rugg, M. S., Fries, E., Milner, C. M., Perretti, M., and Day, A. J. (2002) The link module from human TSG-6 inhibits neutrophil

- migration in a hyaluronan- and inter-alpha -inhibitor-independent manner, *J. Biol. Chem.* 277, 51068-51076.
196. Mahoney, D. J., Mulloy, B., Forster, M. J., Blundell, C. D., Fries, E., Milner, C. M., and Day, A. J. (2005) Characterization of the interaction between tumor necrosis factor-stimulated gene-6 and heparin: implications for the inhibition of plasmin in extracellular matrix microenvironments, *J. Biol. Chem.* 280, 27044-27055.
197. Kuznetsova, S. A., Day, A. J., Mahoney, D. J., Rugg, M. S., Mosher, D. F., and Roberts, D. D. (2005) The N-terminal module of thrombospondin-1 interacts with the link domain of TSG-6 and enhances its covalent association with the heavy chains of inter-alpha-trypsin inhibitor, *J. Biol. Chem.* 280, 30899-30908.
198. Blundell, C. D., Mahoney, D. J., Cordell, M. R., Almond, A., Kahmann, J. D., Perczel, A., Taylor, J. D., Campbell, I. D., and Day, A. J. (2007) Determining the Molecular Basis for the pH-dependent Interaction between the Link Module of Human TSG-6 and Hyaluronan, *J. Biol. Chem.* 282, 12976-12988.
199. Nentwich, H. A., Mustafa, Z., Rugg, M. S., Marsden, B. D., Cordell, M. R., Mahoney, D. J., Jenkins, S. C., Dowling, B., Fries, E., Milner, C. M., Loughlin, J., and Day, A. J. (2002) A novel allelic variant of the human TSG-6 gene encoding an amino acid difference in the CUB module. Chromosomal localization, frequency analysis, modeling, and expression, *J. Biol. Chem.* 277, 15354-15362.
200. Parkar, A. A., and Day, A. J. (1997) Overlapping sites on the Link module of human TSG-6 mediate binding to hyaluronan and chondroitin-4-sulphate, *FEBS Lett.* 410, 413-417.
201. Parkar, A. A., Kahmann, J. D., Howat, S. L. T., Bayliss, M. T., and Day, A. J. (1998) TSG-6 interacts with hyaluronan and aggrecan in a pH-dependent manner via a common functional element: implications for its regulation in inflamed cartilage, *FEBS Lett.* 428, 171-176.
202. Wisniewski, H. G., and Vilcek, J. (2004) Cytokine-induced gene expression at the crossroads of innate immunity, inflammation and fertility: TSG-6 and PTX3/TSG-14, *Cytokine Growth Factor Rev.* 15, 129-146.
203. Kuznetsova, S. A., Issa, P., Perruccio, E. M., Zeng, B., Sipes, J. M., Ward, Y., Seyfried, N. T., Fielder, H. L., Day, A. J., Wight, T. N., and Roberts, D. D. (2006) Versican-thrombospondin-1 binding in vitro and colocalization in microfibrils induced by inflammation on vascular smooth muscle cells, *J. Cell Sci.* 119, 4499-4509.
204. Day, A. J., Aplin, R. T., and Willis, A. C. (1996) Overexpression, purification, and refolding of link module from human TSG-6 in *Escherichia coli*: effect of temperature, media, and mutagenesis on lysine misincorporation at arginine AGA codons, *Protein Expr. Purif.* 8, 1-16.
205. Kahmann, J. D., Koruth, R., and Day, A. J. (1997) Method for quantitative refolding of the link module from human TSG-6, *Protein Expr. Purif.* 9, 315-318.
206. Rodahl, M., Höök, F., Krozer, A., Brzezinski, P., and Kasemo, B. (1995) Quartz crystal microbalance setup for frequency and Q-factor measurements in gaseous and liquid environments, *Rev. Sci. Instrum.* 66, 3924-3930.

- 
207. Weiss, J. N. (1997) The Hill equation revisited: uses and misuses, *FASEB J.* 11, 835-841.
208. Kahmann, J. D., O'Brien, R., Werner, J. M., Heinegård, D., Ladbury, J. E., Campbell, I. D., and Day, A. J. (2000) Localization and characterization of the hyaluronan-binding site on the Link module from human TSG-6, *Structure* 8, 763-774.
209. Day, A. J., Wright, A. J., Blanc, G., Konarev, P., Svergun, D. I., and Hulmes, D. J. S. (2004) Small angle X-ray scattering reveals TSG-6 to be an end-to-end dimer in the presence of excess hyaluronan., In *HASYLAB DESY Annual Report 2004* ([http://hasyweb.desy.de/science/annual\\_reports/2004\\_report/index2.html](http://hasyweb.desy.de/science/annual_reports/2004_report/index2.html)).
210. Baranova, N. S., Nileback, E., Haller, F. M., Briggs, D. C., Svedhem, S., Day, A. J., and Richter, R. P. (2011) The inflammation-associated protein TSG-6 cross-links hyaluronan via hyaluronan-induced TSG-6 oligomers, *J Biol Chem* 286, 25675-25686.
211. de Gennes, P.-G. (1979) *Scaling Concepts in Polymer Physics*, Cornell University Press, Ithaca and London.
212. Rubinstein, M., and Colby, R. H. (2003) *Polymer Physics*, Oxford University Press, Oxford.
213. Heng, B. C., Gribbon, P. M., Day, A. J., and Hardingham, T. E. (2008) Hyaluronan binding to link module of TSG-6 and to G1 domain of aggrecan is differently regulated by pH, *Journal of Biological Chemistry* 283, 32294-32301.
214. Blundell, C. D., Kahmann, J. D., Perczel, A., Mahoney, D. J., Cordell, M. R., Teriete, P., Campbell, I., and Day, A. J. (2002) Getting to grips with HA-protein interactions, In *Hyaluronan* (Kennedy, J. F., Phillips, G. O., Williams, P. A., and Hascall, V. C., Eds.), pp 161-172, Woodhead Publishing Ltd., Abington, Cambridge, UK.
215. Höök, F., Larsson, C., and Fant, C. (2002) Biofunctional Surfaces Studied by Quartz Crystal Microbalance with Dissipation Monitoring, In *Encyclopedia of Surface and Colloid Science*, pp 774-791, Marcel Dekker, Inc., digital publisher.
216. Blundell, C. D., Almond, A., Mahoney, D. J., DeAngelis, P. L., Campbell, I. D., and Day, A. J. (2005) Towards a structure for a TSG-6-hyaluronan complex by modeling and NMR spectroscopy: insights into other members of the link module superfamily, *J. Biol. Chem.* 280, 18189-18201.
217. Higman, V. A., Blundell, C. D., Mahoney, D. J., Redfield, C., Noble, M. E., and Day, A. J. (2007) Plasticity of the TSG-6 HA-binding loop and mobility in the TSG-6-HA complex revealed by NMR and X-ray crystallography, *J. Mol. Biol.* 371, 669-684.
218. Banerji, S., Wright, A. J., Noble, M., Mahoney, D. J., Campbell, I. D., Day, A. J., and Jackson, D. G. (2007) Structures of the Cd44-hyaluronan complex provide insight into a fundamental carbohydrate-protein interaction, *Nat. Struct. Mol. Biol.* 14, 234-239.
219. Fraser, J. R., Laurent, T. C., and Laurent, U. B. (1997) Hyaluronan: its nature, distribution, functions and turnover, *J. Intern. Med.* 242, 27-33.
220. Camaioni, A., Hascall, V. C., Yanagishita, M., and Salustri, A. (1993) Effects of exogenous hyaluronic acid and serum on matrix organization and stability in the mouse cumulus cell-oocyte complex, *J. Biol. Chem.* 268, 20473-20481.

221. Mahoney, D. J., Swales, C., Athanasou, N. A., Bombardieri, M., Pitzalis, C., Kliskey, K., Sharif, M., Day, A. J., Milner, C. M., and Sabokbar, A. (2011) TSG-6 inhibits osteoclast activity via an autocrine mechanism and is functionally synergistic with OPG, *Arthritis Rheum*.
222. Bayliss, M. T., Howat, S. L., Dudhia, J., Murphy, J. M., Barry, F. P., Edwards, J. C., and Day, A. J. (2001) Up-regulation and differential expression of the hyaluronan-binding protein TSG-6 in cartilage and synovium in rheumatoid arthritis and osteoarthritis, *Osteoarthritis Cartilage* 9, 42-48.
223. Discher, D. E., Janmey, P. A., and Wang, Y.-L. (2005) Tissue Cells Feel and Respond to the Stiffness of Their Substrate, *Science* 210, 1139-1143.
224. Discher, D. E., Mooney, D. J., and Zandstra, P. W. (2009) Growth factors, matrices, and forces combine and control stem cells, *Science* 324, 1673-1677.
225. Geiger, B., Spatz, J. P., and Bershadsky, A. D. (2009) Environmental sensing through focal adhesions, *Nat. Rev. Mol. Cell Biol.* 10, 21-33.
226. Wolny, P. M., Banerji, S., Gounou, C., Brisson, A. R., Day, A. J., Jackson, D. G., and Richter, R. P. (2010) Analysis of CD44-hyaluronan interactions in an artificial membrane system: insights into the distinct binding properties of high and low molecular weight hyaluronan, *J. Biol. Chem.* 285, 30170-30180.
227. Andrian, U. H. v., Hasslen, S. R., Nelson, R. D., Erlandsen, S. L., and Butcher, E. C. (1995) A central role for microvillous receptor presentation in leukocyte adhesion under flow, *Cell* 82, 989-999.
228. Russell, D. L., and Salustri, A. (2006) Extracellular matrix of the cumulus-oocyte complex, *Semin Reprod Med* 24, 217-227.
229. Day, A. J., and Sheehan, J. K. (2001) Hyaluronan: polysaccharide chaos to protein organisation, *Curr Opin Struct Biol* 11, 617-622.
230. Kida, D., Yoneda, M., Miyaura, S., Ishimaru, T., Yoshida, Y., Ito, T., Ishiguro, N., Iwata, H., and Kimata, K. (1999) The SHAP-HA complex in sera from patients with rheumatoid arthritis and osteoarthritis, *J Rheumatol* 26, 1230-1238.
231. Hamerman, D., and Sandson, J. (1963) Unusual Properties of Hyaluronateprotein Isolated from Pathological Synovial Fluids, *J Clin Invest* 42, 1882-1889.
232. Zhuo, L., Kanamori, A., Kannagi, R., Itano, N., Wu, J., Hamaguchi, M., Ishiguro, N., and Kimata, K. (2006) SHAP potentiates the CD44-mediated leukocyte adhesion to the hyaluronan substratum, *J Biol Chem* 281, 20303-20314.
233. Lauer, M. E., Cheng, G., Swaidani, S., Aronica, M. A., Weigel, P. H., and Hascall, V. C. (2012) Tumor necrosis factor-stimulated gene-6 (TSG-6) amplifies hyaluronan synthesis by airway smooth muscle cells, *J Biol Chem* 288, 423-431.
234. Milner, C. M., Tongsoongnoen, W., Rugg, M. S., and Day, A. J. (2007) The molecular basis of inter-alpha-inhibitor heavy chain transfer on to hyaluronan, *Biochem Soc Trans* 35, 672-676.
235. Enghild, J. J., Salvesen, G., Thogersen, I. B., Valnickova, Z., Pizzo, S. V., and Hefta, S. A. (1993) Presence of the protein-glycosaminoglycan-protein covalent cross-link in the inter-alpha-inhibitor-related proteinase inhibitor heavy chain 2/bikunin, *J Biol Chem* 268, 8711-8716.

- 
236. Rugg, M. S., Willis, A. C., Mukhopadhyay, D., Hascall, V. C., Fries, E., Fulop, C., Milner, C. M., and Day, A. J. (2005) Characterization of complexes formed between TSG-6 and inter-alpha-inhibitor that act as intermediates in the covalent transfer of heavy chains onto hyaluronan, *J Biol Chem* 280, 25674-25686.
237. Sanggaard, K. W., Sonne-Schmidt, C. S., Krogager, T. P., Kristensen, T., Wisniewski, H. G., Thogersen, I. B., and Enghild, J. J. (2008) TSG-6 transfers proteins between glycosaminoglycans via a Ser28-mediated covalent catalytic mechanism, *J Biol Chem* 283, 33919-33926.
238. Sanggaard, K. W., Sonne-Schmidt, C. S., Krogager, T. P., Lorentzen, K. A., Wisniewski, H. G., Thogersen, I. B., and Enghild, J. J. (2008) The transfer of heavy chains from bikunin proteins to hyaluronan requires both TSG-6 and HC2, *J Biol Chem* 283, 18530-18537.
239. Sanggaard, K. W., Sonne-Schmidt, C. S., Jacobsen, C., Thogersen, I. B., Valnickova, Z., Wisniewski, H. G., and Enghild, J. J. (2006) Evidence for a two-step mechanism involved in the formation of covalent HC x TSG-6 complexes, *Biochemistry* 45, 7661-7668.
240. Milner, C. M., and Day, A. J. (2003) TSG-6: a multifunctional protein associated with inflammation, *J Cell Sci* 116, 1863-1873.
241. Mahoney, D. J., Blundell, C. D., and Day, A. J. (2001) Mapping the hyaluronan-binding site on the link module from human tumor necrosis factor-stimulated gene-6 by site-directed mutagenesis, *J Biol Chem* 276, 22764-22771.
242. Blundell, C. D., Mahoney, D. J., Almond, A., DeAngelis, P. L., Kahmann, J. D., Teriete, P., Pickford, A. R., Campbell, I. D., and Day, A. J. (2003) The link module from ovulation- and inflammation-associated protein TSG-6 changes conformation on hyaluronan binding, *J Biol Chem* 278, 49261-49270.
243. Nentwich, H. A., Mustafa, Z., Rugg, M. S., Marsden, B. D., Cordell, M. R., Mahoney, D. J., Jenkins, S. C., Dowling, B., Fries, E., Milner, C. M., Loughlin, J., and Day, A. J. (2002) A novel allelic variant of the human TSG-6 gene encoding an amino acid difference in the CUB module. Chromosomal localization, frequency analysis, modeling, and expression, *J Biol Chem* 277, 15354-15362.
244. de Gennes, P. G. (1987) Polymers at an Interface. A simplified view., *Adv Colloid Interface Sci* 27, 189-209.
245. Eisele, N. B., Frey, S., Piehler, J., Görlich, D., and Richter, R. P. (2010) Ultrathin nucleoporin FG repeat films and their interaction with nuclear transport receptors, *EMBO Rep* 11, 366-372.
246. Richter, R. P., Hock, K. K., Burkhartsmeier, J., Boehm, H., Bingen, P., Wang, G., Steinmetz, N. F., Evans, D. J., and Spatz, J. P. (2007) Membrane-Grafted Hyaluronan Films: a Well-Defined Model System of Glycoconjugate Cell Coats, *J Am Chem Soc* 127, 5306-5307.
247. Fujimoto, T., Savani, R. C., Watari, M., Day, A. J., and Strauss, J. F., 3rd. (2002) Induction of the hyaluronic acid-binding protein, tumor necrosis factor-stimulated gene-6, in cervical smooth muscle cells by tumor necrosis factor-alpha and prostaglandin E(2), *Am J Pathol* 160, 1495-1502.

248. de Belder, A. N., and Wik, K. O. (1975) Preparation and properties of fluorescein-labelled hyaluronate, *Carbohydr Res* 44, 251-257.
249. Lesley, J., He, Q., Miyake, K., Hamann, A., Hyman, R., and Kincade, P. W. (1992) Requirements for hyaluronic acid binding by CD44: a role for the cytoplasmic domain and activation by antibody, *J Exp Med* 175, 257-266.
250. Gal, I., Lesley, J., Ko, W., Gonda, A., Stoop, R., Hyman, R., and Mikecz, K. (2003) Role of the extracellular and cytoplasmic domains of CD44 in the rolling interaction of lymphoid cells with hyaluronan under physiologic flow, *J Biol Chem* 278, 11150-11158.
251. Lesley, J., Gal, I., Mahoney, D. J., Cordell, M. R., Rugg, M. S., Hyman, R., Day, A. J., and Mikecz, K. (2004) TSG-6 modulates the interaction between hyaluronan and cell surface CD44, *J Biol Chem* 279, 25745-25754.
252. Parkar, A. A., and Day, A. J. (1997) Overlapping sites on the Link module of human TSG-6 mediate binding to hyaluronan and chondroitin-4-sulphate, *FEBS Lett* 410, 413-417.
253. Heng, B. C., Gribbon, P. M., Day, A. J., and Hardingham, T. E. (2008) Hyaluronan binding to link module of TSG-6 and to G1 domain of aggrecan is differently regulated by pH, *J Biol Chem* 283, 32294-32301.
254. Marson, A., Robinson, D. E., Brookes, P. N., Mulloy, B., Wiles, M., Clark, S. J., Fielder, H. L., Collinson, L. J., Cain, S. A., Kielty, C. M., McArthur, S., Buttle, D. J., Short, R. D., Whittle, J. D., and Day, A. J. (2009) Development of a microtiter plate-based glycosaminoglycan array for the investigation of glycosaminoglycan-protein interactions, *Glycobiology* 19, 1537-1546.
255. Mahoney, D. J., Mulloy, B., Forster, M. J., Blundell, C. D., Fries, E., Milner, C. M., and Day, A. J. (2005) Characterization of the interaction between tumor necrosis factor-stimulated gene-6 and heparin: implications for the inhibition of plasmin in extracellular matrix microenvironments, *J Biol Chem* 280, 27044-27055.
256. Getting, S. J., Mahoney, D. J., Cao, T., Rugg, M. S., Fries, E., Milner, C. M., Perretti, M., and Day, A. J. (2002) The link module from human TSG-6 inhibits neutrophil migration in a hyaluronan- and inter-alpha -inhibitor-independent manner, *J Biol Chem* 277, 51068-51076.
257. Colon, E., Shytuhina, A., Cowman, M. K., Band, P. A., Sanggaard, K. W., Enghild, J. J., and Wisniewski, H. G. (2009) Transfer of inter-alpha-inhibitor heavy chains to hyaluronan by surface-linked hyaluronan-TSG-6 complexes, *J Biol Chem* 284, 2320-2331.
258. Luchetti, M. M., Piccinini, G., Mantovani, A., Peri, G., Matteucci, C., Pomponio, G., Fratini, M., Fraticelli, P., Sambo, P., Di Loreto, C., Doni, A., Introna, M., and Gabrielli, A. (2000) Expression and production of the long pentraxin PTX3 in rheumatoid arthritis (RA), *Clin Exp Immunol* 119, 196-202.
259. Yudin, A. I., Cherr, G. N., and Katz, D. F. (1988) Structure of the cumulus matrix and zona pellucida in the golden hamster: a new view of sperm interaction with oocyte-associated extracellular matrices, *Cell Tissue Res* 251, 555-564.
260. Day, A. J., and de la Motte, C. A. (2005) Hyaluronan cross-linking: a protective mechanism in inflammation?, *Trends in Immunology* 26, 637-643.

261. Wisniewski, H. G., and Vilcek, J. (2004) Cytokine-induced gene expression at the crossroads of innate immunity, inflammation and fertility: TSG-6 and PTX3/TSG-14, *Cytokine Growth Factor Rev* 15, 129-146.
262. Fulop, C., Kamath, R. V., Li, Y., Otto, J. M., Salustri, A., Olsen, B. R., Glant, T. T., and Hascall, V. C. (1997) Coding sequence, exon-intron structure and chromosomal localization of murine TNF-stimulated gene 6 that is specifically expressed by expanding cumulus cell-oocyte complexes, *Gene* 202, 95-102.
263. Yoshioka, S., Ochsner, S., Russell, D. L., Ujioka, T., Fujii, S., Richards, J. S., and Espey, L. L. (2000) Expression of tumor necrosis factor-stimulated gene-6 in the rat ovary in response to an ovulatory dose of gonadotropin, *Endocrinology* 141, 4114-4119.
264. Mantovani, A., Garlanda, C., and Bottazzi, B. (2003) Pentraxin 3, a non-redundant soluble pattern recognition receptor involved in innate immunity, *Vaccine* 21 Suppl 2, S43-47.
265. Vouret-Craviari, V., Matteucci, C., Peri, G., Poli, G., Introna, M., and Mantovani, A. (1997) Expression of a long pentraxin, PTX3, by monocytes exposed to the mycobacterial cell wall component lipoarabinomannan, *Infect Immun* 65, 1345-1350.
266. Deban, L., Russo, R. C., Sironi, M., Moalli, F., Scanziani, M., Zambelli, V., Cuccovillo, I., Bastone, A., Gobbi, M., Valentino, S., Doni, A., Garlanda, C., Danese, S., Salvatori, G., Sassano, M., Evangelista, V., Rossi, B., Zenaro, E., Constantin, G., Laudanna, C., Bottazzi, B., and Mantovani, A. (2010) Regulation of leukocyte recruitment by the long pentraxin PTX3, *Nat Immunol* 11, 328-334.
267. Maina, V., Cotena, A., Doni, A., Nebuloni, M., Pasqualini, F., Milner, C. M., Day, A. J., Mantovani, A., and Garlanda, C. (2009) Coregulation in human leukocytes of the long pentraxin PTX3 and TSG-6, *J Leukoc Biol* 86, 123-132.
268. Nagyova, E., Camaioni, A., Prochazka, R., and Salustri, A. (2004) Covalent transfer of heavy chains of inter-alpha-trypsin inhibitor family proteins to hyaluronan in vivo and in vitro expanded porcine oocyte-cumulus complexes, *Biol Reprod* 71, 1838-1843.
269. Day, A. J., Aplin, R. T., and Willis, A. C. (1996) Overexpression, purification, and refolding of link module from human TSG-6 in Escherichia coli: effect of temperature, media, and mutagenesis on lysine misincorporation at arginine AGA codons, *Protein Expr Purif* 8, 1-16.
270. Kahmann, J. D., Koruth, R., and Day, A. J. (1997) Method for quantitative refolding of the link module from human TSG-6, *Protein Expr Purif* 9, 315-318.
271. Riviaccio, V., Esposito, A., Bellofiore, P., Palladino, P., Sassano, M., Colombo, M., and Verdoliva, A. (2007) High-level expression and efficient purification of recombinant human long pentraxin PTX3 in Chinese hamster ovary cells, *Protein Expr Purif* 51, 49-58.
272. Day, A. J., Rugg, M.S., Mahoney, D.J., Milner C.M. (2004) The Role of Hyaluronan-binding proteins in Ovulation, *Matrix Biology Institute*.
273. Wisniewski, H. G., Maier, R., Lotz, M., Lee, S., Klampfer, L., Lee, T. H., and Vilcek, J. (1993) TSG-6: a TNF-, IL-1-, and LPS-inducible secreted glycoprotein associated with arthritis, *J Immunol* 151, 6593-6601.

## References

---

274. Flory, P. (1971) Principles of Polymer Chemistry, *Cornell University Press 1971*.
275. Attili, S. B., O. V.; Richter, R. P. (2012) Films of end-grafted hyaluronan are a prototype of a brush of a strongly charged, semi-flexible polyelectrolyte with intrinsic excluded volume. , *Biomacromolecules*.
276. de Gennes, P. G. (1980) Conformations of Polymers Attached to an Interface, *Macromolecules* 13, 1069-1075.



# List of publications

---

1. Baranova, N. S., Nileback, E., Haller, F. M., Briggs, D. C., Svedhem, S., Day, A. J., and Richter, R. P. (2011) The inflammation-associated protein TSG-6 cross-links hyaluronan via hyaluronan-induced TSG-6 oligomers, *J Biol Chem* 286, 25675-25686.
2. Baranova, N. S., Attili Seetharamaiah, Wolny P.M. and Richter R.P. (2011) The sweet coast of living cells-from supramolecular structure and dynamics to biological function, *Int J Mat Res* 102, 903-905.
3. Baranova, N. S., Foulcer, S.J., Briggs, D.C., Tilakaratna V, Enghild, J.J., Milner, C.M., Day, A.J. and Richter, R.P. Inter- $\alpha$ -inhibitor impairs TSG-6 induced hyaluronan cross-linking, submitted to *J Biol Chem*
4. Baranova, N.S., Inforzato A., Briggs, D.C., Enghild, J.J., Day, A.J. and Richter, R.P. Mechanism of PTX3 incorporation into HA-rich matrices, *manuscript in preparation*.



Date of birth 26/06/1984  
Nationality Ukrainian  
Civil state Married

## Research experience

Since 05/2008 **CIC biomaGUNE, San Sebastian, Spain**  
PhD Student  
Model systems of carbohydrate - rich pericellular coats;  
Supramolecular assembly of the artificial cumulus cells oocyte complex matrix.

01/2007-05/2007 **Wroclaw Polytechnic University, Wroclaw, Poland**  
Internship  
Preparation/purification/characterization of oligomeric hyaluronic acid;  
Protein glycosylation chemistry.

06/2006-05/2007 **Palladin Institute of Biochemistry, Kiev, Ukraine**  
Master Student  
Biotechnological application of hyaluronic acid - cell culture models.

---

## Education

09/2006 – 06/2007 **Kiev National University, Kiev, Ukraine**  
Master of Science in Biochemistry and Biotechnology, *with honor*  
Title: "Preparation and chemical modification of low molecular weight fragments of hyaluronic acid. Impact of high and low molecular weight hyaluronic acid on the phenotype of cultured cells."

09/2001 - 06/2006 **Kiev National University, Kiev, Ukraine**  
Bachelor of Science in Biology

---

## Technical skills

Biochemistry *In vivo* cell culturing and characterization, ELISA, size-exclusion/affinity chromatography (proteins and carbohydrates purification), SDS-PAGE, RT-PCR, flow cytometry, BF and fluorescence microscopy.

Surface characterization *In situ* ellipsometry, QCM-D, RICM.

Surface modification Supported lipid bilayers on silica, self-assembled monolayer on gold.

## *Publications:*

1. **Baranova, N. S.**, Inforzato A., Briggs, D.C., Enghild, J.J., Day, A.J., Richter, R.P. Mechanism of PTX3 incorporation into HA-rich matrices, *manuscript in preparation*.
2. **Baranova, N. S.**, Foulcer, S.J., Briggs, D.C., Tilakaratna V, Enghild, J.J., Milner, C.M., Day, A.J., Richter, R.P. Inter- $\alpha$ -inhibitor impairs TSG-6 induced hyaluronan cross-linking, *submitted to J Biol Chem*
3. **Baranova, N. S.**, Nileback, E., Haller, F. M., Briggs, D. C., Svedhem, S., Day, A. J., and Richter, R. P. (2011) The inflammation-associated protein TSG-6 cross-links hyaluronan via hyaluronan-induced TSG-6 oligomers, *J Biol Chem* 286, 25675-25686.
4. **Baranova, N. S.**, Attili Seetharamaiah , Wolny P.M., Richter R.P. (2011) The sweet coast of living cells-from supramolecular structure and dynamics to biological function, *Int. J. Mat. Res.* 102, 903-905.
5. Yevdokymova, N., Karlova, N. P., **Baranova, N. S.**, and Komisarenko, S. V. (2006). "Methylenebisphosphonic acid alters the pattern of pericellular glycosaminoglycans and binding properties of CD44 in human endothelial cells" *Ukr Biochim Zh* 78, 95-103.

---

## *Teaching experience:*

2012	Tutor of practical sessions, FEBS Whorkshop: Physical chemistry of Biointerfaces, San Sebastian, Spain
2010	Tutor of practical sessions, FEBS Whorkshop: Physical chemistry of Biointerfaces, San Sebastian, Spain
2007	Biochemistry teacher, Kiev Biochemical lyceum.